Thermal Insulation by Heat Resistant Polymers

Ashraf Fathy Ahmed

A Thesis

In the Department

Of

Mechanical and Industrial `Engineering

Presented in Partial Fulfillment of the Requirements

For the Degree of Doctor of Philosophy at

Concordia University

Montreal, Quebec, Canada

June 2009

Your file Votre référence
ISBN: 978-0-494-63379-3
Our file Notre référence
ISBN: 978-0-494-63379-3

Abstract

Thermal Insulation by Heat Resistant Polymers

Ashraf Fathy Ahmed, Ph.D.

Concordia University, 2009

Internal insulation in a solid rocket motor is a layer of heat-barrier material placed between the internal surface of the case and the propellant. The primary function of internal insulation is to prevent the rocket motor case from reaching temperatures that may endanger its structural integrity.

An extensive experimental and theoretical work in the development and characterization of asbestos-free rubbers for use as rocket motor insulators has been performed. The insulation is based on chopped carbon fiber and/or aramid fiber in the pulp form as fillers for Ethylene Propylene Diene Monomer (EPDM). The first aim of the research is to provide an understanding of the mechanism, the principle, and the process for making polymeric thermal insulants. The second aim is to produce thermal insulants based on polymers with different fillers having different compositions which are capable of working under extreme thermal conditions of 2760 °C (5000 °F). This is through an investigation on the processing, installation, physical, mechanical, thermal and ablative properties of these materials. A hybrid of chopped carbon fiber and Kevlar pulp filled EPDM has been shown to exhibit better thermal, mechanical, physical and ablative properties than its asbestos containing counterpart. Also the prediction of thermal conduction of multiphase thermal insulation composite materials was done using series, parallel, Maxwell Euken and effective medium theory models. Comparison with the measured values allows determining which model estimates best the thermal conductivity

of composite insulation material. Development of a suitable optimization technique to reach the best parameters of the selected material was done by doing transient dynamic analysis to determine the response of these materials under a time-varying thermal load. A new type of insulation material using prepregs was developed for the first time. This consists of the development of the prepregs and their assembly to make insulant laminates. This laminate has been shown to exhibit better physical, mechanical, thermal and ablative properties than a hybrid of chopped carbon fiber and Kevlar pulp filled EPDM.

Acknowledgements

Foremost, I would like to thank my supervisor Prof. S. V. Hoa for providing me with the opportunity to complete my PhD thesis at the Concordia University. I especially want to thank him for support and guidance made my thesis work possible. He has been actively interested in my work and has always been available to advise me. I am very grateful for his patience, motivation, enthusiasm, and immense knowledge in the field of composites that, taken together, make him a great mentor.

A few lines are too short to make a complete account of my deep appreciation for my advisory committee members Prof. A Elhakeem, Prof. M Pugh, Prof. P Wood Adams for their unflattering trust and constant encouragements which have been essential to my success through the last three years.

I would like to express my gratitude to the Egyptian armed forces for giving me the possibility to complete this thesis. I want to thank the Department of Mechanical and Industrial engineering, Concordia University, Montreal, Canada for helping me to do this work.

For the non-scientific side of my thesis, I particularly want to thank my wife and my kids for the quiet environment they provided for me to take care of my thesis.

Table of Contents

List of Figures

List of Tables

Nomenclature

EPDM	Ethylene Propylene Diene Monomer
AP	Ammonium Polyphosphate
CCF	Chopped Carbon Fiber
PCA	Peroxide Cross linking Agent
CTPB	Carboxy-terminated polybutadiene
NBR	Nitrile butadiene rubber
SBR	Copolymer of styrene and butadiene
PBAA	Butadiene-Acrylic Acid polymer
ASRM	Advanced Solid Rocket Motor
K	Thermal Conductivity, W m^{-1} K^{-1}
C_p	Specific Heat, J/kg.°k
KP	Kevlar Pulp
DSC	Differential Scanning Calorimetery
TGA	Thermo Gravimetric Analysis
ASTM	American Society for Testing and Materials
α	Thermal diffusivity, mm^2/s
ρ	Density, gm/cm^3
d_i	Configuration factor
k_i	Thermal conductivity of a component (W m^{-1} K^{-1})
K	Effective thermal conductivity of the material (W m^{-1} K^{-1})
m	Number of components inside composite material
v_i	Volume fraction of a component i

U(x, t)	Temperature as function of thickness and time
t	Time
H	Heat source
HTPB	Hydroxyl-terminated polybutadiene
SBR	Butadiene-Styrene copolymers

Chapter 1

Introduction and Literature Review

1.1 Introduction

Solid rocket motors typically include an outer case or shell that houses solid propellant grains. A longitudinal cross section of the rocket main components is shown in Fig (1.1) [1]. The rocket motor case is conventionally manufactured from a rigid, yet durable, material such as steel or filament-wound composite. The propellant is housed within the case and is formulated from a composition designed to undergo combustion and thereby produce the requisite thrust for attaining rocket motor propulsion.

Internal insulation in a solid rocket motor is a layer of heat-barrier material placed between the internal surface of the case and the propellant. The primary function of internal insulation is to prevent the rocket motor case from reaching temperatures that may endanger its structural integrity. In addition, the insulation performs important secondary functions:

- Inhibits burning on certain propellant grain surfaces on which burning is undesirable.
- Buffers the transmission of case strain into the propellant.
- Seals the case, joints, and fittings to prevent loss of pressure and damage from hot combustion products.
- Guides combustion products into the nozzle in laminar flow to the greatest extent possible.
- Good ageing characteristics (minimum 10 years of shelf / useful life).

- Excellent bonding of the insulator with propellant and motor case over the entire range of working temperature.

- Bleed off or dissipate static charges that build up on the insulator surface.

Most insulator materials fail to perform one or more of the secondary functions, but if the primary function is performed well, designers usually are able to modify the design or provide other parts or materials to ensure the performance of secondary functions.

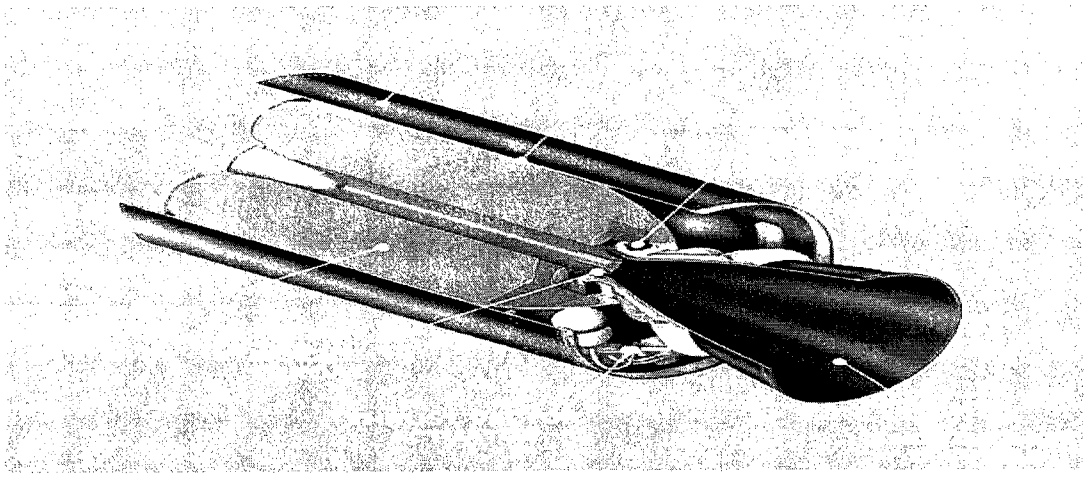

Fig (1.1) Longitudinal cross section of the Rocket motor main components [1]

During operation, a heat insulating layer (insulation) protects the rocket motor case from heat and particle streams generated by the combusting propellant. Fig (1.2) shows a cross section of a solid rocket motor [2]. Typically, the insulation is bonded to the inner surface of the case and is generally fabricated from a composition capable of withstanding the high temperature gases produced when the propellant grains burn. A liner layer (liner) functions to bond the propellant grains to the insulating layer [2-5].

The combustion of solid rocket propellant generates extreme conditions within the case of the rocket motor. For example, temperatures inside the rocket motor case typically reach 2,760° C (5,000° F), and interior pressures may exceed 1,500 psi (10.35 MPa).

These factors combine to create a high degree of turbulence within the rocket motor case. In addition, particles are typically entrained in the gases produced during propellant combustion. Under the turbulent environment, these entrained particles can erode the rocket motor insulation. If the insulating layer and liner are pierced during rocket motor operation, the casing is susceptible to melting or degradation, which can result in failure of the rocket motor. Thus, it is crucial that insulation compositions withstand the extreme conditions experienced during propellant combustion and protect the case from the burning propellant.

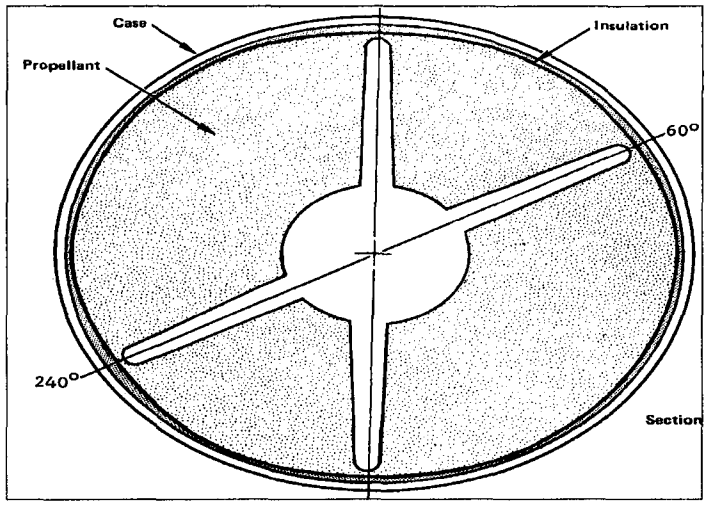

Fig (1.2) Cross section of a solid rocket motor [5]

It is also crucial that insulation compositions possess acceptable shelf life characteristics such that they remain sufficiently pliable, until used in application to the rocket motor casing. This requirement is essential because the production of a given lot of insulation may have to wait in storage for a number of months prior to use [6].

The case insulation design is a hybrid system to optimize weight and performance.

The requirements for an acceptable, functionally effective, insulation for solid propellant rocket motors are well known to be quite severe due to the extreme conditions to which

the insulation is exposed. These conditions not only include exceedingly high temperatures but also severe ablative effects from the hot particles (as well as gases) that traverse and exit the rocket motor interior. Unless the insulation will withstand such conditions, catastrophic failure may (and has) occur.

1.2 Literature Review

Materials used as insulators for solid rocket motors usually are identified by a hybrid name (e.g., fiber/matrix) that identifies a filler or reinforcement material in a matrix or binder. Two classes of materials are used as binders (matrix) for internal insulation: thermosetting and elastomeric plastics [7-12].

The designer of internal insulation must perform the following tasks:

(1) Select the insulation material.

(2) Establish the insulation thickness throughout the motor.

(3) Design flaps, joints, fillets, and inserts that are needed for proper insulator performance.

(4) Try to avoid disadvantages of insulation such as limited shelf life and higher density.

(5) Attain specific requirements of the insulator such as:

a- Excellent bonding of the insulator with propellant and motor case over the entire range of working temperature.

b- Low ablation rate from 0.09 mm/sec to 0.2 mm/sec.

c- Low density from 1.05 gm/cm^3 to 1.5 gm/cm^3.

d- Sufficient tensile strength $\geq$ 0.5 MPa

e- Low thermal conductivity from 0.2 to 0.5 W/m.k.

f- High specific heat from 1000 to 2100 J/kg.K.

g- Porous char with good retention characteristics.

h- Ability to withstand mechanical and thermal stress during storage, handling and curing operations.

i- Low moisture absorption.

j- Good ageing characteristics (minimum 10 years of shelf / useful life).

Knowledge of insulator function is a prerequisite to both selection of material and thickness design. Most current insulators for solid rocket motors function as heat barriers primarily through the mechanism of ablation; i.e., the material absorbs heat by increasing in temperature and changing in chemical or physical state, the changes usually being accompanied by loss of surface material.

1.2.1 Currently used thermoset-based insulations

The first class of material used for internal insulation is reinforced thermosetting resin. The binder resin used in this application is usually a high-temperature phenolic, although phenylsilane and polyamide-modified phenolic have also been used. The resin typically is filled with silica, asbestos, nylon, carbon, or glass cloth. Typical properties of filled thermosets used as insulators are shown in Table (1.1).

Phenolic polymer has good temperature resistance. When heated to 410 ^{o}C, phenolic starts to ablate and completely vaporizes from solid to gaseous state at 1312 ^{o}C. The ablated material is carried away by the hot gas stream. Phenolic is brittle. These thermosets however, crack and/or blister as a result of the rapid temperature and pressure fluctuations experienced during combustion. Although phenolic-based insulations are much more erosion resistant than many insulators which is due to the strong char formed during decomposition, they do not exhibit high strain capability and cannot survive high

aeroheating loads. In order to compensate for this, the rocket consists of many stages. Each stage can only last a fraction of the total required time. As such the rocket has to be very long. This adds weight and is very expensive.

Composition		Thermal properties		Physical properties		
Binder	**Filler**	**K (w /m .°k)**	**C_P (J /kg. °k)**	**Tensile Strength (MPa)**	**Density (gm/cm^3)**	**Elongation (%)**
Phenolic	Asbestos	0.3459	1172.3	6.9	1.52	1
Phenolic	Asbestos	0.6918	1130.4	8.3-45.5	1.76	0.5
Phenolic	Carbon cloth	0.8302	962.9	17.2-151.7	1.43	-
Phenolic	Carbon fiber	0.2940	1256.1	13.8	1.25	0.25
Phenolic	Glass cloth	0.2594	962.9	4.1-689.6	1.87	-
Phenolic	Chopped glass	0.4497	1046.7	34.5	1.85	-
Phenolic	Nylon	0.1729	1297.9	17.2-30.3	1.18	-
Pure aluminum		237	938	135	2.76	60

Table (1.1) Typical properties of filled thermosets used as rocket motor insulators [7-12]

1.2.2 Currently used elastomeric-based insulations

The second class of material used for internal insulation is reinforced elastomers. [13-16] An elastomeric material has the following basic characteristics:

(1) It is relatively soft, and its elastic modulus is low.

(2) It can withstand very high strains, up to 900 percent.

(3)It will return quickly to its original length following strain.

(4) It is noncrystalline, and the glass transition temperature characteristic of the material is well below the normal operating temperatures at which it will be used.

Elastomeric compositions have also been used as rocket motor insulation materials in a large number of rocket motors. The elastomeric compositions have been selected because their mechanical, thermal, and ablative properties are particularly suited for rocket motor applications. The most commonly used elastomer for rocket motor applications is ethylene propylene diene monomer (EPDM) which is available in different forms (rubbery and viscous liquid). However, the ablative properties of elastomers are often inadequate for rocket motor operation. For example, insulation, whether thermosetting or thermoplastic, is characterized by relatively high erosion rates unless reinforced with suitable fillers. The criticality of avoiding such high erosion rates is demonstrated by the severity and magnitude of the risk of failure due to erosion. Most insulation is, of necessity, "man-rated" in the sense that a catastrophic failure can result in the loss of human life—whether the rocket motor is used as a booster for launch of a space shuttle or is carried tactically underneath the wing of an attack aircraft. The monetary cost of failure in satellite launches is well-publicized and can run into the hundreds of millions of dollars. So this leads to reinforcing the elastomers with suitable fillers such as carbon black, asbestos and silica. Filled elastomers are useful in internal insulation both because their thermal properties are excellent and because their high strain capabilities allow the transmission of stress concentrations to be diffused from the case into the solid propellant [17-20].

One of the best reinforcements for elastomers for solid rocket motor applications is asbestos which shows outstanding performance in the physical, mechanical, thermal and ablative properties.

U. S. Patent 3, 347, 047, an early patent describing asbestos fiber filled insulations, states that flame temperatures encountered in the combustion of propellants, particularly when used as source of propulsion, necessitating the confinement of the gases of combustion and ultimate release thereof through orifices, are usually accompanied by extremely turbulent flow conditions. All of these features place considerable stress and strain upon the member defining the escape passageway. While the combustion of the propellant in the case of rockets and the like will usually be of short duration, the temperatures and turbulence encountered have been found to very easily destroy even the strongest and most exotic alloys formed of iron, steel, titanium, magnesium, silicon, chromium, beryllium and the like. As a consequence, the projectile structure fails leading to total destruction thereof through explosion or in the event that only the exit passageway is destroyed, the projectile proceeds in an erratic uncontrollable path since its trajectory or path is at least in part dependent upon the contour of the passageway through which pass the gaseous products of combustion.

Asbestos is made of two incombustible, chemical-resistant, fibrous mineral forms of impure magnesium silicate, used for fireproofing, electrical insulation and thermal insulation. Asbestos is a general name that applies to several types of fibrous silicate minerals. There are two main types of asbestos, the first is known as amphiboles. They are characterized by having very strong and stiff fibers, which makes them a serious health hazard. Amphibolic asbestos fibers can penetrate body tissue, especially in the lungs, and eventually cause tumors to develop. The second type of asbestos is known as serpentine or chrysotile. These fibers are much softer and more flexible than amphibolic asbestos, and they do less damage to body tissue. All types of asbestos are composed of

long chains of silicon and oxygen atoms, locked together with various metals, such as magnesium and iron, to form the whisker-like crystalline fibers that characterize this mineral [21].

Chrysotile is the most commonly used type of asbestos and accounted for about 98% of the worldwide asbestos production in 1988. It is usually white, and is sometimes known as white asbestos, although it can also be amber, gray, or greenish in color. Most chrysotile fibers are about 6.4-12.7 mm long and are usually added to elastomers to provide reinforcement for solid rocket motor applications. Only about 8% of chrysotile fibers are long enough to be spun into fabric or rope.

Asbestos deposits are found underground, and the ore is brought to the surface for processing using conventional mining practices. Chrysotile asbestos is usually found near the surface and can be accessed with an open-pit mine. Other asbestos deposits are found at varying depths and may require tunnels as deep as 300 m to gain access.

Asbestos fibers are formed by the gradual growth of mineral crystals in cracks, or veins, found in soft rock formations. The crystals grow across the vein, and the width of the vein determines the resulting asbestos fiber length. Because the minerals come from the surrounding rock, the chemical composition of the fibers is similar to the rock. As a result the asbestos must be separated from the rocky ore using physical methods, rather than the chemical methods sometimes used to process other ores. It is extracted for use through two main processes, mining and separation.

Chrysotile asbestos is a highly hydrated magnesium silicate with the formula $Mg_3 Si_2 O_5 (OH)_4$ with density 2.53 gm/cm^3. It has a thermal conductivity of 0.8 W/m.K and completely decomposes at 1712 °C.

A current technology describing asbestos fiber filled insulations consists of EPDM (NORDEL 1040) with 50 phr asbestos in addition to 60 phr dechlorane + R powder (a chlorinated flame retardant) and the composition is cured using peroxide cross linking agent with 5 phr. This insulation has the properties shown in Table (1.2).

Property	Unit	Testing value for laminate
Tensile strength	MPa	6.55
Elongation	%	30
Hardness	Shore A	94.6
Density	gm/cm^3	1.205
Specific heat capacity	J/kg.k	1674.7
Thermal diffusivity	mm^2/sec	0.12
Thermal conductivity	W/m.k	0.2421
Ablation rate	mm/sec	0.15
Outer case temperature	°C	139.1
TGA remaining weight	% (at 600 °C)	16

Table (1.2) Asbestos based EPDM properties

For asbestos used with EPDM, the fibers were dispersed in a two-roll mill to reduce agglomerations of fibers. The dispersion was accomplished by tightening the nip (separation between the two rolls) to 0. 75 mm on the two-roll mill and passing the rubber through the nip a minimum of six times. The rubber was then allowed to cool before the second pass.

Typical properties of filled plastics used as insulators with asbestos and other reinforcements are shown in Table (1.3).

Composition		Thermal properties		Physical properties		
Binder	Filler	K (w /m .°k)	C_P (J /kg. °k)	Tensile (MPa)	Density (gm/cm^3)	Elongation (%)
CTPB	Carbon black	0.2076	1800.3	1.89	0.969	350
EPDM	Asbestos	0.2421	1674.7	6.55	0.977	900
NBR	Silica	0.2249	1674.7	11.7-16.9	1.219	-
NBR	Silica + Asbestos	0.2421	1716.6	13.8	1.268	400-623
SBR	Asbestos	0.4324	1674.7	6.9	1.398	400
SBR	Silica	0.2249	1423.5	13.1-27.6	1.174	550-800
PBAA	Asbestos	0.4843	1507.3	1.2	1.331	1
Pure aluminum		237	938	135	2.76	60

Table (1.3) Typical properties of filled plastics used as rocket motor insulators [13-21]

Chase, Michael John, Smith, Derek Anthony and Dudley, Michael Alan [22] provided a solid propellant rocket motor with a liner between the motor case and the propellant, the liner comprising a terpolymer of ethylene, propylene and a nonconjugated diene and inert fillers. Ablative fillers such as heavy metal halides, calcium hydroxide and magnesium hydroxide were included.

Ratte, Jacques, Duchesne, Gonzague and Carignan, Pierre [23] provided an insulation system for use in rocket motors containing solid composite propellants. Some composite rocket propellants are based on carboxyl-terminated polybutadiene (CTPB) and others on hydroxyl-terminated polybutadiene (HTPB) binders. An important requirement of such systems is the ability of the wall insulation to adhere to the combustion chamber and of the composite propellant to adequately adhere to the insulation system. With CTPB propellants, a sheet insulant comprising chrysotile asbestos fibers and floats dispersed in

a CTPB polymeric binder was successfully employed. However, the use of a similar sheet insulant based on HTPB polymeric binder did not prove to be compatible with HTPB propellants. It provides a composite sheet insulation system which is compatible with HTPB propellants including a first layer of sheet material comprising a CTPB binder having a mixture of asbestos fibers and floats dispersed in it and, bonded to it, a second layer of aluminum foil and an economical and effective method of lining a rocket casing propellant chamber.

Junior, Kenneth E. and Byrd, James D. [24] disclosed an elastomeric composition suitable for use as a rocket motor case insulation. The composition consists of a vulcanizable elastomeric composition and reinforcing aramid polymer fibers in combination with powder filler. The embodiment utilizes polyisoprene as the elastomer, KELVAR.RTM. fibers as the aramid polymer fibers, and silica as the powder filler.

Junior, Kenneth E., Byrd, James D. and Hightower, Jr., James O. [25] disclosed an elastomeric composition suitable for use as a rocket motor case insulation. The composition comprises a vulcanizable elastomeric material and reinforcing polybenzimidazole polymer fibers in combination with powder filler. The embodiment utilizes polyisoprene as the elastomer and silica as the powder filler. These compositions have better erosion resistance than asbestos-reinforced compositions, and do not pose the environmental or safety risks associated with asbestos-reinforced insulation.

Byrd, James D., Davis, Robert T. [26] provided an improvement to the process of applying a rocket motor liner to an inside surface of a rocket motor casing by coating the casing with a rocket motor liner composition and then curing the liner composition. Typical rocket motor liner compositions include the product of a hydroxyl-terminated

polybutadiene prepolymer; a diisocyanate curing agent for forming urethane linkages with said prepolymer; a trifunctional aziridine bond promoter; filler; and a curing catalyst comprising maleic anhydride, magnesium oxide, and triphenyl bismuth. This invention uses alkaline carbon black filler and/or a curing catalyst which does not include magnesium oxide.

Herring, Liles G. [27] disclosed a non-asbestos elastomeric insulation materials for rocket motors. The insulation materials comprise 100 parts by weight of a crosslinked elastomer polymer and between about 10 and 100 (preferably 15-75) parts by weight of an organic fiber selected from cotton flock, sisal and a combination of cotton flock and sisal. The insulation materials have notable erosion resistance and can be tailored to have thermal, mechanical and other properties of desired character. The organic fiber advantageously functions as char-forming, low density filler. Other ingredients such as silica, phenolic resin, polybutadiene etc. are included to enhance the utility of the insulation materials.

Herring, Liles G. [28] disclosed a non-asbestos elastomeric insulating materials for rocket motors. The insulating materials are low in density (between about 0.97 and 1.38 g/cm^3) and comprise crosslinked elastomeric polymers (100 parts by weight of a crosslinkable elastomeric polymer that is substantially saturated and about 5-50 parts by weight of a crosslinkable, substantially unsaturated, elastomeric polymer) in which are dispersed between about 10 and 100 (preferably 15-75) parts by weight of a char-forming organic fiber selected from polyaramide pulps, between 1 and 15 parts by weight of a peroxide crosslinker, and between about 0 and 150 parts by weight organic and/or inorganic particulate. The insulating materials issue little smoke, have notable erosion resistance and can be tailored to have thermal, mechanical and other properties of desired character.

Ingredients such as supplemental elastomers, oils and lubricants enhance the processability and green properties such as tack of the insulating materials.

Chang, Suae-Chen [29] claimed a process for forming a low smoke, low erosion rocket motor insulation comprising mixing organic fiber selected from the group polyaramid and polybenzimidazole; an inorganic powder filler; a vulcanizable hydrocarbon elastomer and a non-fluorinated phosphazene polymer.

Guillot, David [30] provided another rocket motor insulation composition. An important component of such insulation composition is a thermoplastic liquid crystal polymer. Such a polymer provides an ablative insulation which has good performance characteristics during operation of the rocket motor. One such thermoplastic liquid crystal polymer is wholly aromatic polyester known as VECTRA.RTM. The insulation also includes fillers such as fibrous fillers and particulate fillers. Typical fibrous fillers include glass or carbon fibers. Typical particulate fillers include materials such as silica, alumina, powdered coal, and the like.

Also Guillot, David [31] disclosed thermoplastic elastomeric ablative insulation having low density. The ablative insulation is based upon a thermoplastic elastomeric polymer resin containing a polyamide polymer and a maleic anhydride modified EPDM polymer. The ratio of polyamide polymer to maleic anhydride modified EPDM is in the range from about 20:80 to about 40:60. Carefully selected fillers provide suitable charring and ablative insulation performance without unduly increasing the insulation density. Typical fillers include a phosphorus-containing compound, such as ammonium polyphosphate, a polyhydric alcohol, such as pentaerythritol, silicone resin, chopped fibers, an antioxidant, a butadiene polymer, and peroxide.

Graham, Mark, Levi, Lane and Clarke, Brett [32] provided an insulation for rocket motors that uses two ingredients not previously combined in such insulation before. These ingredients are ammonium sulfate and antimony oxide (hybrid flame retardant), which when combined, have a synergistic effect that reduces the ablation rate significantly. Such insulation also includes EPDM rubber and aramid fibers. The insulation also exhibits better tear resistance and propellant-to-insulation bond peel strength, compared with prior art rocket motor insulation.

Hutchens, Dale E., Cohen, Norman [33] provided a formulation which is capable of performing as a liner layer between a rocket motor casing and the propellant grain disposed within the interior of the rocket motor casing. The composition produces relatively little smoke during the operation of the rocket motor and is capable of securely bonding a wide range of conventional propellants to a wide range of conventional casings. The liner consists of from about 50% to about 75% oxygen containing polymer; from about 3 % to about 15 % curing agent; from about 5% to about 50 % filler and from about 0.01 % to about 0.5 % cure catalyst.

Pennington, William L., Skolnik, Edward G. and Davidson, Thomas F. [34] described an insulation material for a rocket motor, which is composed of a glass fabric, a resin binder, and a fire retardant. The resin binder preferably is composed of a phenolic resin and a Buna-N rubber, and the fire retardant is preferably alumina trihydrate. A method of manufacturing the insulation material is also described.

Harvey, Albert R. and Ellertson, John W. [35] claimed a rocket motor insulation including an elastomer base polymer with improved processability by the addition of silica particles treated with a hydrophobic coating. The insulation also preferably includes

a metallic coagent cross-linker, which when used in combination with the hydrophobic silica particles increases the tear strength and the elasticity of the insulation, while at the same time not adversely affecting the bonding characteristics of the insulation.

Harvey, Albert R. and Ellertson, John W. [36] claimed insulation for a rocket motor. The insulation includes a cured elastomer and vapor-grown carbon fibers dispersed in the cured elastomer. The cured elastomer is preferably formed from a precursor composition comprising an EPDM terpolymer. Generally, the vapor-grown carbon fibers have an internal graphitized tube surrounded by a sheath of vapor-deposited amorphous carbon.

Guillot, David [37] provided a new method for EPDM-based insulation. This method permits manufacturing EPDM rocket motor insulation in which carbon fibers are dispersed and immobilized in the EPDM polymeric matrix but are not excessively fractured or fragmentized, i.e., broken into smaller fragments, when encountering degrees of shear necessary to homogeneously or otherwise distribute or disperse the carbon fibers in the EPDM polymeric matrix. The method is substantially solvent free and is performed via distributive/reduced shear mixing to distribute the fragile carbon fibers into a rubber matrix without excessive damage. At least about 50% of the elastomer composition introduced into the mixing apparatus is liquid EPDM terpolymer having sufficiently low molecular weight and high diene content to permit dispersion of the carbon fibers in the EPDM without substantial fragmentation of the fibers. Mixing takes place in a kneader capable of rotating a screw having a discontinuous screw thread about the screw axis while superimposing an axially reciprocating stroke to the screw. The kneader imparts low shear distributive mixing of the carbon fibers in the EPDM terpolymer.

Fan, Jun-Ling and Ho, Wen-Dar [38] claimed rocket motor insulation formed of a solid EPDM rubber, liquid EPDM rubber, an inorganic hydrophilic filler, and polyaramide fiber in place of asbestos of the conventional insulation. The hydrophilic filler takes the form of powder. The fine particles of the filler powder are encapsulated with a rubber material. The encapsulated particles of the filler are provided with protection against interference by moisture contents of other ingredients of a compounding recipe, relative humidity of a processing environment, and a shearing stress brought about in the course of preparation. The vulcanized end product of the insulation has an excellent physical property of ablative resistance.

Fan, Jun-Ling [39] disclosed non-asbestos elastomeric insulating materials for solid propellant rocket motors. The insulating materials are composed of EPDM rubber, polyaramide fiber, liquid EPDM rubber, magnesium hydroxide or aluminum hydroxide, silicon dioxide, chlorinated flame retardant compound and zinc hydroxystannate. The char-forming organic fiber is used to substitute for asbestos in traditional insulating materials that are believed to cause serious environmental problems. These fillers in the formulation, which when combined, have a synergistic effect that reduces the ablation rate significantly. Also, use of zinc hydroxystannate to substitute for Sb_2O_3, further reduces density of the insulator and smoke density and smoke toxicity of exhausted gas from the rocket motor.

Fan, Jun-Ling, Tsai, Shr-Hau, Tu Fu-Hua and Tu Yao-Tsai [40] provided a composition of elastomeric insulation. This composition is suitable to be used as a non-asbestos insulation in a solid rocket motor. In this embodiment, an EPDM rubber, a polyaramide fiber, a liquid EPDM rubber and an aluminum hydroxide are used to substitute for the

hazardous asbestos in traditional insulation materials to prevent environmental contamination. With careful formulation control, density of the composition based on this embodiment can be tailored to lower than 1.0 gm/cm^3. Thus enable the insulation to be especially applicable in the areas of lower ablation rate in a solid rocket motor to reduce tare weight of the rocket motor. Moreover, since no chlorinated organic fire retardant compound is used therein, the additional advantage of low smoke density and low smoke toxicity is exhibited.

Gajiwala, Himansu M. and Guillot, David G. [41] provided an insulation composition that comprises at least one nitrile butadiene rubber ("NBR") having an acrylonitrile content that ranges from approximately 26% by weight to approximately 35% by weight and polybenzoxazole ("PBO") fibers. The NBR is a copolymer of acrylonitrile and butadiene and it was presented in the insulation composition in a range of from approximately 45% by weight to approximately 56% by weight of a total weight of the insulation composition. The PBO fibers were presented in a range of from approximately 3% by weight to approximately 10% by weight of a total weight of the insulation composition. A rocket motor including the insulation composition and a method of insulating a rocket motor are also disclosed.

Guillot, David and Harvey, Albert R. [42] claimed a novel and improved EPDM formulation for a solid propellant rocket motor described wherein hexadiene EPDM monomer components are replaced by alkylidene norbornene components and with appropriate adjustment of curing and other additives functionally-required rheological and physical characteristics are achieved with the desired compatibility with any one of a

plurality of solid filler materials, e.g. powder silica, carbon fibers or aramid fibers, and with appropriate adhesion and extended storage or shelf life characteristics.

Gajiwala, Himansu M. [43] provided an insulation material comprising a low-density EPDM polymer, at least one flame-retardant, and organic filler. The insulation material is used in an insulation layer of a rocket motor. The organic filler is polymeric, organic filler such as polyvinyl chloride. A rocket motor comprising an insulation material is also disclosed. The insulation material comprises a low-density EPDM polymer, at least one flame-retardant, and polymeric, organic filler and is applied between an inner surface of a case of the rocket motor and a propellant. A method of insulating a rocket motor is also disclosed.

Table (1.4) summarizes the different insulation compositions that are currently used as solid rocket motor insulation.

Composition		advantages	disadvantages
Binder	**Filler**		
EPDM	Heavy metal halides + calcium hydroxide + magnesium hydroxide	- Asbestos free	- High ablation rates
CTPB	Asbestos	- Perfect bonding to case and propellant	- Using Asbestos
NBR	Aramid staple	- Asbestos free - Good thermal insulation	- High ablation rates
NBR	Cotton flock + sisal	- Low ablation rates - Asbestos free	- Not completely uniform master batch (matrix rich areas)
EPDM + Polyisoprene	Aramid R	- Low density - Good thermal insulation	- High ablation rates
SBR + natural rubber	Polybenzimidazole	- Low density - Good thermal insulation	- High ablation rates
polyester	Glass fibers + alumina	- Low ablation rates	- Low strain capability - High densities
EPDM + polyamide	Ammonium polyphosphate + chopped carbon fibers	- Low ablation rates	- High case temperature - High densities
EPDM	Ammonium sulfate + antimony oxide + aramid staple	- Better tear resistance - Better bond strength	- High ablation rates
Phenolic + N-rubber	Glass fabric + aluminatrihydrate	- Low ablation rates	- Low strain capability - High densities
NBR	Hydrophobic Silica	- Better tear resistance - Better bond strength	- High electrical resistance
EPDM (hexadiene)	Chopped carbon fibers	- Low ablation rates	- High case temperatures - High densities
EPDM	Hydrophilic Silica	- Low ablation rates	- High affinity to water - High electrical resistance
NBR	Polybenzoxazole	- Low density - Good thermal insulation	- High ablation rates
EPDM (Alkylidene norbornene instead of hexadiene))	Carbon fibers + silica	- Low ablation rates	- High case temperatures - High densities
EPDM	Polyvinyl Chloride	- Low density - Good thermal insulation	- High ablation rates

Table (1.4) Current used insulators

1.3 Justification of the work

The currently used insulators have deficiencies in at least one of the primary requirements of the insulator material. For reinforced thermosets, there are cracks and/or blisters as a result of the rapid temperature and pressure fluctuations experienced during combustion. This is because the insulation based on these materials has very low elongation, in addition to relatively high density as shown in table (1.1). Although phenolic-based insulation are much more erosion resistant than many insulators which is due to the strong char formed during decomposition, it does not exhibit high strain capability and cannot survive high aeroheating loads.

For elastomers filled with carbon black the ablation resistance of the whole insulation is inadequate to withstand the high stresses and erosion rates resulting from the combustion gases. In addition the International Agency for Research on Cancer (IARC) evaluates that Carbon black is possibly carcinogenic to humans.

Also for the insulators based on elastomers filled with asbestos the mechanical properties and the ablation resistance of the whole insulation are adequate to withstand the high stresses and erosion rates resulting from the combustion gases. However asbestos are banned from use due to its health hazards.

For elastomers filled with silica the ablation resistance of the whole insulation is inadequate to withstand the high stresses and erosion rates resulting from the combustion gases. Also current silica-filled elastomeric insulation materials are electrically insulating, exhibiting high volume resistivities, and, hence, a poor ability to dissipate static charge. The ability to dissipate static charge is considered to be an important quality for the thermal insulator. An insulator possessing this quality is able to bleed off or dissipate

charges that build up on the insulator surface. An insulator having a high electrical resistivity does not dissipate static charge timely, thus creating a potential for static charge to build up to a dangerous level. When the electric field increases to the point that breakdown of the air occurs or a path to ground for the static charge is inadvertently provided, the discharge can be dangerous. Physical harm to personnel and flash fires are possible. Conventional silica-filled EPDM insulation is electrically insulating, having resistivities ranging from 1×10^{14} to 1×10^{16} Ohm · cm. An insulator is considered to be able to dissipate static charge if its volume resistivity is in the range of from 1×10^{5} to 1×10^{12} Ohm · cm. Asbestos-filled NBR, which is one of the few currently used insulation materials that is considered to be able to dissipate static charge, has a volume resistivity in the range of 1×10^{11} to 1×10^{12} Ohm · cm. However, the use of asbestos in rocket motors has lost favor due to reported health dangers associated with asbestos. [46].

Another approach to address the problem is the use of an elastomeric matrix such as Ethylene Propylene Diene Monomer (EPDM) reinforced with chopped carbon fibers. This composite material has two phases. The rubber (EPDM) provides flexibility to conform and to bond to the surface of the container. It is also light weight. However the EPDM has low decomposition point and it can not stand temperature above 496 $^{\circ}$C. In order to compensate for this deficiency, chopped carbon fibers have been used. Chopped carbon fibers have high temperature resistance (melting point of carbon fibers is 3425 $^{\circ}$C) and as such it can withstand high temperature. The problem with this approach is that carbon fibers have high coefficient of thermal conductivity (6.4 W m^{-1} K^{-1}). As such heat is conducted quickly from the inside of the container to the steel structural part. Once the steel structural part reaches its critical temperature, it will lose its usefulness.

Therefore any replacement insulation should exhibit at least comparable temperature resistant and ablation characteristics in addition to physical, mechanical and thermal properties at least equivalent to that of current insulators, yet should not otherwise significantly alter the formulation techniques employed for the production of such rocket motor thermal insulation. Additionally, due to the large and growing quantities of solid propellant rocket motor insulation required by the industry, any such replacement candidate should be abundantly available now and into the foreseeable future.

One well known potential point of failure is the appearance of voids or cracks in the insulation which could lead to the penetration of the rocket motor casing itself. The resultant dispersion of hot gases may not only lead to destruction of the motor generally or can at least lead to its being thrown of its intended course or trajectory with several unhappy results. In such events, either the vehicle itself will self-destruct, or will be intentionally destroyed, or the satellite will be launched into a useless orbit.

Therefore, one of the most difficult tasks in the solid propellant rocket motor industry is the development of a suitable, acceptable insulation composition that will meet and pass a large number of test criteria to lead to its acceptability.

1.3.1 Requirements of the new material

The insulation material at least must have a flame retardant agent to increase its resistance to propellant combustion flame and an example of already used flame retardant agents is chlorinated compounds such as dechlorane products and phosphate compounds such as ammonium polyphosphate products.

The insulation material at least must have a crosslinking agent to crosslink the elastomer during curing. Examples of already used crosslinking agents are sulphur and organic peroxides.

The processing of insulation starting from the ingredient materials mainly consists of [44-45]:

(a) Mixing of the ingredients (the filler, the flame retardant agent and the crosslinking agent) with the elastomeric matrix to obtain a homogenous mixture as a master batch,

(b) Molding of the master batch inside a suitable mold,

(c) Curing the mixture under a press using measured and calculated pressure and temperature,

(d) Demold the insulation product for future assembly inside the rocket motor case.

An extensive experimental and theoretical work in the development and characterization of asbestos-free rubbers for use as rocket motor insulators has been performed. The insulation is based on chopped carbon fiber and/or aramid fiber in the pulp form as filler for Ethylene Propylene Diene Monomer (EPDM). The aim of the research is to provide an understanding of the mechanism, the principle, and the process of making polymeric thermal insulants and to produce thermal insulants based on polymers with different fillers having different compositions which are capable of working under extreme thermal conditions 2760 °C (5000 °F). This is through an investigation on the processing, installation and testing of physical, mechanical, thermal and ablative properties of these materials.

The thesis includes

1- The study of the characteristics of different fillers such as chopped carbon fiber and Kevlar pulp which may succeed as filler with polymers to produce a thermal insulant. These characteristics include physical, mechanical, thermal and ablative properties.

2- The development of a mathematical model for the prediction of thermal conduction of multiphase thermal insulation composite material.

3- The development of a suitable optimization technique to reach the best parameters of the selected material (polymers & fillers).

4- The development of a new thermal insulant based on EPDM rubber for thermal insulation. These should show improvement over current insulators.

Research methods on different formulations of the new fillers (chopped carbon fiber or Kevlar pulp and their hybrids) with EPDM polymer were prepared to investigate the physical, mechanical, thermal and ablative properties to choose a new insulant with the best properties.

In the proposed work the development and characterization of hybrid reinforcements for elastomers where the insufficient thermal properties (thermal conductivity, specific heat capacity, thermal diffusivity) of CCF filled elastomers is complemented by the outstanding new insulator (in 2005) of Dupont Kevlar pulp (IF 453) (thermal conductivity 0.04 W/m.k, Specific heat capacity 1420 J/kg.K).

The characteristics of CCF and Kevlar pulp, using this hybrid mixture (CCF, Kevlar pulp) provides outstanding performance in ablation resistance and decomposition temperatures.

Chapter 2

Experimental Techniques

2.1 Materials

2.1.1 EPDM

EPDM is a hydrocarbon rubber [47-53] designed for molded and extruded applications; it is ideally suited for general purpose moldings. The combination of low viscosity and low crystallinity allows for good balance of process ability and product performance. There are many EPDM products depending on the relative amounts of ethylene, propylene and diene content. The most suitable for rocket motor applications is EPDM IP 4640 (chemical formula is shown in Fig (2.1)) which is available as a solid rubbery form. Typical properties are shown in Table (2.1).

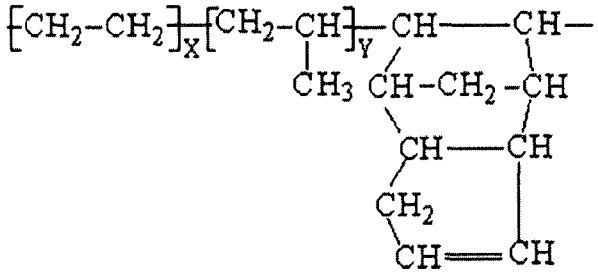

Fig (2.1) EPDM (Nordel ip 4640) chemical structure

With this type of EPDM (rubbery form) it is difficult to mix and disperse well the fragile chopped carbon fiber so the liquid form of EPDM is required (TRILENE products) [54].

Property	units	Nordel ip 4640
Density	g/cm^3	0.86
Diene content	%	5
Ethylene/propylene ratio	By weight	55/40
Mooney Viscosity at 125 °C	-	40
Ash content	%	≤ 0.1
Volatiles content	%	≤ 0.5
Color	-	Pale yellow
Heat capacity	J/kg.K	2177.1
Thermal conductivity	W/m.K	0.3559

Table (2.1): Typical properties of EPDM (Nordel ip 4640)

TRILENE liquid polymers are a family of viscous, low molecular weight ethylene-propylene diene terpolymers developed by Uniroyal Chemical Company, Inc. They are polymerized randomly to produce liquid elastomers with stable, saturated hydrocarbon backbones. TRILENE may be used alone or in combination with solid EPDMs to allow curing of a conventional rubber along with the processing versatility of a liquid. TRILENE liquid polymers can be used in a wide variety of applications. The lower viscosity of TRILENE, compared with traditional EPDM polymers, provides advantages in the areas of processing and product preparation. TRILENE polymers offer a combination of rapid cure rate and good aging resistance not previously available with liquid hydrocarbon elastomers. They can be cross linked using peroxide or sulfur. Also, they offer superior thermal stability and UV resistance. A number of TRILENE polymer grades are available to allow customers latitude in choosing the balance of cure rate and

aging resistance which best fits their needs. The most suitable type for rocket motor insulations is TRILENE 67 which has the properties shown in Table (2.2) and its chemical structure has shown in Fig (2.2).

Property	Units	Trilene 67
Density	g/cm^3	0.86
Diene content	%	9.5
Ethylene/propylene ratio	By weight	46/54
Molecular weight	-	42000
Viscosity at 60 °C	cps	$0.9x\ 10^6$
Viscosity at 100 °C	cps	$0.128x\ 10^6$
Ash content	%	≤ 0.1
Volatiles content	%	≤ 0.5
Color	-	Pale yellow
Heat capacity	J/kg.k	2177.1
Thermal conductivity	w/m.k	0.3559

Table (2.2): Typical properties of EPDM (TRILENE 67)

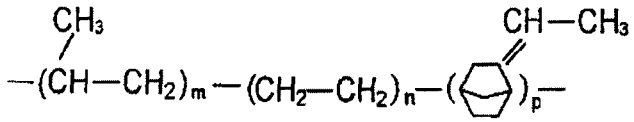

Fig (2.2): Liquid EPDM (TRILENE 67) chemical structure

A photo of TRILENE 67 in a bag is shown in Fig (2.3)

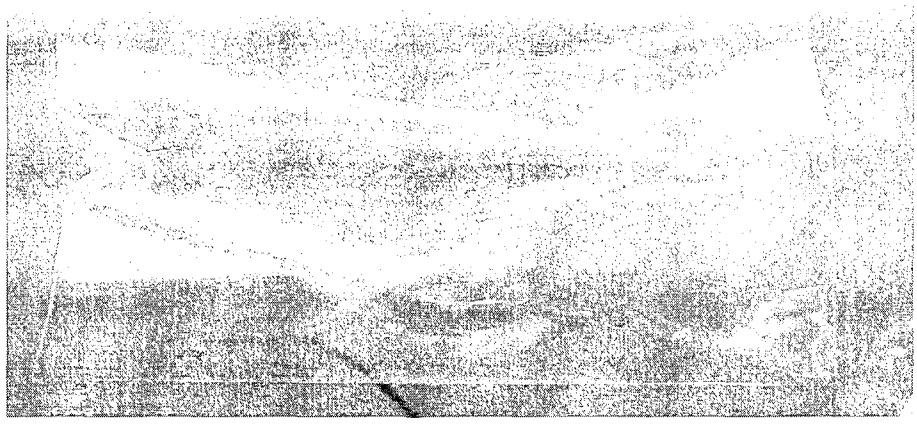

Fig (2.3) TRILENE 67 in a bag

The process of forming a 3 – D structure from the linear EPDM is called cross linking [55-57]. In general, cross linking is a process of forming a three-dimensional network structure from a linear polymer by a chemical or physical method. The cross linking of EPDM is usually done by chemical methods where a cross linking reaction can proceed via a radical pathway by using peroxides. A wide variety of peroxides can be used to crosslink most types of elastomers. In general, the diacyl peroxides are useful for the cross linking of silicone elastomers, while the ketal and diakyl peroxides are used primarily for diene and ethylene-propylene elastomers. Compared with sulfur vulcanization, cross linking by peroxides is a relatively simple process.

The advantages of peroxide cross linking are:

1- Short cross linking time

2- Simple compounding

3- Good heat-aging resistance

4- No mold contamination

5- Transparent rubbers possible

For EPDM cross linking diakyl peroxides are suitable cross linking agents. The peroxide cross linking mechanism is shown in Scheme 1.

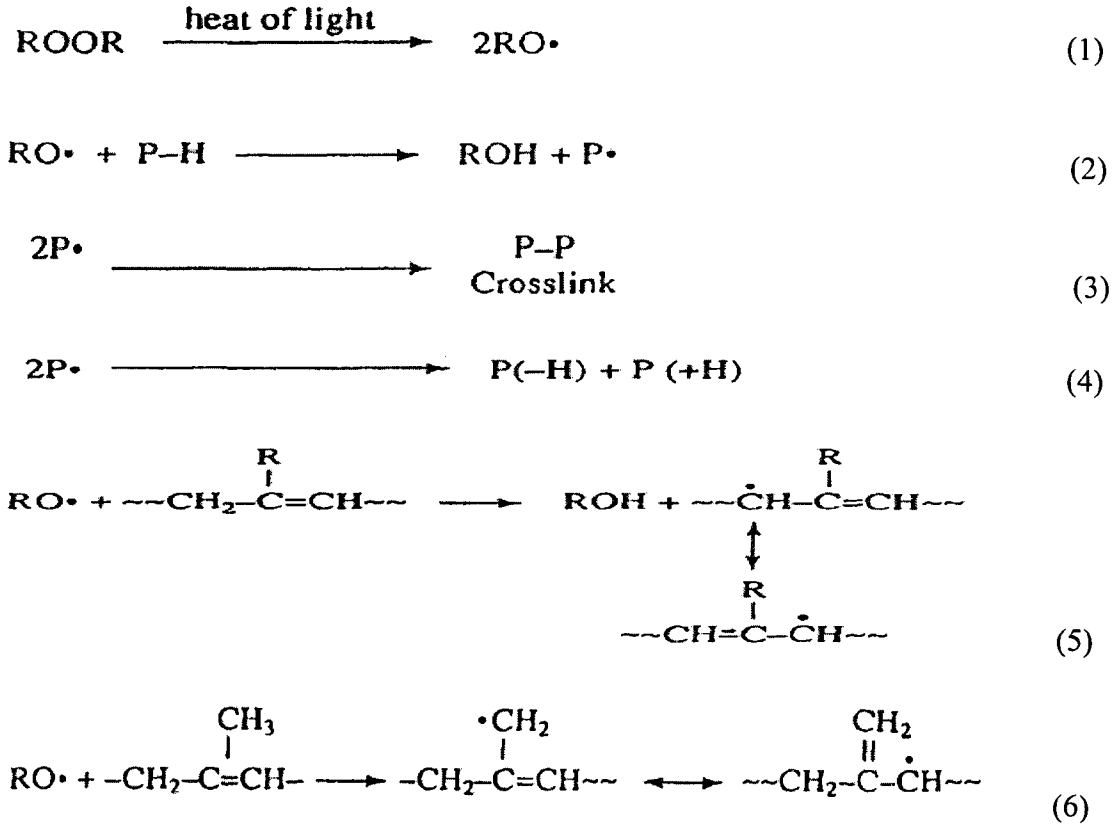

Scheme (2.1) Peroxide cross linking mechanism. P-H = saturated of unsaturated elastomer.

The cross linking reactions involve the homolytic decomposition of the peroxide to produce alkoxy radicals [eqn (1)] followed by hydrogen-atom abstraction [eqn (2)]. Studies with model compounds indicate that the hydrocarbon radicals predominantly undergo coupling [eqn (3)] rather than disproportionation [eqn (4)]. The coupling reaction forms crosslinks between polymer chains. For polydiene elastomers, experimental evidence indicates that the primary radical formed by peroxide decomposition abstracts a hydrogen atom from a carbon alpha to the double bond [eqn (5)]. In natural rubber, the methyl group is also reactive towards hydrogen-atom

abstraction [eqn (6)]. There are several important limitations to peroxide cross linking of rubbers. Antioxidants can react with peroxide-generated radicals; this can result in reduced cross linking efficiency for the peroxide cross linking reaction and in the destruction of the antioxidants.

The chemical name of the peroxide cross linking agent used to crosslink EPDM is 2, 5-dimethyl-2,5-di (tert-butylperoxy) hexane on an inert filler and it is supplied as white powder.

2.1.2 Chopped carbon fiber

Carbon fibers, after a 40 year period of development and use in specialized applications, are now on the brink of broad commercialization. Their use is growing rapidly, fueled by significant price reductions during the 1990s and increasing availability. Changes in the performance / price ratio have resulted in the increased penetration of composites into applications formerly held by metals and has enabled their use in other applications previously not possible with existing materials. Additionally, market conditions increasingly favor designs for commercial products that are lighter, stronger, faster, and more fuel efficient—designs that are possible with carbon fibers. No longer relegated to aerospace, carbon fiber composites are now being adopted in fields such as automotive and civil infrastructure.

The manufacturing of carbon fibers depends on the type of precursor used. Precursor sources used, in order of volume, are PAN, pitch, and rayon. Although the specific processing details for each precursor is different, all follow a basic sequence involving spinning, stabilization, carbonization, and application of a finish or sizing to facilitate handling, as shown in Fig (2.4).

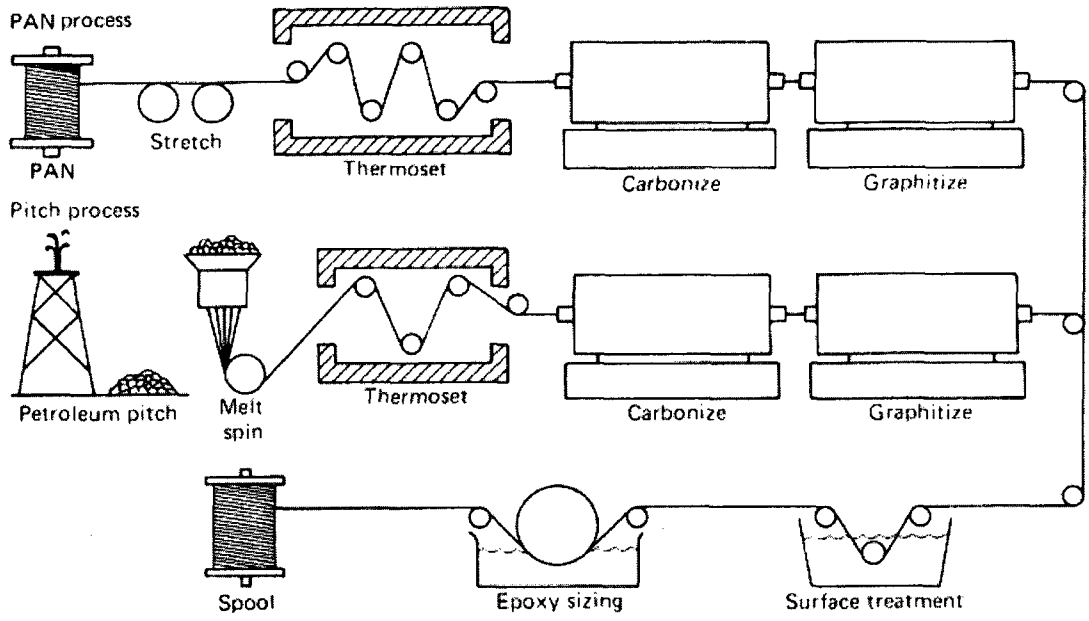

Fig (2.4) The processing sequence for polyacrylonitrile (PAN) and mesophase-pitch-based precursor fibers [58]

The majority of all carbon fibers used today are made from PAN precursor, which is a form of acrylic fiber. Precursor manufacture is accomplished by spinning the PAN polymer into filaments using variants of standard textile fiber manufacturing processes. The PAN fibers are white in color, with a density of approximately 1.17 g/cm^3 and a molecular structure comprised of oriented, long chain molecules. Stabilization involves stretching and heating the PAN fibers to approximately 200 to 300 °C in an oxygen-containing atmosphere to further orient and then crosslink the molecules, such that they can survive higher-temperature pyrolysis without decomposing. Stretching after spinning and during stabilization helps develop the highly oriented molecular structure that allows development of a high tensile modulus and improved tensile strength upon subsequent heat treatment. Carbonization of standard and intermediate modulus fiber typically involves pyrolyzing the fibers to temperatures ranging from 1000 to 1500°C in an inert

atmosphere, typically to 95% carbon content. An additional high heat treatment step is included just after carbonization for some very high-modulus fibers.

During carbonization, the fibers shrink in diameter and lose approximately 50% in weight. Restraint on longitudinal shrinkage helps develop additional molecular orientation, further increasing mechanical properties. After carbonization, the fibers may be run through a surface treatment step designed to clean and attach functional groups to the fiber surface, which increases bond strength with matrix resins. Most manufacturers use an electrolytic oxidation process that creates carboxyl, carbonyl, and hydroxyl groups on the surface for enhanced bonding. A sizing or finish is then applied to minimize handling damage during spooling and enhance bonding with matrix resins. The fiber is then spooled.

A general carbon fiber is a long, thin strand of material about 0.005-0.010 mm in diameter and composed mostly of carbon atoms. The carbon atoms are bonded together in microscopic crystals that are more or less aligned parallel to the long axis of the fiber. The crystal alignment makes the fiber incredibly strong for its size. Several thousand carbon fibers are twisted together to form a yarn, which may be used by itself or woven into a fabric.

Chopped carbon fibers are originally long regular carbon fibers yarns cut to small length (6-50 mm). These are generally used for reinforcement in thermoplastic molding compounds requiring high strength and modulus, low density, electrical conductivity, dimensional stability, low thermal expansion and excellent friction/wear properties. They do not melt or soften with heat, allowing them to be used in such high temperature applications as rocket nozzles and aircraft brakes. In fact, their strength actually increases

with temperature in non-oxidizing atmospheres. These unique properties are the result of the fiber microstructure, in both the axial and transverse directions. The selected chopped carbon fiber as a candidate for reinforcement of elastomers as a rocket motor insulation is a product of Zoltek Corporation under the trade name Panex 33 and have a properties shown in Table (2.3). [58-62]

Panex 33 has superior properties due to the additional heat treatment of the fibers by doing additional carbonization where the carbon content increases to 95.5%. During compounding chopped carbon fibers distribute easily improving process and product performance. Fig (2.5) shows chopped carbon fibers in a bag.

Property	**Units**	**Chopped carbon fiber (panex 33)**
Tensile Strength	MPa	3800
Tensile Modulus	GPa	228
Electrical Resistivety	ohm-cm	0.00172
Density	g/cm^3	1.81
Fiber Diameter	microns	7.2
Carbon Content	%	95.5
Fiber length	mm	6
Specific heat	J / kg.K	660
Thermal conductivity	W/ m.K	6.4
Coeff. Of thermal expansion	$x\ 10^{-6}$ /°C	-0.75
Decomposition temp.	°C	3445

Table (2.3) Typical properties of chopped carbon fibers (Panex 33)

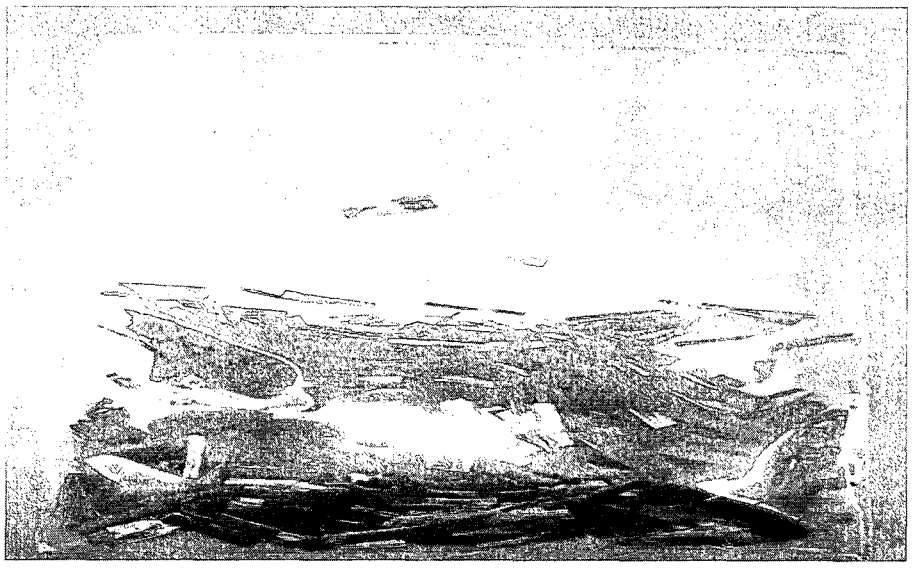

Fig (2.5) Chopped carbon fibers in a bag

2.1.3 Aramid fiber (Kevlar pulp)

In the mid- 1960s, nylon and polyester represented the state of the art in man-made fibers. However, to achieve maximum tenacity (break strength) and initial modulus, the polymer molecules had to be in extended chain configuration and almost perfect crystaline packing. With flexible-chain polymers, such as nylon or polyester, this could be accomplished only by mechanically drawing the fiber after melt spinning. This required chain disentanglement and orientation in the solid phase, so tenacity and modulus levels were far from the theoretically possible values.

In 1965, scientists at Du Pont discovered a new method of producing an almost perfect polymer chain extension. The polymer poly-p-benzamide was found to form liquid crystalline solutions due to the simple repetitiveness of its molecular backbone. The key structural requirement for the backbone is the key para orientation on the benzene ring, which allows the formation of rod-like molecular structures. These developments led the company to the current formulation for kevlar.

To illustrate the difference between liquid crystalline polymers and flexible, "melt" polymers, consider what happens when rod – like polymer molecules are dissolved, as opposed to molecules with flexible chains. With flexible chain polymers, random coil configuration is obtained in solution, and even increasing the polymer concentration cannot generate a higher degree of order. In contrast, with rigid polymers, as the concentration increases, the rods begin to associate in parallel alignment. Randomly oriented domains of internally highly oriented polymer chains then develop as shown in fig (2.6), (2.7).

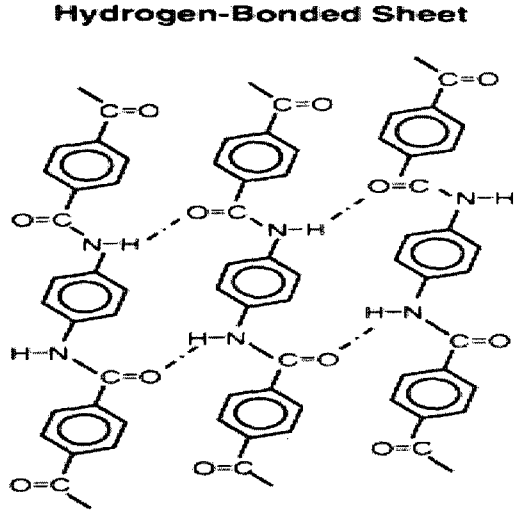

Fig(2.6) Rod-like fiber structure by the radial stacking of hydrogen- bonded sheets

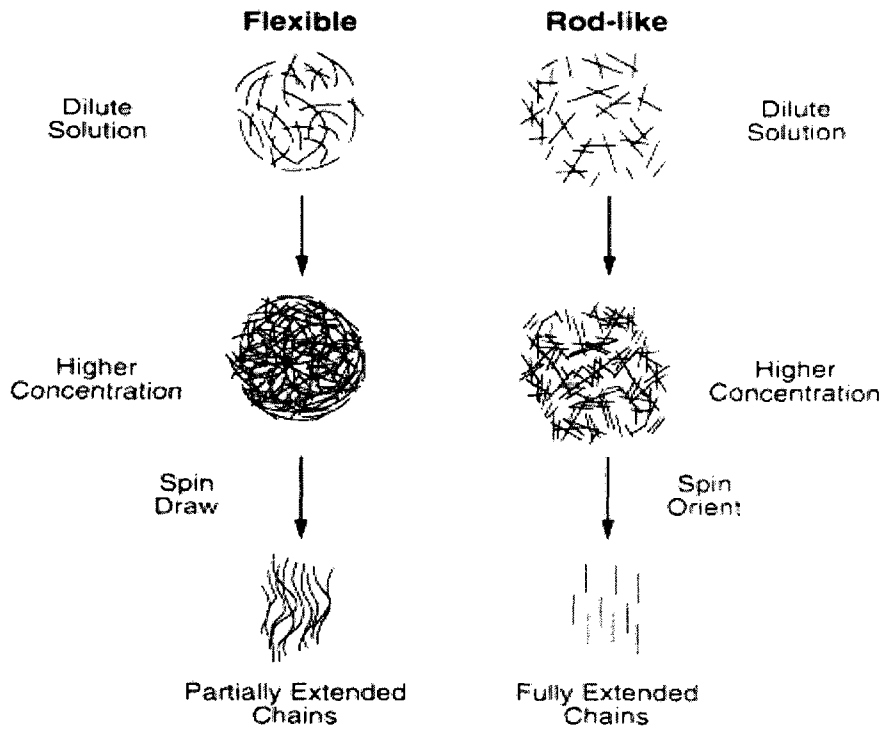

Fig (2.7) Differences in behavior during spinning between flexible and rigid polymers

Liquid crystalline polymer solutions display a unique behavior under shear. This unique aspect opened up new dimensions in fiber manufacturing and processing. Under shear forces, as the solutions pass through a spinneret (orifice), the randomly oriented domains become fully oriented in the direction of the shear and emerge with near perfect molecular orientation. The molecular structure is almost entirely preserved in the as – spun filament structure due to very slow relaxation of the shear- induced orientation. This process is a novel, low – energy way to highly orient polymer molecules and to achieve very strong fibers. Du Pont utilized this technology to develop a fiber of poly-para-phenylene terephthalamide, which was introduced as high strength KEVLAR aramid fiber consisting of long molecular chains. The chains are highly oriented with strong

interchain bonding, which results in a unique combination of properties such as high modulus, high tensile strength at low weight, low electrical conductivity, high chemical resistance, low thermal shrinkage, high toughness, excellent dimensional stability and excellent flame resistance.

KEVLAR is an organic fiber in the aromatic polyamide family. The unique properties and the distinct chemical composition of wholly aromatic polyamides (aramids) distinguish them, and especially KEVLAR from other commercial, manmade fibers properties. KEVLAR fibers have long been used in a wide variety of demanding applications because of an impressive list of physical and thermal properties. It combines high tensile strength (5 times that of steel on an equal weight basis), high modulus, and low elongation to break with excellent wear properties, temperature stability and chemical resistance. It was developed for demanding industrial and advanced aerospace technology applications. It has a wide range of properties and forms; the most suitable and combatable with elastomers is the pulp form. A high grade of Kevlar pulp having very low thermal conductivity (0.04 W/m.K) is developed by DEPONT in 2005 under the trade name KEVLAR PULP IF 453.

Fig (2.8) shows a photograph of KEVLAR PULP IF 453 and Fig (2.9) shows a photomicrograph of KEVLAR PULP IF 453 [63-64].

KEVLAR pulp is a highly fibrillated form of fiber which can be dispersed in different matrix systems, the fibrillation results in high surface area (7 – 10 m^2/g).

Fig (2.8): Photograph of Kevlar pulp ((10 X) [64]

Fig (2.9): Photomicrograph of Kevlar pulp (500X) [64]

It is also non brittle, so standard mixing and dispersion equipment will not affect the fiber size. KEVLAR pulp enhances the performance of elastomers, thermoplastic and thermoset resins especially where high temperature performance is required. The selected Kevlar pulp as a candidate for reinforcement of elastomers for rocket motor insulation is a product of Dupont under the trade name Kevlar pulp IF 453 and has properties shown in Table (2.4) [65-66].

Property	Units	Aramid (Kevlar pulp)
Tensile Strength	MPa	3600
Tensile Modulus	GPa	83
Elongation at break	%	3.6
Density	g/cm^3	1.44
Moisture level	%	7
Specific heat	J / kg.K	1420
Thermal conductivity	W/ m.K	0.04
Decomposition temp.	°C	427-482
Specific surface area	m^2/g	7-10

Table (2.4): Typical properties of Kevlar pulp (IF 453)

A photo of Kevlar pulp IF 453 in a bag is shown in Fig (2.10).

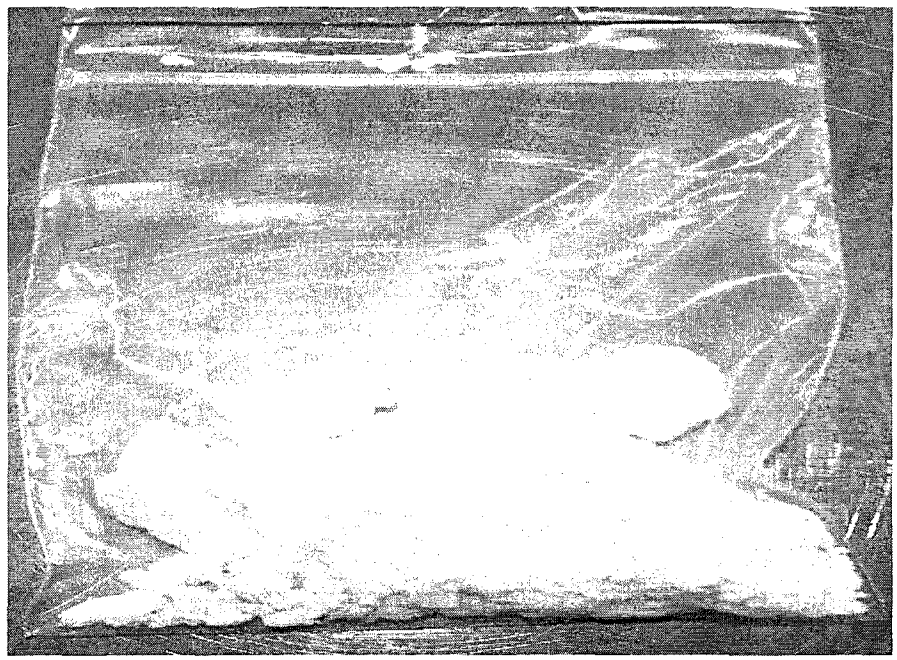

Fig (2.10) Kevlar pulp IF 453 in a bag

2.1.4 Peroxide cross linking agent

Peroxide cross linking agents are mainly used for the vulcanization or cross-linking of most elastomers and polyolefins. Peroxide curing is an alternative to sulfur vulcanization that offers superior heat-aged performance. In addition to final properties such as dynamic flexibility, tear resistance, and tensile strength are comparable or superior to sulfur-cured systems with much better heat-aged performance. It also has the added benefit of significantly improving adhesion to metal and fiber reinforcing materials when vulcanized. The chemical name of the peroxide cross linking agent used to crosslink EPDM is 2,5-dimethyl-2,5-di (tert-butylperoxy) hexane on an inert filler and it is supplied as white powder. A photo of PCA is shown in Fig (2.11) [67].

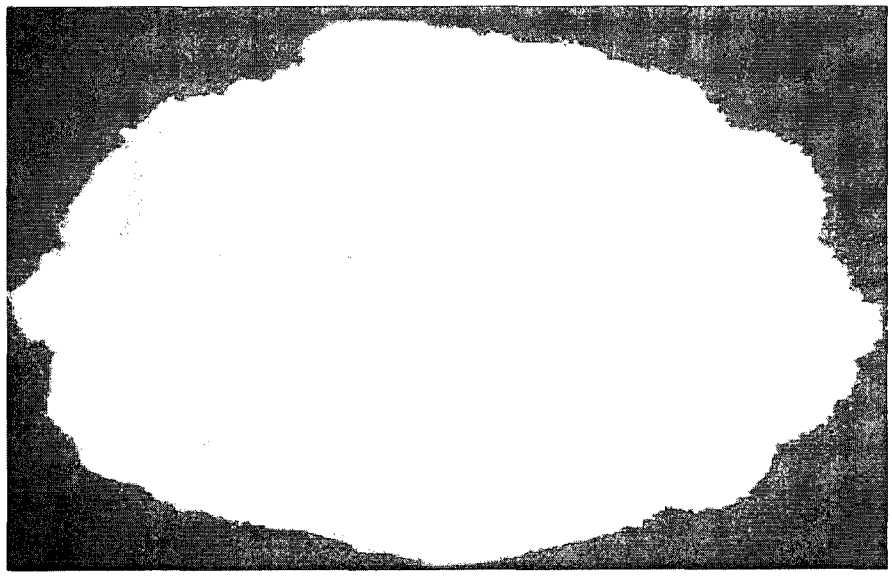

Fig (2.11) 2,5-dimethyl-2,5-di (tert-butylperoxy) hexane (PCA)

2.1.5 Ammonium polyphosphate flame retardant agent

Ammonium polyphosphate is an inorganic salt of polyphosphoris acid and ammonia containing both chains and possibly branching. Its chemical formula is $[NH_4\ PO_3]_n$ showing that each monomer consists of an orthophosphate radical of a phosphorus atom

with three oxygens and one negative charge neutralized by an ammonium anion leaving two bonds free to polymerize. In the branched cases some monomers are missing the ammonium anion and instead link to three other monomers. The chemical structure of AP is shown in fig (2.12) [68].

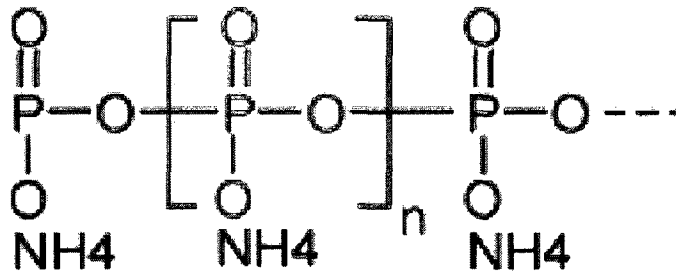

Fig (2.12) AP chemical structure

The properties of AP depend on the number of monomers in each molecule and to a degree on how often it branches. Shorter chains are more soluble and less thermally stable. AP is a stable, non-volatile compound. It starts to decompose at temperatures above 300 °C to polyphosphoric acid and ammonia. It acts as a flame retardant by a chemical effect in the condensed phase called "Intumescence" as shown in Fig (2.13).

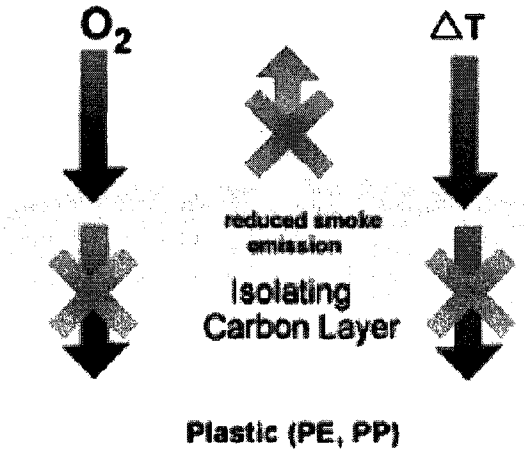

Fig (2.13) AP flame retardant mechanism of action

When plastic or other materials which contain AP are exposed to an accidental fire or heat, the flame retardant starts to decompose, commonly into polymeric phosphoric acid and ammonia. The polyphosphoric acid reacts with hydroxyl to form a non stable phosphate ester. In the next step the dehydration of the phosphate ester follows. Carbon foam is built up on the surface against the heat source (charring). The carbon barrier acts as an insulation layer, preventing further decomposition of the material. The chemical mechanism of action is shown in fig (2.14).

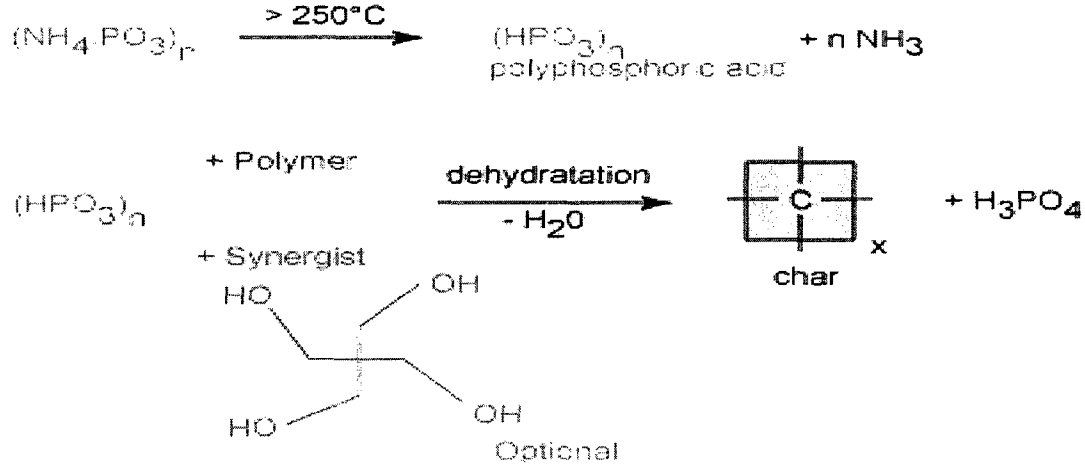

Fig (2.14) AP flame retardant chemical mechanism of action

In order to obtain optimum material performances, AP needs to:

- Be dispersed properly into the polymer

- Be compatible with the polymer matrix

- Be insoluble in water for better weathering performances

Moreover, to facilitate the processing of formulations, AP needs to have:

- Good flow ability

- Good thermal stability to provide a larger processing window.

To fulfill all these requirements PHOS-CHEK has developed finer and coated AP grades which provide significant improvements in terms of material process ability and performances. These finer and coated grades of AP have good properties such as low hydrolysis, low solubility in water, low acidity, better compatibility with polymers, better thermal stability, easier processing and good abrasion over the uncoated grades as shown in fig (2.15).

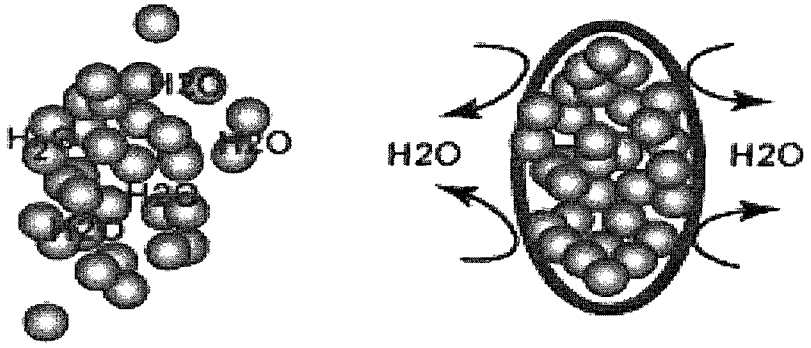

Uncoated AP **Coated AP**

Fig (2.15) Coated and uncoated AP flame retardant agent

The AP flame retardant agent used in the thermal insulation compositions is a product of PHOS-CHEK under trade name PHOS-CHEK P – 30. A photo of PHOS-CHEK P – 30 is shown in fig (2.16)

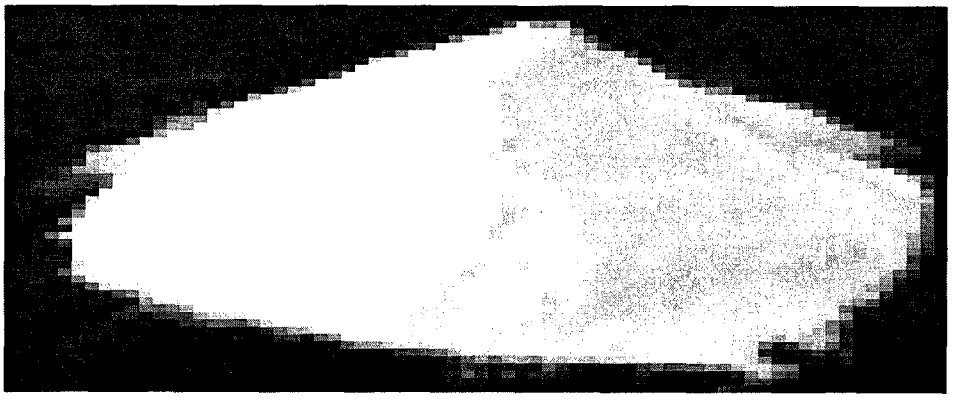

Fig (2.16) PHOS- CHEK P – 30

2.1.6 Teflon release film

The type of Teflon release film used in this thesis is Teflon coated glass fabric. The physical properties of the Teflon coated glass fabric combine good temperature resistance (from -190°C up to + 260°C, for short time up to + 300°C) and excellent glue repellence; almost non-flammable, resistant to most chemicals, smooth surface, almost no water absorption, little thermo extension and impermeable. The thickness of the film used is 0.075 mm and the standard roll width is 94 cm. The film is used without adhesive to provide the high degree of repellence from the insulation material after curing. A Teflon coated glass fabric is shown in Fig (2.17).

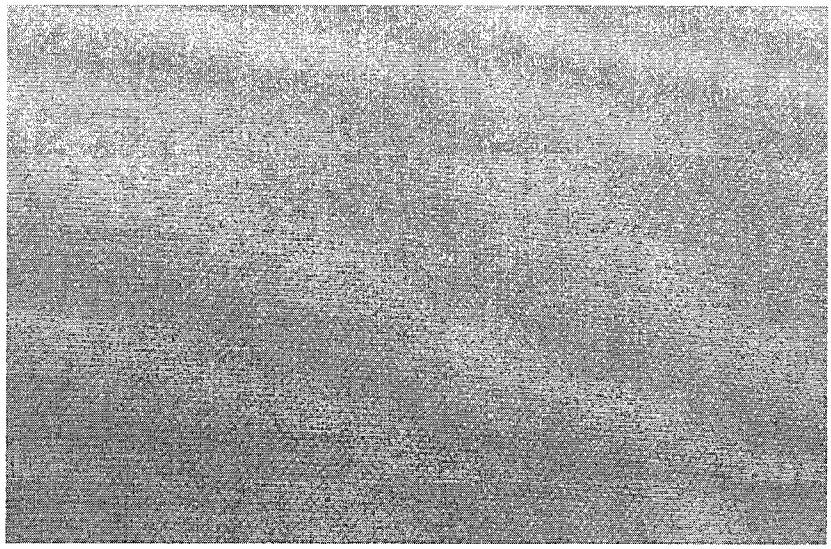

Fig (2.17) Teflon coated glass fabric with thickness 0.075 mm

Teflon-based glass fabric are constructed with high-quality and backing materials to deliver superior performance. Additional properties to those mentioned above are:

- Optimal release
- Low friction
- Electrical insulation

• Dimensional stability

• Non-stick surface

• High tensile strength

The Teflon based glass fabric is used as a release layer to repel insulation samples from the mold after curing

2.1.7 High temperature adhesive

The high temperature adhesive used in the thesis is EPON 828 and EP cure. EPON 828 resin is an undiluted clear difunctional bisphenol A/epichlorohydrin derived liquid epoxy resin. When cross-linked or hardened with appropriate curing agents, very good mechanical, adhesive, dielectric and chemical resistance properties are obtained. Because of this versatility, EPON Resin 828 has become a standard epoxy resin used in formulation, fabrication and fusion technology.

One of the most widely recognized properties of cured EPON Resin 828 is strong adhesion to a broad range of substrates. Such systems exhibit shear strength of up to 6,000 psi (41 MPa). One factor which contributes to this property is the low shrinkage shown by these systems during cure. Compared to other polymers, epoxy resins have low internal stresses resulting in strong and durable finished products.

To formulate the adhesive for this work we should have the primary components of the resin formula. These are the epoxy resin and the hardener or curing agent. To prepare the adhesive one part of the hardner (EP cure) is added to two parts of resin (EPON 828).

This adhesive is used to glue insulation samples to standard steel plates for ablation test and it needs 18 hours at room temperature to full cure.

2.2 Instruments and machines

2.2.1 Furnace

A regular furnace is used to heat the EPDM from 20 °C to 80 °C where its viscosity decreased from 1.7x 10^6 cps to 0.15 x 10^6 cps. This is essential to allow the material to flow into the C. W. Bra bender mixing chamber easily where a uniform dispersion of the fiber and the reinforcing filler inside EPDM can be achieved with very low shear stress to keep the reinforcements with complete dimensions without fragmentization.

2.2.2 C.W. Bra bender mixer

The C. W. Bra bender mixer is a 3-Piece Mixer that provides the latest method for predicting the processability of polymers. The mixer is shown in Fig (2.18) [69].

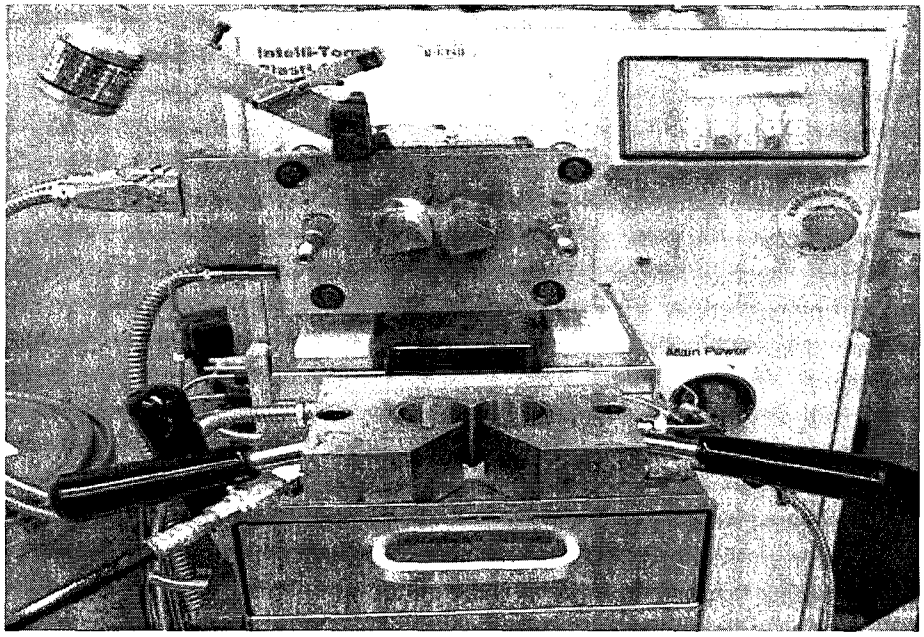

Fig (2.18) C. W. Bra bender mixer

It is classified as 3 piece mixer where the mixing chamber mainly consists of three parts. Also it considered to be the most universal mixer/measuring head with a capacity of 60 to 120 ml.

The machine was originally equipped with two Banbury blades. Banbury Blades are designed to duplicate the mixing action of a Banbury Mixer with a medium shear-rate mixing action ideal for mixing elastomeric materials. But this medium shear stress provided by Banbury blades can fragmentize chopped carbon fiber into small fragments negating its reinforcing characteristics. Sigma Blades are mixer blades providing very low shear stress during mixing which creates a tumbling and kneading force within the mixer without imposing a strong compressing force. This results in attaining uniform dispersion of the fiber and the reinforcing filler inside EPDM without breaking of the reinforcements. Sigma blades are removable blades made from 304 Stainless Steel. The zone in the center of the mixer between the two blades is characterized by excellent distributive and dispersive mixing ability with high shear rates.

2.2.3 Wabash press

A Wabash press is a hydraulic press specifically designed to mold test samples of materials. It has an adjustable clamp force of 1 to 30 tons. Fully guided, heated and insulated platens are 19" x 19" with operating temperature to 500° C. It also has integral hydraulic system, fully programmable controls and fully guarded clamp area with interlocked operator gate. The Wabash press is shown in Fig (2.19).

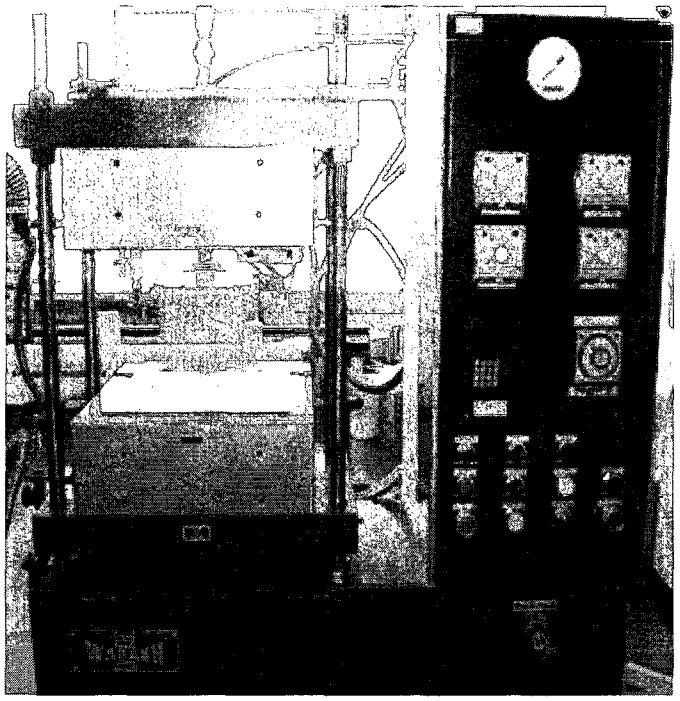

Fig (2.19) Wabash press

2.2.4 MTS machine

The MTS Load Frame is suitable for tensile, compressive and flexural loading. The upper crosshead can be positioned to accommodate a specific specimen by loosening the bolts, clamping it to the columns to raise or lower it to the required position. After the desired position is reached, the bolts must be re-tightened. This positioning is usually a pre-test setup, done ahead of time. The load cell or transducer and a grip (tension test) are attached to the crosshead. A grip is also attached to the movable piston. The grips are opened or closed using the valve controls. The MTS Load Frame provides load up to 100 KN.

It is used for the determination of the tensile strength and elongation of vulcanized rubber according to ASTM Designation: D 412-02. It consists of:

a- Testing Machine

A power – driven machine equipped with a suitable dynamometer, a recording device for measuring the applied force within ± 2%.

b- Grips

The tester has two grips; one of which is stable and the other is connected to the dynamometer. Also it contains a mechanism for separating the grips at a uniform rate of 500 ± 50 mm/min.

The entire tension tests were performed on a standard temperature of 23 ± 2 °C according ASTM standards.

The MTS machine with load up to 100 KN is shown in Fig (2.20).

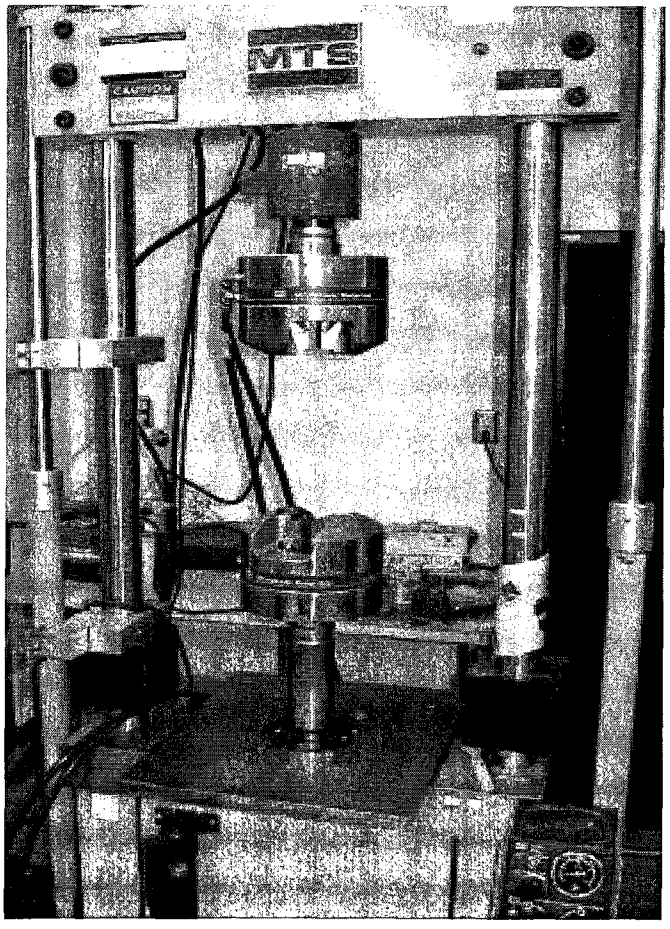

Fig (2.20) MTS machine

2.2.5 Laser extensometer

This machine measures the elongation by subjecting a vertical laser light to the specimen where there is a laser sensitive paper is glued. The measurement is done by taking the difference between the original and final laser light length over the original length. The laser extensometer is shown in Fig (2.21).

Fig (2.21) laser extensometer

2.2.6 Shore A durometer

Shore A duremeter have high contrast LCD display with backlighting and large easy to read numbers. It has a test counter that automatically counts the number of tests and number of parts. It has RS-232 Serial Port to send results to printer or computer for analysis and processing [70]. The test method for measuring shore A hardness for insulation sheet describes a procedure for measuring the hardness of rubber according to

ASTM: D2240-91. Fig (2.22) (a), (b) show the shore A hardness durometer during calibration and testing respectively.

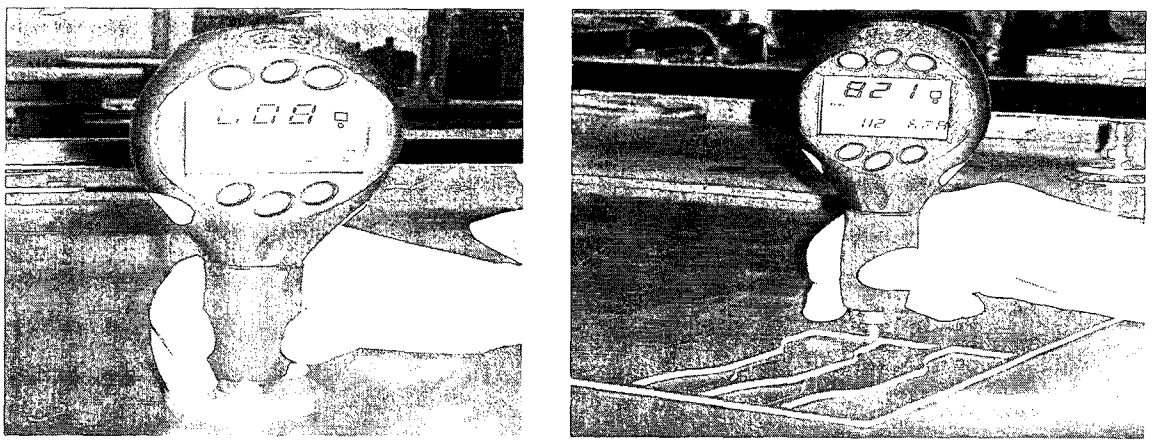

(a) (b)

Fig (2.22) The INSTRON Shore A hardness durometer during (a) calibiration (b) testing

2.2.7 Nanoflash

The nanoflash technique is one of the most widely used methods for the determination of the thermal diffusivity of metals, graphite, coatings, composites, ceramics, polymers and

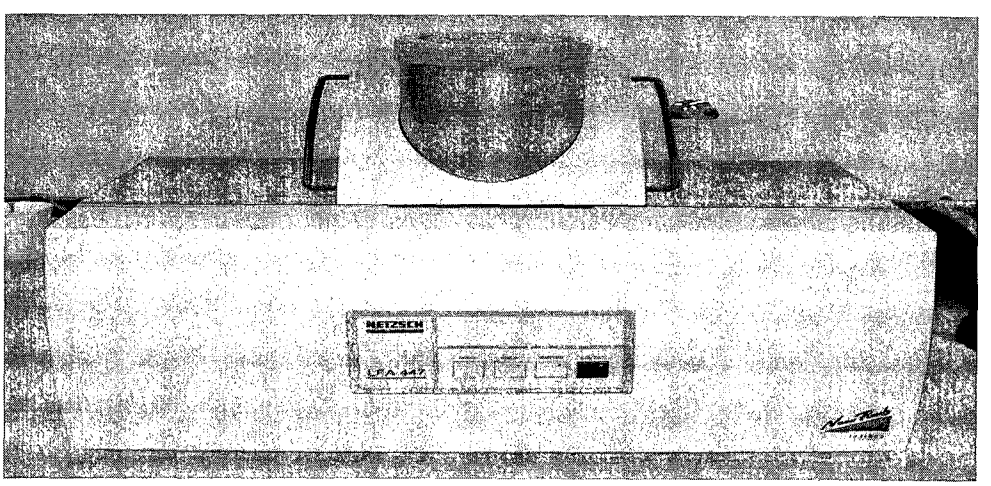

Fig (2.23) The nanoflash instrument

other materials. Fig (2.23) shows a photo of the Nanoflash instrument.

The instrumentation includes sophisticated hardware and simple menu-driven software to provide fast, accurate, and safe measurements. The Nanoflash works to the flash method according to international standards and it satisfies the requirements for measurements of thermal diffusivities according to ASTM E 1461 [71].

Using this method, the front side of a plane – parallel sample with a well-defined thickness is heated by a short light or laser pulse. The resulting temperature rise on the back surface is measured versus time using an infrared detector. Analyzing the measured detector signal with appropriate mathematical models yields information on various thermophysical properties of the material, Short testing times, easy sample preparation and a broad thermal diffusivity range are only some of the advantages of this non – contact, non destructive measurement technique.

The Nanoflash is equipped with a furnace capable of operation from room temperature to 300°C. The system is equipped with a software-controlled automatic sample changer allowing measurement of up to 4 samples at the same time. The temperature rise on the back face of the sample is measured using an In-Sb detector. Data acquisition and evaluation are accomplished using a comprehensive 32-bit MS-Windows software package.

The analysis of the flash diffusivity data requires that the energy be absorbed on the surface of the sample. It also requires that only the sample surface temperature is measured by the IR detector. Some materials are transparent at visible and near IR wavelengths of the Xenon flash. A sputter-coated metal film (typically gold) is used on both sides of the sample to minimize the radiation heat transfer within the sample and to prevent the detector from viewing temperature changes within the sample. The required

film thickness is approximately 1000 Å, and can be controlled by the settings used during the coating process. As a guide, most unfilled polymers and many ceramics and glasses will require a metal film or graphite coating. A missing or insufficient coating shows a high temperature increase in the detector signal directly after the shot (spike) [71-73].

Fig (2.24) shows the main components of the nanoflash instrument.

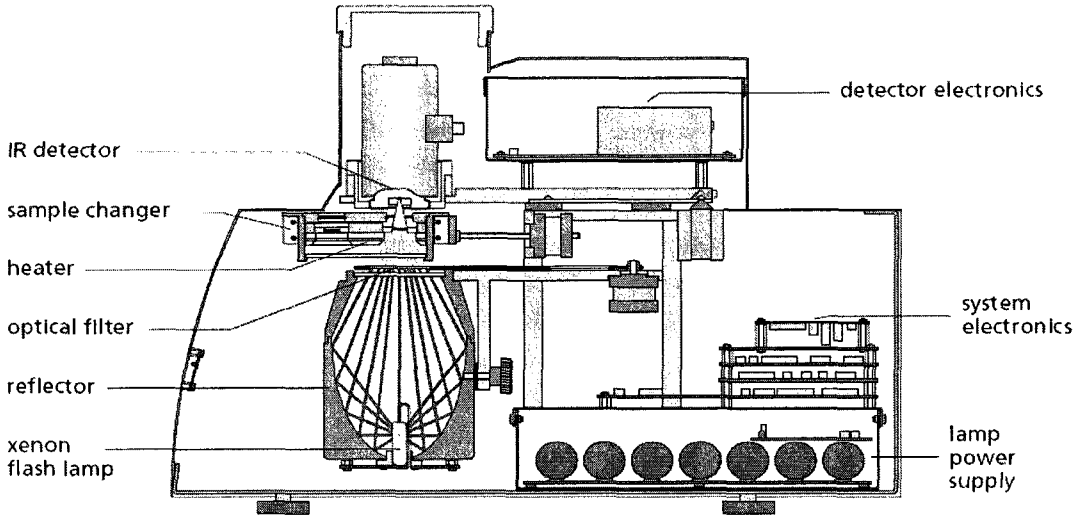

Fig (2.24) The nanoflash instrument main measurement components

2.2.8 Differential Scanning Calorimeter (DSC)

The Differential Scanning Calorimeter (DSC) determines the temperature and heat flow associated with material transitions as a function of time and temperature. It also provides quantitative and qualitative data on endothermic (heat absorption) and exothermic (heat evolution) processes of materials during physical transitions that are caused by phase changes, melting, oxidation, and other heat-related changes. This information helps the scientist or engineer identify processing and end-use performance. The DSC instrument works in conjunction with a controller and associated software to make up a thermal analysis system [74].

Differential Scanning Calorimetry (DSC) is the most widely used technique of all the thermal analysis methods. In DSC machine the substance which shall be measured is placed in an aluminium pan whereas an empty aluminium pan serves as the reference. These two pans are put on an electrically heated plate in order to make sure that the temperature in the sample is the same as in the reference. Via those plates and the pans heat is transferred to the sample and the reference with the use of a defined computer controlled heating program (the rates of the heating can be adjusted). The differential heat flux to the sample and the reference as well as the sample temperature are measured. The output of a DSC measurement, the so called thermogram is a plot of the difference of heat delivered to the sample and to the reference as a function of the sample temperature. If a physical or a chemical process which is endothermic (consuming energy as heat) is taking place, in order to maintain the same temperature of the two pans, more heat must be delivered to the sample pan than to the reference pan. The effect is a positive or negative peak in the thermogram (the sign of the peak is depending on the definition of the sign for the direction of the heat flow). The opposite is true for an exothermic process. Since the enthalpy change of the transition is linearly related to the area under the curve of the thermogram. Fig (2.25) shows a DSC machine.

The DSC Heat Capacity analysis however, calculates the actual specific heat capacity at any temperature in the DSC scan. The measurement is made by heating a test specimen at a fixed rate over a designated temperature range, where the specimen is held in thermal equilibrium before and after dynamic heating. The heat flow obtained from the specimen

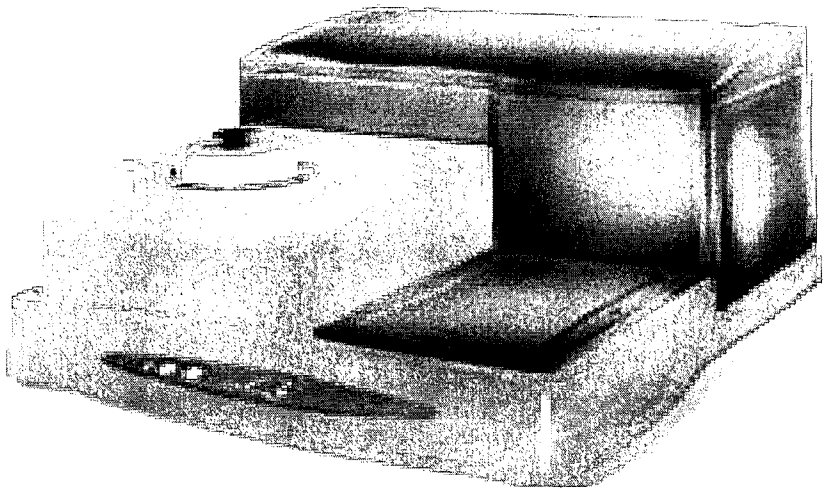

Fig (2.25) DSC machine

is recorded as a function of the actual sample temperature. This heat flow, normalized to the specimen mass and heating rate, is directly proportional to the specimen's specific heat capacity. To obtain specific heat capacity analysis one needs three DSC graphs: a sample, a baseline, and a reference. The baseline data is used for baseline subtraction from the reference and sample data. Typically sapphire is used as the reference material, but other materials (such as water for liquids) may be used. Two DSC scans were carried out for each material to ensure reproducibility.

2.2.9 Thermo gravimetric analyzer (TGA)

Thermo gravimetric Analyzer (TGA) is a thermal weight-change analysis instrument, used in conjunction with a TA Instruments thermal analysis controller and associated software, to make up a thermal analysis system [75].

The Thermo gravimetric Analyzer measures the amount and rate of weight change in a material, either as a function of increasing temperature, or isothermally as a function of time, in a controlled atmosphere. It can be used to characterize any material that exhibits a weight change and to detect phase changes due to decomposition, oxidation, or

dehydration. This information helps the scientist or engineer identify the percent weight change and correlate chemical structure, processing, and end-use performance.

The TGA has six major components:

• The balance, which provides precise measurement of sample weight. The balance is the key to the TGA system.

• The sample platform, which loads and unloads the sample to and from the balance.

• The furnace, which controls the sample atmosphere and temperature.

• The cabinet, where the system electronics and mechanics are housed.

• The heat exchanger, which dissipates heat from the furnace.

• The TGA has two mass flow controllers, which control the purge gas to the balance and furnace. Fig (2.26) shows a TGA machine

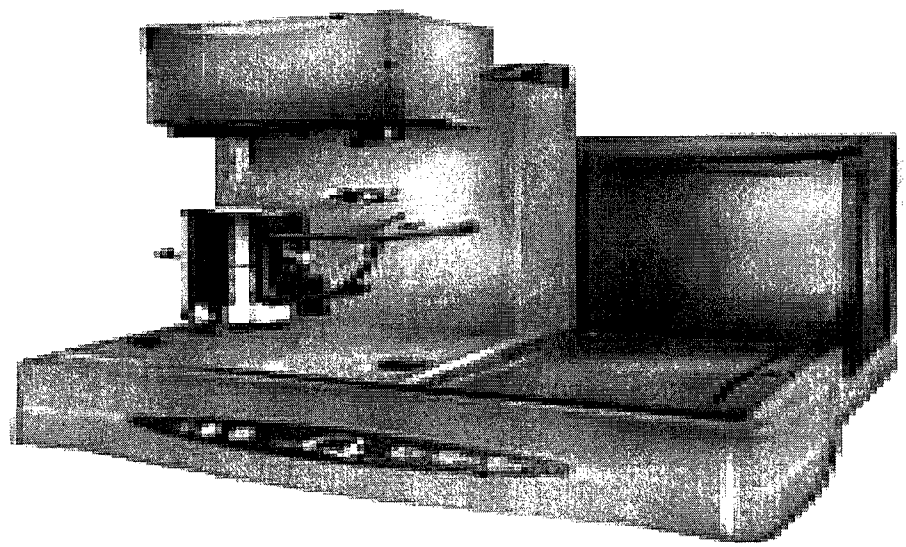

Fig (2.26) TGA machine

2.2.10 Molds for curing

Two molds from steel with cavity dimensions (300 x 150 x 3 mm, 300 x 150 x 1 mm) were made for curing of different samples with two thicknesses (1 mm and 3 mm) for

investigation of the physical, mechanical, thermal and ablative properties according to ASTM standards. Each mold consists of three pieces with additional spacers to control the thickness of the cured sheet. In compression molding a master batch (the materials mixture after mixing) is placed between two halves of a mold and is then squeezed under temperature and pressure into the shape of the cavity.

2.2.11 MAPP torch

It is a surface mix torch. The fuel and oxygen are carried through a multitude of tiny tubes which bring them out on the face of the torch to ignite and burn. It is a specially-designed gas composed of liquefied stabilized methyl acetylene propadiene compound. It has a good sized flame and can put out 2010 °C [76]. Fig (2.27) shows the MAPP torch used to do ablation test.

Fig (2.27) MAPP torch

2.2.12 Ablation test kit

The test kit is constructed mainly from steel with a horizontal base with dimensions 250 x 150 x 4 mm. Two vertical steel columns with dimensions 300 x 25 x 8 mm are welded to the horizontal base where the sample can be held using a two screw clamps. A high temperature, sensitive digital thermocouple is attached to the kit. The thermocouple can read temperature of the surface up to 1200 °C accurately.

Fig (2.28) shows a photo of the ablation kit used to perform ablation test for all samples

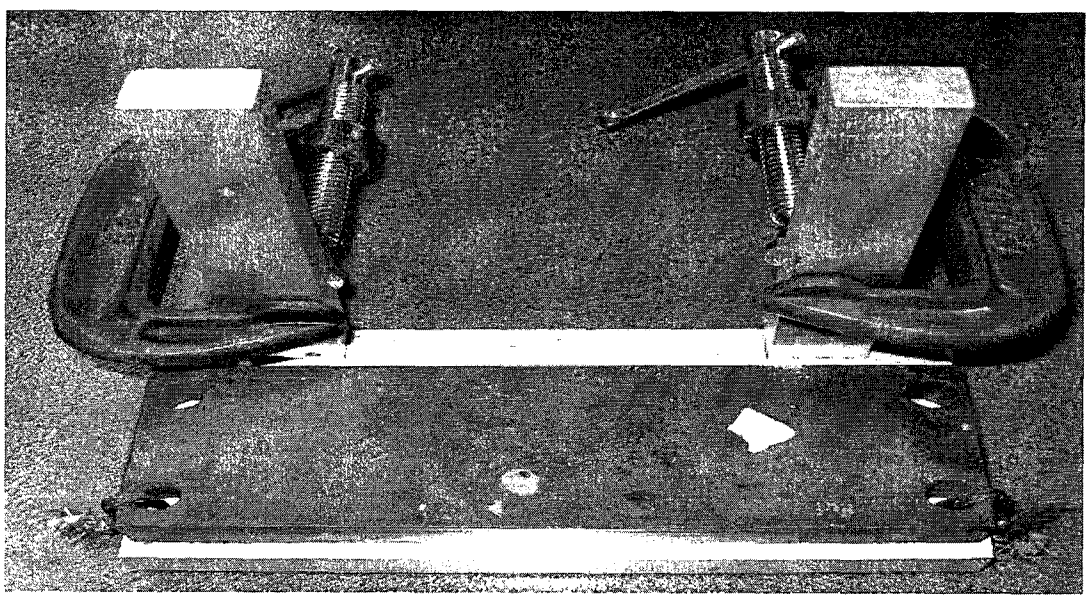

Fig (2.28) Ablation test kit

2.2.13 ASTM cutting die

ASTM cutting die (type C) used to cut samples from the cured sheet of the insulation to be tested using tensometer and laser extensometer for the determination of the tensile strength and elongation according to ASTM D 412-02.

Fig (2.29) show the ASTM cutting die type C which is used to cut samples from insulation sheets for the determination of the tensile strength and elongation.

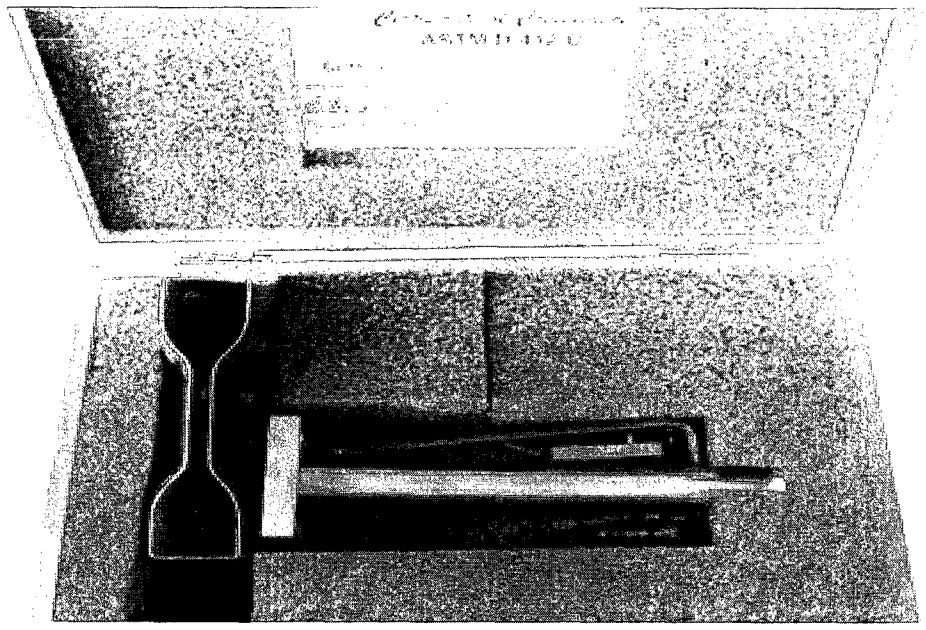

Fig (2.29) ASTM cutting die type C.

The common tensile specimen is of the dumbbell shape. It has tabbed ends for gripping in the test machine and a tapering to control a constricted section of a uniform width. Six different shapes of dies for clicking out dumbbell specimens are permitted by ASTM Designation D412-92 [77]. The piece of rubber to be tested is, whenever possible flat, not less than 1.5 mm and nor more than 3 mm in thickness and of size permitting cutting a dumbbell specimen by means of one of the saturated dies.

2.2.14 Micrometer

The micrometer used to measure the thicknesses of the sheets is a digital one with high accuracy. This micrometer used to measure the thickness of a flat specimen is capable of exerting a pressure of 0.2 kg/ cm^2 on the specimen according to ASTM Designation: D3767.

2.2.15 Scanning electron microscope

The scanning electron microscope (SEM) is a microscope that images the sample surface by scanning it with a high-energy beam of electrons in a raster scan pattern. The electrons interact with the atoms that make up the sample producing signals that contain information about the sample's surface topography, composition and other properties such as electrical conductivity. SEM micrographs have a very large depth of field yielding a characteristic three-dimensional appearance useful for understanding the surface structure of a sample. A wide range of magnifications is possible, from about x 25 (about equivalent to that of a powerful hand-lens) to about x 250,000, about 250 times the magnification limit of the best light microscopes. All samples must also be of an appropriate size to fit in the specimen chamber and are generally mounted rigidly on a specimen holder called a specimen stub.

For conventional imaging in the SEM, specimens must be electrically conductive, at least at the surface and electrically grounded to prevent the accumulation of electrostatic charge at the surface. Composite objects require little special preparation for SEM except for cleaning and mounting on a specimen stub. Nonconductive specimens tend to charge when scanned by the electron beam, and especially in secondary electron imaging mode, this causes scanning faults and other image artifacts. They are therefore usually coated with an ultrathin coating of electrically-conducting material. Coating prevents the accumulation of static electric charge on the specimen during electron irradiation.

2.2.16 Balance

High accurate balance to weigh ingredients is used. The accuracy of this balance is ± 0.0001 gram.

2.2.17 Agilent High Resistance Meter

The high resistance meter used is HP 4339B type. It is used to measure the volumetric electrical resistivity of a material. The electrical resistivity (also known as specific electrical resistance or volume resistivity) is a measure of how strongly a material opposes the flow of electric current. A low resistivity indicates a material that readily allows the movement of electrical charge. The SI unit of electrical resistivity is the ohm meter (Ω m).

The 4339B high-resistance meter is Agilent Technologies most advanced tool for making precision high-resistance measurements. The HP Agilent 4339B High Resistance Meter is a single channel solution for accurate high resistance and low current measurements. The test sequence program function provides an automatic measurement process (charge-measure-discharge).

Features of the Agilent 4339B High Resistance Meter include:

(a) Wide measurement range: 1×10^3 ohm to 1.6×10^{16} ohm

(b) High-speed measurement: 10 ms

(c) Stable test fixtures: resistivity cell, component test fixture

(d) Volumetric resistivity calculations

The HP Agilent 4339B High Resistance Meter main components are shown in Fig (2.30).

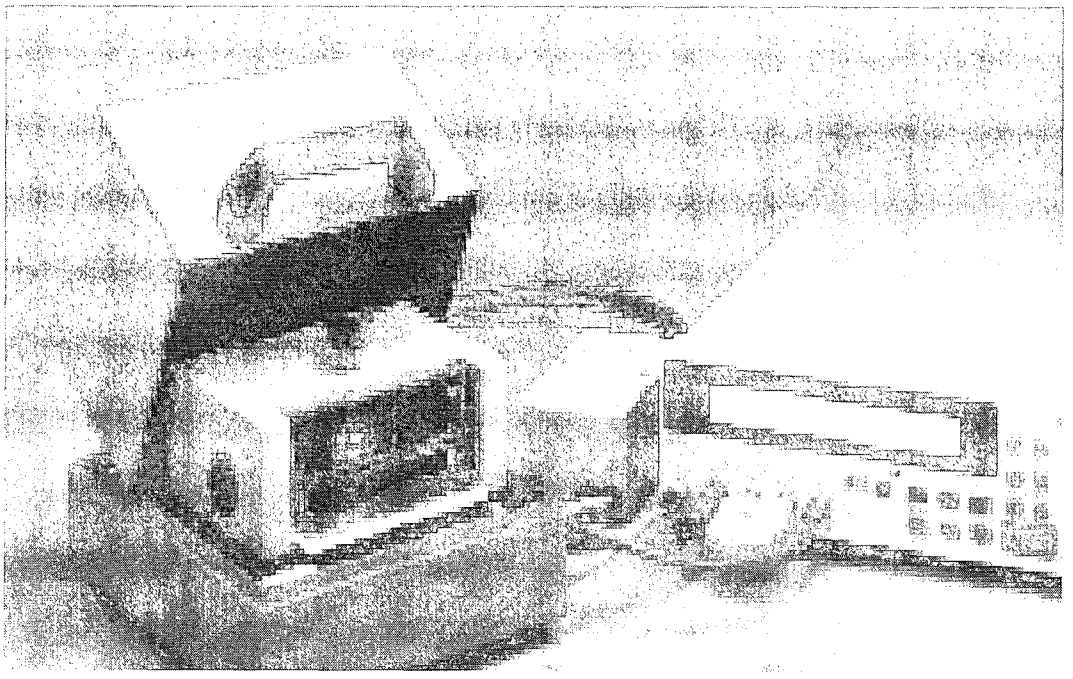

Fig (2.30) The HP Agilent 4339B High Resistance Meter main components

2.3 Processing of materials

2.3.1 Mixing of samples

There are different processing methodologies for mixing and curing of the available types of the elastomers compounds due to the wide variety of polymers and a wide range of compound specifications with different types of fillers. However broad guidelines have been suggested.

For rubbery EPDM elastomers mixing, the fine mixing is obtained using two- roll mixing mill. For viscous liquid EPDM elastomers, it is difficult to be mixed in a two-roll mill since these are usually highly loaded with fillers and oils.

C.W. Bra bender mixer is preferred for viscous liquid EPDM elastomers. The optimum mixing is achieved by following accurately the mixing cycle. The basic requirement of EPDM elastomers processing for rocket motor insulation is the compounding of the

insulating material at a temperature below which the elastomer does not cure and permit the loss of compounding ingredients. Normally, the safer processing temperature was found to be around 90 °C.

Uniform dispersion of the fiber and the reinforcing filler is one of the major problems associated with mixing fiber loaded compositions. An accurate method describes the incorporation of fragile fibers like chopped carbon fibers in the EPDM elastomers matrix via distributive and reduced shear mixing without excessive fracture or fragmentation of the fiber. The mixing which involves chopped carbon fiber can be done by C.W. Bra bender mixer equipped with 2 sigma blades (not with the regular Banbury blades).

The mixing procedure for mixing the master batch of the insulation which includes chopped carbon fiber by using the C.W. Bra bender is as follows:

1- Warm the specified amount of Trilene 67 inside a beaker on the furnace at 90 °C for 30 min. to allow easy flow into the mixing chamber of the C.W. Bra bender mixer

2- Operate the mixer at 50 rpm and 90 °C and then put the Trilene 67 amount in for 5 min.

3- Put the specified amount of the ammonium polyphosphate for 5 min.

4- Put the specified amount of reinforcement

- If chopped carbon fiber is used the required time is 10 min.
- If Kevlar pulp is used the required time is 15 min.
- If chopped carbon fiber + Kevlar pulp is used the required time is 13 min.

5- Put the specified amount of peroxide cross linking agent for 5 min.

6- Stop the Bra Bender and Extract the master batch (in about 5 minutes) for curing.

The mixing cycle is shown in fig (2.31).

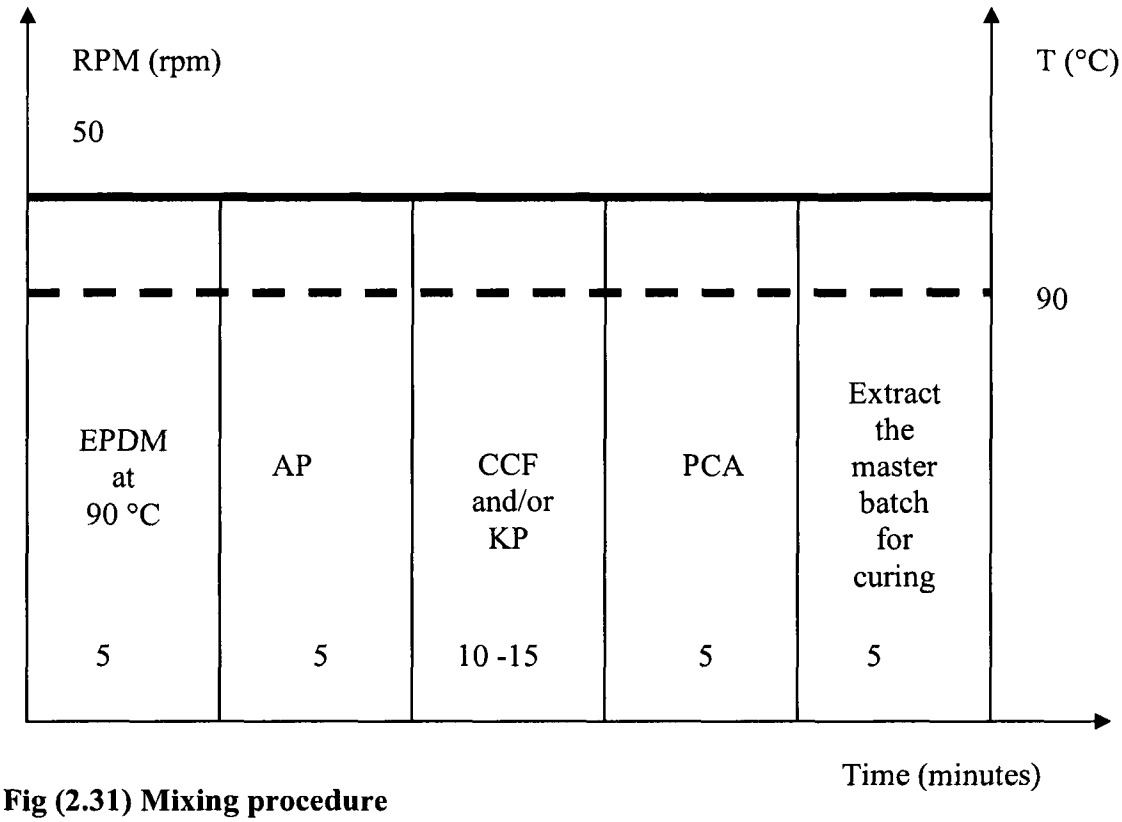

Fig (2.31) Mixing procedure

This means that the total time to mix a master batch of 60 cm^3 is from 30 to 35 minutes according to the type of reinforcement used in addition to 30 minutes to warm Trilene 67 inside the furnace. So the total time to mix a master batch of 60 cm^3 is from 60 to 65 minutes.

Since the curing of the two sheets required for physical, mechanical, thermal and ablative properties testing needs 240 cm^3 of the materials, 4 master batches have been mixed with mixing total time from 240 to 260 minutes for each sample.

2.3.2 Curing of samples

The mold for fabrication of thermal insulation is designed according to the shape and the thickness of the required thermal insulant material. The curing of the insulation is usually done under a press by compression molding where the homogenous mixture as a master

batch is placed inside the mold with specific weight calculated by density and size of insulant material.

Compression molding is the process by which polymers are usually formed as shown in Fig (2.32).

The compression molding process involves placing the polymer master batch into the die cavity. This master batch is carefully measured to avoid waste and minimise the amount of 'flashing' (fine, thin webs attached to the molding) around the finished article.

With the die platens apart, the prepared polymer 'master batch' is placed into the cavity and with the die platens closed, the article is formed and the small amount of flashing on each side will be removed later.

When the die is closed, heat and pressure are maintained until the polymer cross linking process is completed.

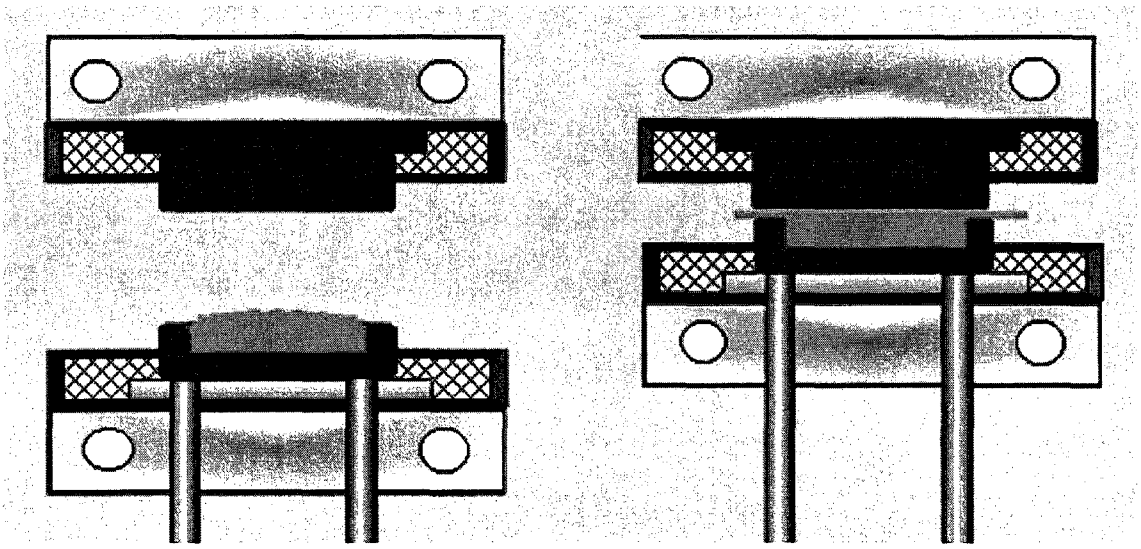

Fig (2.32) Compression molding for curing of polymers

Specific pressure of 2.5 MPa and 170 °C temperature are applied and for a duration of 90 min. The specific curing cycle for all samples based on different reinforcement is shown in Fig (2.33).

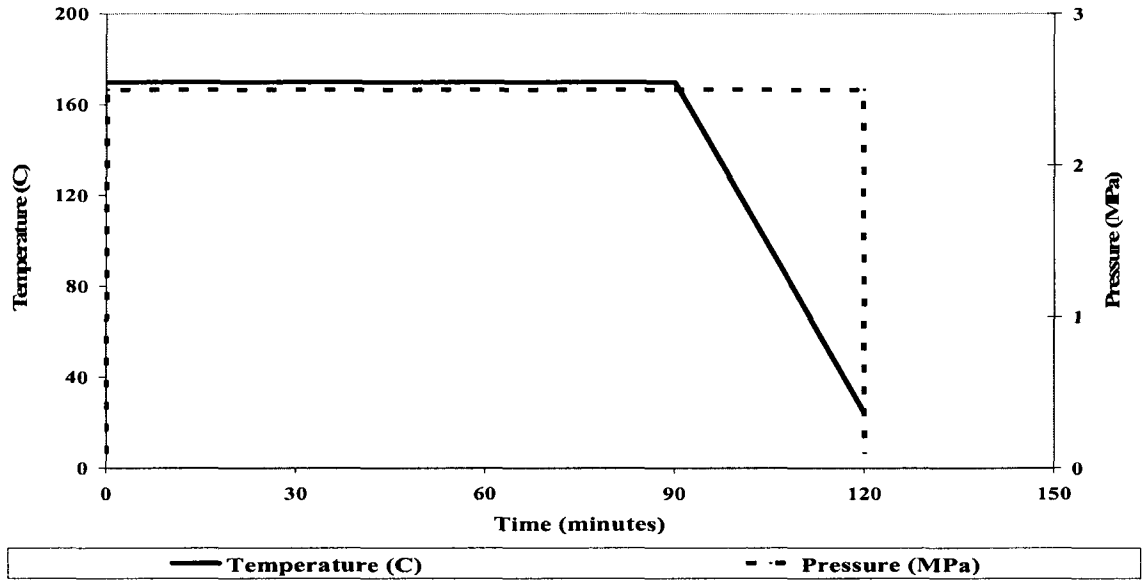

Fig (2.33) The curing conditions for the samples

2.4 Testing of materials

2.4.1 Tensile strength and elongation

ASTM cutting die (type C) was used to cut samples from the cured sheet of the insulation. There were tested on MTS machine and using laser extensometer for the determination of the tensile strength and elongation of vulcanized rubber according to ASTM D 412-02.

These test methods cover procedures used to evaluate the tensile (tension) properties of vulcanized rubbers. Specimens are in the shape of dumbbells. All the insulation samples were tested under the same conditions. The standard temperature for testing was 23 ± 2°C [78].

2.4.2 Density and Hardness

The test method for measuring shore A hardness for insulation sheet describes a procedure for measuring the hardness of rubber. The hardness was obtained by the

difference in penetration depth of a specified dimension ball of indenter when forced into the material under specified conditions. The indentation hardness is inversely related to the penetration and is dependent on the elastic modulus and viscoelastic behavior of the material. The differential penetration was taken at a specified time and converted to a hardness scale value according to ASTM D2240-05.

The surfaces of the specimens were flat and parallel over an area to permit the presser foot to contact the specimen over an area having a radius of at least 6.0 mm from the indentor point. The specimens were suitably supported to provide for positioning and stability. A suitable hardness determination cannot be made on an uneven or rough point of contact with the indentor. The standard temperature for testing was 23 ± 2°C.

There are rubber reference block(s) (calibration standards) provided for checking durometer operation and state of calibration [79].

The determination of Density of solid rubber sheets was done by using the densities and volume fractions for all constituents in the rule of mixture formula for composites ($\rho = \sum_{i=1,..,n} v_i \rho_i$).

2.4.3 Thermal diffusivity

The test method covers the determination of the thermal diffusivity of primarily homogeneous fully dense solid materials according to ASTM E1461 - 07 [80].

In principle, the thermal diffusivity is obtained from the thickness of the sample and from a characteristic time function describing the propagation of heat from the front surface of the sample to its back surface.

A small square sample (12.7x 12.7x1 mm) was cut from the material sheets and using a standard sample provided by the instrument manufacturer having a nearly similar density

as the tested sample such as vesbel standard sample. By entering the calculated densities to the thermal Nanoflash instrument we can get the thermal diffusivity for the material. Fig (2.34) (a) shows the material and vespel reference samples. Fig (2.34) (b) shows the Nanoflash instrument samples holder which contains four windows each one holding one sample.

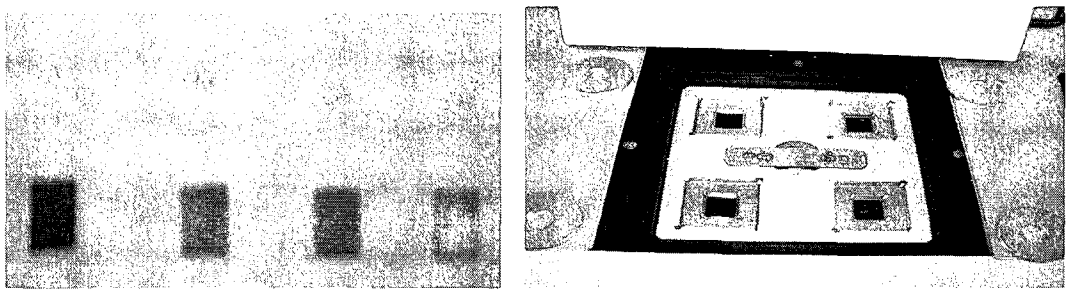

(a) (b)

Fig (2.34) The nanoflash instrument (a) samples (b) samples tray holder

2.4.4 Specific heat capacity

The test method covers the determination of specific heat capacity by differential scanning calorimetry. It is generally applicable to thermally stable solids and liquids according to ASTM E 1269 – 01 [81]. Differential scanning calorimetric measurements provide a rapid, simple method for determining specific heat capacities of materials.

Since milligram quantities of specimen are used, it is essential that specimens are homogeneous and representative. The occurrence of chemical changes or mass loss on heating during the measurement may invalidate the test.

To get the specific heat capacity for insulation composition, DSC must be done with a specific procedure as a requirement of the TA DSC instrument (equilibrium at 25 C then isothermal for 10 min. then heating to 300 C then isothermal for 10 min. again) and using

sapphire calibrant as a reference and do DSC for base line (without sample), DSC of the material samples was done using samples around 8 mg.

2.4.5 Thermal conductivity

The thermal conductivity of a solid material is the time rate of steady heat flow through unit thickness of an infinite slab of a homogeneous material in a direction perpendicular to the surface, induced by unit temperature difference. The property must be identified with a specific mean temperature, since it varies with temperature [82].

The fundamental relationship between thermal diffusivity (α), thermal conductivity (K), specific heat capacity (Cp), and density (ρ) is:

$$K = \rho \, . \, \alpha \, . \, C_p \qquad (2.1)$$

This allows the calculation of thermal conductivity, with the knowledge of the other properties.

2.4.6 Decomposition temperatures

Another important aspect of the characterization of the material compositions includes defining the primary reactions in the decomposition of the material. TGA analysis is a tool used to establish the primary reactions that occur. The data are useful in obtaining decomposition temperatures of the whole material composition. Thermogravimetry provides a rapid method for determining the temperature-decomposition profile of a material according to ASTM E 1641 – 99 [83-86].

This test method consists of heating a specimen, taken from the original sample, through its decomposition region. The specimen mass is recorded continuously as a function of temperature. The temperatures for constant conversion are determined from the resultant mass loss curves.

TGA of the insulation samples was performed using samples of around 12 mg in a temperature range from 25 °C to 1000 °C with a heating rate 40 °C/min. TGA with higher heating rates provides a good datum upon which to base insulation/case bondline temperature crifical in rocket motors.

2.4.7 Ablation Test

The test method covers the screening of ablative materials to determine the relative thermal insulation effectiveness when tested as a flat panel in an environment of a steady flow of hot gas provided by a torch. This test method is used to measure and describe the properties of materials in response to heat and flame under controlled laboratory conditions [87-88].

Hot combustion gases are directed along the normal to the specimen until burn-through is achieved. The ablation rate of the material is determined by dividing the difference between the original and the final thicknesses by the time of burn-through. The insulating effectiveness is determined from the back-face temperature.

The specimen and the calorimeter were supported in a suitable fixture arranged in such a fashion that it can hold the specimen with the thermocouple when subjected to the torch during the whole duration of the test.

According to ASTM-E-285-02 [89] the ablation test was done by preparing a sample of the insulation material with 3 mm thickness, length 20 cm and width 20 cm and the sample is weighed before the test. Then it is glued to a steel piece with the same dimensions using the special adhesive Epon 828 and Epicure curing agent which is specified for gluing of rubber to steel and with adhesive thickness approximately 0.3 mm. Then a thermocouple is fixed in the back of steel sheet and the insulation material is

subjected to MAPP torch (2010 °C) for 60 seconds. During the test the temperature was measured and recorded with time using the thermocouple. After the test the weight and final thickness of the insulation were measured. A photo representation of ablation test is shown in Fig (2.35) (a), (b).

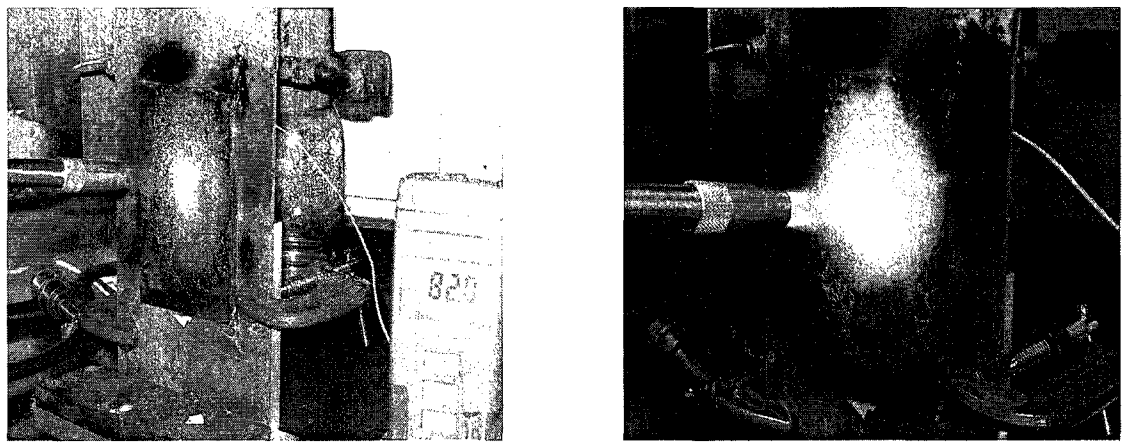

(a) (b)

Fig (2.35) Ablation test representation

2.4.8 Microscopic observation

This was done by cutting small specimens from the insulation samples. Microscopic observations were performed using scanning electron microscope (SEM). The resultant photos [(2.45), (2.54), (2.62)] which describe the distribution of the constituents are of length 250 μm and width 150 μm.

2.4.9 Electrical resistivity

The electrical resistivity is known as specific electrical resistance or volume resistivity. It is a measure of how strongly a material opposes the flow of electric current. A low resistivity indicates a material that readily allows the movement of electrical charge. The SI unit of electrical resistivity is the ohm meter (Ω m).

Electrical resistivity ρ is defined by,

$$\rho = \frac{E}{J} \qquad (2.2)$$

Where

ρ is the static resistivity (measured in volt-metres per ampere, Vm/A);

E is the magnitude of the electric field (measured in volts per metre, V/m);

J is the magnitude of the current density (measured in A/m^2).

The electrical resistivity ρ can also be given by,

$$\rho = R\frac{A}{L} \qquad (2.3)$$

Where

ρ is the static resistivity (measured in Ω.m);

R is the electrical resistance of a uniform specimen of the material (measured in Ω);

L is the length of the piece of material (measured in m);

A is the cross-sectional area of the specimen (measured in m^2).

Finally, electrical resistivity is also defined as the inverse of the conductivity σ as shown in equation (2.4)

$$\rho = \frac{1}{\sigma} \qquad (2.4)$$

A small square or circular sample with well defined thickness was cut from the material sheets and was introduced to Agilent 4339B High Resistance Meter to measure electrical resistivity.

The ability to dissipate static charge is considered to be an important quality for the thermal insulator. An insulator possessing this quality is able to bleed off or dissipate charges that build up on the insulator surface. An insulator having a high electrical

resistivity does not dissipate static charge timely, thus creating a potential for static charge to build up to a dangerous level. When the electric field increases to the point that breakdown of the air occurs or a path to ground for the static charge is inadvertently provided, the discharge can be dangerous. Physical harm to personnel and flash fires are possible. Conventional silica-filled EPDM insulation is electrically insulating, having resistivities ranging from 1×10^{14} to 1×10^{16} Ohm · cm. An insulator is considered to be able to dissipate static charge if its volume resistivity is in the range of from 1×10^{5} to 1×10^{12} Ohm · cm.

2.4.10 Bond strength test

Bond strength (ply adhesion) is the amount of force required (per unit width) to separate plies of material or materials in peeling mode plus the force to bend the plies.

It has been widely discussed in the literature that bond strength of flexible multi-ply materials is measured by doing tensile test of an unaxial sample according to the standard test method for determining the bond strength (ply adhesion) of composites (ASTM Designation: D 7005 – 03).

2.5 Compositions and results

For this purpose, 30 samples were prepared (mixed, molded and cured under specific temperature and pressure, then demolded) representing 30 types of insulants. An investigation on the processing, installation, physical, mechanical, thermal and ablative properties of these insulation compositions was carried out. This was done by measuring the following properties: tensile strength, elongation, hardness, density, thermal conductivity, specific heat, thermal diffusivity, initial decomposition temperature, final decomposition temperature, microscopic observation and ablation rate.

2.5.1 CCF based compositions

Different formulations (5 samples) of chopped carbon fiber (30- 50 phr) with EPDM polymer were prepared. All the formulations contain 100 phr EPDM, 60 phr AP and 6 phr PCA.

Because the capacity of the C. W. Bra bender mixer is around $60cm^3$, in order to have around 240 gm of the material as a requirement for curing the required samples for testing, four master batches (cycles for mixing) were done for every composition. The curing molds were cleaned and prepared for curing where a Teflon release sheet with same size of the samples (300 x 150 mm) was prepared and placed between the mold parts and the material for releasing and easy demolding after curing.

A list of tensile strength and elongation values are shown in Table (2.5) and Fig (2.36). The values are average for 3 measured samples for every composition with a standard deviation of ± 0.5 MPa and 1.2 % respectively.

Sample No/Composition (phr)	CCF content (phr)	Tensile Strength (MPa)	Elongation (%)
(1) 100 EPDM + 60 AP + CCF + 6 PCA	30	2.21	25.3
(2) 100 EPDM + 60 AP + CCF + 6 PCA	35	2.64	20.3
(3) 100 EPDM + 60 AP + CCF + 6 PCA	40	2.97	16.4
(4) 100 EPDM + 60 AP + CCF + 6 PCA	45	3.59	14.9
(5) 100 EPDM + 60 AP + CCF + 6 PCA	50	3.9	12.3
Asbestos reinforced EPDM [45]		6.55	30

Table (2.5) Tensile Strength & Elongation for CCF based samples

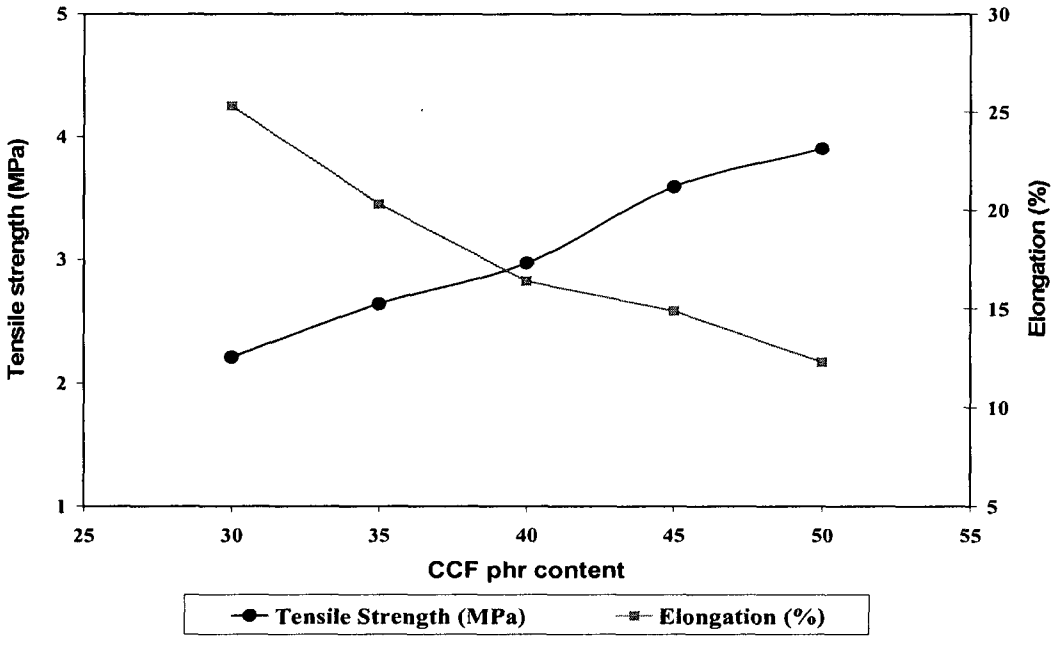

Fig (2.36) Tensile Strength & Elongation as a function of CCF phr content

Increasing phr content of CCF in EPDM increases the tensile strength of the material while elongation decreases.

A list of hardness values is shown in Table (2.6) and Fig (2.37). Hardness increases with increasing CCF content in EPDM. The values are average for 3 measured samples for every composition with a standard deviation of ± 0.2 Shore A.

Sample No/Composition (phr)	CCF content (phr)	Density (g/cm^3)	Hardness (shore A)
(1) 100 EPDM + 60 AP + CCF + 6 PCA	30	1.241	82.3
(2) 100 EPDM + 60 AP + CCF + 6 PCA	35	1.252	83.5
(3) 100 EPDM + 60 AP + CCF + 6 PCA	40	1.273	84.9
(4) 100 EPDM + 60 AP + CCF + 6 PCA	45	1.281	86.1
(5) 100 EPDM + 60 AP + CCF + 6 PCA	50	1.293	87.2
Asbestos reinforced EPDM [45]		1.205	94.6

Table (2.6) Hardness & Density for CCF based samples

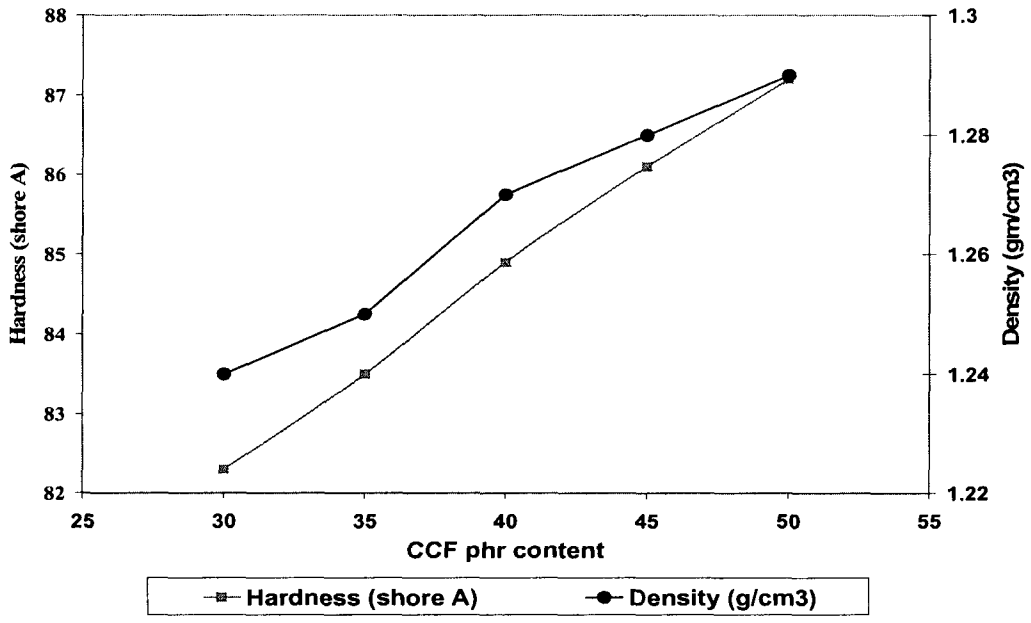

Fig (2.37) Hardness & Density as a function of CCF phr content

A list of density values are shown in Table (2.6) and Fig (2.37). Density increases with increasing CCF content in EPDM. This is because of the higher density of CCF (1.81 g/cm^3) as compared to EPDM (0.86 g/cm^3).

Thermal diffusivities for the insulation compositions with different CCF phr content at 200 °C are shown in Table (2.7) and Fig (2.38). The values are average for 3 measured samples for every composition with a standard deviation of ± 0.002 mm^2/s.

Sample No/Composition (phr)	CCF content (phr)	Thermal Diffusivity (mm^2/s)	Specific heat Capacity (J/Kg.C)
(1) 100 EPDM + 60 AP + CCF + 6 PCA	30	0.147	1757
(2) 100 EPDM + 60 AP + CCF + 6 PCA	35	0.169	1725
(3) 100 EPDM + 60 AP + CCF + 6 PCA	40	0.184	1698
(4) 100 EPDM + 60 AP + CCF + 6 PCA	45	0.211	1635
(5) 100 EPDM + 60 AP + CCF + 6 PCA	50	0.242	1549
Asbestos reinforced EPDM [45]		0.12	1674.7

Table (2.7) Thermal diffusivity & specific heat capacity for CCF based samples

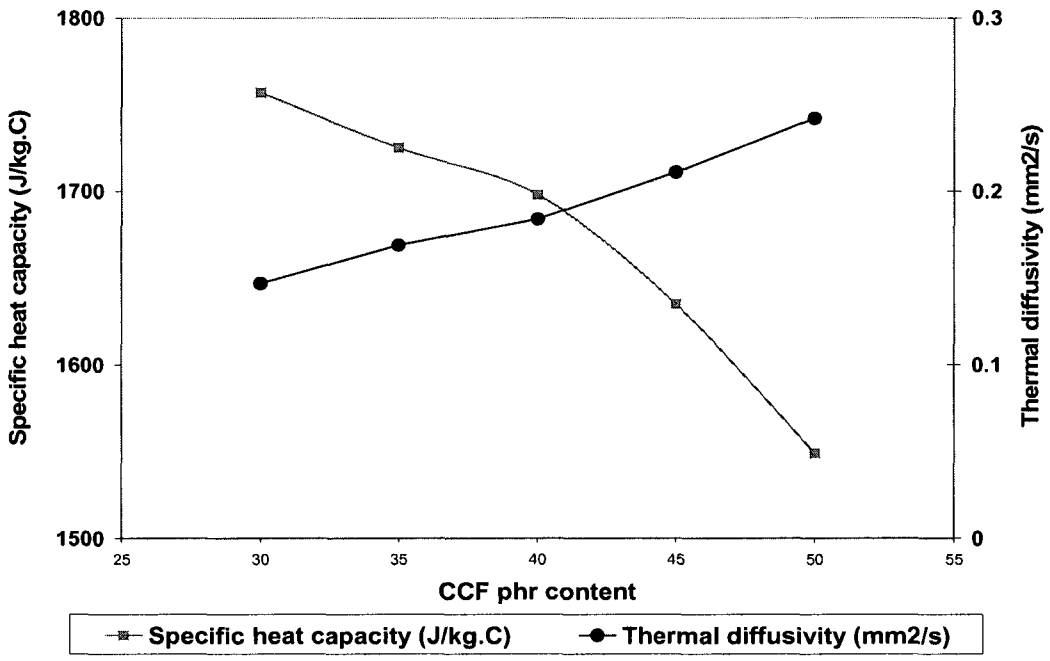

Fig (2.38) Thermal diffusivity and specific heat capacity as a function of CCF phr content

DSC curve for sample (5) was selected for representation which represents the final phr content for CCF as shown in Fig (2.39). From DSC curves, the relation between the specific heat capacities for every material composition with the temperature is obtained. Specific heat capacities for the different material compositions at 200 °C are shown in Table (2.7) and Fig (2.38). It appeared that increasing CCF phr content in the material will result in decreasing the specific heat capacity of the material. This is due to the lower specific heat capacity of CCF (660 J/kg.C) (reinforcement) compared to EPDM (the matrix) (2177 J/kg.C).

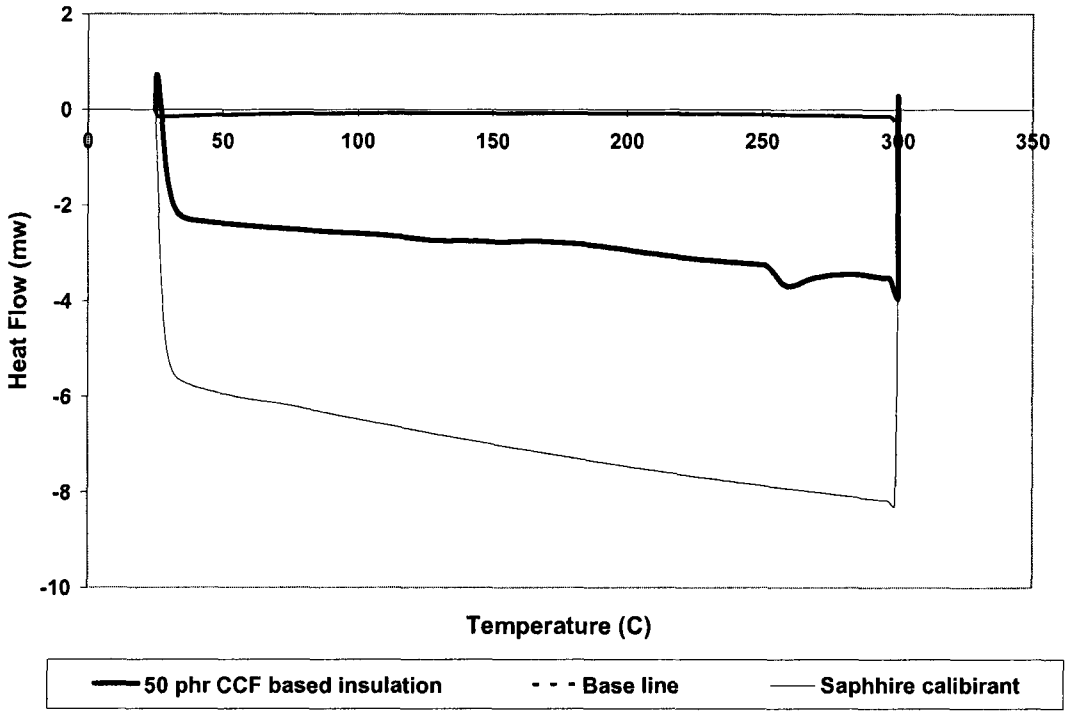

Fig (2.39) DSC curve for insulation composition sample 5 (50 phr CCF based EPDM)

Thermal conductivities for the CCF based compositions at 200 °C are shown in Table (2.8) and Fig (2.40).

Sample No/Composition (phr)	CCF content (phr)	Thermal Conductivity (W/m.C)
(1) 100 EPDM + 60 AP + CCF + 6 PCA	30	0.297
(2) 100 EPDM + 60 AP + CCF + 6 PCA	35	0.359
(3) 100 EPDM + 60 AP + CCF + 6 PCA	40	0.364
(4) 100 EPDM + 60 AP + CCF + 6 PCA	45	0.372
(5) 100 EPDM + 60 AP + CCF + 6 PCA	50	0.453
Asbestos reinforced EPDM		0.2421

Table (2.8) Thermal conductivity for CCF based samples

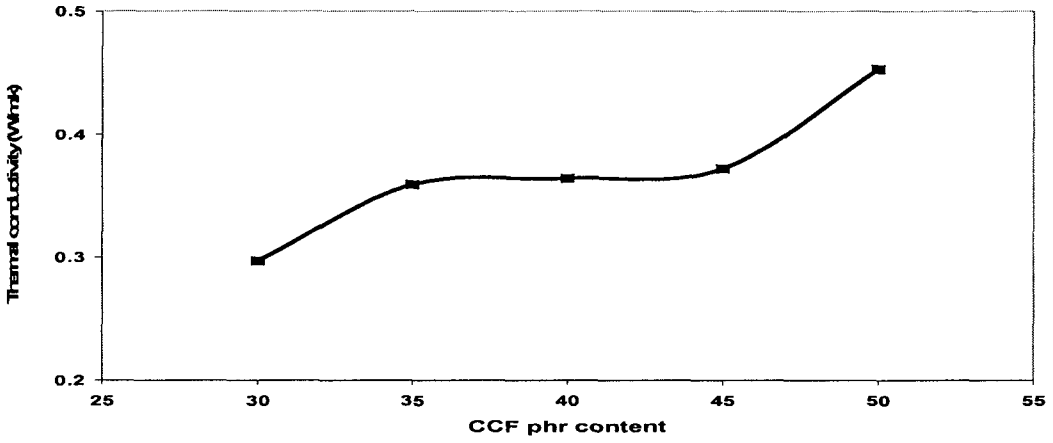

Fig (2.40) Thermal conductivity as a function of CCF phr content

It appears that increasing CCF phr content in the material will result in increasing the thermal conductivity of the material. This is due to the higher thermal conductivity of CCF (6.4 W/m.°C) compared to EPDM (0.36 W/m.°C). This goes against the requirement of the insulation material to have a very low thermal conductivity.

The resultant TGA curves which relate the weight % for every insulation composition sample with temperature for 30 phr CCF and 50 phr CCF based samples [samples (1), (5)] [Fig (2.41)].

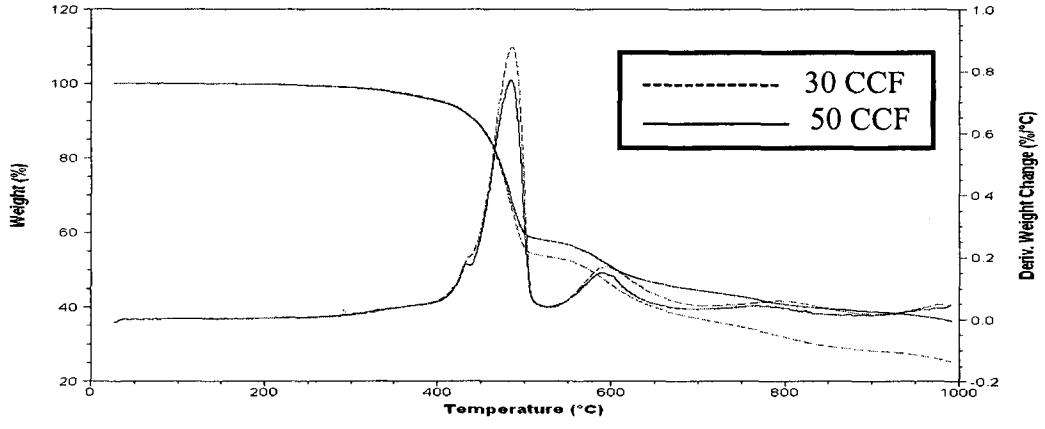

Fig (2.41) TGA, DTGA curves for insulation compositions (1), (5) [30 CCF, 50CCF based EPDM]

The TGA tests indicate for all compositions that an initial decomposition temperature for EPDM (matrix) occurs around 410 °C and the final decomposition is at 547 °C where EPDM decomposes to carbonaceous residue of carbon. These provide a net effect of strong carbon based char which is highly erosion resistant. Also the tests indicate that an initial decomposition temperature for ammonium polyphosphate (flame retardant agent) occurs around 575 °C and the final decomposition is at 722 °C.

In addition TGA for the individual CCF was carried out. The TGA curve for CCF is shown in Fig (2.42).

The only stable ingredient above 1000 °C is CCF which is stable up to 3445°C, in addition to the carbon based char remains from decomposition of EPDM. However not all 100 % of chopped carbon fiber will be stable up to 3445 °C since up to 13 % of it decomposes as shown in Fig. (2.42), which represents the TGA curve for CCF alone. This represents the epoxy sizing of the chopped carbon fiber which was added to protect it during handling and processing.

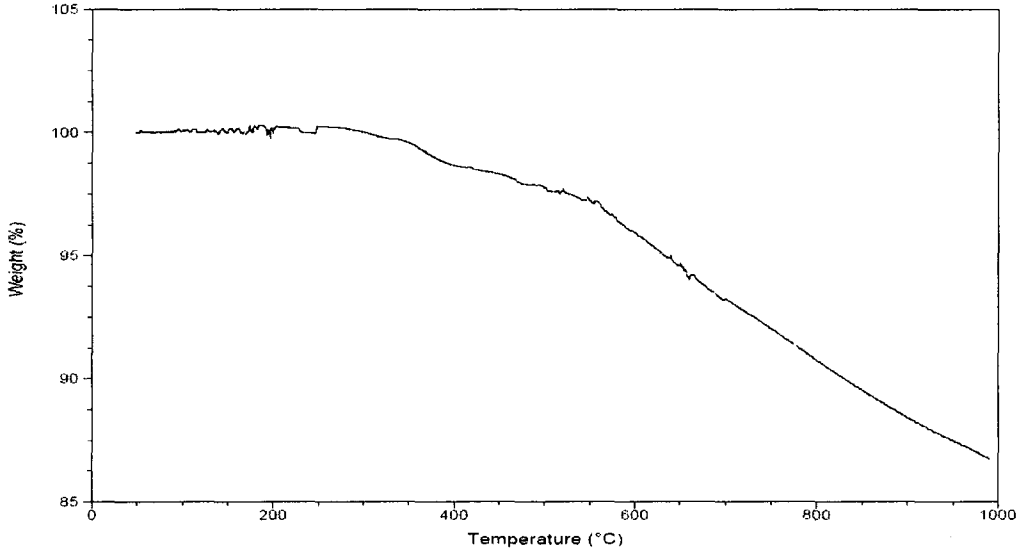

Fig (2.42) TGA curve for CCF alone

For TGA analysis for the matrix and flame retardant agent (AP and EPDM) alone was done as shown in Figures (2.43), (2.44) respectively. It appeared that the initial decomposition temperatures for EPDM and AP are 401 °C and 502 °C respectively and the final decomposition temperatures for EPDM and AP are 496 °C and 643 °C respectively. These temperatures are lower than those obtained from TGA of the whole insulation because CCF works as active shield for EPDM and AP against decomposition.

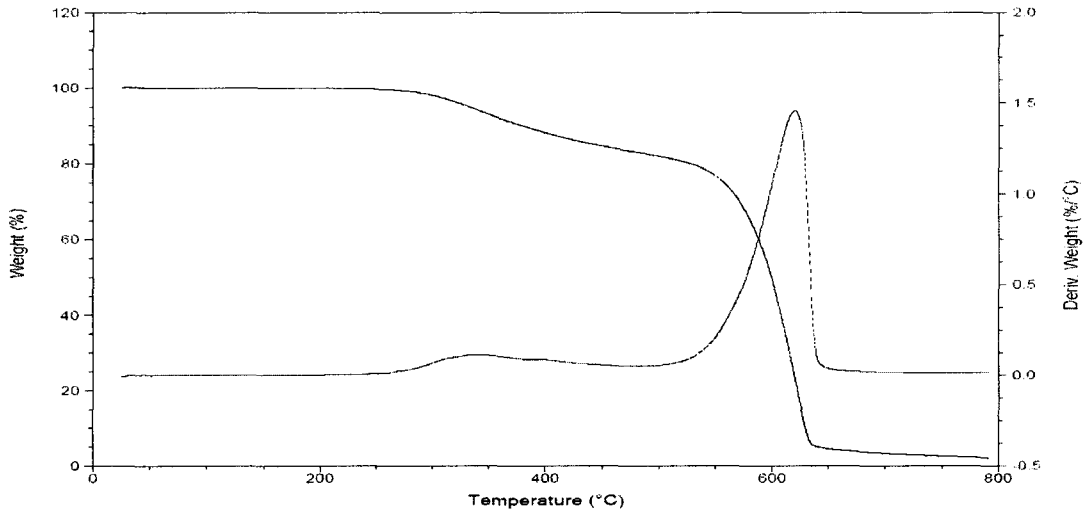

Fig (2.43) TGA, DTGA curves for Ammonium Polyphosphate (AP) alone

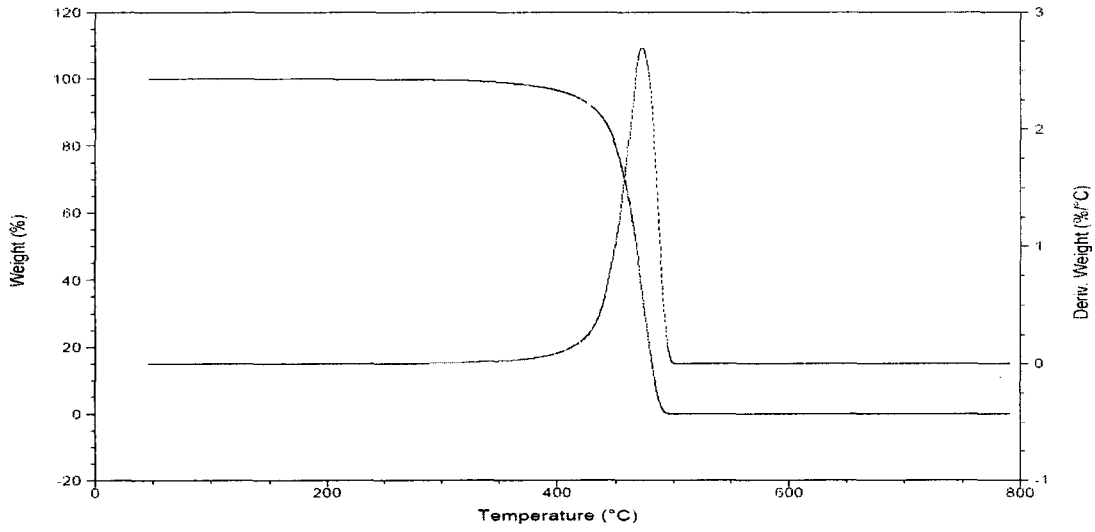

Fig (2.44) TGA, DTGA curves for EPDM alone

So as the phr of CCF increases inside EPDM the insulation efficiency increases with respect to decomposition. This is clear where the remaining weight for sample 1 insulation composition just before 1000 °C is 25 % of the total insulation weight while for sample (5) insulation composition is 38 % of the total insulation weight as shown in Fig (2.41). This is because CCF (stable up to 3445 °C) works as a shield to EPDM.

For ablation resistance of sample (5), its characteristics before and after the test are shown in Table (2.9). The resultant ablation rate (0.01 mm/sec) which corresponds to CCF with 50 phr content is outstanding for rocket motor insulation (as compared to the asbestos based EPDM rate of 0.09 to 0.2 mm/sec). This is due to the CCF content which itself has very high ablation resistance and stability up to 3445 °C. The temperature at the back of the ablation test sample after 60 seconds (317 °C) indicates that the insulation containing CCF is a conductive material. This goes against the requirement of the insulation material to have very low heat conduction.

Sample Number	**EPDM + 50 phr CCF**	
Property	**Before**	**after**
Thickness of the sample (mm)	3	2.39
weight of the sample (gm)	36	35.2
Time (seconds)	60	
Temp. in front of sample (°C)	2010	
Temp. in back of sample (°C)	317	
Ablation rate (mm/sec.)	0.01± 0.0002	
Regular ablation rate [52] (mm/sec.)	0.09-0.2	

Table (2.9) Ablation rate test results for sample (5)

From SEM of sample 5 (50 phr CCF content)[Fig (2.45)], it appears that mixing using C. W. Bra bender permits homogeneous dispersion of CCF in the EPDM polymeric matrix in which most of the chopped carbon fibers are aligned. This homogenous distribution of

CCF inside EPDM improves the performance of EPDM with respect to mechanical properties and ablation resistance while reducing the performance with respect to thermal properties (thermal diffusivity, specific heat capacity, thermal conductivity).

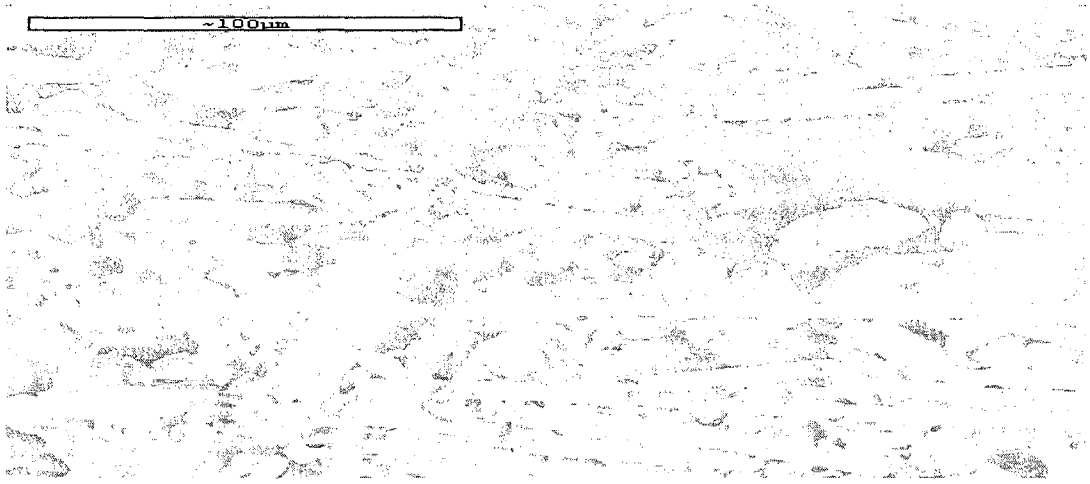

Fig (2.45) SEM photo for sample 5 (50 phr CCF content)

Electrical Resistivity's for the insulation compositions with different CCF phr content are shown in Table (2.10) and Fig (2.46).

Sample No/Composition (phr)	CCF content (phr)	Electrical Resistivity (Ω.cm)
(1) 100 EPDM + 60 AP + CCF + 6 PCA	30	1.8×10^{8}
(2) 100 EPDM + 60 AP + CCF + 6 PCA	35	9.4×10^{7}
(3) 100 EPDM + 60 AP + CCF + 6 PCA	40	4.5×10^{7}
(4) 100 EPDM + 60 AP + CCF + 6 PCA	45	2.2×10^{7}
(5) 100 EPDM + 60 AP + CCF + 6 PCA	50	9.6×10^{6}
Asbestos reinforced EPDM [45]		1×10^{11} to 1×10^{12}

Table (2.10) Electrical resistivity for CCF based samples

It appears that increasing CCF phr content in the material will result in decreasing the Electrical Resistivity of the material. This is due to the higher electrical conductivity of CCF compared to EPDM.

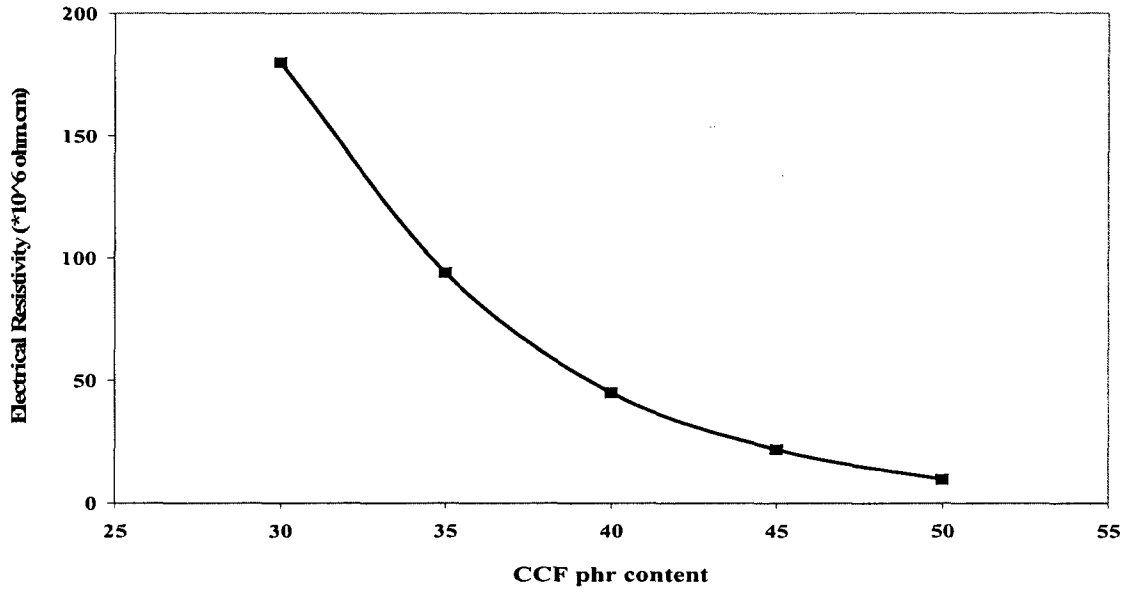

Fig (2.46) Electrical resistivity as a function of CCF phr content

2.5.2 KP based compositions

Different formulations (5 samples) of Kevlar pulp (10- 30 phr) with EPDM polymer were prepared. All the formulations contain 100 phr EPDM, 60 phr AP and 6 phr PCA.

A list of tensile strength and elongation values are shown in Table (2.11) and Fig (2.47).

The values are average for 3 measured samples for every composition with a standard deviation of ± 0.6 MPa and 0.8 % respectively.

Sample No/Composition (phr)	KP content (phr)	Tensile Strength (MPa)	Elongation (%)
(6) 100 EPDM + 60 AP + KP + 6 PCA	10	5.13	31.4
(7) 100 EPDM + 60 AP + KP + 6 PCA	15	6.08	26.9
(8) 100 EPDM + 60 AP + KP + 6 PCA	20	7.19	21.3
(9) 100 EPDM + 60 AP + KP + 6 PCA	25	8.24	15.6
(10) 100 EPDM + 60 AP + KP + 6 PCA	30	9.35	11.7
Asbestos reinforced EPDM [45]		6.55	30

Table (2.11) Tensile Strength & Elongation for KP based samples

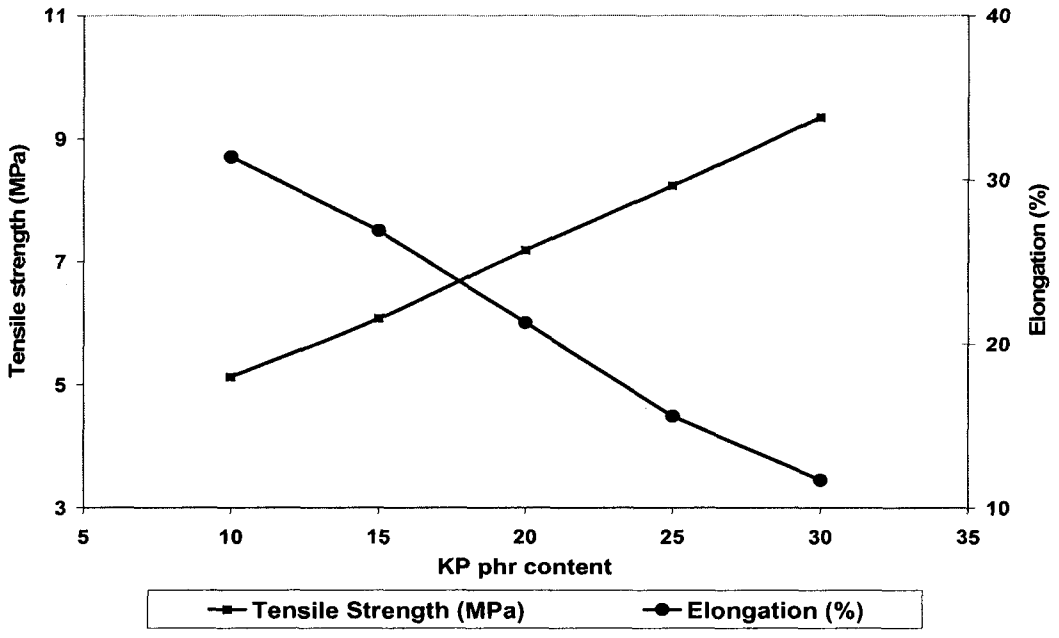

Fig (2.47) Tensile Strength & Elongation as a function of KP phr content

Increasing phr content of KP in EPDM will increase the tensile strength of the material while elongation decreases.

A list of hardness values is shown in Table (2.12) and Fig (2.48). The values are average for 3 measured samples for every composition with a standard deviation of ± 0.3 Shore A. Hardness increases with increasing KP content in EPDM.

Sample No/Composition (phr)	KP content (phr)	Density (g/cm^3)	Hardness (shore A)
(6) 100 EPDM + 60 AP + KP + 6 PCA	10	1.156	87.8
(7) 100 EPDM + 60 AP + KP + 6 PCA	15	1.163	89.9
(8) 100 EPDM + 60 AP + KP + 6 PCA	20	1.171	91.1
(9) 100 EPDM + 60 AP + KP + 6 PCA	25	1.179	92.3
(10) 100 EPDM + 60 AP + KP + 6 PCA	30	1.185	93.4
Asbestos reinforced EPDM [45]		1.205	94.6

Table (2.12) Hardness & Density for KP based samples

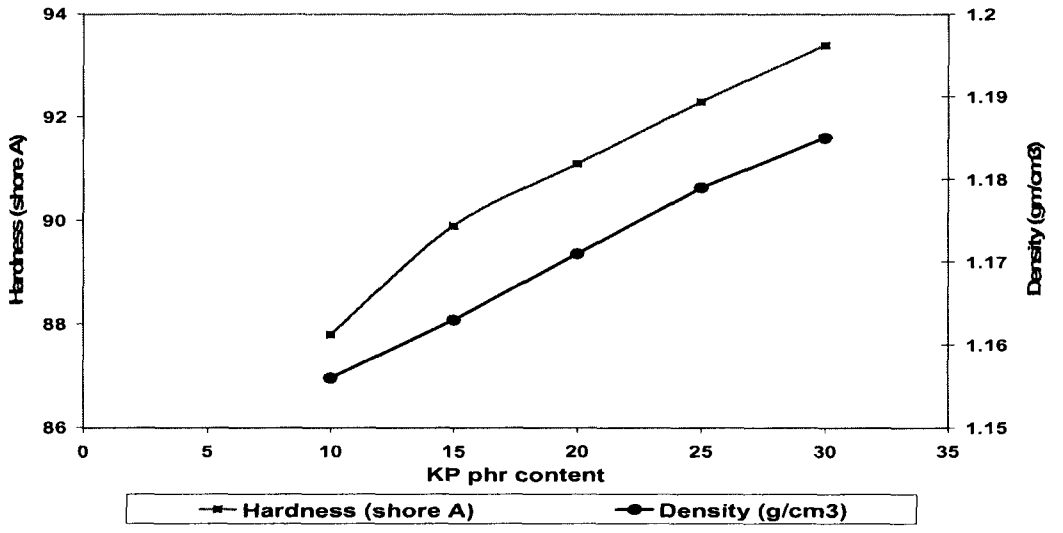

Fig (2.48) Hardness & Density as a function of KP phr content

Density values are shown in Table (2.12) and Fig (2.48). Density increases with increasing KP content. This is because of the higher density of KP (1.44 g/cm^3) as compared to EPDM (0.86 g/cm^3).

Thermal diffusivities for the insulation compositions with different KP phr content at 200 °C are shown in Table (2.13) and Fig (2.49). The values are average for 3 measured samples for every composition with a standard deviation of ± 0.0015 mm^2/s.

Sample No/Composition (phr)	KP content (phr)	Thermal Diffusivity (mm^2/s)	Specific heat Capacity (J/Kg.C)
(6) 100 EPDM + 60 AP + KP + 6 PCA	10	0.111	2302
(7) 100 EPDM + 60 AP + KP + 6 PCA	15	0.103	2179
(8) 100 EPDM + 60 AP + KP + 6 PCA	20	0.096	2053
(9) 100 EPDM + 60 AP + KP + 6 PCA	25	0.088	1919
(10) 100 EPDM + 60 AP + KP + 6 PCA	30	0.081	1778
Asbestos reinforced EPDM [45]		0.12	1674.7

Table (2.13) Thermal diffusivity & specific heat capacity for KP based samples

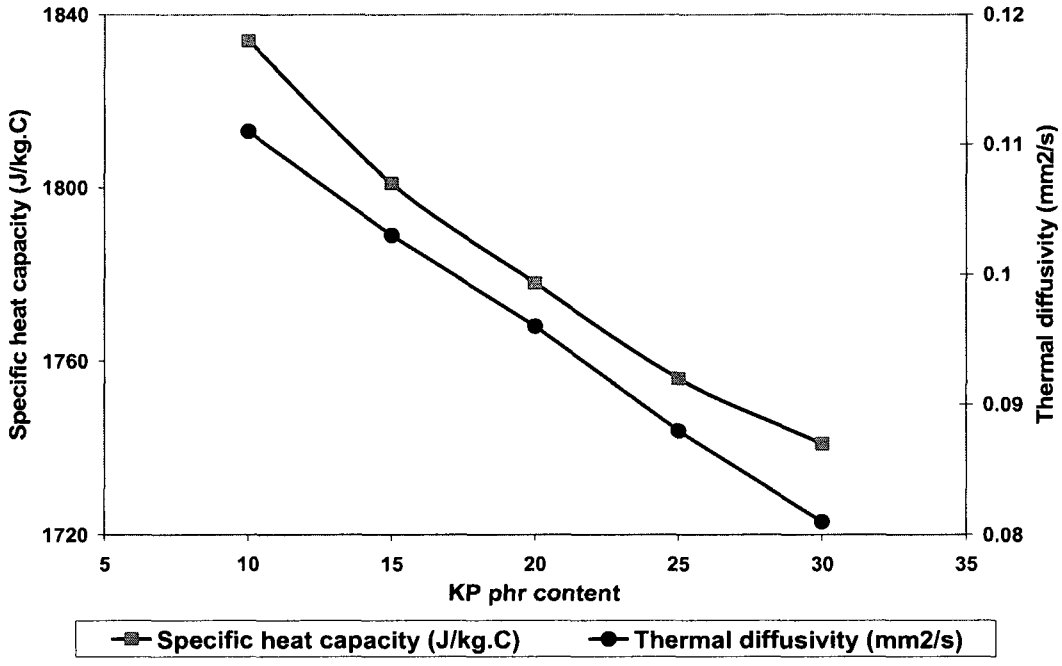

Fig (2.49) Thermal diffusivity and specific heat capacity as a function of KP phr content

DSC curve for sample (10) was selected for representation which represents the final phr content for KP as shown in Fig (2.50). From DSC curves, the relation between the specific heat capacities for every material composition with the temperature is obtained. Specific heat capacities for the different material compositions at 200 °C are shown in Table (2.13) and Fig (2.49). It appears that increasing KP phr content in the material will result in decreasing the specific heat capacity of the material. This is due to the lower specific heat capacity of KP (1420 J/kg.C) (reinforcement) compared to EPDM (the matrix) (2177 J/kg.C).

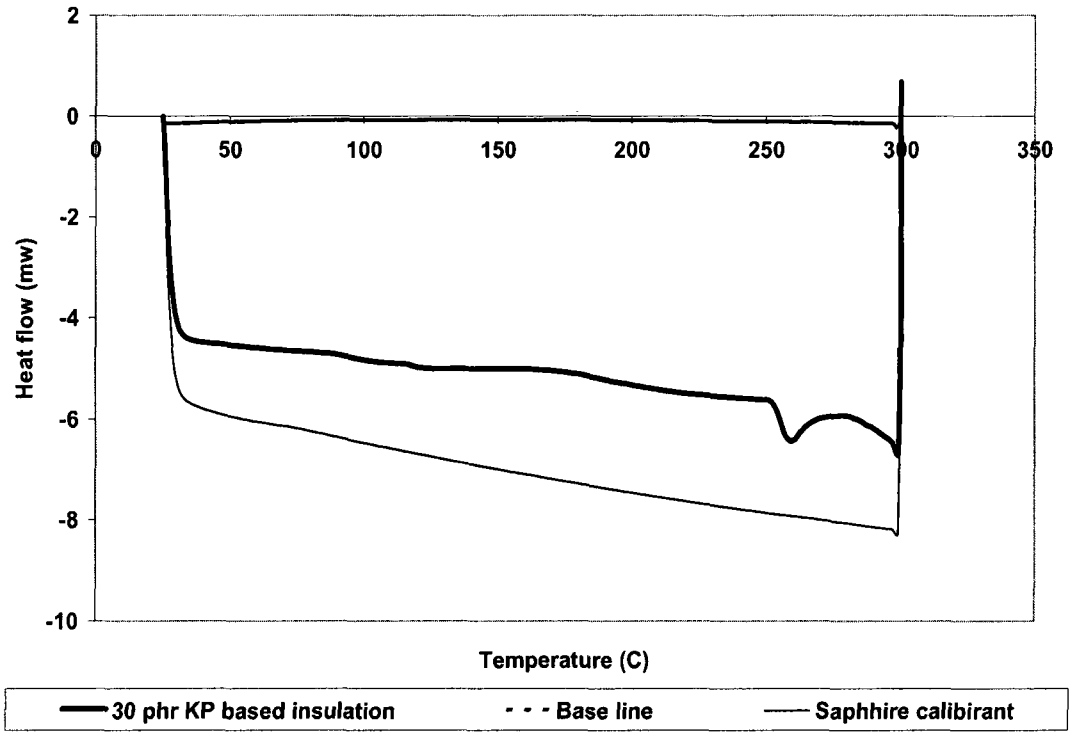

Fig (2.50) DSC curve for insulation composition sample 10 (30 phr KP based EPDM)

Thermal conductivities for the KP based compositions at 200 °C are shown in Table (2.14) and Fig (2.51).

Sample No/Composition (phr)	KP content (phr)	Thermal Conductivity (W/m.C)
(6) 100 EPDM + 60 AP + KP + 6 PCA	10	0.295
(7) 100 EPDM + 60 AP + KP + 6 PCA	15	0.261
(8) 100 EPDM + 60 AP + KP + 6 PCA	20	0.231
(9) 100 EPDM + 60 AP + KP + 6 PCA	25	0.199
(10) 100 EPDM + 60 AP + KP + 6 PCA	30	0.171
Asbestos reinforced EPDM [45]		0.2421

Table (2.14) Thermal conductivity for KP based samples

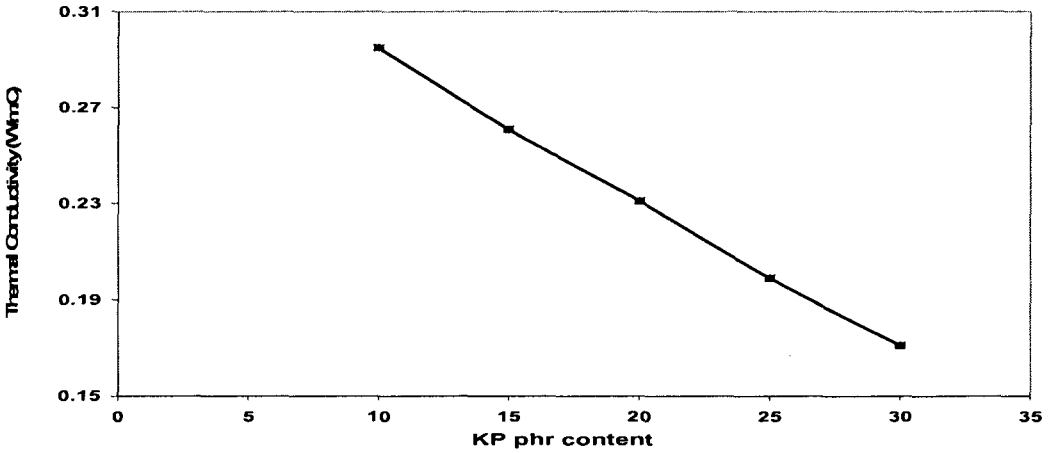

Fig (2.51) Thermal conductivity as a function of KP phr content

It appears that increasing KP phr content in the material will result in decreasing its thermal conductivity. This is due to the lower thermal conductivity of KP (0.04 W/m.K) as compared to EPDM (0.36 W/m.K). This satisfies the requirement of the insulation material to have a very low thermal conductivity.

The resultant TGA curves which relate the weight % for every insulation composition sample with temperature for 10 phr KP and 30 phr KP based samples [samples (6), (10)] [Fig (2.52)].

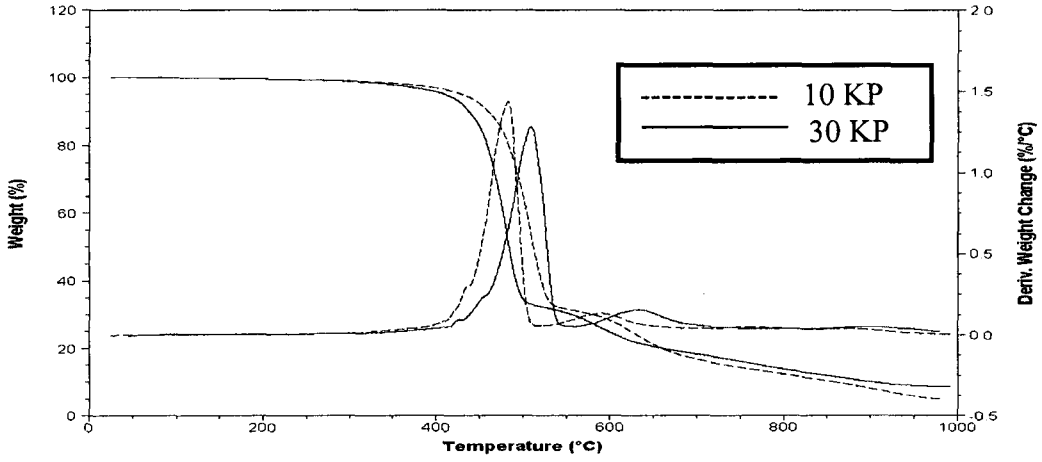

Fig (2.52) TGA, DTGA curves for insulation compositions (6), (10) [10 KP, 30 KP]

The TGA tests indicate for all compositions that an initial decomposition temperature for EPDM (matrix) occurs around 410 °C and the final decomposition is at 547 °C where EPDM decomposes to carbonaceous residue of free carbon. These provide a net effect of strong carbon based char which is highly erosion resistant. Also the tests indicate that an initial decomposition temperature for ammonium polyphosphate (flame retardant agent) occurs around 575 °C and the final decomposition is at 722 °C.

In addition TGA for the individual KP was carried out. The TGA curve for KP is shown in Fig (2.53).

The only stable ingredient above 1000 °C is KP which is stable up to 1450 °C, in addition to the carbon based char remains from decomposition of EPDM. Also not all 100 % of Kevlar pulp will be stable up to 1450 °C since up to 80 % of it decomposes. The remaining 20 % represents carbon based char which is highly erosion resistant. This is shown in Figure (2.53) which represents the TGA curve for KP alone.

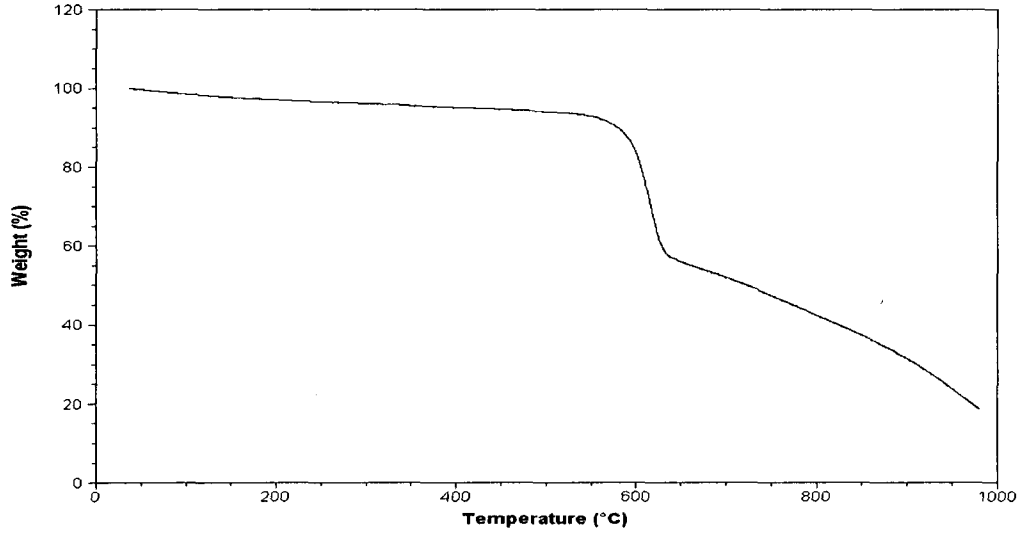

Fig (2.53): TGA curve for KP alone

So as the phr of KP increases, the insulation efficiency increases with respect to decomposition. This is clear where the remaining weight for sample (6) insulation

composition just before 1000 °C is 7 % of the total insulation weight while for sample (10) insulation composition is 9 % of the total insulation weight as shown in Fig (2.52). This is due to KP (stable up to 1450 °C) works as a shield to EPDM.

For ablation resistance of sample (10), its characteristics before and after the test are shown in Table (2.15). The resultant ablation rate (0.015 mm/sec) which corresponds to KP with 30 phr content is outstanding for rocket motor insulation (as compared to the current rate of 0.09 to 0.2 mm/sec). This is due to the KP content which itself has very high ablation resistance and stability up to 1450 °C.

The temperature at the back of the ablation test sample after 60 seconds (79 °C) indicates that the insulation which contains KP is outstanding thermal insulation material. This satisfies the requirement of the insulation material to have very low heat conduction.

Sample Number	**EPDM + 30 phr KP**	
Property	**Before**	**after**
Thickness of the sample (mm)	3	2.12
weight of the sample (gm)	33	29.1
Time (seconds)	60	
Temp. in front of sample (°C)	2010	
Temp. in back of sample (°C)	79	
Ablation rate (mm/sec.)	0.015 ± 0.0003	
Regular ablation rate [52] (mm/sec.)	0.09-0.2	

Table (2.15) Ablation rate test results

For sample 10 (30 phr KP content) [Fig (2.54)], it appears that the mixing using C. W. Bra bender permits homogeneous dispersion of Kevlar pulp in the EPDM polymeric matrix. This homogenous distribution of KP inside EPDM improves the performance of EPDM with respect to mechanical properties and thermal resistance.

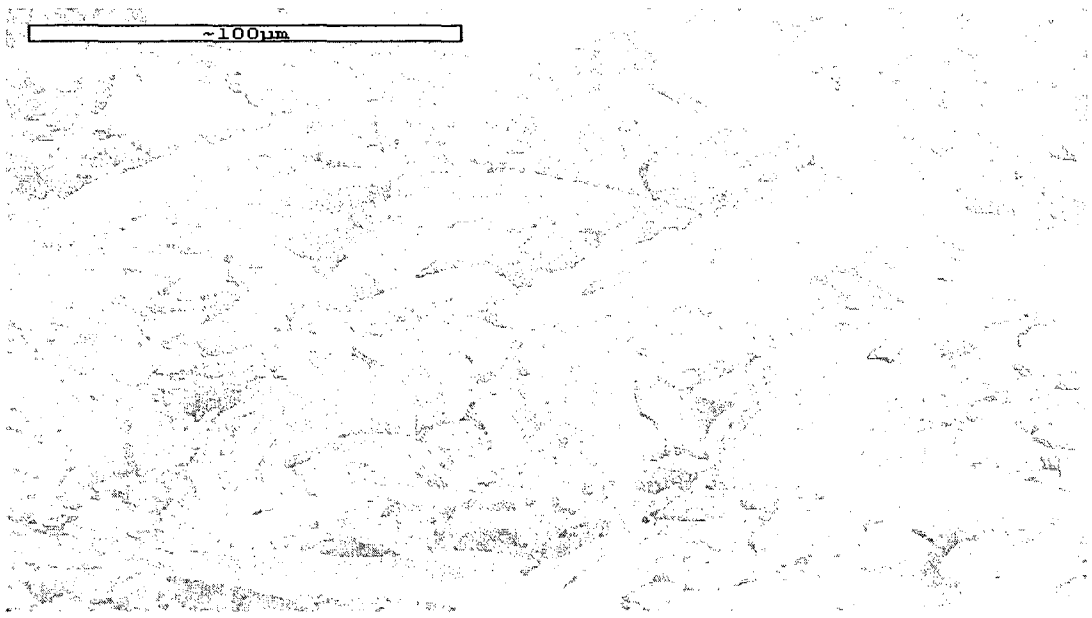

Fig (2.54) SEM photo for sample 10 (30 phr KP content)

Electrical Resistivity's for the insulation compositions with different KP phr content are shown in Table (2.16) and Fig (2.55).

Sample No/Composition (phr)	KP content (phr)	Electrical Resistivity (Ω.cm)
(6) 100 EPDM + 60 AP + KP + 6 PCA	10	2.7×10^{10}
(7) 100 EPDM + 60 AP + KP + 6 PCA	15	9.8×10^{10}
(8) 100 EPDM + 60 AP + KP + 6 PCA	20	2.6×10^{11}
(9) 100 EPDM + 60 AP + KP + 6 PCA	25	4.5×10^{11}
(10) 100 EPDM + 60 AP + KP + 6 PCA	30	9.2×10^{11}
Asbestos reinforced EPDM [45]		1×10^{11} to 1×10^{12}

Table (2.16) Electrical resistivity for KP based samples

It appears that increasing KP phr content in the material will result in increasing the Electrical Resistivity of the material. This is due to the lower electrical conductivity of KP compared to EPDM.

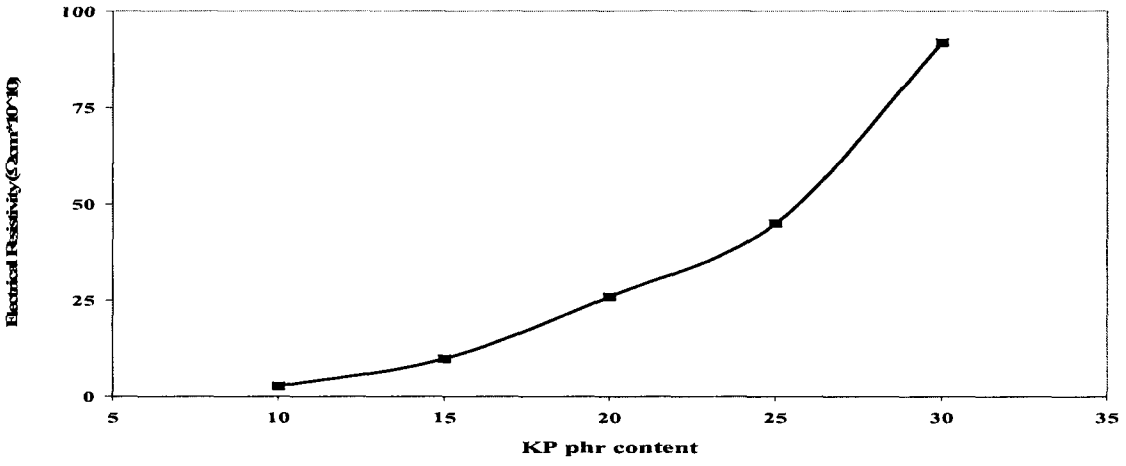

Fig (2.55) Electrical resistivity as a function of KP phr content

2.5.3 CCF + KP based compositions

Different formulations (9 samples) of CCF + KP (10- 50 phr) with EPDM polymer were prepared. All the formulations contain 100 phr EPDM, 60 phr AP and 6 phr PCA

A list of tensile strength and elongation values are shown in Table (2.17) and Fig (2.56). The values are average for 3 measured samples for every composition with a standard deviation of ± 0.4 MPa and 0.7 % respectively.

Sample No/Composition (phr)	Phr		Tensile Strength (MPa)	Elongation (%)
	CCF	KP		
(11) 100 EPDM + 60 AP + CCF + KP + 6 PCA	5	5	3.9	24.9
(12) 100 EPDM + 60 AP + CCF + KP + 6 PCA	7.5	7.5	4.6	22.9
(13) 100 EPDM + 60 AP + CCF + KP + 6 PCA	10	10	5.3	19.4
(14) 100 EPDM + 60 AP + CCF + KP + 6 PCA	12.5	12.5	6.1	17.3
(15) 100 EPDM + 60 AP + CCF + KP + 6 PCA	15	15	6.8	15.5
(16) 100 EPDM + 60 AP + CCF + KP + 6 PCA	17.5	17.5	7.2	12.4
(17) 100 EPDM + 60 AP + CCF + KP + 6 PCA	20	20	8.3	10.2
(18) 100 EPDM + 60 AP + CCF + KP + 6 PCA	22.5	22.5	9.6	8.5
(19) 100 EPDM + 60 AP + CCF + KP + 6 PCA	25	25	11	7.4
Asbestos reinforced EPDM [45]			6.55	30

Table (2.17) Tensile Strength & Elongation for CCF + KP based samples

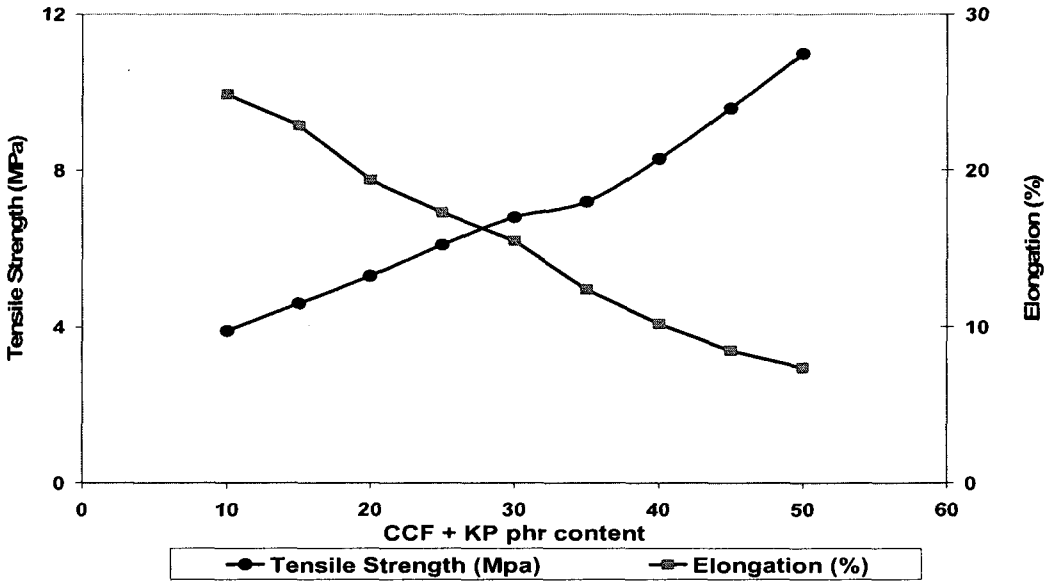

Fig (2.56) Tensile Strength & Elongation as a function of CCF + KP phr content

Increasing phr content of CCF + KP in EPDM will increase the tensile strength of the material while elongation decreases.

A list of hardness values are shown in Table (2.18) and Fig (2.57). The values are average for 3 measured samples for every composition with a standard deviation of ± 0.1 Shore A. Hardness increases with increasing CCF + KP content in EPDM.

Sample No/Composition (phr)	Phr content		Density (g/cm^3)	Hardness (shore A)
	CCF	KP		
(11) 100 EPDM + 60 AP + CCF + KP + 6 PCA	5	5	1.166	86.1
(12) 100 EPDM + 60 AP + CCF + KP + 6 PCA	7.5	7.5	1.181	87.6
(13) 100 EPDM + 60 AP + CCF + KP + 6 PCA	10	10	1.192	88.9
(14) 100 EPDM + 60 AP + CCF + KP + 6 PCA	12.5	12.5	1.203	90.5
(15) 100 EPDM + 60 AP + CCF + KP + 6 PCA	15	15	1.215	91.9
(16) 100 EPDM + 60 AP + CCF + KP + 6 PCA	17.5	17.5	1.225	93.1
(17) 100 EPDM + 60 AP + CCF + KP + 6 PCA	20	20	1.238	94.6
(18) 100 EPDM + 60 AP + CCF + KP + 6 PCA	22.5	22.5	1.246	95.6
(19) 100 EPDM + 60 AP + CCF + KP + 6 PCA	25	25	1.256	96.4
Asbestos reinforced EPDM [45]			1.205	94.6

Table (2.18) Hardness & Density for CCF + KP based samples

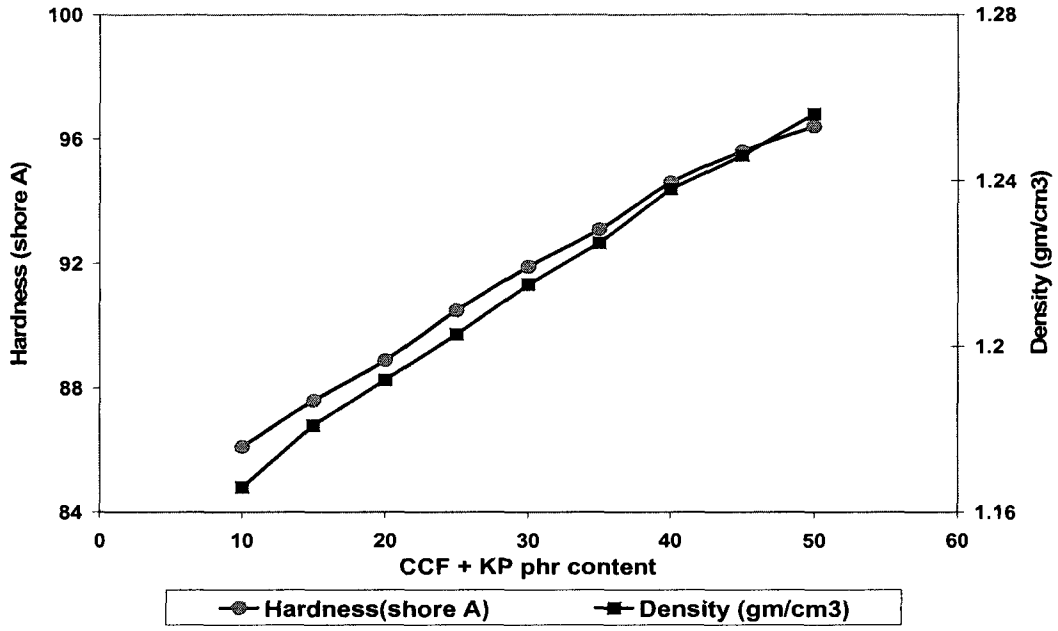

Fig (2.57) Hardness & Density as a function of CCF + KP phr content

A list of density values are shown in Table (2.18) and Fig (2.57). Density increases with increasing CCF content in EPDM. This is because of the higher density of CCF (1.81 g/cm^3) and KP (1.44 g/cm^3) compared to EPDM (0.86 g/cm^3).

Thermal diffusivities for the insulation compositions with different CCF + KP phr content at 200 °C are shown in Table (2.19) and Fig (2.58). The values are average for 3 measured samples for every composition with a standard deviation of ± 0.001.

Sample No/Composition (phr)	Phr content		Thermal Diffusivity (mm^2/s)	Specific heat Capacity (J/Kg.C)
	CCF	KP		
(11) 100 EPDM + 60 AP + CCF + KP + 6 PCA	5	5	0.124	2315
(12) 100 EPDM + 60 AP + CCF + KP + 6 PCA	7.5	7.5	0.117	2271
(13) 100 EPDM + 60 AP + CCF + KP + 6 PCA	10	10	0.11	2254
(14) 100 EPDM + 60 AP + CCF + KP + 6 PCA	12.5	12.5	0.104	2175
(15) 100 EPDM + 60 AP + CCF + KP + 6 PCA	15	15	0.098	2119
(16) 100 EPDM + 60 AP + CCF + KP + 6 PCA	17.5	17.5	0.092	2087
(17) 100 EPDM + 60 AP + CCF + KP + 6 PCA	20	20	0.088	2066
(18) 100 EPDM + 60 AP + CCF + KP + 6 PCA	22.5	22.5	0.083	1999
(19) 100 EPDM + 60 AP + CCF + KP + 6 PCA	25	25	0.08	1973
Asbestos reinforced EPDM [45]			0.12	1674.7

Table (2.19) Thermal diffusivity & specific heat capacity for CCF + KP based samples

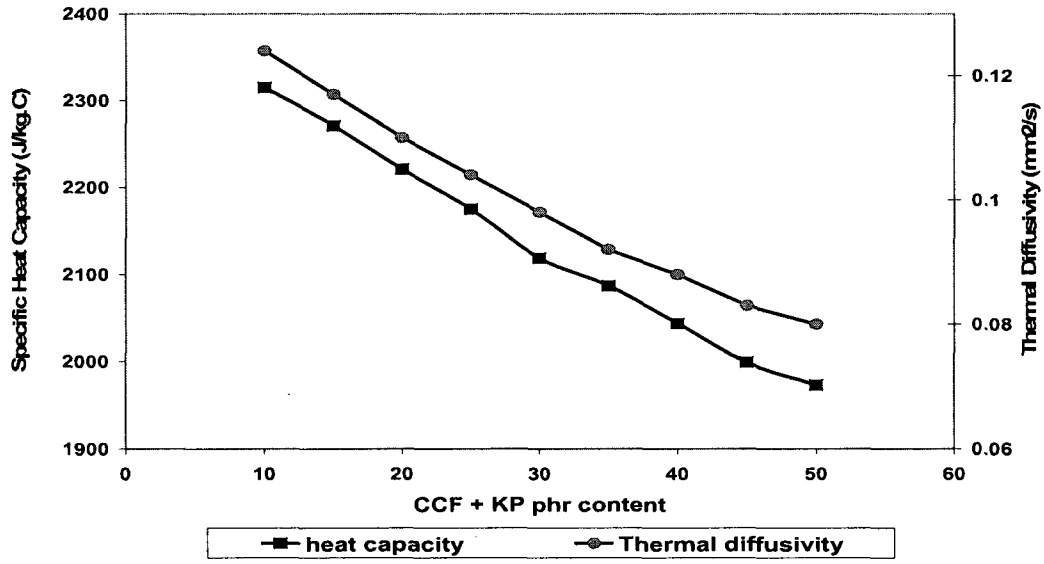

Fig (2.58) Thermal diffusivity and specific heat capacity of the material as a function of CCF + KP phr content

DSC curve for sample (19) was selected for representation which represents the final phr content for CCF + KP as shown in Fig (2.59). Specific heat capacities for the different

material compositions at 200 °C are shown in Table (2.19) and fig (2.58). It appears that increasing CCF + KP phr content in the material will result in decreasing the specific heat capacity of the material. This is due to the lower specific heat capacity of CCF (660 J/kg.C) and KP (1450 J/kg.C) (reinforcement) compared to EPDM (the matrix) (2177 J/kg.C).

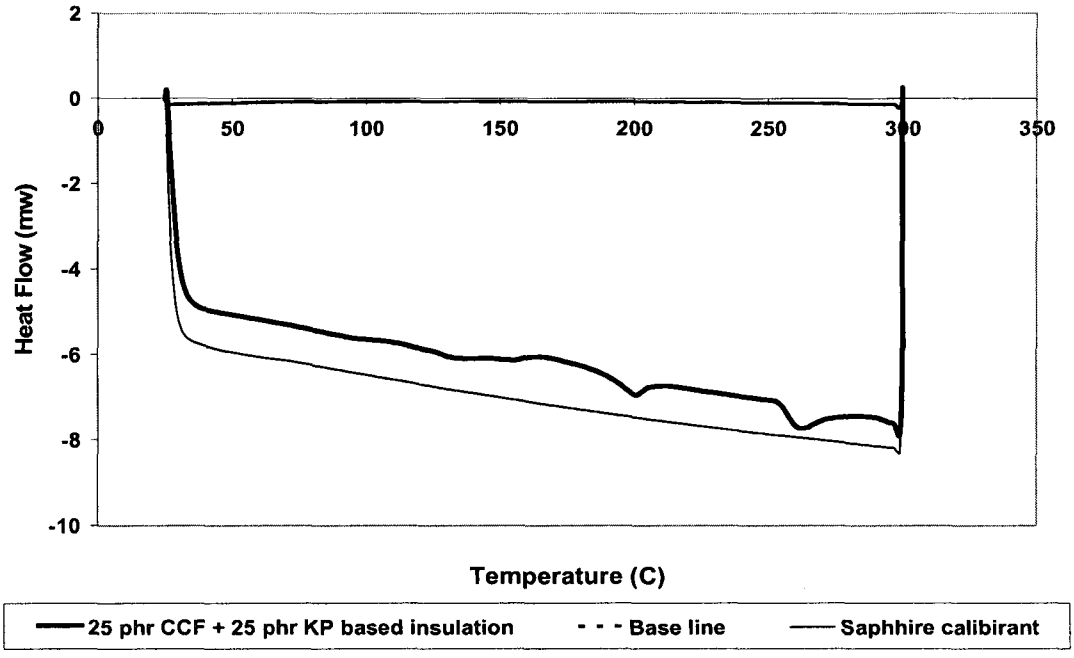

Fig (2.59) DSC curve for insulation composition sample 19 (25 phr KP +25 phr CCF based EPDM)

Thermal conductivities for the CCF + KP based compositions at 200 °C are shown in Table (2.20) and Fig (2.60).

Sample No/Composition (phr)	Phr content		Thermal Conductivity (W/m.C)
	CCF	KP	
(11) 100 EPDM + 60 AP + CCF + KP + 6 PCA	5	5	0.334
(12) 100 EPDM + 60 AP + CCF + KP + 6 PCA	7.5	7.5	0.313
(13) 100 EPDM + 60 AP + CCF + KP + 6 PCA	10	10	0.296
(14) 100 EPDM + 60 AP + CCF + KP + 6 PCA	12.5	12.5	0.271
(15) 100 EPDM + 60 AP + CCF + KP + 6 PCA	15	15	0.252
(16) 100 EPDM + 60 AP + CCF + KP + 6 PCA	17.5	17.5	0.235
(17) 100 EPDM + 60 AP + CCF + KP + 6 PCA	20	20	0.225
(18) 100 EPDM + 60 AP + CCF + KP + 6 PCA	22.5	22.5	0.207
(19) 100 EPDM + 60 AP + CCF + KP + 6 PCA	25	25	0.198
Asbestos reinforced EPDM [45]			0.2421

Table (2.20) Thermal conductivity for CCF + KP based samples

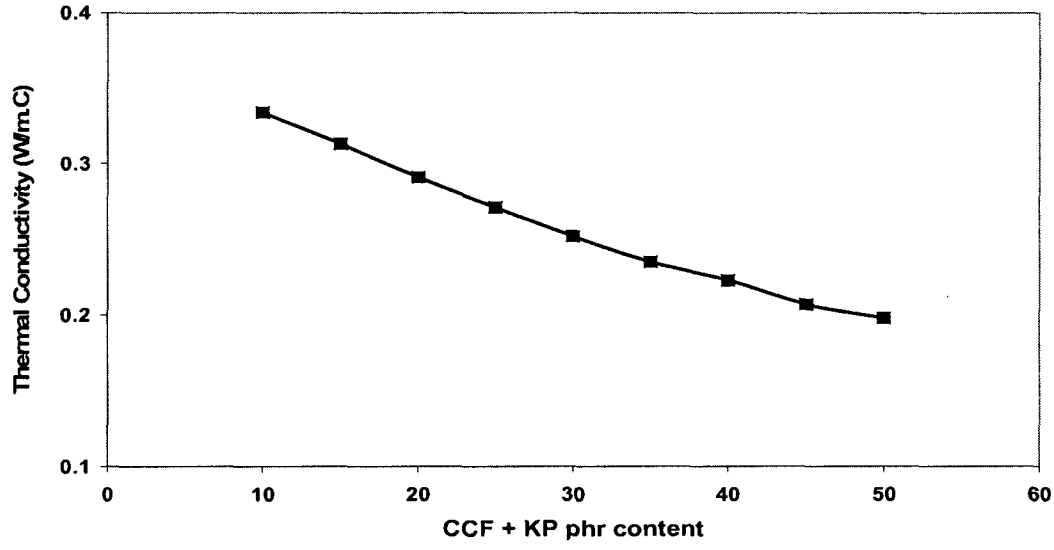

Fig (2.60) Thermal conductivity as a function of CCF + KP phr content

It appears that increasing CCF + KP phr content in the material will result in decreasing the thermal conductivity of the material. This is due to function of KP to serve as an insulation shield around the conductive chains of CCF. This satisfies the requirement of the insulation material to have a very low thermal conductivity.

The resultant TGA curves which relate the weight % for every insulation composition sample with temperature for 5 phr CCF + 5 phr KP and 25 phr CCF + 25 phr KP based samples [samples (11), (19)] [Fig (2.61)].

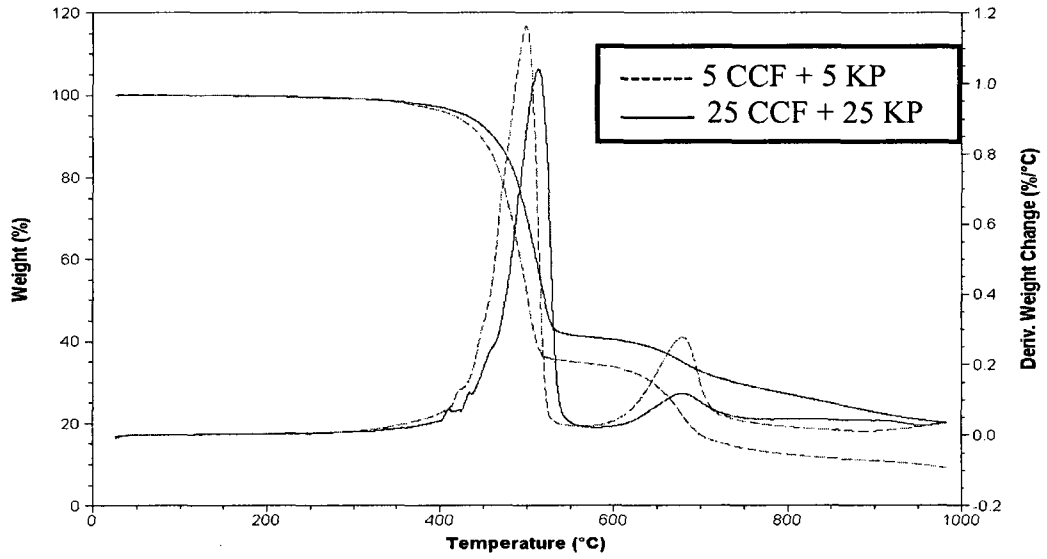

Fig (2.61) TGA, DTGA curves for insulation compositions (11), (19) [5 CCF + 5 KP, 25 CCF + 25 KP]

The TGA tests indicate for all compositions that an initial decomposition temperature for EPDM (matrix) occurs at around 415 °C and the final decomposition is at 551 °C where EPDM decomposes to carbonaceous residue of free carbon. These provide a net effect of strong carbon based char which is highly erosion resistant. Also the tests indicate that an initial decomposition temperature for ammonium polyphosphate (flame retardant agent) occurs at around 575 °C and the final decomposition is at 722 °C.

The only stable ingredients above 1000 °C is CCF and KP which are stable up to 3445°C and 1450°C respectively, in addition to the carbon based char remains from decomposition of EPDM.

So as the phr of CCF + KP increases inside EPDM the insulation efficiency increases with respect to decomposition. This is clear where the remaining weight for sample 11 insulation composition just before 1000 °C is 10 % of the total insulation weight while for sample (19) insulation composition is 23 % of the total insulation weight as shown in fig (2.61). This is due to CCF + KP work as a shield to EPDM.

For ablation resistance of sample (19), its characteristics before and after the test are shown in Table (2.21). The resultant ablation rate (0.005 mm/sec) which corresponds to 25 phr CCF + 25 phr KP content is outstanding for rocket motor insulation (as compared to the current rate of 0.09 to 0.2 mm/sec). This is due to the CCF content which itself has very high ablation resistance and stability up to 3445 °C.

Sample Number	**EPDM + 25 phr CCF + 25 phr KP**	
Property	**Before**	**after**
Thickness of the sample (mm)	3	2.71
weight of the sample (gm)	36	35.4
Time (seconds)	60	
Temp. in front of sample (°C)	2010	
Temp. in back of sample (°C)	82	
Ablation rate (mm/sec.)	0.005 ± 0.0001	
Regular ablation rate [52] (mm/sec.)	0.09-0.2	

Table (2.21) Ablation rate test results for sample (19) [25 CCF + 25 KP based]

The temperature at the back of the ablation test sample after 60 seconds (82 °C) indicates that the insulation which contains CCF + KP is a nonconductive material. This satisfies the requirement of the insulation material to have very low heat conduction.

For sample 19 (25 phr CCF + 25 phr KP), it appears that mixing using C. W. Bra bender mixer permits homogeneous dispersion of chopped carbon fibers and Kevlar pulp in the EPDM polymeric matrix. This homogenous distribution of CCF and KP inside EPDM

improves the performance of EPDM with respect to mechanical, thermal and ablative properties. KP with lower density (1.44 gm / cm^3) [i.e. higher volume material] works as insulation shield around the conductive chains of CCF with higher density (1.81 gm / cm^3) [i.e. lower volume material] as shown in Fig (2.62) where the CCF is totally impeded inside KP and cannot be seen.

Fig (2.62) SEM photo for sample 19 (25 phr CCF + 25 phr KP content)

Electrical Resistivity's for the insulation compositions with different CCF + KP phr content are shown in Table (2.22) and Fig (2.63).

It appears that increasing CCF + KP phr content in the material will result in decreasing the Electrical Resistivity of the material. This is due to the higher electrical conductivity of CCF compared to KP and EPDM.

Sample No/Composition (phr)	Phr content		Electrical Resistivity (Ω.cm)
	CCF	KP	
(11) 100 EPDM + 60 AP + CCF + KP + 6 PCA	5	5	7.2×10^8
(12) 100 EPDM + 60 AP + CCF + KP + 6 PCA	7.5	7.5	3.1×10^8
(13) 100 EPDM + 60 AP + CCF + KP + 6 PCA	10	10	1.1×10^8
(14) 100 EPDM + 60 AP + CCF + KP + 6 PCA	12.5	12.5	5.7×10^7
(15) 100 EPDM + 60 AP + CCF + KP + 6 PCA	15	15	3.1×10^7
(16) 100 EPDM + 60 AP + CCF + KP + 6 PCA	17.5	17.5	1.7×10^7
(17) 100 EPDM + 60 AP + CCF + KP + 6 PCA	20	20	0.9×10^7
(18) 100 EPDM + 60 AP + CCF + KP + 6 PCA	22.5	22.5	4.8×10^6
(19) 100 EPDM + 60 AP + CCF + KP + 6 PCA	25	25	2.8×10^6
Asbestos reinforced EPDM [45]			1×10^{11} to 1×10^{12}

Table (2.22) Electrical resistivity for CCF + KP based samples

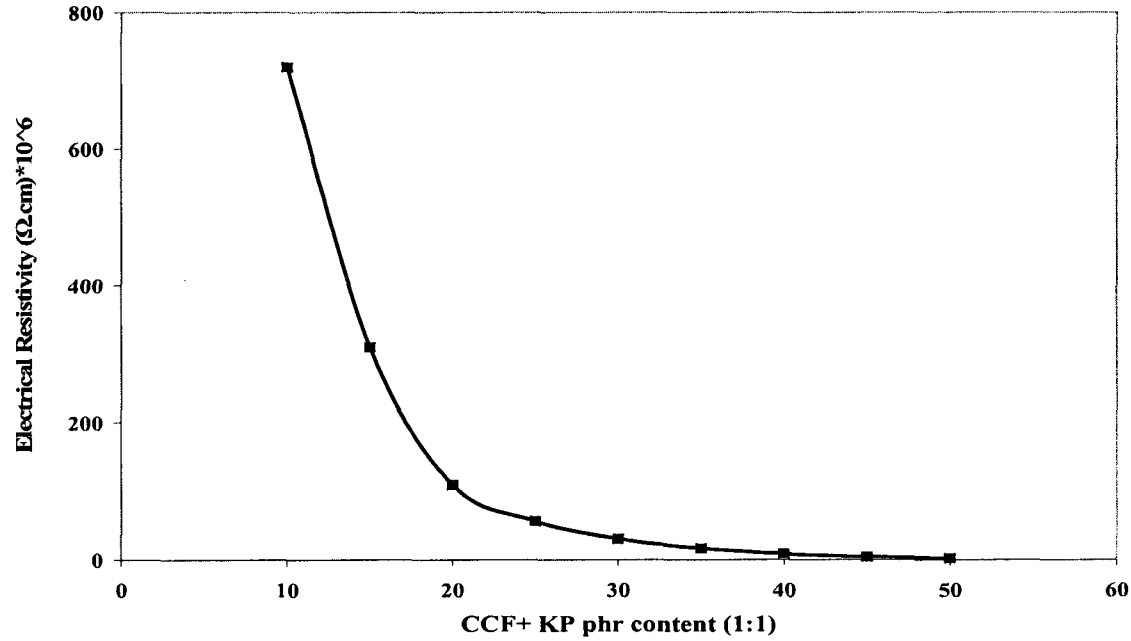

Fig (2.63) Electrical resistivity as a function of CCF + KP phr content

2.5.4 Optimization of CCF + KP based compositions

Different formulations (8 samples) of CCF + KP (50 phr) with EPDM polymer were prepared. All the formulations contain 100 phr EPDM, 60 phr AP, 50 phr reinforcements (CCF + KP) and 6 phr PCA.

A list of tensile strength and elongation values are shown in Table (2.23) and Fig (2.64). The values are average for 3 measured samples for every composition with a standard deviation of ± 0.3 MPa and 0.4 % respectively.

Sample No/Composition (phr)	Phr		Tensile Strength (MPa)	Elong. (%)
	CCF	KP		
(20) 100 EPDM + 60 AP + CCF + KP + 6 PCA	5	45	6.1	5.4
(21) 100 EPDM + 60 AP + CCF + KP + 6 PCA	10	40	6.4	5.9
(22) 100 EPDM + 60 AP + CCF + KP + 6 PCA	15	35	7.9	6.5
(23) 100 EPDM + 60 AP + CCF + KP + 6 PCA	20	30	10.5	7
(24) 100 EPDM + 60 AP + CCF + KP + 6 PCA	30	20	9.9	9.2
(25) 100 EPDM + 60 AP + CCF + KP + 6 PCA	35	15	8.1	9.9
(26) 100 EPDM + 60 AP + CCF + KP + 6 PCA	40	10	6.9	10.8
(27) 100 EPDM + 60 AP + CCF + KP + 6 PCA	45	5	5.8	11.1
Asbestos reinforced EPDM [45]			6.55	30

Table (2.23) Tensile Strength & Elongation for CCF + KP based samples

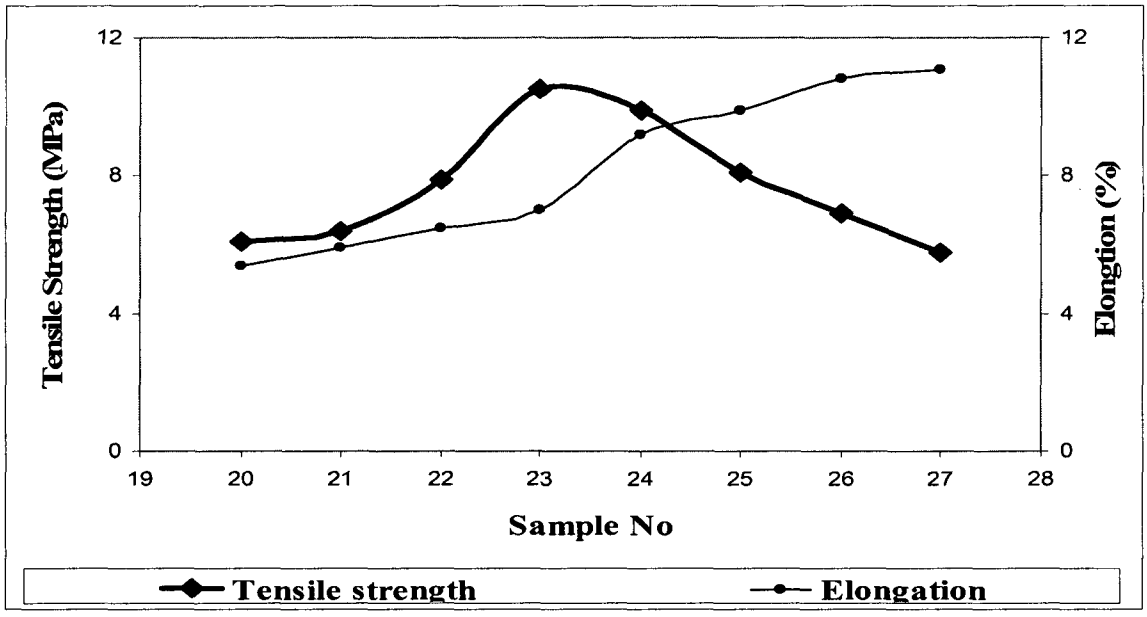

Fig (2.64) Tensile Strength & Elongation as a function of CCF + KP phr content

Increasing phr content of KP over 30 in EPDM inside the hybrid (decreasing CCF phr content) (CCF + KP = 50) will decrease the tensile strength of the material. This is due to the very high surface area of KP (7-10 m^2/gm) where over 30 phr of KP not all the fibers are wetted by the matrix during the mixing resulting in the decrease in tensile strength. While the elongation will increase with increasing the CCF phr content inside the hybrid (decreasing KP phr content).

A list of hardness values are shown in Table (2.24) and Fig (2.65). The values are average for 3 measured samples for every composition with a standard deviation of ± 0.1 Shore A. Hardness increases with increasing KP content inside the hybrid (decreasing CCF phr content) (CCF + KP = 50).

Sample No/Composition (phr)	Phr		Density (g/cm^3)	Hardness (shore A)
	CCF	KP		
(20) 100 EPDM + 60 AP + CCF + KP + 6 PCA	5	45	1.218	99.7
(21) 100 EPDM + 60 AP + CCF + KP + 6 PCA	10	40	1.227	99.1
(22) 100 EPDM + 60 AP + CCF + KP + 6 PCA	15	35	1.235	98.3
(23) 100 EPDM + 60 AP + CCF + KP + 6 PCA	20	30	1.244	97.7
(24) 100 EPDM + 60 AP + CCF + KP + 6 PCA	30	20	1.262	94.9
(25) 100 EPDM + 60 AP + CCF + KP + 6 PCA	35	15	1.271	93
(26) 100 EPDM + 60 AP + CCF + KP + 6 PCA	40	10	1.279	90.8
(27) 100 EPDM + 60 AP + CCF + KP + 6 PCA	45	5	1.288	88.6
Asbestos reinforced EPDM [45]			1.205	94.6

Table (2.24) Hardness & Density for CCF + KP based samples

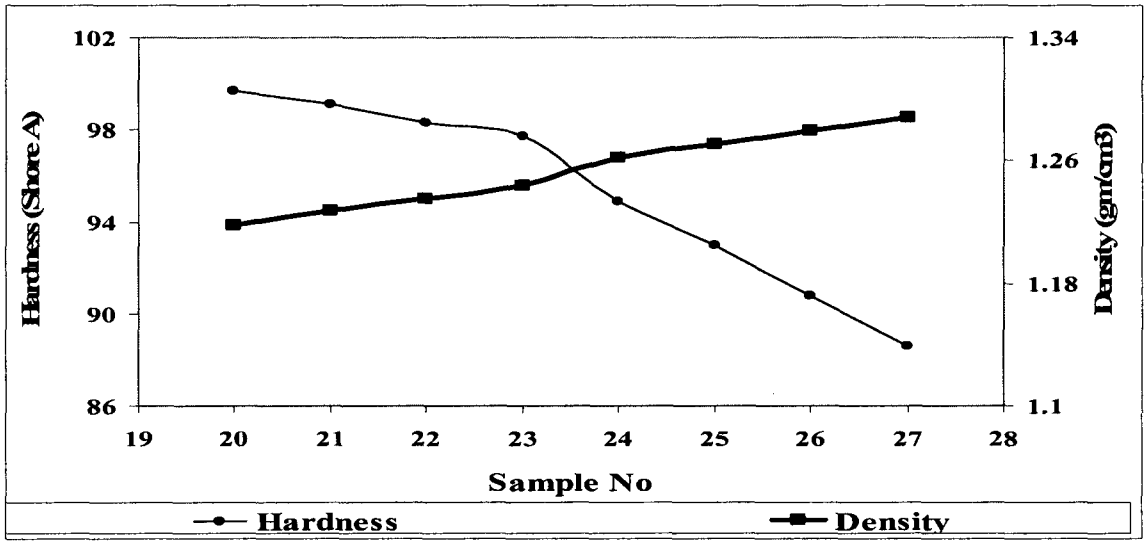

Fig (2.65) Hardness & Density as a function of CCF + KP phr content

Density values are shown in Table (2.24) and Fig (2.65). Density increases by increasing CCF content inside the hybrid (decreasing KP phr content) (CCF + KP = 50). This is because of the higher density of CCF (1.81 g/cm^3) compared to EPDM (0.86 g/cm^3) and KP (1.44 g/cm^3).

Thermal diffusivities for the insulation compositions with different CCF + KP phr content at 200 °C are shown in Table (2.25) and Fig (2.66). The values are average for 3 measured samples for every composition with a standard deviation of ± 0.0015 mm^2/s.

Sample No/Composition (phr)	Phr		Thermal Diffusiv. (mm^2/s)	Specific heat Capacity (J/Kg.C)
	CCF	KP		
(20) 100 EPDM + 60 AP + CCF + KP + 6 PCA	5	45	0.05	2151
(21) 100 EPDM + 60 AP + CCF + KP + 6 PCA	10	40	0.056	2096
(22) 100 EPDM + 60 AP + CCF + KP + 6 PCA	15	35	0.063	2056
(23) 100 EPDM + 60 AP + CCF + KP + 6 PCA	20	30	0.071	2027
(24) 100 EPDM + 60 AP + CCF + KP + 6 PCA	30	20	0.108	1731
(25) 100 EPDM + 60 AP + CCF + KP + 6 PCA	35	15	0.143	1662
(26) 100 EPDM + 60 AP + CCF + KP + 6 PCA	40	10	0.176	1639
(27) 100 EPDM + 60 AP + CCF + KP + 6 PCA	45	5	0.208	1619
Asbestos reinforced EPDM [45]			0.12	1674.7

Table (2.25) Thermal diffusivity & sp. heat capacity for CCF + KP based samples

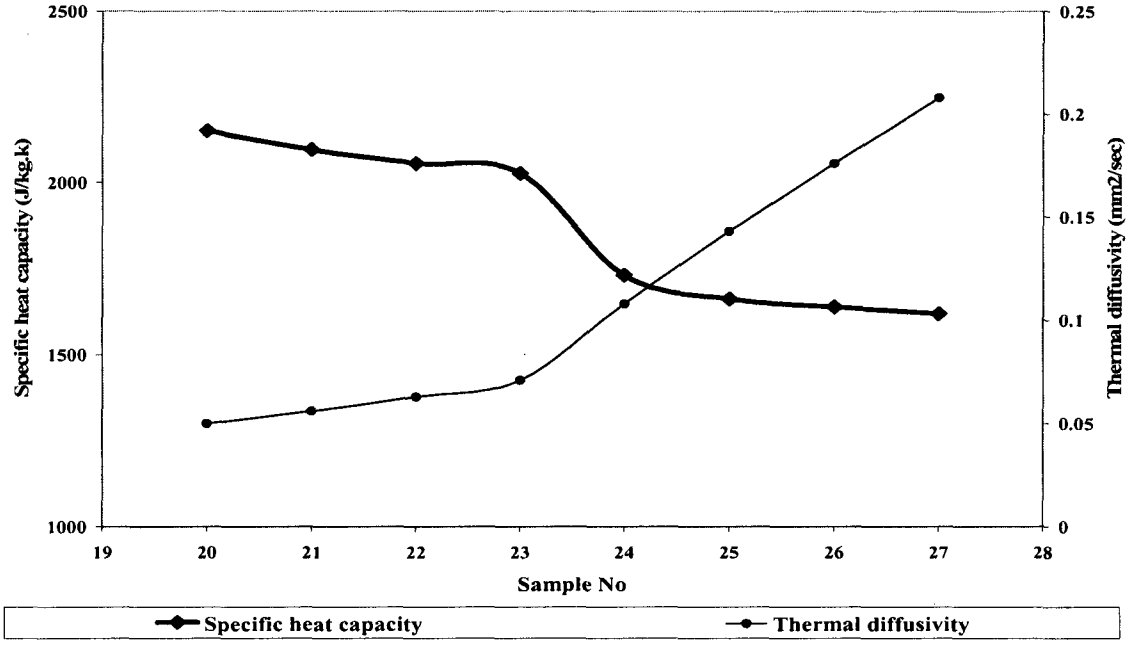

Fig (2.66) Thermal diffusivity and specific heat capacity of the material as a function of CCF + KP phr content

Specific heat capacities for the different material compositions at 200 °C are shown in Table (2.25) and Fig (2.66). It appears that increasing CCF content inside the hybrid (decreasing KP phr content) (CCF + KP = 50) in the material will result in decreasing the specific heat capacity of the material. This is due to the lower specific heat capacity of CCF (660 J/kg.C) compared to KP (1450 J/kg.C) (reinforcement) and EPDM (the matrix) (2177 J/kg.C).

Thermal conductivities for the CCF + KP based compositions at 200 °C are shown in Table (2.26) and Fig (2.67).

Sample No/Composition (phr)	Phr		Thermal Conductivity (W/m.C)
	CCF	KP	
(20) 100 EPDM + 60 AP + CCF + KP + 6 PCA	5	45	0.131
(21) 100 EPDM + 60 AP + CCF + KP + 6 PCA	10	40	0.144
(22) 100 EPDM + 60 AP + CCF + KP + 6 PCA	15	35	0.16
(23) 100 EPDM + 60 AP + CCF + KP + 6 PCA	20	30	0.179
(24) 100 EPDM + 60 AP + CCF + KP + 6 PCA	30	20	0.236
(25) 100 EPDM + 60 AP + CCF + KP + 6 PCA	35	15	0.302
(26) 100 EPDM + 60 AP + CCF + KP + 6 PCA	40	10	0.369
(27) 100 EPDM + 60 AP + CCF + KP + 6 PCA	45	5	0.434
Asbestos reinforced EPDM [45]			0.2421

Table (2.26) Thermal conductivity for CCF + KP based samples

It appears that increasing CCF content inside the hybrid (decreasing KP phr content) (CCF + KP = 50) in the material will result in increasing the thermal conductivity of the material. This is due to the higher thermal conductivity of CCF (6.4 W/m.K) compared to KP (0.04 W/m.K).

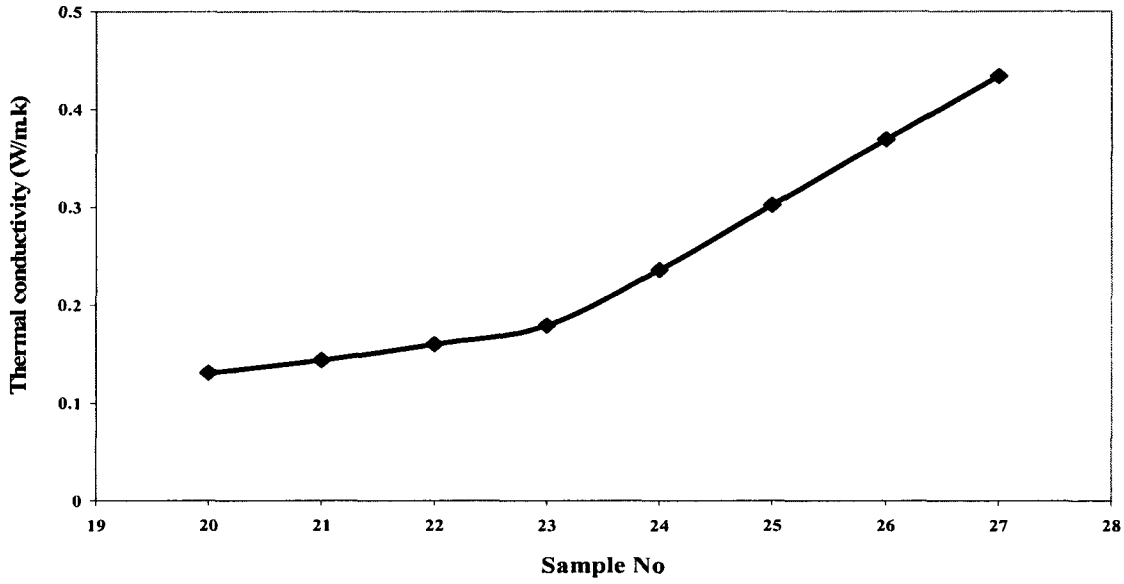

Fig (2.67) Thermal conductivity as a function of CCF + KP phr content

The resultant TGA curves which relate the weight % for every insulation composition sample with temperature for 5 phr CCF + 45 phr KP and 45 phr CCF + 5 phr KP based samples [samples (20), (27)] are shown in Fig (2.68) and Fig (2.69) respectively.

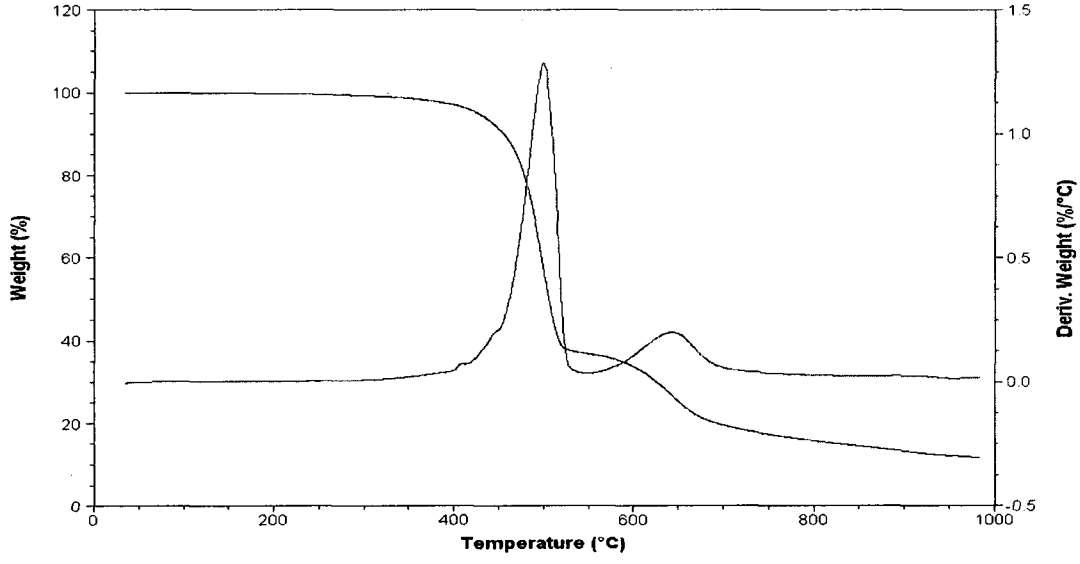

Fig (2.68) TGA, DTGA curves for 5 CCF + 45 KP based insulation [sample (20)]

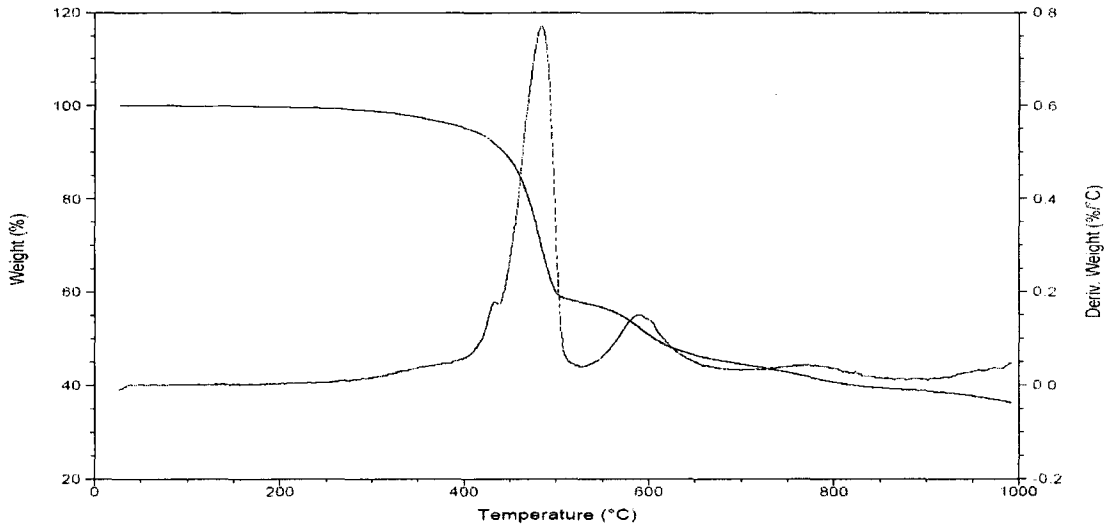

Fig (2.69) TGA, DTGA curves for 45 CCF + 5 KP based insulation [sample (27)]

The TGA tests indicate for all compositions that an initial decomposition temperature for EPDM (matrix) occurs around 411 °C and the final decomposition is at 549 °C where EPDM decomposes to carbonaceous residue of free carbon. These provide a net effect of strong carbon based char which is highly erosion resistant. Also the tests indicate that an initial decomposition temperature for ammonium polyphosphate (flame retardant agent) occurs around 577 °C and the final decomposition is at 725 °C.

The only stable ingredients above 1000 °C is CCF and KP which are stable up to 3445°C and 1450°C respectively, in addition to the carbon based char remains from decomposition of EPDM.

So CCF content increases inside the hybrid (decreasing KP phr content) (CCF + KP = 50) inside EPDM will result in the insulation efficiency increases with respect to decomposition. This is clear where the remaining weight for sample 20 (5 phr CCF + 45 phr KP based insulation) just before 1000 °C is 15 % of the total insulation weight as shown in Fig (2.68) while for sample (27) (45 phr CCF + 5 phr KP based insulation)

insulation composition is 36 % of the total insulation weight as shown in Fig (2.69). This is because CCF is more stable than KP with respect to decomposition.

As a conclusion, it appears that as CCF content increases [inside the hybrid (decreasing KP phr content) (CCF + KP = 50)] inside EPDM there will be improvement in the performance of EPDM as solid rocket motor insulation with respect to decomposition and ablation resistance while reduce the performance of EPDM as solid rocket motor insulation with respect to thermal (thermal diffusivity and specific heat capacity) and mechanical properties.

2.5.5 Comparison

Comparison between the best composition in every class of materials is done. For CCF based compositions, the best composition for the whole measured physical, mechanical, thermal and ablative properties is 50 phr CCF based EPDM.

For KP based compositions, the best composition in the whole measured physical, mechanical, thermal and ablative properties is 30 phr KP based EPDM.

For CCF + KP based compositions, the best composition for the whole measured physical, mechanical, thermal and ablative properties is 25 phr CCF + 25 phr KP based EPDM.

A comparison between these 3 samples in the physical and mechanical properties is shown in Fig (2.70).

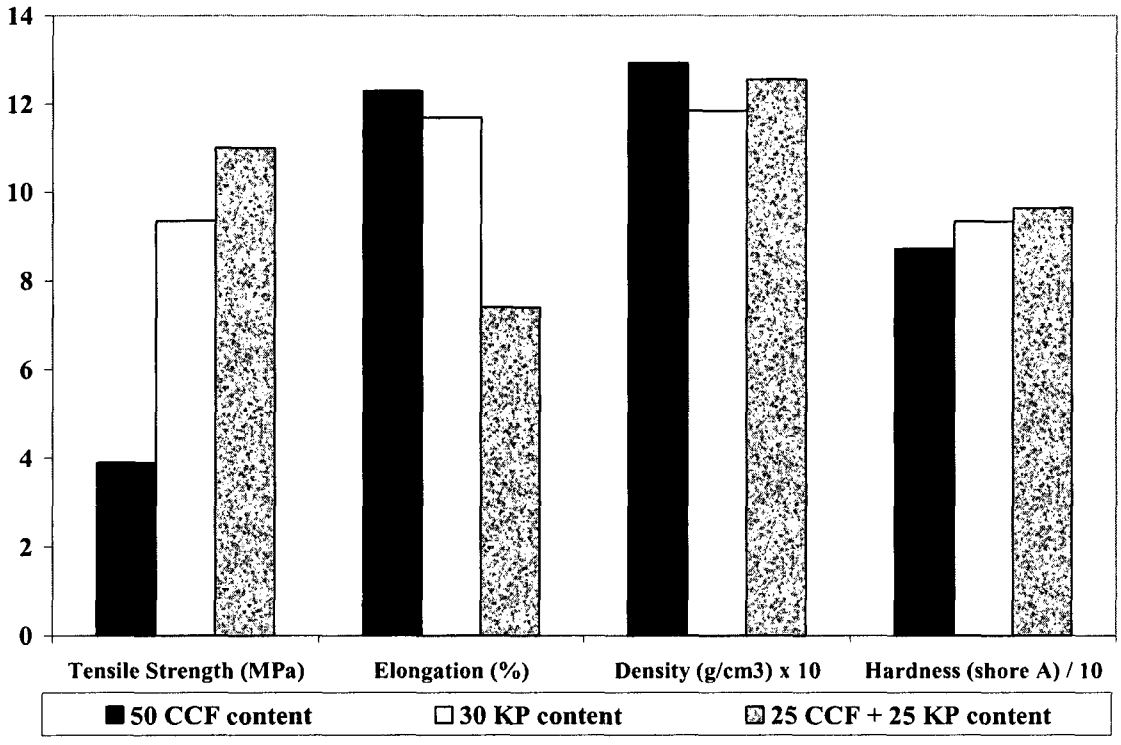

Fig (2.70) Physical and mechanical properties comparison

It appears that the best composition in tensile strength as solid rocket motor application is 25 phr CCF + 25 phr KP based EPDM. And the best composition in elongation and hardness as solid rocket motor application is 50 phr CCF based EPDM. Also the best composition in density as solid rocket motor application is 30 phr KP based EPDM as shown in Fig (2.70).

A comparison between these 3 samples in the thermal and ablative properties is shown in Fig (2.71).

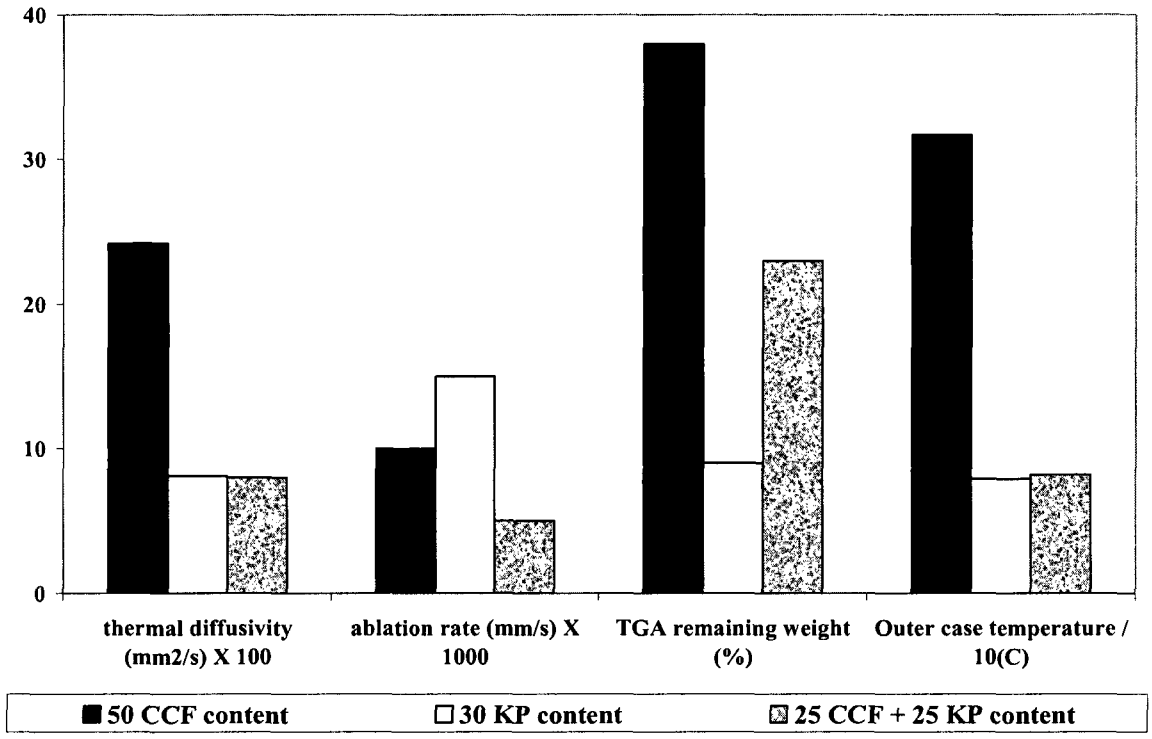

Fig (2.71) Thermal and ablative properties comparison

It appears that the best composition in thermal diffusivity and ablation rate is 25 phr CCF + 25 phr KP based EPDM. And the best composition in TGA remaining weight at 1000 °C is 50 phr CCF based EPDM. And the best composition in the outer case temperature is 30 phr KP based EPDM as shown in Fig (2.71).

Table (2.27) shows the priorities for physical, mechanical, thermal and ablative properties as solid rocket motor application.

Taking into consideration the priority of the properties, 25 phr CCF + 25 phr KP based EPDM shows the best performance (physical, mechanical, thermal and ablative properties) as solid rocket motor application.

property	priority
Outer case temperature	1
Ablation rate	2
TGA remaining weight	3
Density	4
Thermal diffusivity	5
Tensile strength	6
Elongation	7
Hardness	8

Table (2.27) The priorities of the physical, mechanical, thermal and ablative properties in application

Chapter 3

Thermal Conduction Modeling

3.1 Analytical calculations

The thermal conductivity of any material can be calculated using the relation:

$$K = \rho \, . \, \alpha \, . \, C_p \qquad (3.1)$$

Where K, ρ, α and C_p are the thermal conductivity, density, thermal diffusivity and heat capacity of the material respectively.

Modeling the effective thermal conductivity of heterogeneous or composite materials is of interest in many heat transfer applications. A substantial number of effective thermal conductivity models [90-92] has been proposed, some of which have been intended for highly specific applications, while others have wider applicability. A question arises on how good is the agreement with data coming from experimental measurements.

A heterogeneous material's effective thermal conductivity is strongly affected by its composition and structure. And, as yet, there does not appear to be any single model equation that is applicable to all types of structure. Instead, a common approach has been used to develop a set of equations based on a conceptual 'parent' model that is modified to varying extents to account for variations in composition and structure. Another common way of estimating effective thermal conductivity for composite materials with known microstructures is to make rigorous numerical simulations using the finite difference or finite element methods. However, analytical models are preferred over numerical models in many applications due to their ability to show relations, rapid and

low cost of calculation, and reasonable accuracy even when the microstructure is uncertain.

Many (if not most) effective thermal conductivity models found in the literature are based on one or more of four basic structural models; specifically, the Series, Parallel, Maxwell–Eucken and Effective Medium Theory (EMT) models. According to the present concepts, any effective property of filled polymer composites is defined by partial properties of individual components and the volume fraction of the dispersed phase. Ideal adhesion contact between the phases (filler and polymer) is assumed. On the basis of such assumption, equations have been obtained to define the effective thermal conduction of a filled polymer composite.

A unifying equation for the four fundamental effective thermal conductivity structural models (Series, Parallel, Maxwell–Eucken and Effective Medium Theory) is [93-99]:

$$K = \frac{\sum_{i=1}^{m} k_i v_i \frac{d_i \bar{k}}{(d_i - 1)\bar{k} + k_i}}{\sum_{i=1}^{m} v_i \frac{d_i \bar{k}}{(d_i - 1)\bar{k} + k_i}} \qquad (3.2)$$

Where

d_i configuration factor

k_i thermal conductivity of a component (W m^{-1} C^{-1})

K effective thermal conductivity of the material (W m^{-1} C^{-1})

m number of components inside composite material

v_i volume fraction of a component i

The physical structures assumed in the derivations of the Series and Parallel models consist of layers of the components aligned either perpendicular or parallel to the heat flow, as indicated in Fig (3.1) (a), (b) respectively.

Series model is obtained from equation (3.2) by substituting $d_i = 1$ or $\bar{k} \to 0$. We can evaluate the effective thermal conductivity for multiphase composite as shown in formula (3.3).

$$K = \frac{1}{\sum_{i=1}^{m} \frac{v_i}{k_i}} \tag{3.3}$$

Where parallel model is obtained from equation (3.2) by substituting $d_i \to \infty$ or $\bar{k} = k_i$. We can evaluate the effective thermal conductivity for multiphase composite as shown in formula (3.4).

$$K = \sum_{i=1}^{m} k_i v_i \tag{3.4}$$

The Maxwell–Eucken model assumes a dispersion of small spheres within a continuous matrix of a different component, with the spheres being far enough apart such that the local distortions to the temperature distributions around each of the spheres do not interfere with their neighbors' temperature distributions as shown in Fig (3.1) (c). Maxwell–Eucken model is obtained from equation (3.2) by substituting $d_i = 3$ or $\bar{k} = k_1$ so we can evaluate the effective thermal conductivity for multiphase composite as shown in formula (3.5).

$$K = \frac{\sum_{i=1}^{m} k_i v_i \frac{3k_1}{2k_1 + k_i}}{\sum_{i=1}^{m} v_i \frac{3k_1}{2k_1 + k_i}} \tag{3.5}$$

The EMT model assumes a completely random distribution of all the components as shown in Fig (3.1) (d). EMT model is obtained from equation (3.2) by substituting $d_i = 3$ or $\bar{k} = K$ so we can evaluate the effective thermal conductivity for multiphase composite as shown in formula (3.6).

$$K = \frac{\sum_{i=1}^{m} k_i v_i \frac{3K}{2K + k_i}}{\sum_{i=1}^{m} v_i \frac{3K}{2K + k_i}} \tag{3.6}$$

Series, Parallel, Effective Medium Theory and the Maxwell–Eucken models are used to calculate the effective thermal conductivity for the rocket motor insulation compositions based on CCF and/or KP reinforcement. Now the formulas for Series, Parallel, the Maxwell–Eucken and Effective Medium Theory models can be derived from equations (3.3), (3.4), (3.5), (3.6) respectively by substituting i = 1,2. The resulting formulas are (3.7), (3.8), (3.9), (3.10) respectively.

$$K = \frac{1}{(v_f / k_f) + (v_m / k_m)} \tag{3.7}$$

$$K = k_f v_f + k_m v_m \tag{3.8}$$

$$K = k_m \frac{k_f + 2k_m + 2v_f(k_f - k_m)}{k_f + 2k_m - v_f(k_f - k_m)} \tag{3.9}$$

$$v_f \frac{k_f - K}{k_f + 2K} + v_m \frac{k_m - K}{k_m + 2K} = 0 \tag{3.10}$$

Where K is the effective thermal conductivity of the whole composite material, k_m and k_f are the thermal conductivities of the matrix (EPDM) and fiber (CCF and/or KP)

respectively, ν_f and ν_m are the volume fractions of the fiber (CCF and/or KP) and matrix (EPDM) respectively.

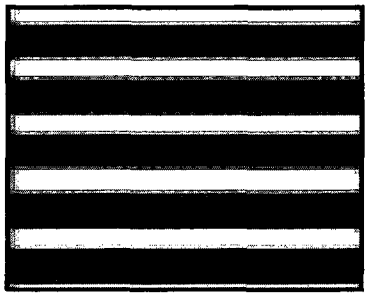

Series model

(a)

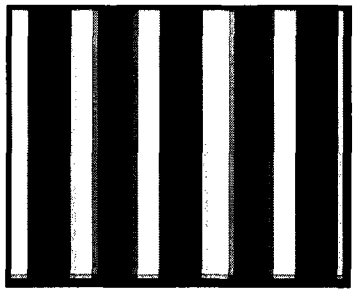

Parallel model

(b)

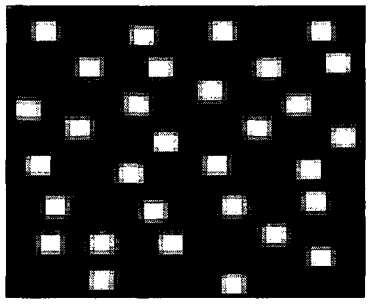

Maxwell–Eucken 1

(c)

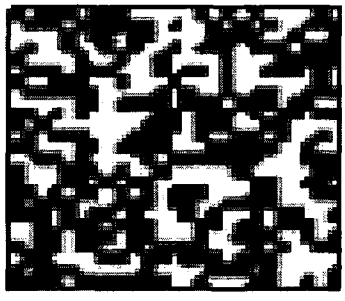

EMT model

(d)

Fig (3.1) Models based on the structure of the homogenous phase and dispersed phase

Formulas (3.7), (3.8), (3.9), (3.10) are used to calculate the effective thermal conductivity for the rocket motor insulation compositions based on CCF and/or KP reinforcement. The results are shown in Table (3.1) and compared with the experimental values.

Property / Composition No	Calc. K_{eff} (w/m.k) (maxwell eucken)	Calc. K_{eff} (w/m.k) (parallel)	Calc. K_{eff} (w/m.k) (series)	Calc. K_{eff} (w/m.k) (EMT)	Measured K_{eff} (w/m.k)
1 (30 CCF)	0.623	1.754	0.461	0.76	0.297
2 (35 CCF)	0.665	1.926	0.477	0.858	0.359
3 (40 CCF)	0.706	2.086	0.493	0.956	0.364
4 (45 CCF)	0.746	2.234	0.509	1.062	0.372
5 (50 CCF)	0.786	2.373	0.525	1.167	0.453
6 (10 KP)	0.320	0.331	0.208	0.319	0.295
7 (15 KP)	0.304	0.318	0.176	0.301	0.261
8 (20 KP)	0.289	0.307	0.154	0.284	0.231
9 (25 KP)	0.276	0.296	0.138	0.271	0.199
10 (30 KP)	0.264	0.286	0.126	0.258	0.171
11 (5 CCF + 5 KP)	0.379	0.62	0.273	0.383	0.334
12 (7.5 CCF + 7.5 KP)	0.388	0.733	0.247	0.395	0.313
13 (10 CCF + 10 KP)	0.395	0.837	0.227	0.408	0.296
14 (12.5 CCF + 12.5 KP)	0.403	0.932	0.211	0.419	0.271
15 (15 CCF + 15 KP)	0.410	1.02	0.198	0.431	0.252
16 (17.5 CCF + 17.5 KP)	0.416	1.101	0.188	0.444	0.235
17 (20 CCF + 20 KP)	0.423	1.177	0.179	0.456	0.225
18 (22.5 CCF + 22.5 KP)	0.428	1.248	0.172	0.465	0.207
19 (25 CCF + 25 KP)	0.434	1.313	0.165	0.479	0.198

Table (3.1) Calculated and measured thermal conductivities for compositions with different phr contents of CCF and/or KP

Figs (3.2), (3.3), (3.4) show the difference between the calculated values using parallel, series, effective medium theory and the Maxwell–Eucken models with the measured values for the thermal conductivities of the CCF and/or KP based insulants.

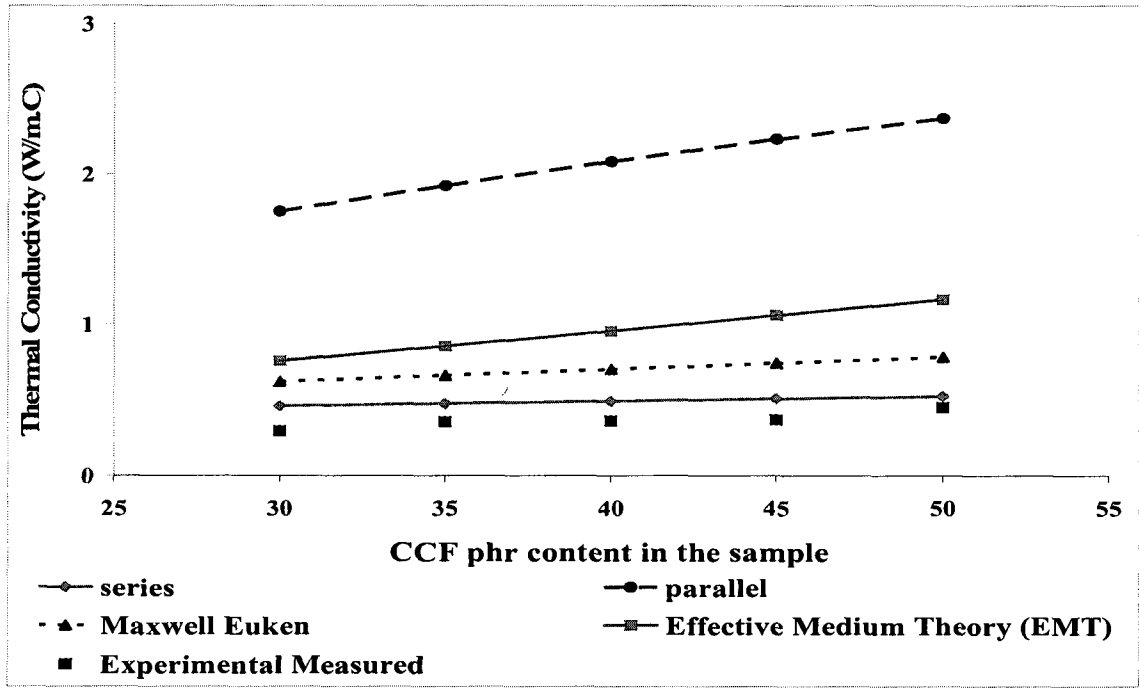

Fig (3.2) Calculated and measured thermal conductivities as function of CCF phr content

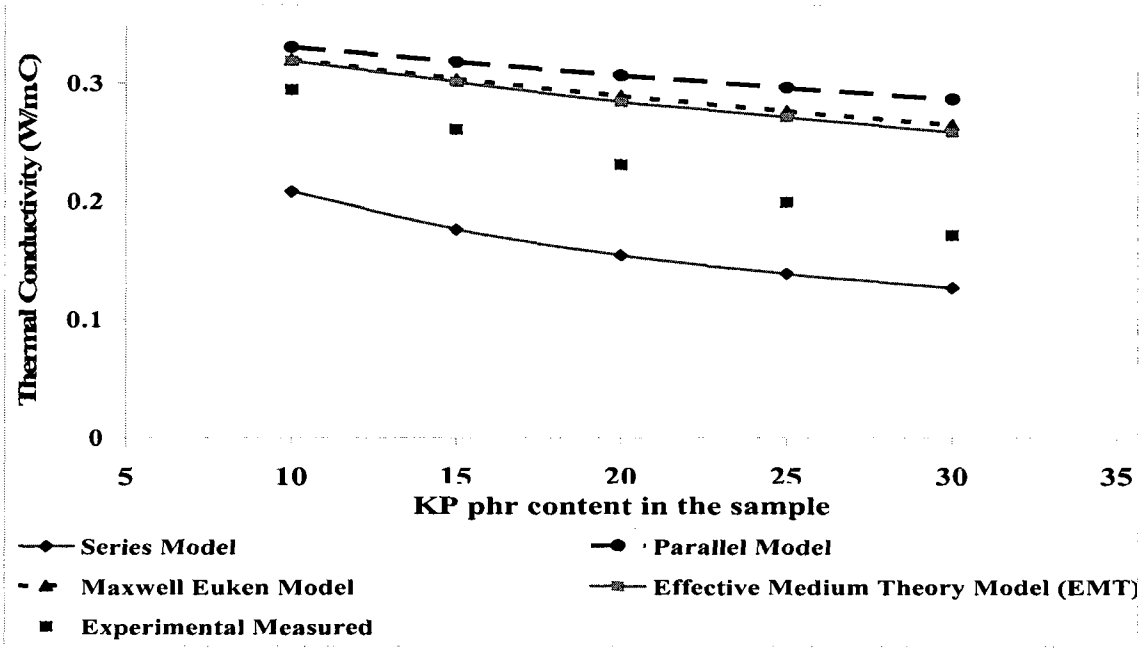

Fig (3.3)) Calculated and measured thermal conductivities as function of KP phr content

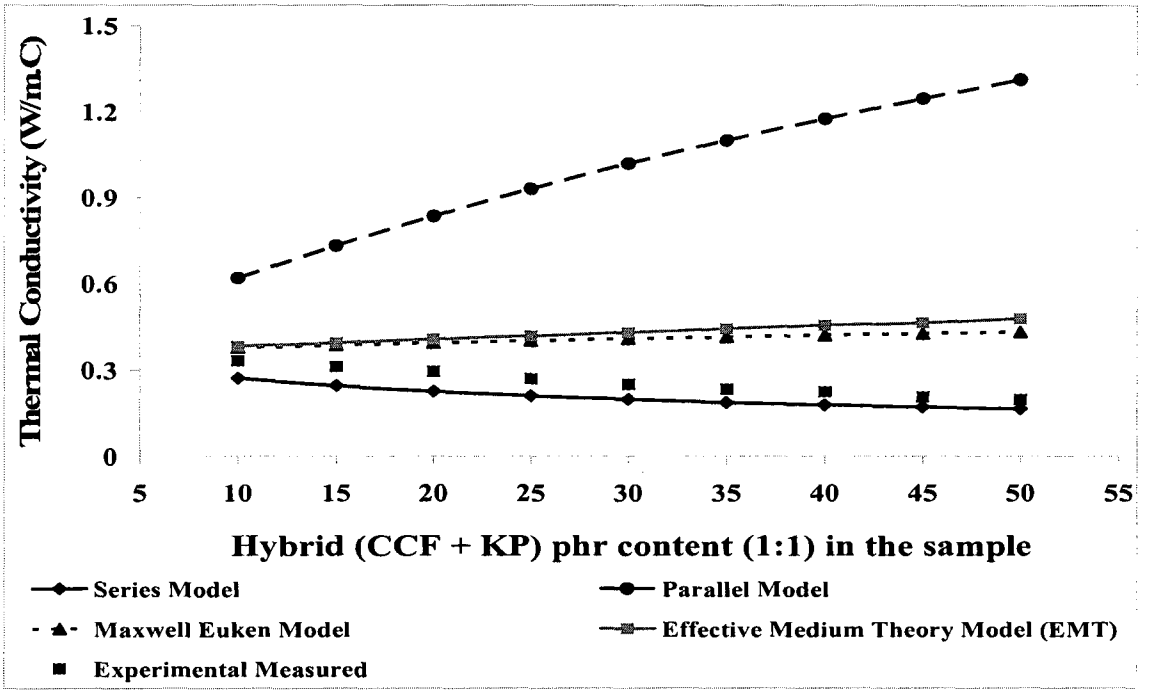

Fig (3.4) Calculated and measured thermal conductivities as function of CCF + KP phr content

It appears in Table (3.1) and Figs (3.2), (3.3), (3.4) that there is difference between the calculated (based on all existing models) and measured thermal conductivities.

It appears that the closest model to the experimental measurements for CCF based compositions is the series model which assumes layers of the components aligned perpendicular to the heat flow as shown in Fig (3.2). The difference is within 16 % to 55 % of the measured values. As a result the thermal conductivity of CCF reinforced EPDM can be estimated by the formula:

$$K = 0.68 \frac{1}{(v_{CCF} / k_{CCF}) + (v_{EPDM} / k_{EPDM})} \qquad (3.11)$$

With an accuracy ± 20 %.

Microscopic observations were performed using scanning electron microscope (SEM).

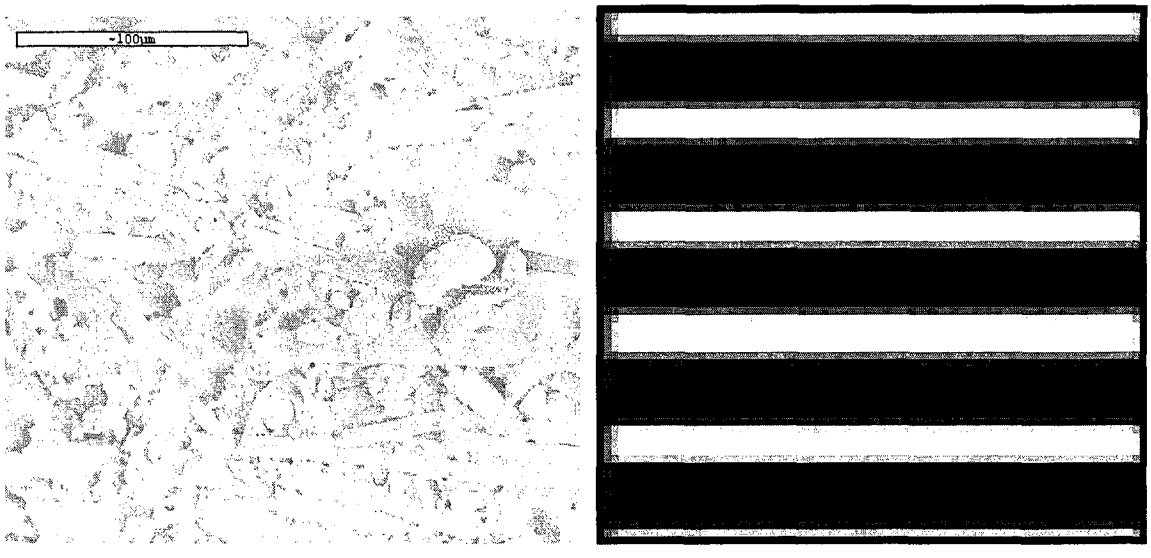

Fig (3.5) SEM photo for sample 5 (50 phr CCF content) versus series model

From SEM for sample 5 (50 phr CCF content)[Fig (3.5), it appears that mixing using C. W. Bra bender permits homogeneous dispersion of CCF in the EPDM polymeric matrix in which most of the chopped carbon fibers are aligned perpendicular to the heat flow.

This alignment of CCF inside EPDM makes the CCF based insulation close to series model.

Also the closest model to the experimental measurements for KP based compositions is the series model which assumes layers of the components aligned perpendicular to the heat flow as shown in Fig (3.3). The difference is within 26.3 % to 29.5 % of the measured values.

As a result the thermal conductivity of KP reinforced EPDM can be estimated by the formula:

$$K = 1.28 \frac{1}{(v_{KP} / k_{KP}) + (v_{EPDM} / k_{EPDM})} \qquad (3.12)$$

With an accuracy ± 2 %.

For sample 10 (30 phr KP content) [Fig (3.6)], it appears that the mixing using C. W. Bra Bender permits homogeneous dispersion of Kevlar pulp in the EPDM polymeric matrix. This homogenous distribution of KP inside EPDM makes the KP based insulation close to series model.

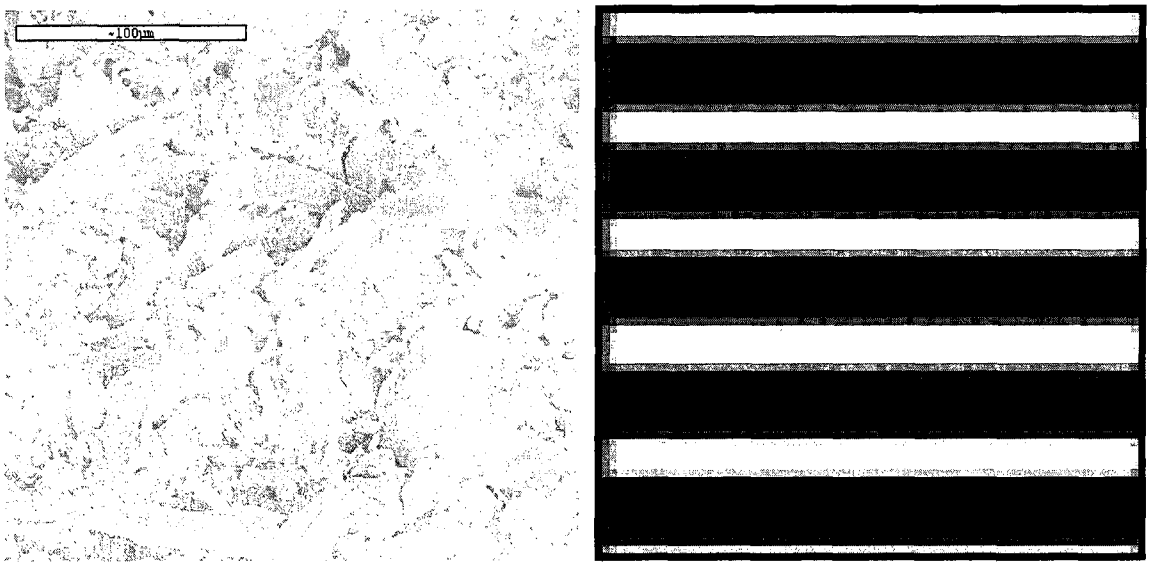

Fig (3.6): SEM photo for sample 10 (30 phr KP content) versus series model

And finally the closest model to the experimental measurements for CCF + KP based compositions is the series model which assumes layers of the components aligned perpendicular to the heat flow. The difference is within 16.7 to 18.3 % of the measured values.

As a result the experimental thermal conductivity of CCF + KP reinforced EPDM can be experimentally fitted to yield:

$$K = 1.175 \frac{1}{(v_{CCF} / k_{CCF}) + (v_{KP} / k_{KP}) + (v_{EPDM} / k_{EPDM})} \qquad (3.13)$$

With an accuracy ± 0.8 %.

For sample 19 (25 phr CCF + 25 phr KP) [Fig (3.7)], it appears that mixing using C. W. Bra bender mixer permits homogeneous dispersion of chopped carbon fibers and Kevlar pulp in the EPDM polymeric matrix. This homogenous distribution of CCF and KP inside EPDM makes the CCF + KP based insulation close to series model.

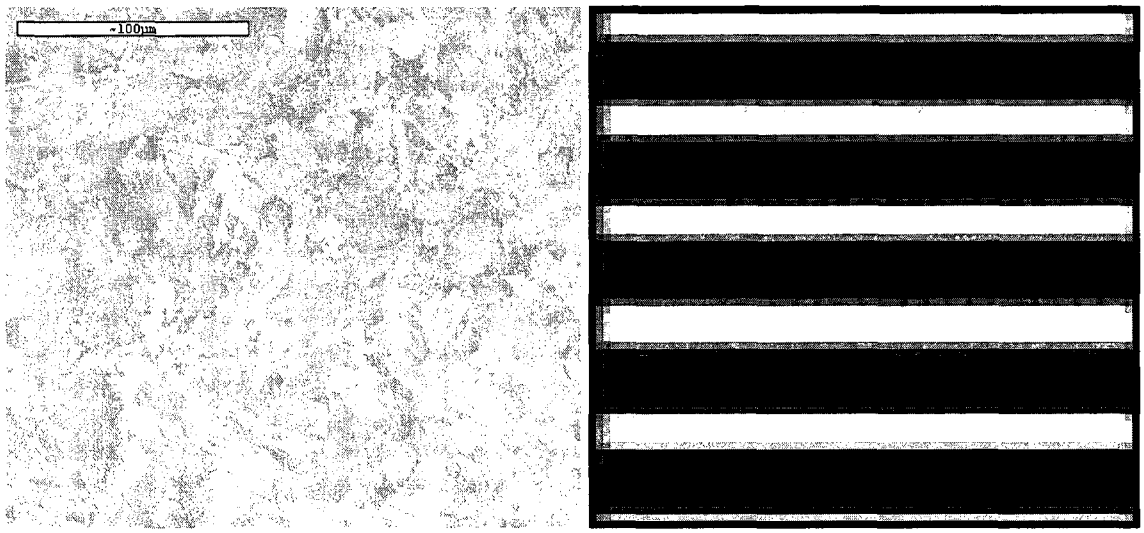

Fig (3.7) SEM photo for sample 19 (25 phr CCF + 25 phr KP content) versus series model

Formulas (3.7), (3.8), (3.9), (3.10) are used to calculate the effective thermal conductivity for the rocket motor insulation compositions based on a hybrid of CCF and KP (unequal volume fraction of CCF and KP inside the hybrid) reinforcement. The results are shown in Table (3.2) and compared with the experimental values.

Fig (3.8) shows the difference between the calculated values using parallel, series, effective medium theory and the Maxwell–Eucken models with the measured values for the thermal conductivities of a hybrid of CCF and KP (total reinforcement 50 phr) (unequal volume fraction of CCF and KP inside the hybrid) based insulants.

Property / Composition No	Calc. K_{eff} (w/m.°C) (max.-euck.)	Calc. K_{eff} (w/m. °C) (parallel)	Calc. K_{eff} (w/m. °C) (series)	Calc. K_{eff} (w/m. °C) (EMT)	Measured K_{eff} (w/m. °C)
20 (5 CCF + 45 KP)	0.249	0.46	0.107	0.245	0.131
20 (10 CCF + 40 KP)	0.291	0.68	0.117	0.291	0.144
20 (15 CCF + 35 KP)	0.334	0.89	0.13	0.342	0.16
20 (20 CCF + 30 KP)	0.381	1.1	0.16	0.404	0.179
20 (30 CCF + 20 KP)	0.491	1.53	0.192	0.574	0.236
20 (35 CCF + 15 KP)	0.553	1.73	0.228	0.687	0.302
20 (40 CCF + 10 KP)	0.622	1.95	0.28	0.823	0.369
20 (45 CCF + 5 KP)	0.67	2.16	0.367	0.983	0.434

Table (3.2) Calculated and measured thermal conductivities for compositions with different phr contents of CCF and/or KP (unequal)

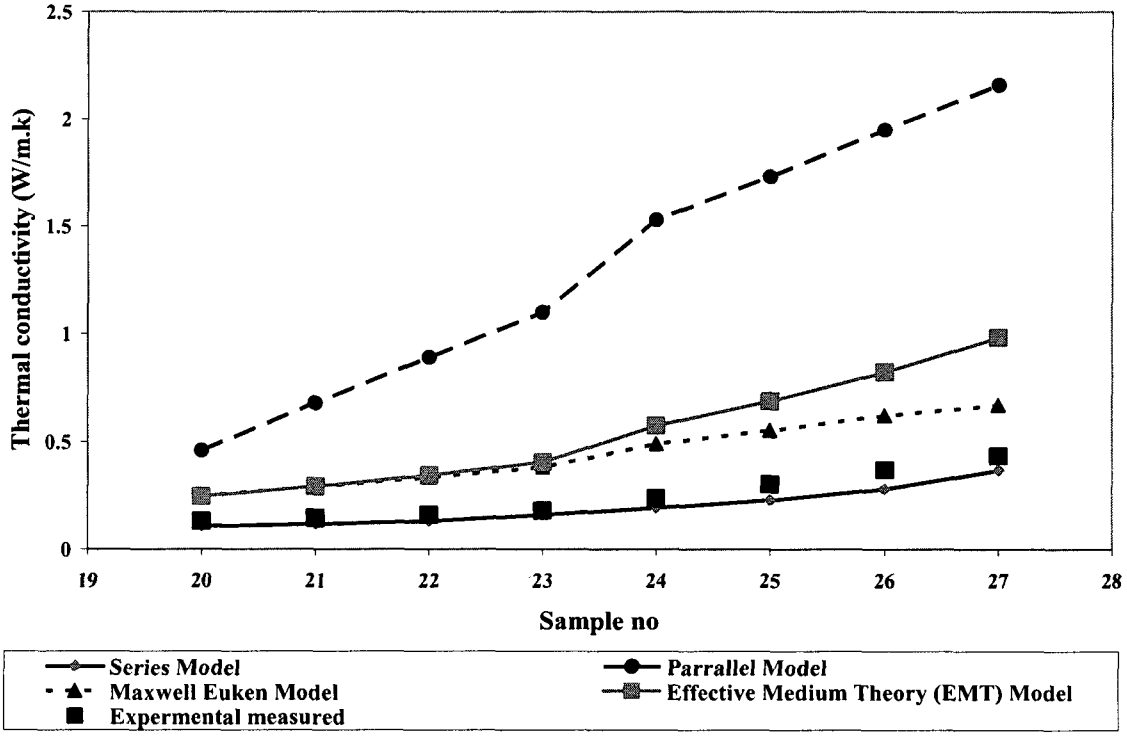

Fig (3.8) Calculated and measured thermal conductivities as function of CCF + KP phr content (unequal phr of CCF and KP) (total reinforcement 50 phr)

There is a step increase for thermal conductivity in the curves from sample 23 to sample 24 as shown in fig (3.8). This is because the sample for equal phr of CCF and KP (25, 25) was not included in between sample (23), (24).

If we want to include this sample and give the sample numbers 20, 21, 22, 23, 24, 25, 26, 27 and 19 a new identifications as 28, 29, 30, 31, 32, 33, 34, 35 and 36 respectively.

Fig (3.9) shows the difference between the calculated values using parallel, series, effective medium theory and the Maxwell–Eucken models with the measured values for the thermal conductivities of a hybrid of CCF and KP (equal and unequal volume fraction of CCF and KP inside the hybrid) (total reinforcement 50 phr) based insulants where there is no step increase.

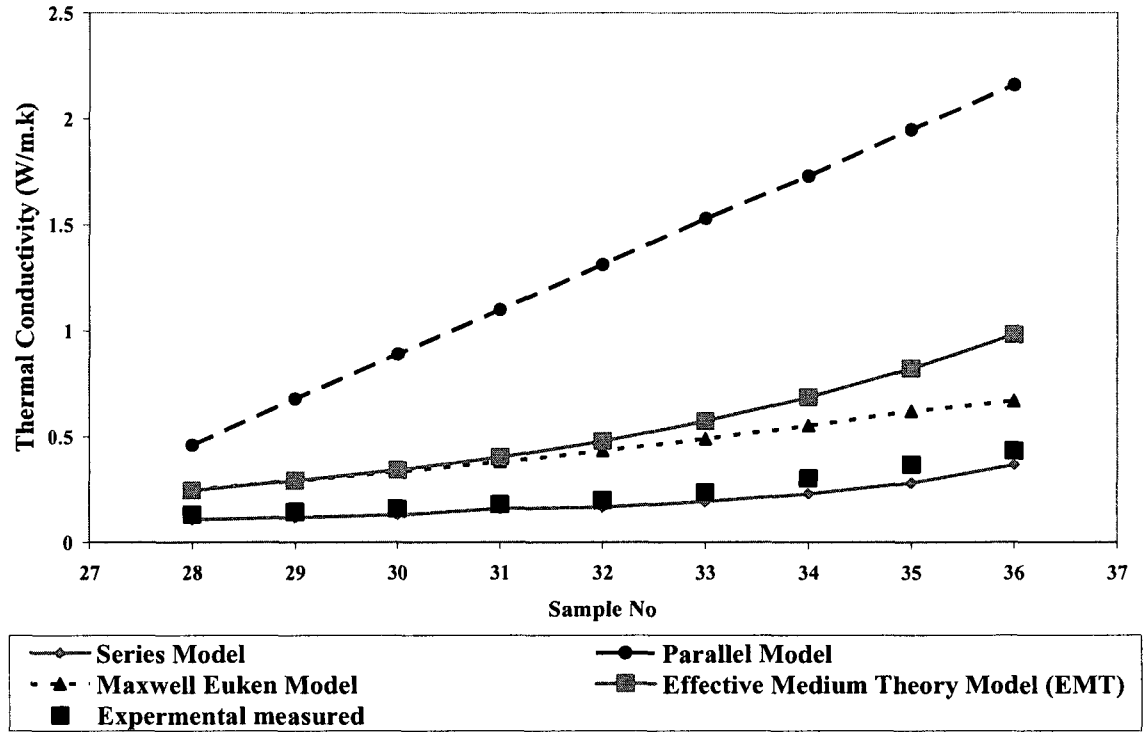

Fig (3.9) Calculated and measured thermal conductivities as function of CCF + KP phr content (unequal phr of CCF and KP) (total reinforcement 50 phr)

And finally the closest model to the experimental measurements for CCF + KP (unequal amounts) based compositions is the series model which assumes layers of the components aligned perpendicular to the heat flow. The difference is within 15.5 and not to 18.3 % of the measured values.

As a result the thermal conductivity of CCF + KP (unequal amounts) reinforced EPDM can be estimated by the formula:

$$K = 1.169 \frac{1}{(v_{CCF} / k_{CCF}) + (v_{KP} / k_{KP}) + (v_{EPDM} / k_{EPDM})} \qquad (3.14)$$

with an accuracy ± 1.4 %.

For samples 28 to 36 [Fig (3.9)], it appears that mixing using C. W. Bra bender mixer permits homogeneous dispersion of chopped carbon fibers and Kevlar pulp in the EPDM

polymeric matrix. This homogenous distribution of CCF and KP inside EPDM makes the CCF + KP based insulation close to series model.

As a general result the closest model to predict the thermal conduction inside multiphase thermal insulation composite material based on CCF and/or KP is the series model which assumes layers of the components aligned perpendicular to the heat flow.

3.2 Numerical model

The general equation governing the heat transfer in a thin sheet of thermal insulation composite material is:

$$\rho C_p \frac{\partial U}{\partial t} = \frac{\partial}{\partial x}(K_{xx} \frac{\partial U}{\partial x}) + \frac{\partial}{\partial y}(K_{yy} \frac{\partial U}{\partial y}) + \frac{\partial}{\partial z}(K_{zz} \frac{\partial U}{\partial z}) + H \qquad (3.15)$$

Where

K is the thermal conductivity of the material

C_p is the specific heat capacity of the material

ρ is the density of the material

U is the temperature

t is the time

H is the heat source

Assume that heat loss or gain through the surface of the sample by convection and radiation is small. Also assume that there is no heat source or sink in the sample (H = 0). Assume also that the thermal conductivity is constant with respect to the thickness direction. This reduces the problem to that of a one – dimensional heat conduction problem across the thickness of the composite as:

$$\rho C_p \frac{\partial U}{\partial t} = K \frac{\partial^2 U}{\partial x^2} \qquad (3.16)$$

Or

$$\frac{\partial^2 U}{\partial x^2} = \frac{1}{\alpha} \frac{\partial U}{\partial t} \qquad (3.17)$$

Where:

α is the thermal diffusivity of the material = $K/\rho C_p$

K is the thermal conductivity of the material along the thickness direction

C_p is the specific heat capacity of the material

ρ is the density of the material

U is the temperature

t is the time

This one dimensional heat equation can be solved analytically and numerically.

3.2.1 Analytical solution

In order to solve the heat equation we must give the initial conditions. The temperature at every point in the sheet at time t = 0 is:

$U(x, 0) = U_0(x)$ for $0 \leq x \leq L$ (3.18)

This function is known as the initial temperature distribution.

Boundary conditions

$U(0, t) = T_0$ $U(L, t) = T_L$ for all $t > 0$ (3.19)

Now we can set up an initial boundary value (IBV) problem. Combining the heat equation with the initial conditions and boundary conditions, the problem is to find U(x, t) such that

$\mathbf{U_t(x, t) = \alpha U_{xx}(x, t)}$ $0 \leq x \leq L$ and $t > 0$ (3.20)

$$U(x, 0) = U_0(x) \qquad 0 \le x \le L \qquad (3.21)$$

$$U(0, t) = T_0 \qquad U(L, t) = T_L \qquad t > 0 \qquad (3.22)$$

Where $U_t(x, t)$ is the temperature first derivative with respect to time t and $U_{xx}(x, t)$ is the temperature second derivative with respect to thickness coordinate x.

This is the general form for the heat equation as an IBV problem.

Since the heat equation is linear we can find a linear combination of two solutions to equal another solution.

$$U = U_S + V \qquad (3.23)$$

Where U_S is the steady state solution for IVP and V is the transient solution for IVP

$$\mathbf{U_S(x) = x(T_L - T_0)/L + T_0} \qquad (3.24)$$

The remaining part of $U = U_S + V$ is V. where $V = U - U_S$ so that it satisfies the IBV problem

$$\mathbf{V_t(x, t) = \alpha U_{xx}(x, t)} \qquad 0 \le x \le L \text{ and } t > 0 \qquad (3.25)$$

$$V(x, 0) = U_0(x) - U_S(x) \qquad 0 \le x \le L \qquad (3.26)$$

$$V(0, t) = U(0, t) - U_S(0, t) = T_0 - T_0 = 0 \qquad t > 0 \qquad (3.27)$$

$$V(L, t) = U(L, t) - U_S(L, t) = T_L - T_L = 0 \qquad (3.28)$$

The purpose of doing this is, V has homogenous boundary conditions which makes finding a solution much easier. This allows using separation of variables to find a solution for V because separation of variables requires the problem to be homogenous.

Therefore we want to find product solution of the form:

$$V(\mathbf{x, t}) = X(x)T(t)$$

Substitute this solution into IVP in (3.25)

$$X(x)T'(t) = \alpha X''(x)T(t) \qquad (3.29)$$

$[T'(t)/ \alpha T(t)] = X''(x)/ X(x)$ (3.30)

Since x and t are independent variables the only way for these two equations to be equal is if they are equal to a constant $-\lambda^2$.

$T'(t)/ \alpha T(t) = -\lambda^2$

$X''(x)/ X(x) = -\lambda^2$

$T'(t) + \alpha \lambda^2 T(t) = 0$ (3.31)

$X''(x) + \lambda^2 X(x) = 0$ (3.32)

$X(x) = a \cos \lambda x + b \sin \lambda x$ (3.33)

With the boundary conditions

$V(0, t) = 0$

$V(0, t) = X(0) T(t)$

$X(0) = 0$ which means $a = 0$

$V(L, t) = 0$

$V(L, t) = X(L)T(t)$

$X(L) = 0$ gives $b \sin \lambda L = 0$ this implies that $\lambda L = n \pi$

$$X(x) = b \sin \frac{n \pi x}{L}$$

Since we are looking for non – zero solutions we set $b = 1$

$$X_n(x) = \sin \frac{n \pi x}{L}$$

Let $\lambda^2_n = n^2 \pi^2 / L^2$ is an eigen value of the problem and $X_n(x)$ is an eigenfunction

To find the solution of the equation $T'(t) + \alpha \lambda^2 T(t) = 0$

$T(t) = C e^{mt}$ Substitute this solution into the problem

$mC e^{mt} + \alpha \lambda^2 C e^{mt} = 0$ (3.34)

so $m = -\alpha \lambda^2$

$T(t) = C e^{-\lambda 2\, \alpha t}$

The complete solution to the problem is the group of eigenvalues and eigenfunctions for $n = 1$ to $n = \infty$.

$$V(x, t) = \sum_{n=1}^{\infty} b_n e^{-n^2\pi^2 \alpha t / L^2} \sin \frac{n\pi x}{L} \tag{3.35}$$

$$b_n = \frac{2}{L} \int_o^L \upsilon_0(x) \sin \frac{n\pi x}{L} dx$$

So the general solution is

$U = U_S + U_T$

$$U(x, t) = x(T_L - T_0)/L + T_0 + \sum_{n=1}^{\infty} b_n e^{-n^2\pi^2 at / L^2} \sin \frac{n\pi x}{L} \tag{3.36}$$

$$U(x,0) = (\sum_{n=1}^{\infty} b_n \sin \frac{n\pi x}{L}) + x(T_L - T_0)/L + T_0$$

Item 1.

For the purpose of heat transfer modeling, the insulant can be considered to be a flat plate with thickness L as shown in Fig (3.10). The plate is initially at room temperature (20°C). At time $t = 0$, the upper face ($x = 0$) is subjected to a temperature T_o (2010 °C). The duration of operation is about 60 seconds. During that time the plate gets heated up, the layers that are exposed to the high temperature may ablate which reduces the effective thickness of the sample. The temperature inside the plate increases and the temperature at the back of the supporting steel piece will be increased above 20°C. The heat transfer across the insulant during the rocket operation is complex. In order to provide a good understanding of the model, the modeling will be presented in two steps, the first one is

simplified to present the governing equations, and the second step presents the procedure to handle the more realistic situation.

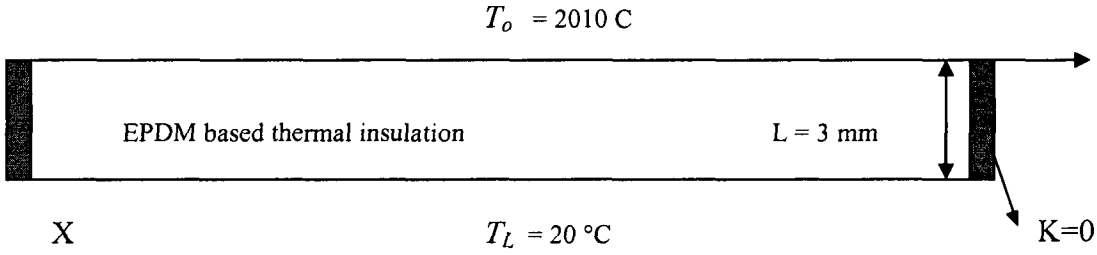

Fig (3.10) Insulant presented as a plate for heat transfer modeling

3.2.1.1 First approximation of the heat transfer across the insulant

As a first approximation, the thickness of the plate is assumed to remain constant during the whole operation, and the thermal diffusivity, density, and specific heat of the insulant do not change. Let U(x,t) represent the temperature of any point in the plate at any time, the initial and boundary values conditions are:

Initial conditions:

$U(x,0) = U_o(x)$ for $0 \leq x \leq L$ (3.37)

Boundary conditions:

$U(0,t) = T_o$ $U(L,t) = T_L$ for $t > 0$ (3.38)

Item 2:

The transient solution can then be written as:

$$V(x,t) = b_n \sin \frac{n\pi x}{L} e^{-\frac{n^2\pi^2\alpha t}{L^2}} \quad (3.39)$$

and the expression for the temperature is:

$$U(x,t) = T_o + (T_L - T_o)\frac{x}{L} + b_n \sin \frac{n\pi x}{L} e^{-\frac{n^2\pi^2\alpha t}{L^2}} \quad (3.40)$$

The expression above satisfies the differential equation and the boundary conditions for each of the value of the positive integer n. However in order for the function (3.21) to satisfy the initial condition (3.18), we would have to choose the coefficient b_n in such a manner that:

$$U(x,0) = T_L = T_L + (T_o - T_L)(1 - \frac{x}{L}) + b_n \sin\frac{n\pi x}{L}$$

or

$$(T_L - T_o)(1 - \frac{x}{L}) = b_n \sin\frac{n\pi x}{L} \tag{3.41}$$

The use of only a single value of b_n may not satisfy equation (3.22). The solution U(x,t) therefore needs to be in the form of a series solution as:

$$U(x,t) = T_o + (T_L - T_o)\frac{x}{L} + \sum_{n=1}^{\infty} b_n \sin\frac{n\pi x}{L} e^{-\frac{n^2\pi^2 at}{L^2}} \tag{3.42}$$

Yielding

$$(T_L - T_o)(1 - \frac{x}{L}) = \sum_{n=1}^{\infty} b_n \sin\frac{n\pi x}{L} \tag{3.43}$$

This last expression is recognized as the half-range of the function on the left hand side in a sine series. Using this property, it can be shown that:

$$b_n = \frac{2}{L}\int_0^L (T_L - T_o)(1 - \frac{x}{L})\sin\frac{n\pi x}{L} dx \tag{3.44}$$

The final form of the solution for the problem is:

$$U(x,t) = T_o + (T_L - T_o)\frac{x}{L} + \frac{2}{L}\sum_{n=1}^{\infty}\left(\int_0^L (T_L - T_o)(1 - \frac{x}{L})\sin\frac{n\pi x}{L} dx\right)\sin\frac{n\pi x}{L} e^{-\frac{n^2\pi^2 at}{L^2}} \tag{3.45}$$

In the special case where T_o = 20 °C, T_L = 2010 °C, L = 3 mm, α = 0.08 mm^2/s, the solution is:

$$b_n = \int_0^3 (1990)(1-\frac{x}{3})\sin\frac{n\pi x}{3}dx$$

$$= \frac{-5970(-n\pi + \sin(n\pi))}{n^2\pi^2}$$

$$U(x,t) = 20 + (1990)\frac{x}{3} + \frac{2}{3}\sum_{n=1}^{\infty}\left(\frac{-5970(-n\pi + \sin(n\pi))}{n^2\pi^2}\right)\sin\frac{n\pi x}{3}e^{-\frac{n^2\pi^2 at}{9}} \qquad (3.46)$$

A plot of the function U as a function of time (at x = 1.5 mm) is shown in Fig (3.11).

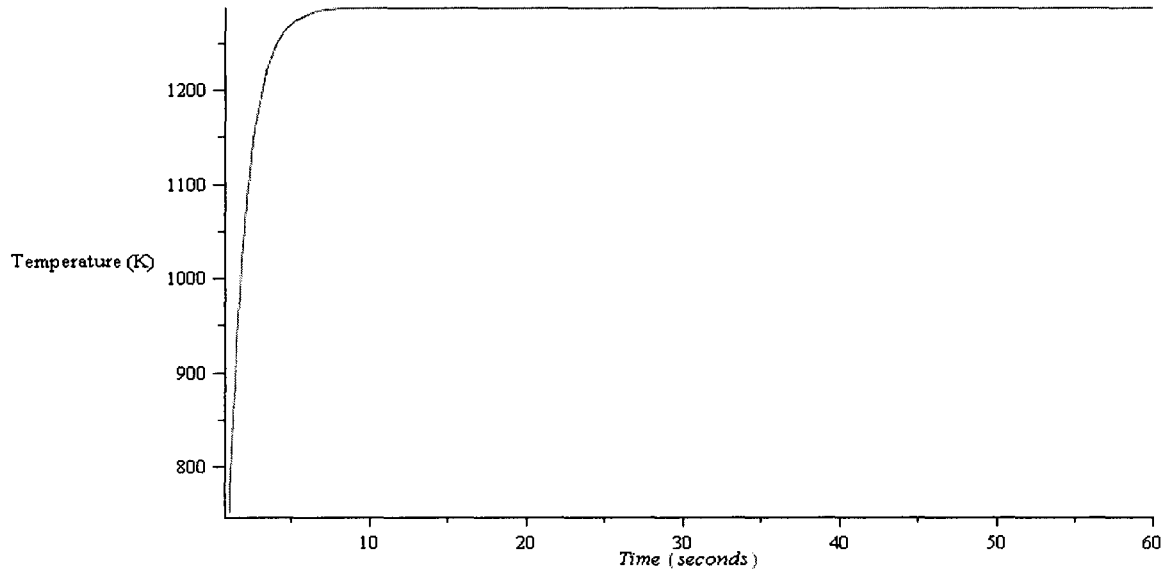

Fig (3.11) U as a function of time (at x = 1.5 mm)

3.2.1.2 Procedure for determination of the temperature profile

The above equation assumes that the plate does not lose any thickness during the course of the operation and that the material properties do not change. In reality, due to the ablation, the thickness of the place is reduced as time goes on. The temperature at the back of the support steel plate is also increasing, and the thermal conductivity of the charred material may also be reduced. In order to better represent the heat transfer situation, the duration of the operation is divided into increments. The geometry of the plate and its thermal properties are assumed to be the same during that increment. At the

end of the time increment, the geometry of the plate is reduced by the rate of ablation, and the thermal properties of the segments along the thickness are also modified to reflect the modification due to charring. The temperature at the back of the support plate is also adjusted. These new parameters are used again for another subsequent problem. The procedure continues until the end of the operation.

This means that for every insulation material composition we have a different solution because we have different properties for the material and at the same time the solution is valid for only one layer of the material so it can not be applied to insulation layer glued to steel piece (two materials). As a result the numerical solution will be more suitable for analysis.

3.2.2 Numerical solution

The numerical solution is done by using Matlab PDE tool. Although Partial Differential Equation Toolbox software offers a great deal of flexibility in the ways that we can approach the problems and interact with the toolbox functions, there is a suggested method of choice for modeling and solving PDE problems using the pdetool. The objectives of Partial Differential Equation Toolbox software are to provide tools that define a PDE problem, e.g., define 2-D regions, boundary conditions, and PDE coefficients.

The general one dimensional heat equation that applies is:

$$d\frac{\partial u}{\partial t} - \nabla .(c \nabla u) + au = f \qquad (3.47)$$

For this dimensional heat equation with no internal heat generation, assuming a triangular mesh on Ω and $t \geq 0$, expands the solution to the PDE (as a function of x) in the Finite Element Method basis:

$$u(x,t) = \sum_i U_i(t)\phi_j(x) \qquad (3.48)$$

Substituting the expansion into the PDE, multiplying with a test function Φ_j, integrating over Ω, and applying Green's formula and the boundary conditions yields the solution.

This method is traditionally called method of lines semidiscretization. Solving using pdetool by this method yields the solution to the PDE at each node x_i and time t.

Explicit time integrators are forced by stability requirements to very short time steps while implicit solvers can be expensive since they solve an elliptic problem at every time step. The numerical integration of the ODE system is performed by the MATLAB ODE Suite functions, which are efficient for this class of problems. The time step is controlled to satisfy a tolerance on the error, and factorizations of coefficient matrices are performed only when necessary. When coefficients are time dependent, the necessity of reevaluating and refactorizing the matrices each time step may still make the solution time consuming, although parabolic reevaluates only that which varies with time.

The material properties of all sub-layers are entered in every run to the math lab PDE tool. Modeling the ablation test appears to be a simple one dimensional heat equation where there is heat conduction thought the thickness. There are two aspects which make this model more complicated. The first aspect is the reduction of the material thickness with time and the second one is the variation of material properties with time. To make the model simple in calculations we will make few assumptions. We will start with the model as a one dimensional heat equation with reduction in the thickness of the material and assume the material properties are constant with time. Finally we will do the model with both reduction in the thickness and variation of material properties with time.

The model was done by considering a sample of the insulation material with known properties (based on CCF and\or KP reinforcement) with 3 mm thickness and width 20 cm. The sample is bonded to a steel piece with the same dimensions. Assuming perfect contact between the insulation material and the steel piece with known properties and the temperature at the top surface of the insulation material is the same temperature of the torch used (2010° C). The bottom surface of steel is subjected to convection heat transfer by air with coefficient of heat convection 10 $W/m^2.K$. as shown in Fig (3.12).

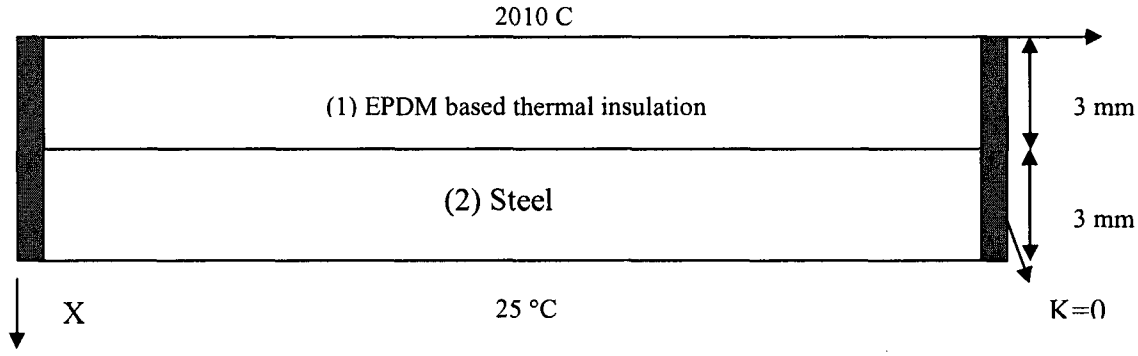

Fig (3.12) Ablation geometric model (1 layer), at t = 0 second

Solving the problem for 60 seconds of total time and with increment of 0.01 second for any 4 sub steps of time (for example from 0 to 1, 1 to 10, 10 to 30 and 30-60 seconds). These 4 sub duration of time is selected to reduce the time of solution and the validation of these theoretical results was done by comparison with experimental values as shown in Figures (3.58), (3.59), (3.60).

1- Solving from 0 -1 second (with 25° C reference temperature through all the thickness, the geometry of the model will be as shown in Fig (3.12). After 1 second the insulation material loses Δx_1 mm of thickness which corresponds to

the experimental ablation rate of this material and the case temperature is T_1 (= 25° C +ΔT_1) as shown in Fig (3.13).

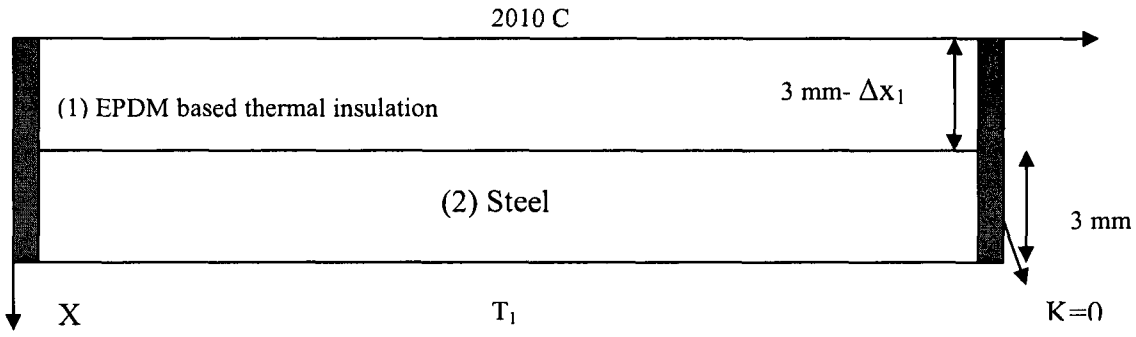

Fig (3.13) Ablation geometric model (1 layer), at t = 1 second

2- Solving from 1 -10 seconds (with the temperature distribution through the thickness result from step 1 as reference temperature), for the geometry shown in Fig (3.13). After 9 seconds the insulation material loses Δx_2 mm of thickness. The total reduction in thickness after 10 seconds will be $\Delta x_1 + \Delta x_2$ mm and the case temperature is T_2 (= 25° C +$\Delta T_1 + \Delta T_2$) as shown in fig (3.14).

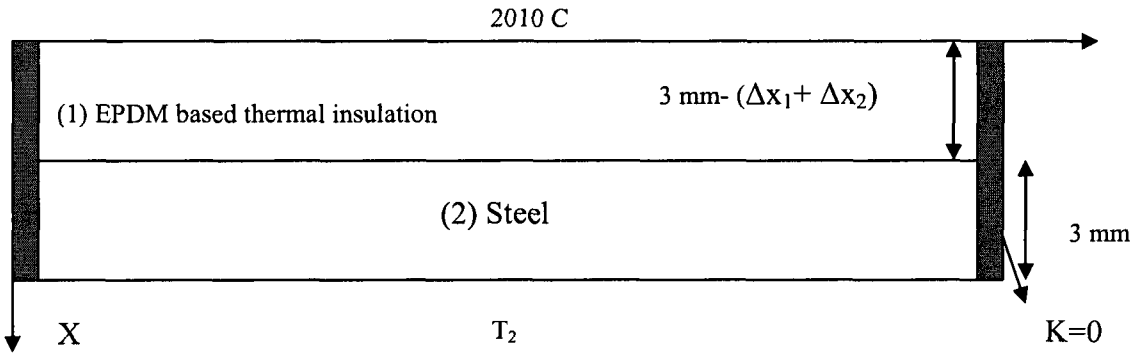

Fig (3.14) Ablation geometric model (1 layer), at t = 10 second

3- Solving from 10 -30 seconds (with the temperature distribution through the thickness result from step 2 as reference temperatures), for the geometry shown in Fig (3.14). After 19 seconds the insulation material loses Δx_3 mm of thickness. The total reduction in

thickness after 30 seconds will be $\Delta x_1 + \Delta x_2 + \Delta x_3$ mm and the case temperature is T_3 (= 25° C $+\Delta T_1 + \Delta T_2 + \Delta T_3$) as shown in Fig (3.15).

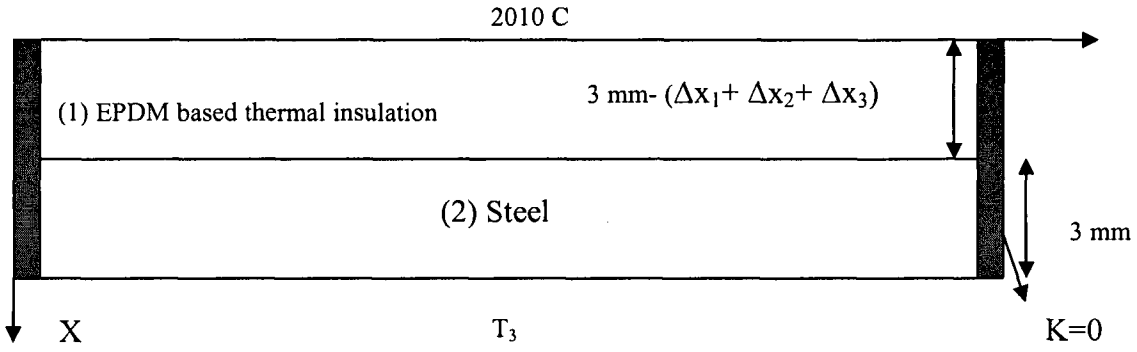

Fig (3.15) Ablation geometric model (1 layer), at t = 30 second

4- Solving from 30 -60 seconds (with the temperature distribution through the thickness result from step 3 as reference temperatures), for the geometry shown in Fig (3.15). After 29 seconds the insulation material loses Δx_4 mm of thickness. The total reduction in thickness after 60 seconds will be $\Delta x_1 + \Delta x_2 + \Delta x_3 + \Delta x_4$ mm and the case temperature is T_4 (= 25° C $+\Delta T_1 + \Delta T_2 + \Delta T_3 + \Delta T_4$) as shown in Fig (3.16).

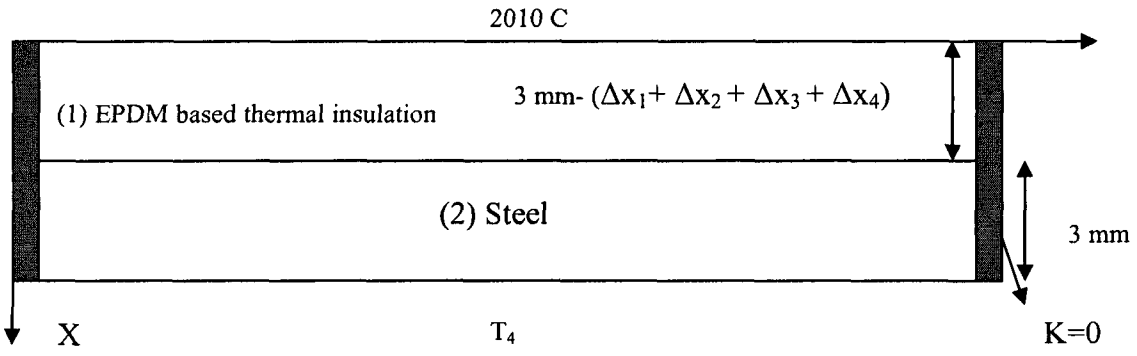

Fig (3.16) Ablation geometric model (1 layer), at t = 60 second

3.2.2.1 Ablation test without considering the properties of char

In this section the sample is assumed to have reduction in thickness but constant K. The ablation test model was done by considering a one dimensional heat equation through the thickness of the insulation material.

3.2.2.1.1 Ablation model for 1 layer of insulation

3.2.2.1.1.1 Ablation model for CCF + KP/ EPDM

By creating the geometry as shown in Fig (3.17) in the Mat lab PDE tool and by entering the properties of insulation material and steel as shown in Table (3.3), the thickness of the insulation material is reduced after each time interval due to ablation.

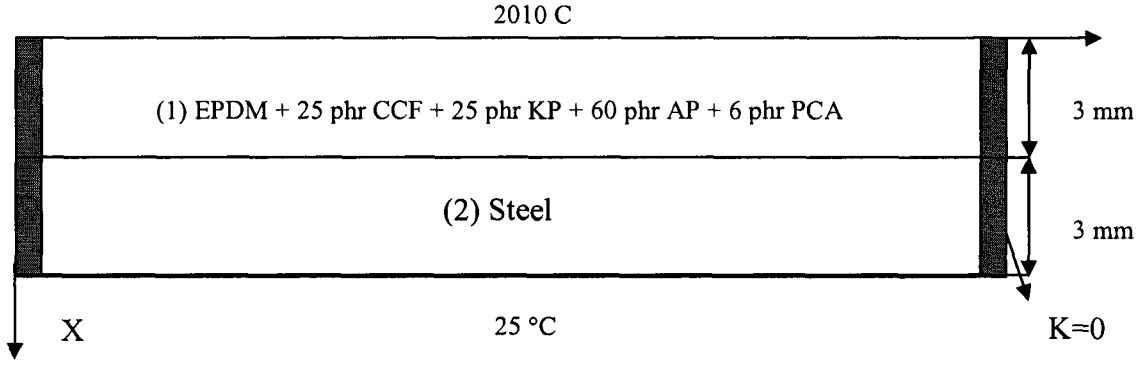

Fig (3.17) Ablation geometric model (1 layer), at t = 0 second

Material number	Material type	Thermal conductivity (W/m.K)	Heat capacity (J/kg.K)	Density (gm/cm^3)	Ablation rate (mm/s)
(1)	EPDM + 25 phr CCF + 25 phr KP + 60 phr AP + 6 phr PCA	0.198	1973	1.256	0.005
(2)	steel	32.1	822	7.85	-

Table (3.3) Material properties (experimentally measured) [25 phr CCF + 25 phr KP based EPDM & steel] [Ch 2]

Solving the problem for 60 seconds of total time and with increment of 0.01 second for 4 sub steps of time:

1- Solving from 0 -1 second, the geometry of the model will be as shown in Fig (3.17). After 1 second the insulation material loses 0.005 mm of thickness which corresponds to the experimental ablation rate of this material. The temperature distribution in the whole thickness of insulation + steel as a function of thickness at 1 second time is shown in Fig (3.18). The total reduction in thickness after 1 second will be 0.005 mm as shown in Fig (3.19).

2- Solving from 1 -10 seconds, for the geometry shown in Fig (3.19). After 9 seconds the insulation material loses 0.045 mm of thickness. The temperature distribution as a function of thickness at 10 seconds time is shown in Fig (3.18). The total reduction in thickness after 10 seconds will be 0.05 mm as shown in Fig (3.20).

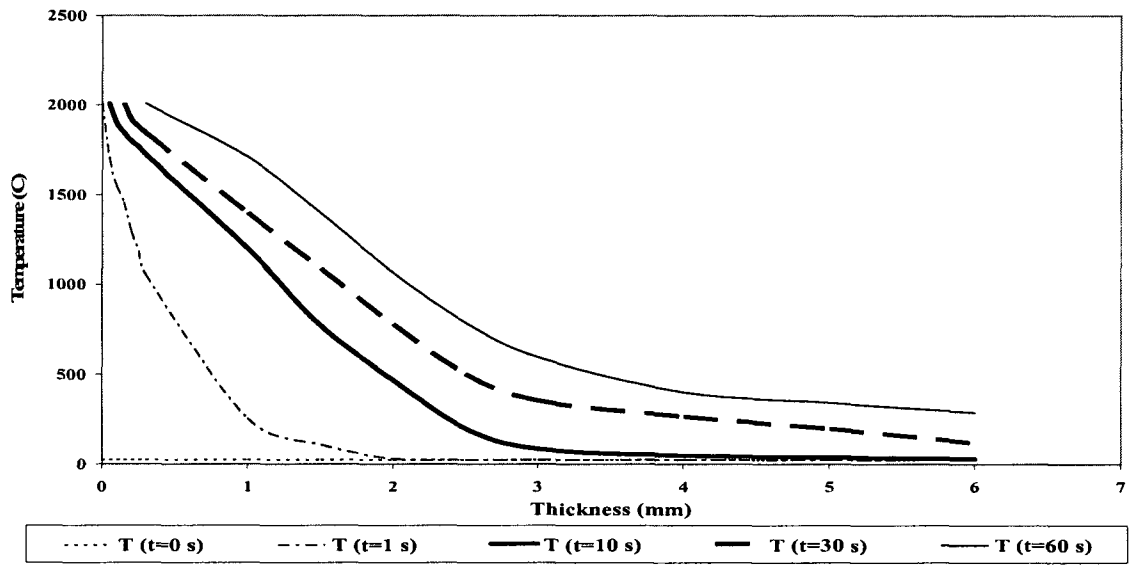

Fig (3.18) Temperature distribution as a function of thickness at different times for CCF + KP based insulation

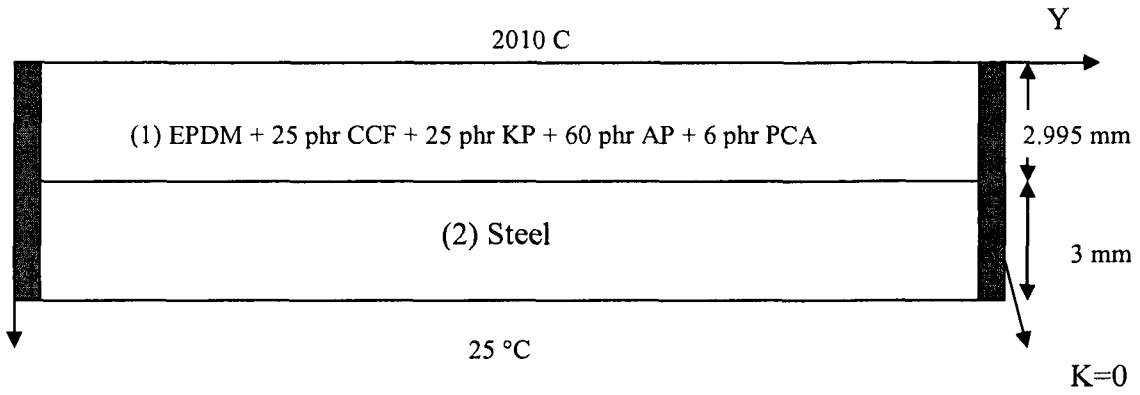

Fig (3.19) Ablation geometric model (1 layer CCF + KP based insulation), t = 1 second

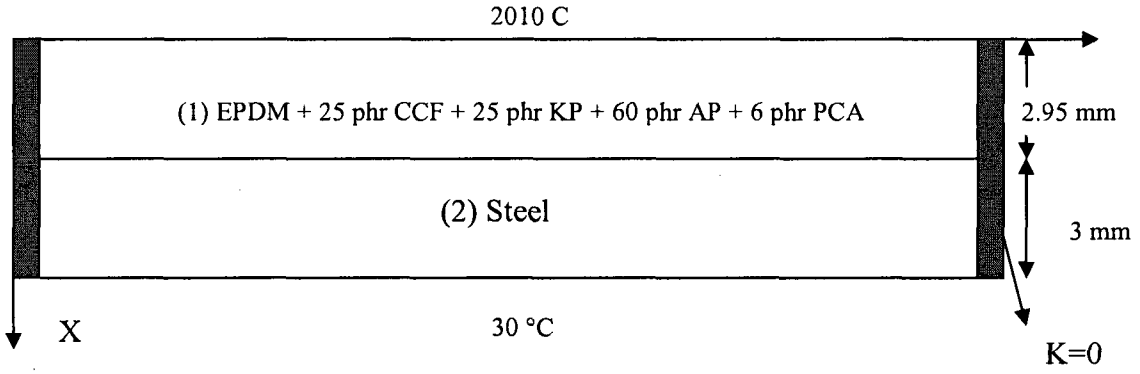

Fig (3.20) Ablation geometric model (1 layer CCF + KP based insulation), t = 10 second

3- Solving from 10 -30 seconds, for the geometry shown in Fig (3.20). After 19 seconds the insulation material loses 0.095 mm of thickness. The temperature distribution as a function of thickness at 30 seconds time is shown in Fig (3.18). The total reduction in thickness after 30 seconds will be 0.15 mm as shown in Fig (3.21).

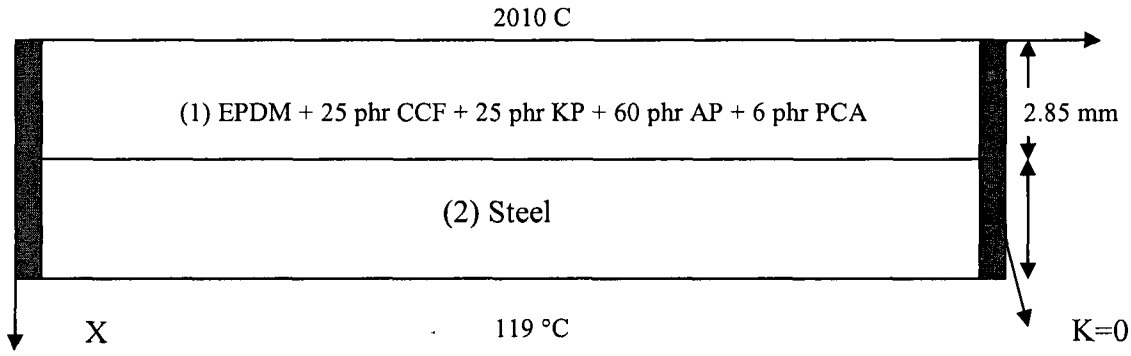

Fig (3.21) Ablation geometric model (1 layer CCF + KP based insulation), t = 30 second

4- Solving from 30 -60 seconds, for the geometry shown in Fig (3.21). After 29 seconds the insulation material loses 0.145 mm of thickness. The temperature distribution as a function of thickness at 60 seconds time is shown in Fig (3.18). The total reduction in thickness after 60 seconds will be 0.3 mm as shown in Fig (3.22).

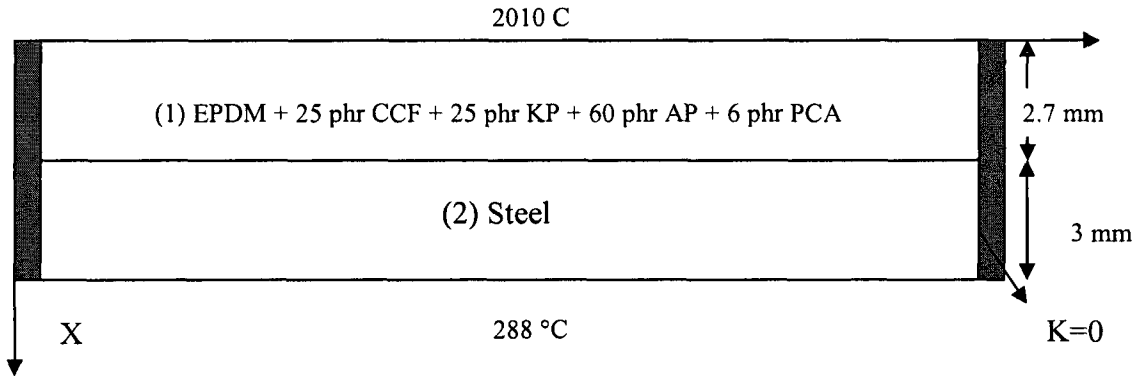

Fig (3.22) Ablation geometric model (1 layer CCF + KP based insulation), t = 60 second

3.2.2.1.1.2 Ablation model for KP/ EPDM

By using the same geometry [as shown in Fig (3.17)] used before but with layer of insulation material based on KP alone in the mat lab PDE tool and by entering the

properties of insulation material and steel as shown in Table (3.4) and taking into account the reduction in thickness of the insulation material due to ablation.

Material number	Material type	Thermal conductivity (W/m.K)	Heat capacity (J/kg.K)	Density (gm/cm^3)	Ablation rate (mm/s)
(1)	EPDM + 30 phr KP + 60 phr AP + 6 phr PCA	0.171	1778	1.185	0.015
(2)	steel	32.1	822	7.85	-

Table (3.4) Material properties (experimentally measured) [30 phr KP based EPDM & steel] [Ch 2]

Solving the problem for 60 seconds of total time and with increment of 0.01 second for 4 sub steps of time:

1- Solving from 0 -1 second, the geometry of the model will be as shown in Fig (3.17). After 1 second the insulation material loses 0.015 mm of thickness which corresponds to the experimental ablation rate of this material. The temperature distribution as a function of thickness at 1 second time is shown in Fig (3.23). The total reduction in thickness after 1 second will be 0.015 as shown in Fig (3.24)

2- Solving from 1 -10 seconds, for the geometry shown in Fig (3.24). After 9 seconds the insulation material loses 0.135 mm of thickness. The temperature distribution in the whole thickness of insulation + steel as a function of thickness at 10 seconds time is shown in Fig (3.23). The total reduction in thickness after 10 seconds will be 0.15 mm as shown in Fig (3.25).

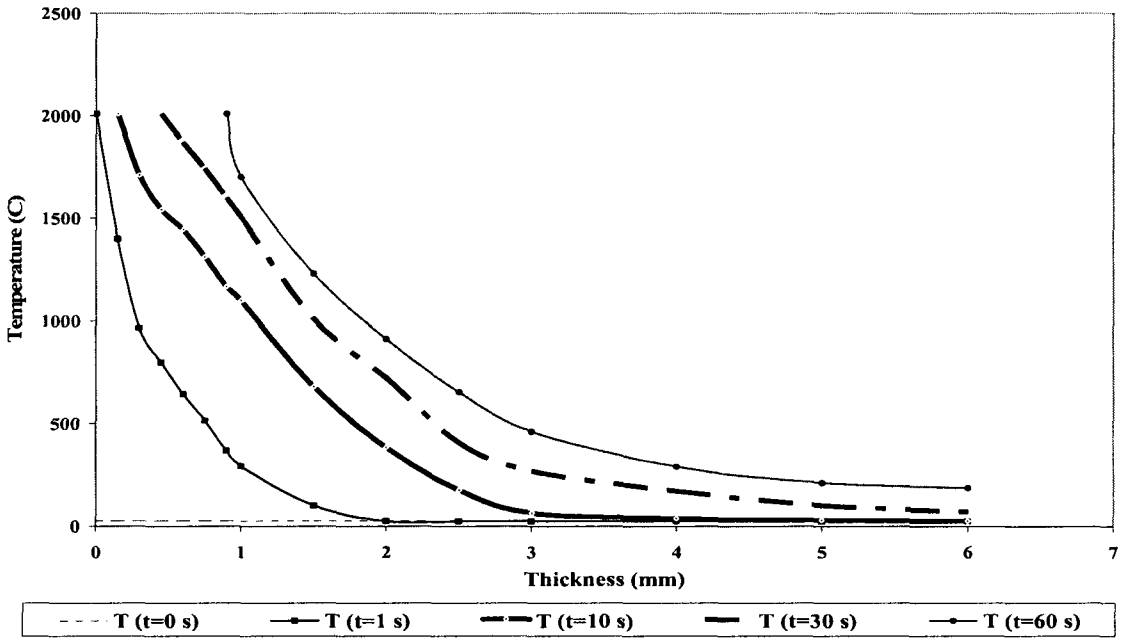

Fig (3.23) Temperature distribution as a function of thickness at different times for KP based insulation

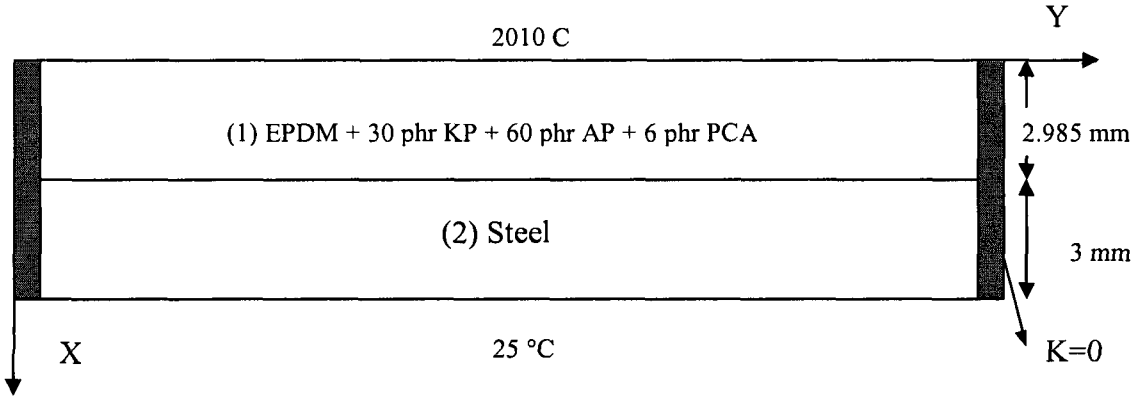

Fig (3.24) Ablation geometric model (1 layer KP based insulation), t = 1 second

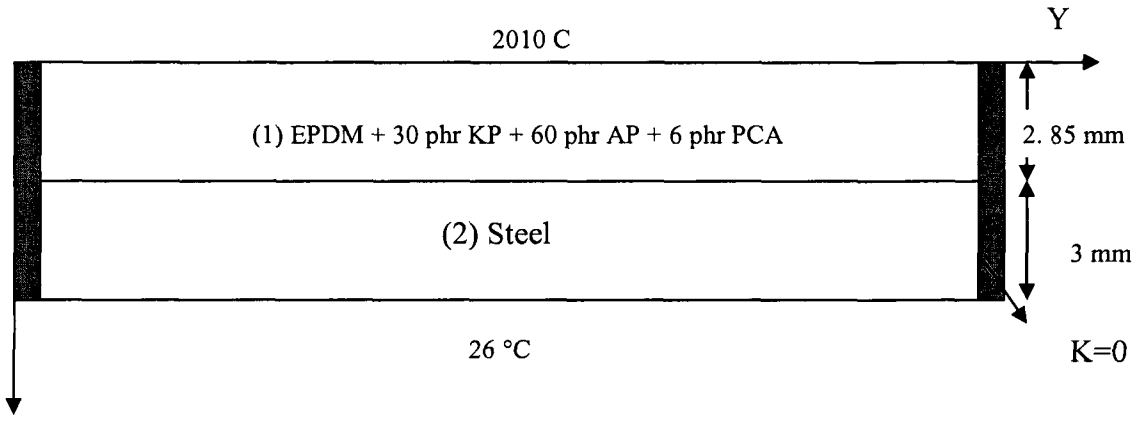

Fig (3.25) Ablation geometric model (1 layer KP based insulation), t = 10 second

3- Solving from 10 -30 seconds, for the geometry shown in Fig (3.25). After 19 seconds the insulation material loses 0.285 mm of thickness. The temperature distribution as a function of thickness at 30 seconds time is shown in Fig (3.23). The total reduction in thickness after 30 seconds will be 0.45 mm as shown in Fig (3.26).

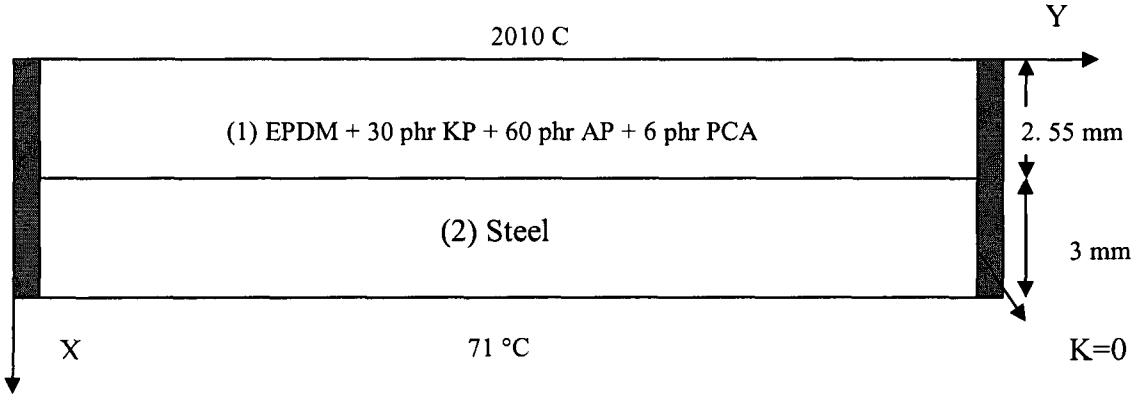

Fig (3.26) Ablation geometric model (1 layer KP based insulation), t = 30 second

4- Solving from 30 -60 seconds, for the geometry shown in Fig (3.26). After 29 seconds the insulation material loses 0.435 mm of thickness. The temperature distribution as a function of thickness at 60 seconds time is shown in Fig (3.23). The total reduction in thickness after 60 seconds will be 0.9 mm as shown in Fig (3.27).

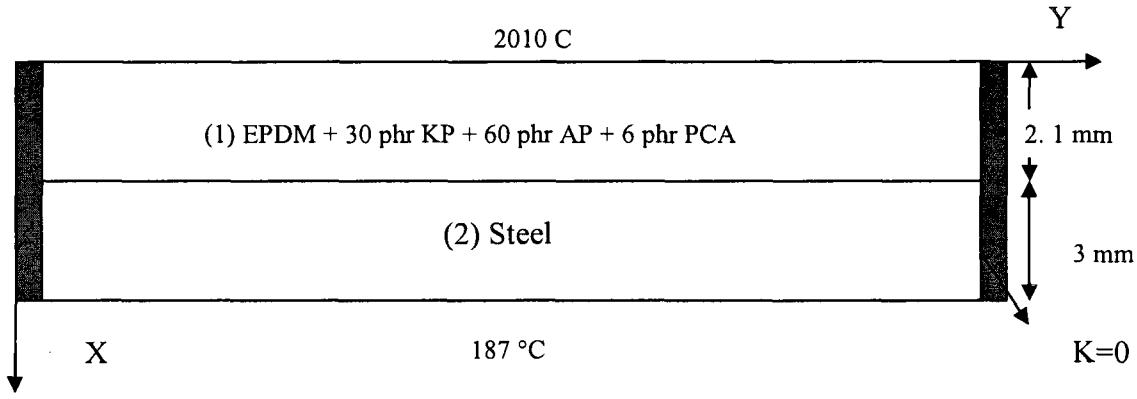

Fig (3.27) Ablation geometric model (1 layer KP based insulation), t = 60 second

3.2.2.1.1.3 Ablation model for CCF / EPDM

By using the same geometry [as shown in Fig (3.17)], But with layer of insulation material based on CCF alone in the mat lab PDE tool and by entering the properties of insulation material and steel as shown in Table (3.5) and taking into account the reduction in thickness of the insulation material due to ablation.

Material number	Material type	Thermal conductivity (W/m.K)	Heat capacity (J/kg.K)	Density (gm/cm^3)	Ablation rate (mm/s)
(1)	EPDM + 50 phr CCF + 60 phr AP + 6 phr PCA	0.453	1549	1.293	0.01
(2)	steel	32.1	822	7.85	-

Table (3.5) Material properties (experimentally measured) [50 phr CCF based EPDM & steel] [Ch 2]

Solving the problem for 60 seconds of total time and with increment of 0.01 second for 4 sub steps of time:

1- Solving from 0 -1 second, the geometry of the model will be as shown in Fig (3.17). After 1 second the insulation material loses 0.01 mm of thickness which corresponds to the experimental ablation rate of this material. The temperature distribution as a function

of thickness at 1 second time is shown in Fig (3.28). The total reduction in thickness after 1 second will be 0.01 mm as shown in Fig (3.29).

2- Solving from 1 -10 seconds, for the geometry shown in Fig (3.29). After 9 seconds the insulation material loses 0.09 mm of thickness. The temperature distribution as a function of thickness at 10 seconds time is shown in Fig (3.28). The total reduction in thickness after 10 seconds will be 0.1 mm as shown in Fig (3.30).

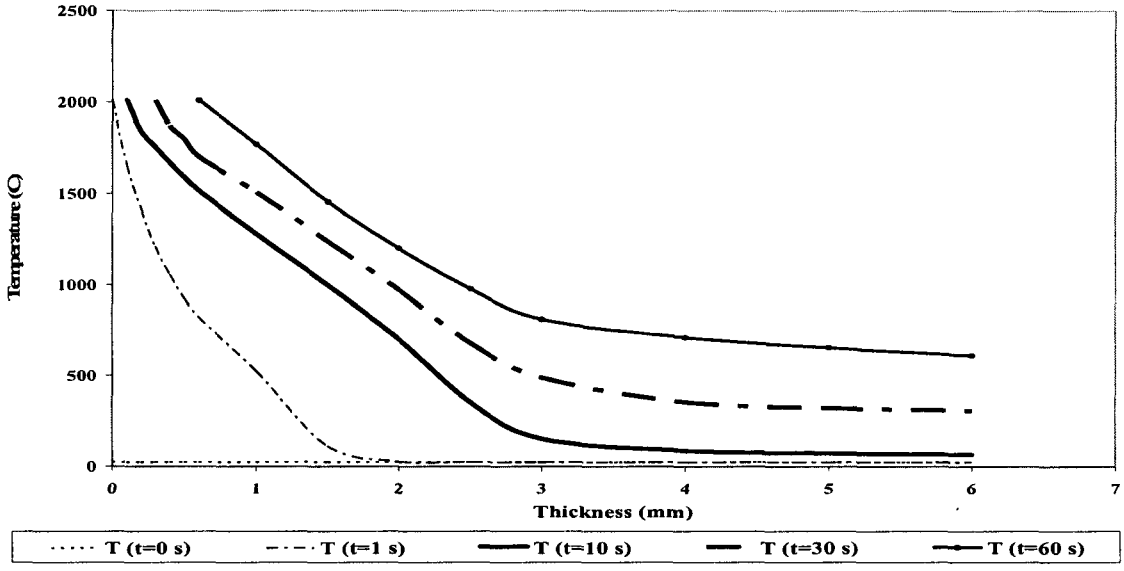

Fig (3.28) Temperature distribution as a function of thickness at different times for CCF based insulation

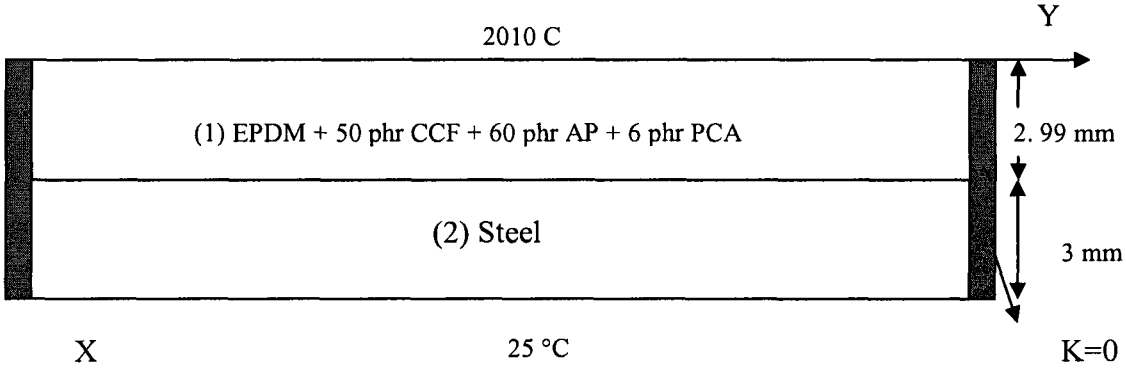

Fig (3.29) Ablation geometric model (1 layer CCF based insulation), t = 1 second

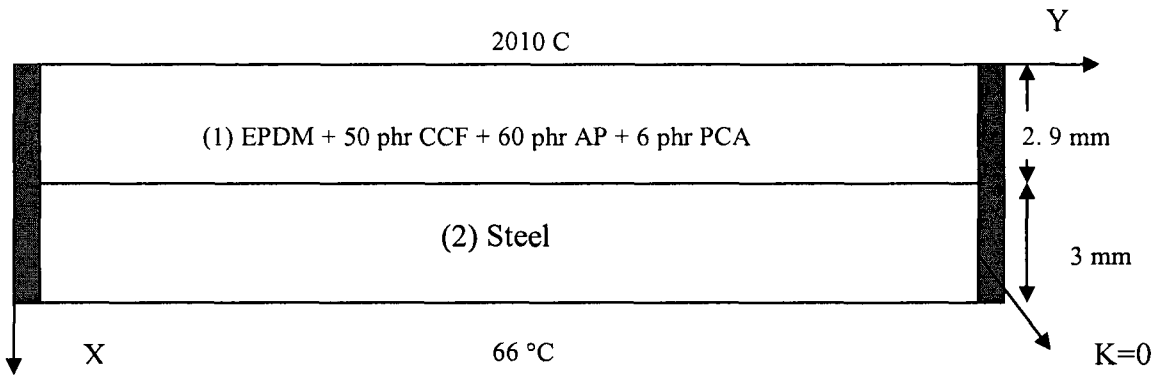

Fig (3.30) Ablation geometric model (1 layer CCF based insulation), t = 10 seconds

3- Solving from 10 -30 seconds, for the geometry shown in Fig (3.30). After 19 seconds the insulation material loses 0.19 mm of thickness. The temperature distribution as a function of thickness at 30 seconds time is shown in Fig (3.28). The total reduction in thickness after 30 seconds will be 0.3 mm as shown in Fig (3.31).

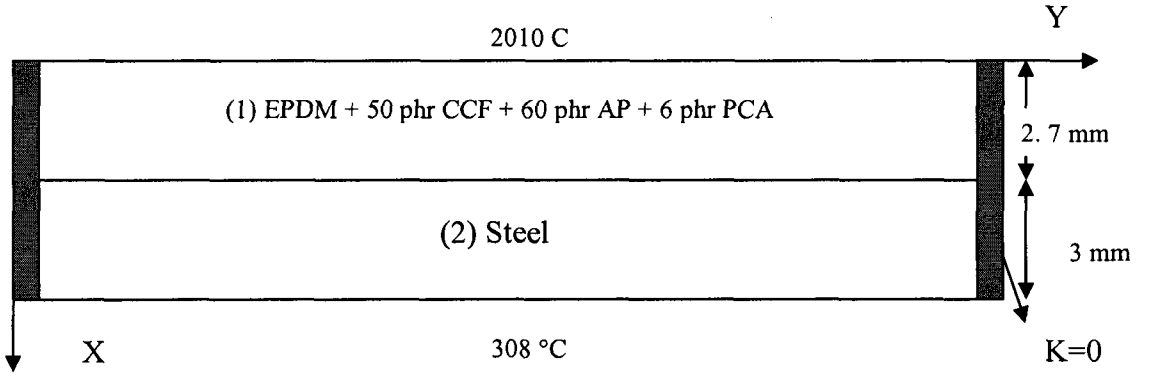

Fig (3.31) Ablation geometric model (1 layer CCF based insulation), t = 30 seconds

4- Solving from 30 -60 seconds, for the geometry shown in Fig (3.31). After 29 seconds the insulation material loses 0.29 mm of thickness. The temperature distribution as a

function of thickness at 60 seconds time is shown in Fig (3.28). The total reduction in thickness after 60 seconds will be 0.6 mm as shown in Fig (3.32).

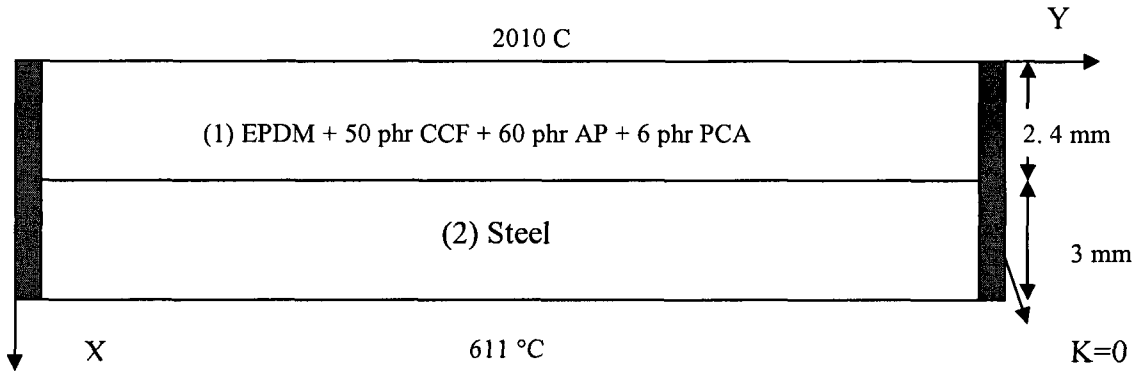

Fig (3.32) ablation geometric model (1 layer CCF based insulation), t = 60 seconds

3.2.2.1.2 Ablation model for 2 alternative layers of insulation

By creating a new geometry as shown in Fig (3.33) in the mat lab PDE tool which represent 2 alternative layers of CCF based insulation and KP based insulation respectively. Entering the properties of insulation material and steel as shown in Table (3.6) and taking into account the reduction in thickness of the insulation material due to ablation.

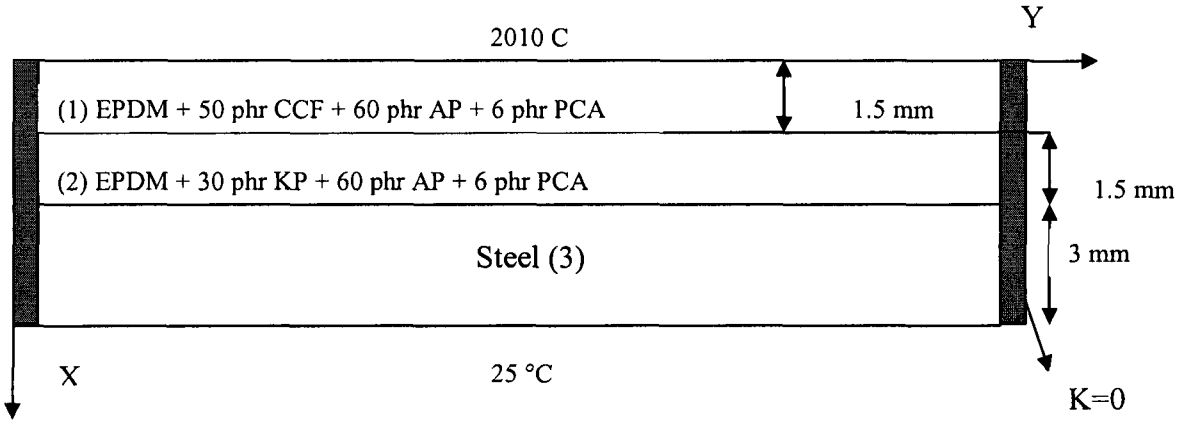

Fig (3.33) ablation geometric model (2 layers, 1 CCF based, 1 KP based)

Material number	Material type	Thermal conductivity (W/m.K)	Heat capacity (J/kg.K)	Density (gm/cm^3)	Ablation rate (mm/s)
(1)	EPDM + 50 phr CCF + 60 phr AP + 6 phr PCA	0.453	1549	1.293	0.01
(2)	EPDM + 30 phr KP + 60 phr AP + 6 phr PCA	0.171	1778	1.185	0.015
(3)	steel	32.1	822	7.85	-

Table (3.6) Material properties (experimentally measured) [50 phr CCF or 30 phr KP based EPDM & steel] [Ch 2]

Solving the problem for 60 seconds of total time and with increment of 0.01 second for 4 sub steps of time,

1- Solving from 0 -1 second, for the geometry shown in Fig (3.33). After 1 second the insulation material loses 0.01 mm of thickness. The temperature distribution as a function of thickness at 1 second time is shown in Fig (3.34). The total reduction in thickness after 1 second will be 0.01 mm as shown in Fig (3.35).

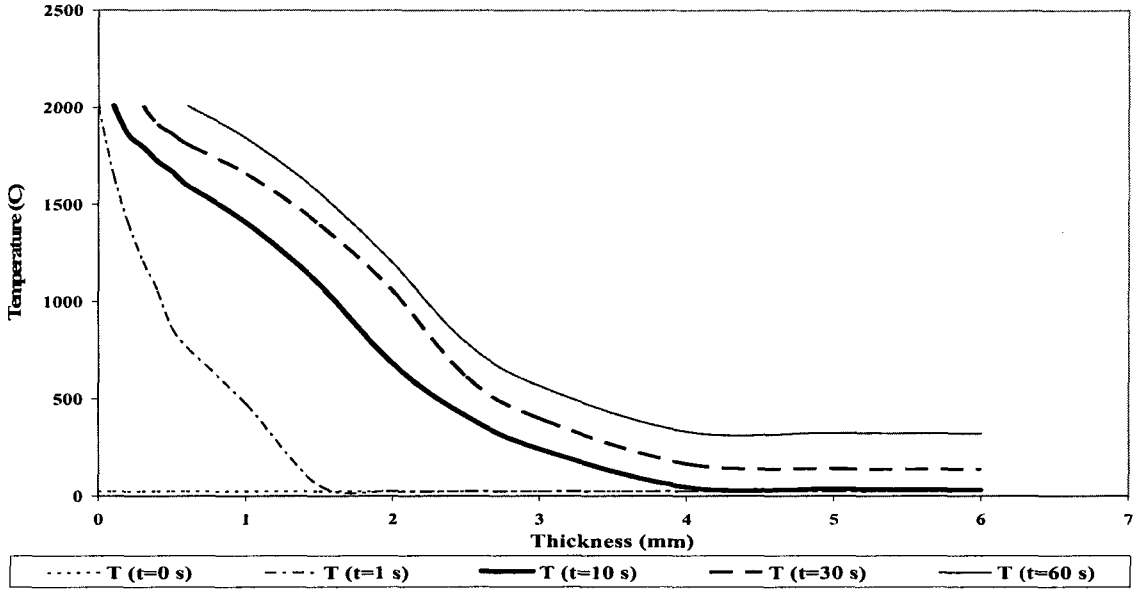

Fig (3.34) Temperature distribution as a function on of thickness at different times for 2 layers (CCF or KP) based insulation

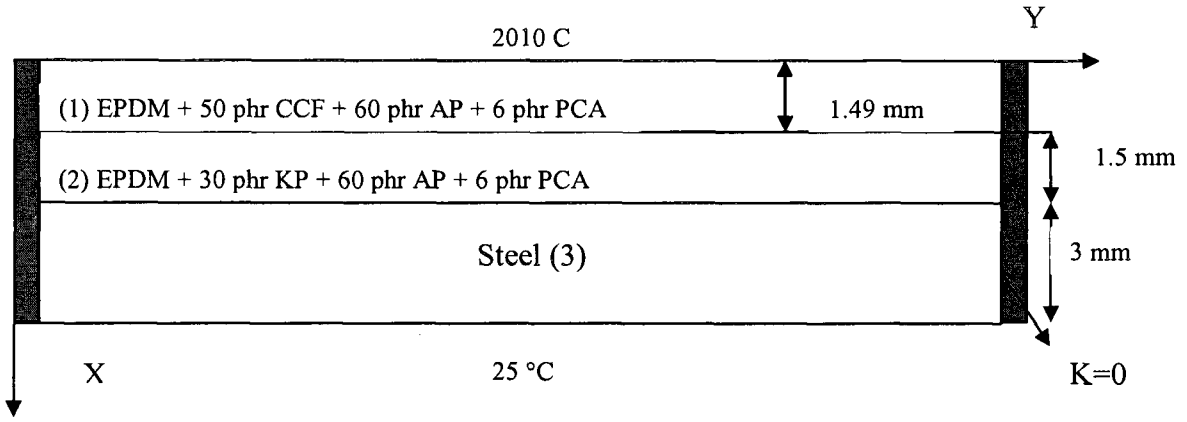

Fig (3.35) Ablation geometric model (2 layers, 1 CCF based, 1 KP based), t = 1 seconds

2- Solving from 1 -10 second, for the geometry shown in Fig (3.35). After 9 seconds the insulation material loses 0.09 mm of thickness. The temperature distribution as a function of thickness at 10 seconds time is shown in Fig (3.34). The total reduction in thickness after 10 seconds will be 0.1 mm as shown in Fig (3.36).

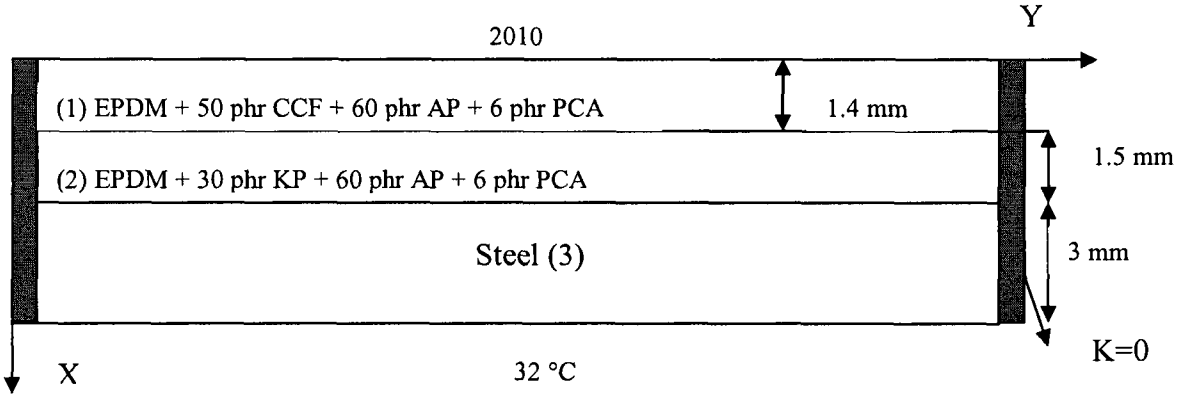

Fig (3.36) Ablation geometric model (2 layers, 1 CCF based, 1 KP based), t = 10 seconds

3- Solving from 10 -30 second, for the geometry shown in Fig (3.36), After 19 second the insulation material loses 0.19 mm of thickness. The temperature distribution as a function

of thickness at 30 seconds time is shown in Fig (3.34). The total reduction in thickness after 30 seconds will be 0.3 mm as shown in Fig (3.37).

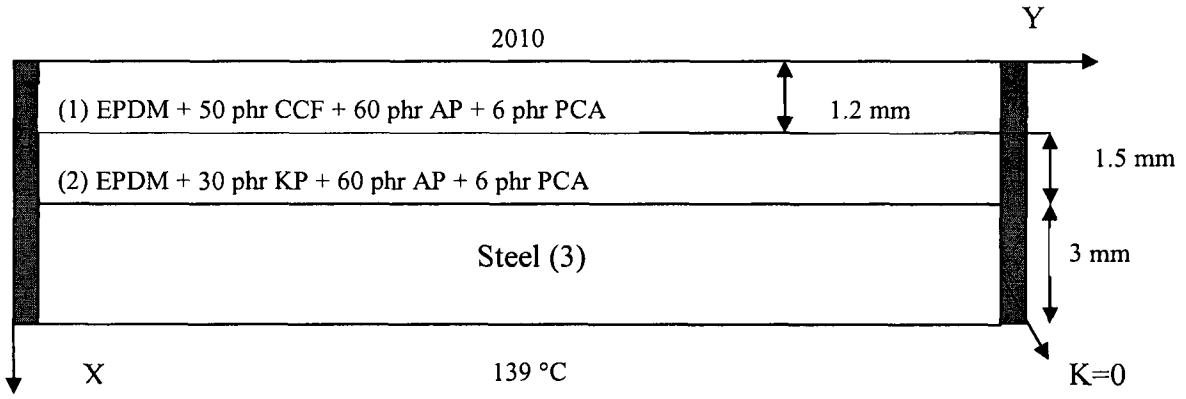

Fig (3.37) Ablation geometric model (2 layers, 1 CCF based, 1 KP based), t = 30 seconds

4- Solving from 30 -60 second, for the geometry shown in Fig (3.37). After 29 second the insulation material loses 0.29 mm of thickness, the temperature distribution as a function of thickness at 60 seconds time is shown in Fig (3.34). The total reduction in thickness after 60 seconds will be 0.6 mm as shown in Fig (3.38).

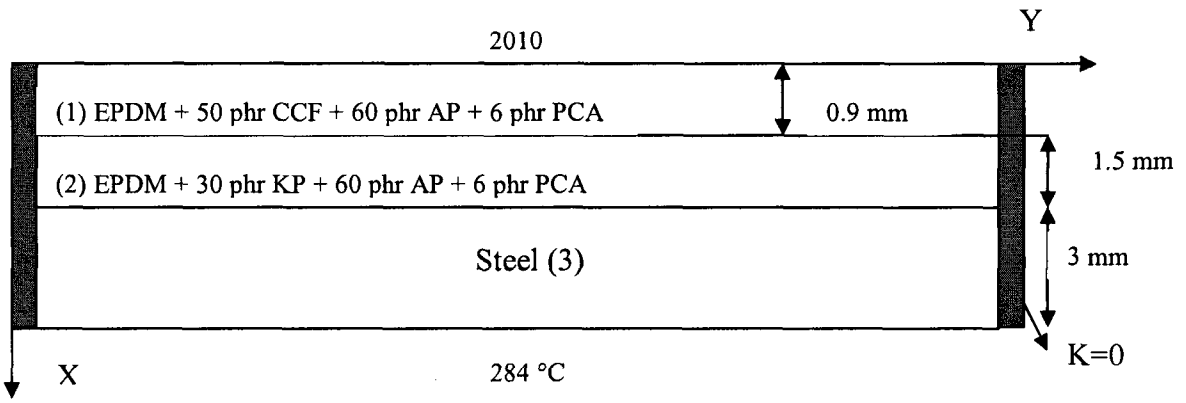

Fig (3.38) ablation geometric model (2 layers, 1 CCF based, 1 KP based), t = 60 seconds

3.2.2.1.3 Ablation model for 4 alternative layers of insulation

By creating a new geometry as shown in Fig (3.39) in the mat lab PDE tool which represent 4 alternative layers of CCF based insulation and KP based insulation respectively. Entering the properties of insulation material and steel as shown in Table (3.6) and taking into account the reduction in thickness of the insulation material due to ablation. Solving the problem for 60 seconds of total time and with increment of 0.01 second for 4 substeps of time:

1- Solving from 0 -1 second, for the geometry shown in Fig (3.39). After 1 second the insulation material loses 0.01 mm of thickness. The temperature distribution as a function of thickness at 1 second time is shown in Fig (3.40). The total reduction in thickness after 1 second will be 0.01 mm as shown in Fig (3.41).

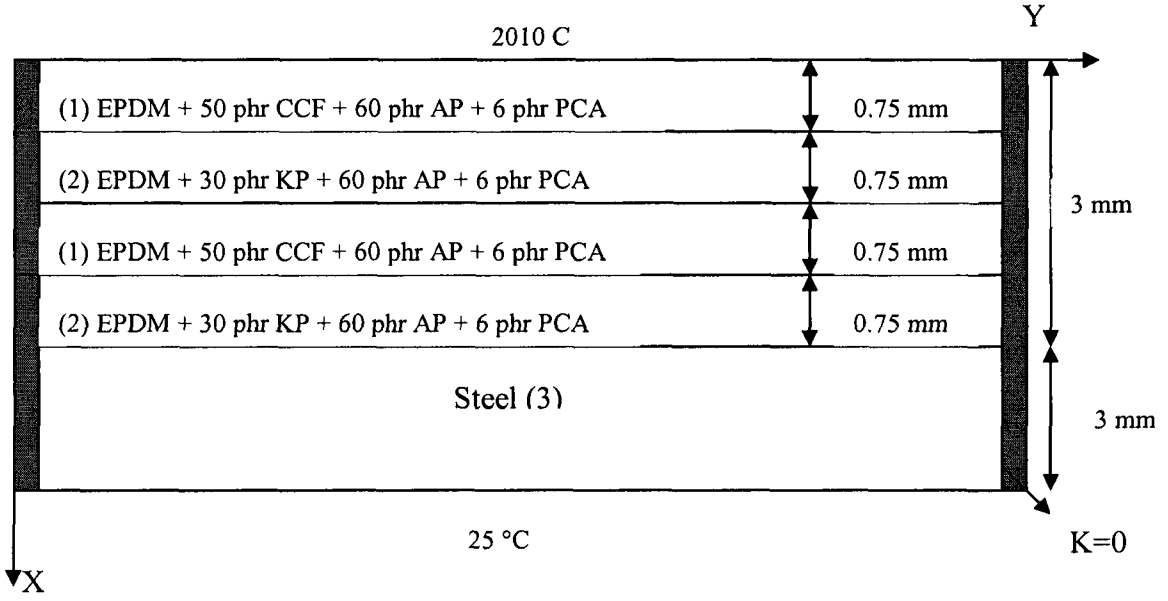

Fig (3.39) Ablation geometric model (4 layers, 2 CCF based, 2 KP based), t = 0 seconds

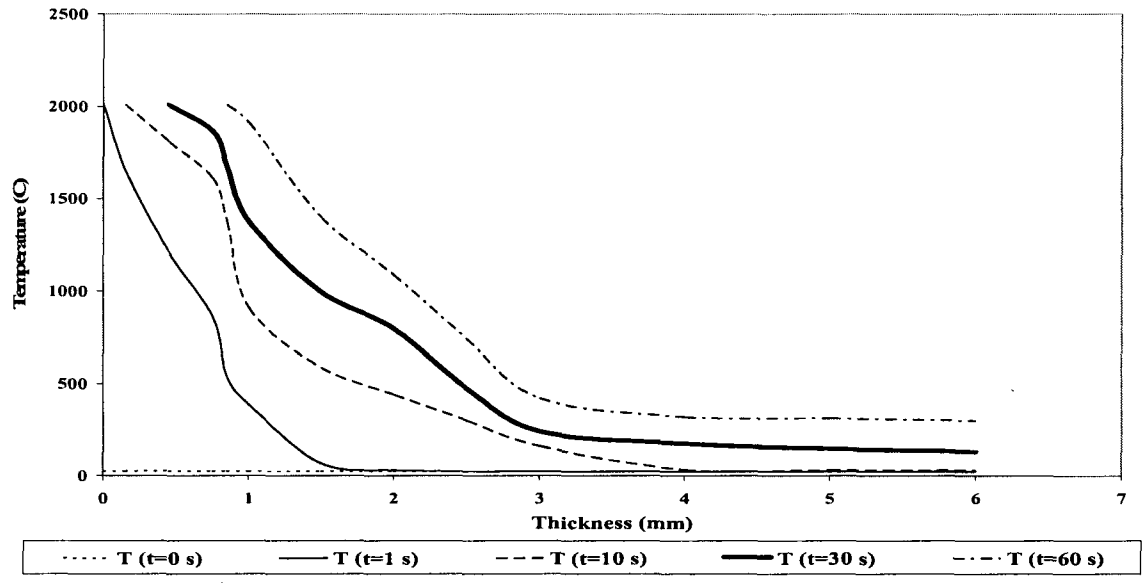

Fig (3.40) Temperature distribution as a function on of thickness at different times for 4 layers (CCF or KP) based insulation

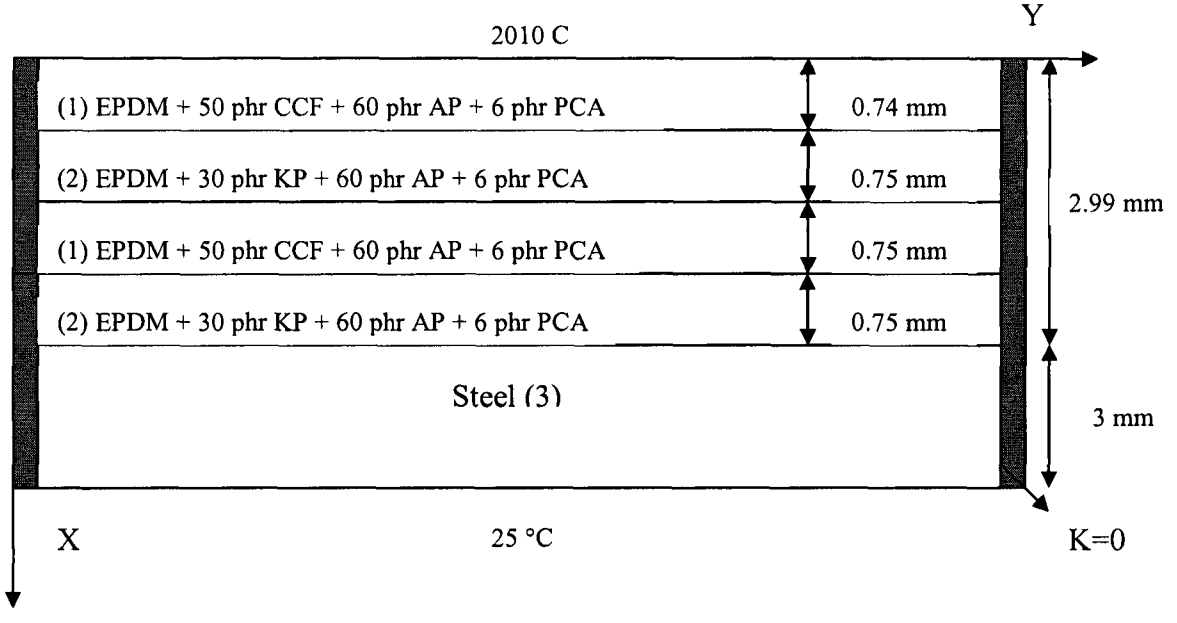

Fig (3.41) Ablation geometric model (4 layers, 2 CCF based, 2 KP based), t = 1 seconds

2- Solving from 1 -10 second, for the geometry shown in Fig (3.41). After 9 second the insulation material loses 0.09 mm of thickness, the temperature distribution as a function

of thickness at 10 seconds time is shown in Fig (3.40). The total reduction in thickness after 10 seconds will be 0.1 mm as shown in Fig (3.42).

3- Solving from 10 -30 second, for the geometry shown in Fig (3.42). After 19 second the insulation material loses 0.19 mm of thickness, the temperature distribution as a function of thickness at 30 seconds time is shown in Fig (3.40). The total reduction in thickness after 30 seconds will be 0.3 mm as shown in Fig (3.43).

4- Solving from 30 -60 second, for the geometry shown in Fig (3.43), After 29 second the insulation material loses 0.29 mm of thickness, the temperature distribution as a function of thickness at 60 seconds time is shown in Fig (3.40). The total reduction in thickness after 60 seconds will be 0.6 mm as shown in Fig (3.44).

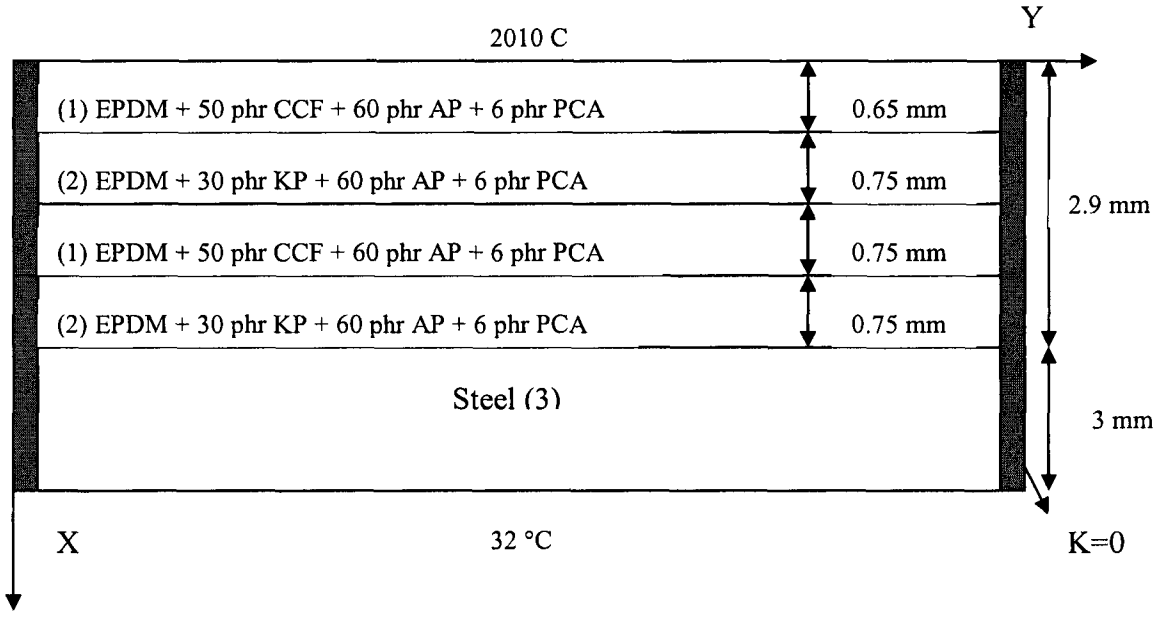

Fig (3.42) Ablation geometric model (4 layers, 2 CCF based, 2 KP based), t = 10 seconds

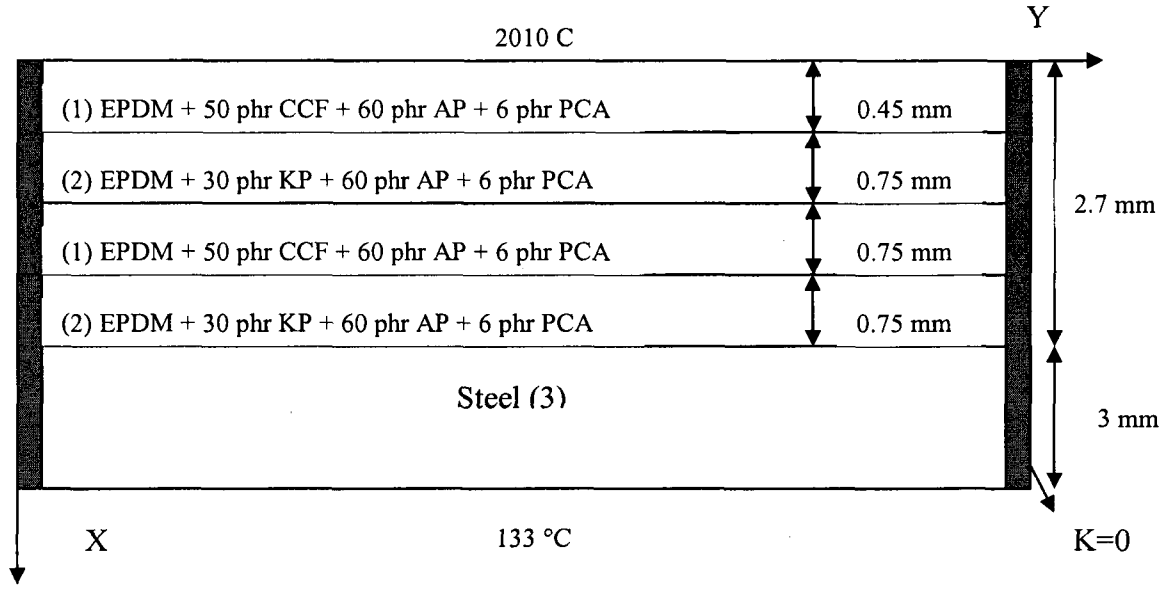

Fig (3.43) Ablation geometric model (4 layers, 2 CCF based, 2 KP based), t = 30 seconds

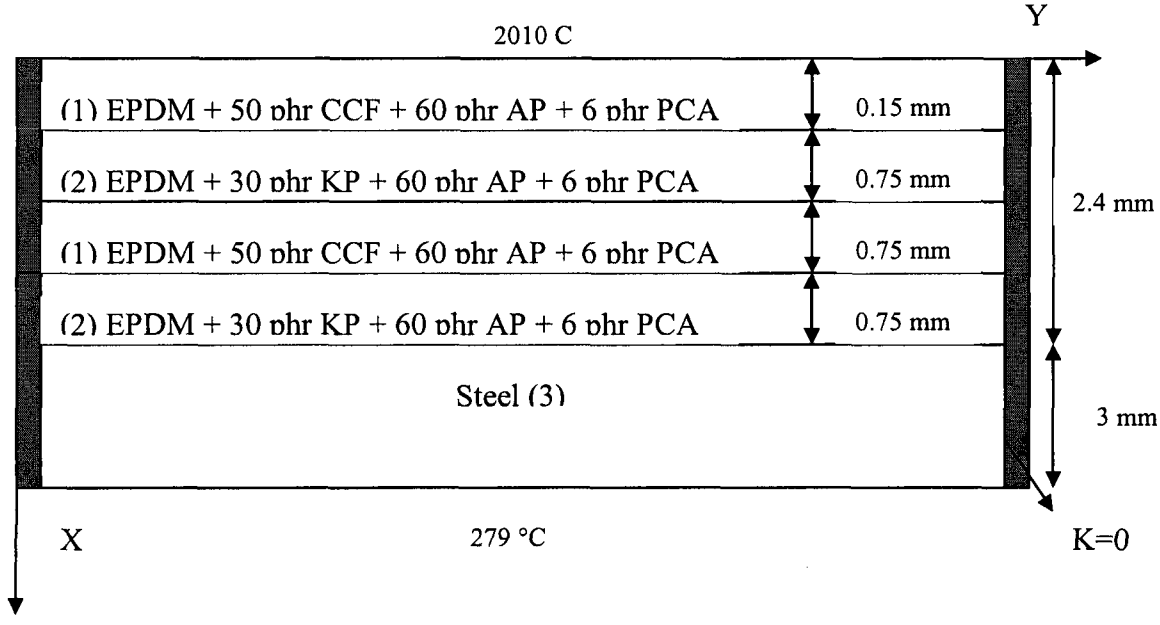

Fig (3.44) Ablation geometric model (4 layers, 2 CCF based, 2 KP based), t = 60 seconds

3.2.2.1.4 Ablation model for 6 alternative layers of insulation

By creating a new geometry as shown in Fig (3.45) in the mat lab PDE tool and by entering the properties of insulation material and steel as shown in Table (3.6) and taking into account the reduction in thickness of the insulation material due to ablation.

Solving the problem for 60 seconds of total time and with increment of 0.01 second for 4 sub steps of time:

1- Solving from 0 -1 second, for the geometry shown in Fig (3.45). After 1 second the insulation material loses 0.01 mm of thickness. The temperature distribution as a function of thickness at 1 second time is shown in Fig (3.46). The total reduction in thickness after 1 second will be 0.01 mm as shown in Fig (3.47).

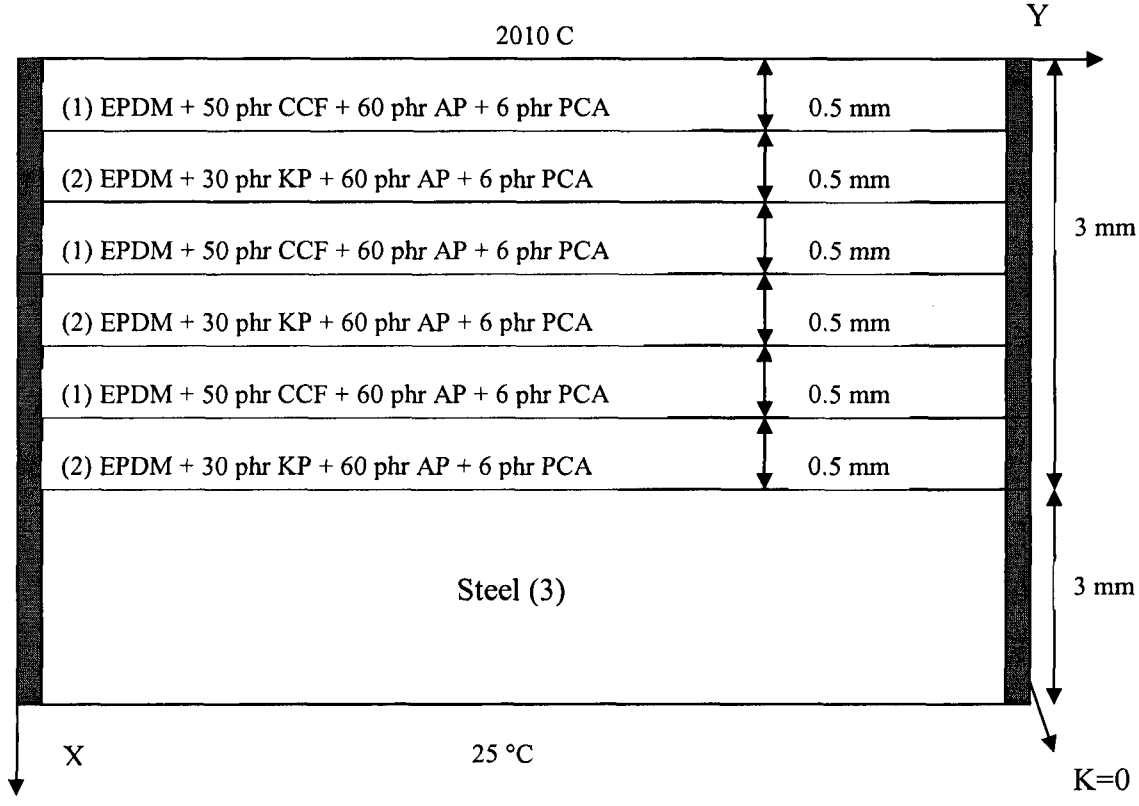

Fig (3.45) Ablation geometric model (6 layers, 3 CCF based, 3 KP based), t = 0 seconds

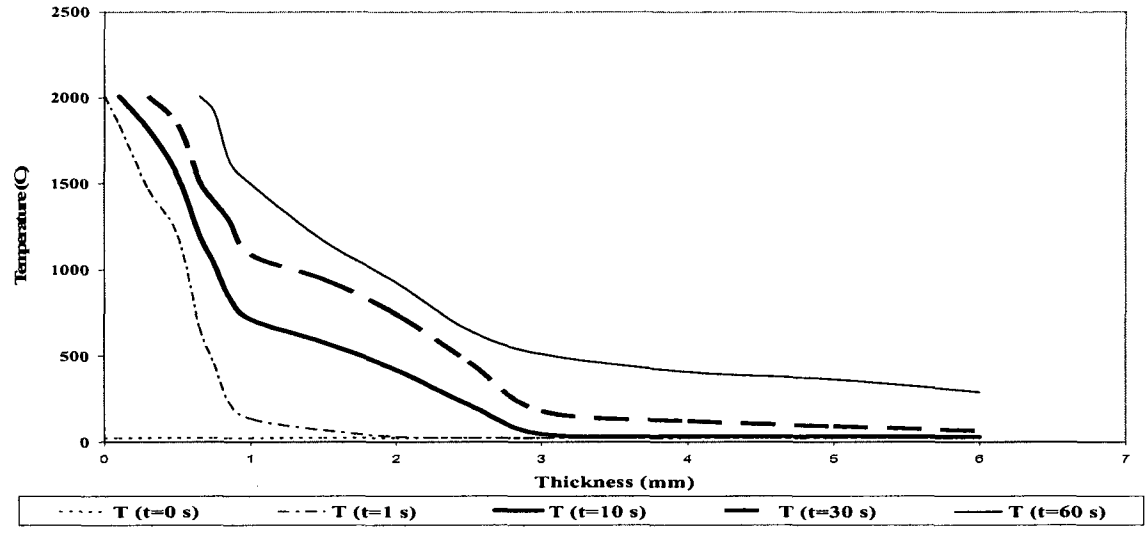

Fig (3.46) Temperature distribution as a function on of thickness at different times for 6 layers (CCF or KP) based insulation

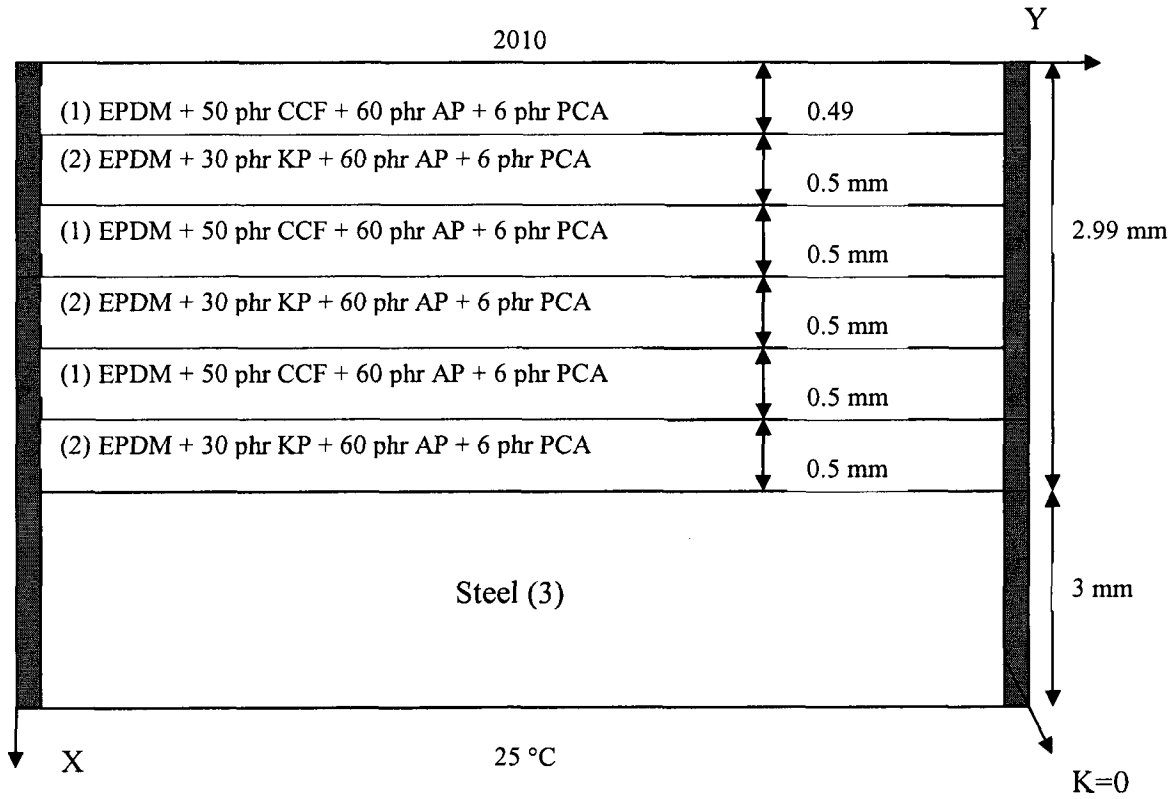

Fig (3.47) Ablation geometric model (6 layers, 3 CCF based, 3 KP based), t = 1 seconds

2- Solving from 1 -10 second, for the geometry shown in Fig (3.47), After 9 second the insulation material loses 0.09 mm of thickness. The temperature distribution as a function of thickness at 10 seconds time is shown in Fig (3.46). The total reduction in thickness after 10 seconds will be 0.1 mm as shown in Fig (3.48).

3- Solving from 10 -30 second, for the geometry shown in Fig (3.48), After 19 second the insulation material loses 0.19 mm of thickness. The temperature distribution as a function of thickness at 30 seconds time is shown in Fig (3.46). The total reduction in thickness after 30 seconds will be 0.3 mm as shown in Fig (3.49).

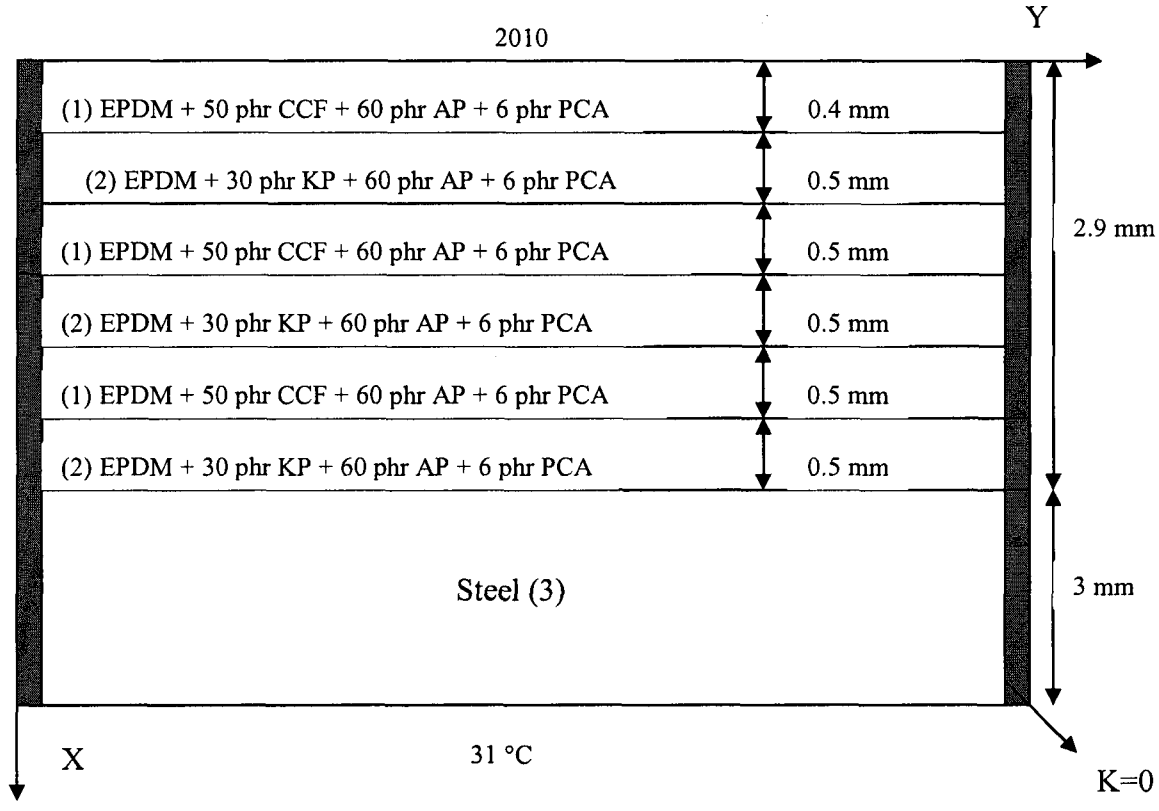

Fig (3.48) Ablation geometric model (6 layers, 3 CCF based, 3 KP based), t = 10 seconds

4- Solving from 30 -60 second, for the geometry shown in Fig (3.49), After 29 second the insulation material loses 0.34 mm of thickness. The temperature distribution as a function of thickness at 60 seconds time is shown in Fig (3.46). The total reduction in thickness after 60 seconds will be 0.65 mm as shown in Fig (3.50).

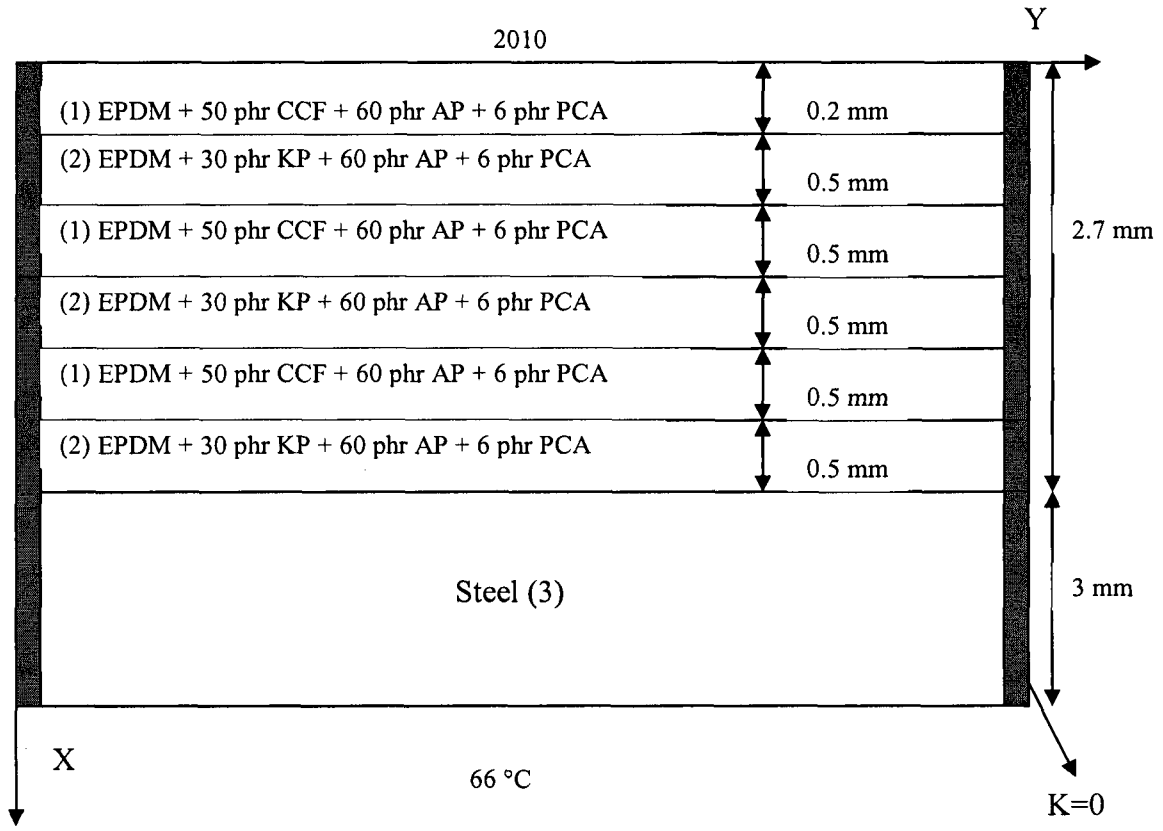

Fig (3.49) Ablation geometric model (6 layers, 3 CCF based, 3 KP based), t = 30 seconds

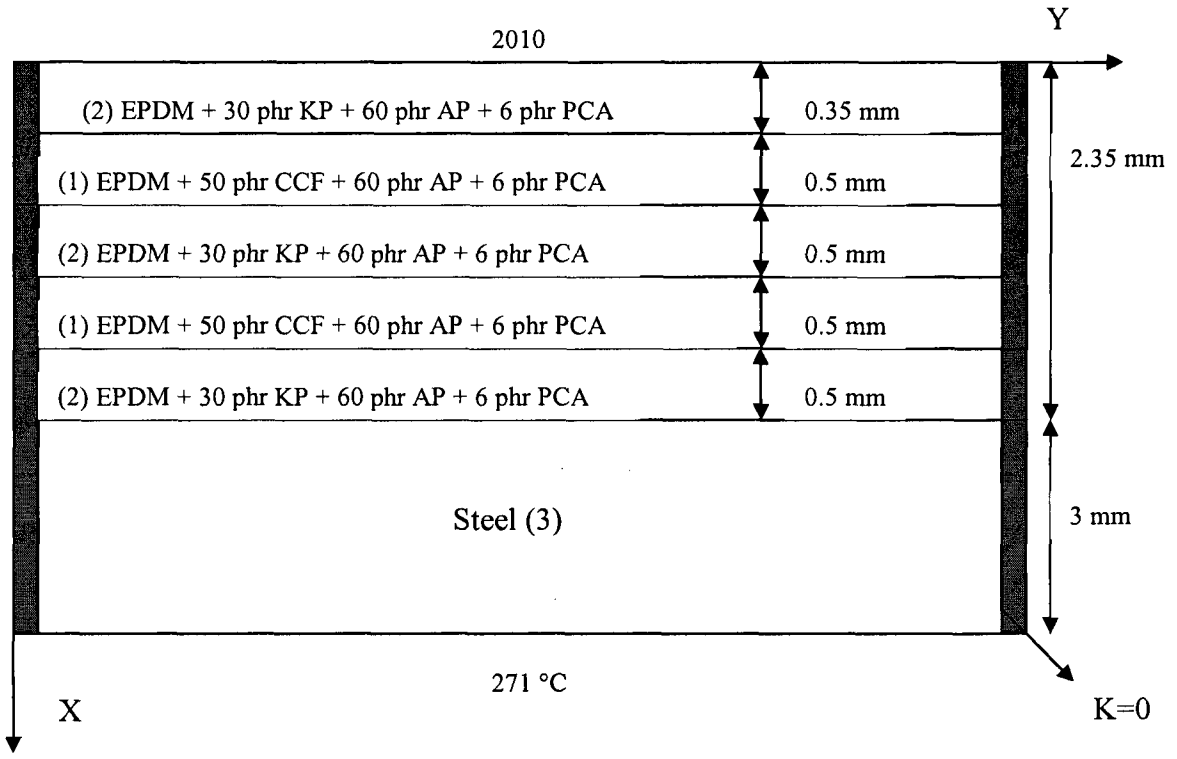

Fig (3.50) Ablation geometric model (6 layers, 3 CCF based, 3 KP based), t = 60 second

It appears from all the analysis that the temperature of a point in the bottom surface of steel vary as shown in Table (3.7).

N	Layers geometry	Temperature at surface of steel (°C)
1	1 layer of hybrid (CCF + KP) based insulation	288
2	1 layer of CCF based insulation	611
3	1 layer of KP based insulation	187
4	2 layers of single reinforcement (CCF or KP) based insulation	284
5	4 layers placed alternatively of single reinforcement (CCF or KP) based insulation	279
6	6 layers placed alternatively of single reinforcement (CCF or KP) based insulation	271

Table (3.7) Temperature comparison for different insulations geometries at the bottom surface of steel

It appears from Table (3.7) that the contribution of the torch (2010 °C) in the temperature of the outside steel surface decreases by increasing the number of alternating layers of CCF or KP based insulation.

3.2.2.2 Ablation test with consideration of the properties of char

Knowledge of insulator function is a prerequisite to both selection of material and thickness design. Most current insulators for solid rocket motors function as heat barriers primarily through the mechanism of ablation; i.e., the material absorbs heat by increasing in temperature and changing in chemical or physical state, the changes usually being accompanied by loss of surface material. The best current knowledge of the ablative insulation function divides the material into three zones as shown in Fig (3.51) [100-103].

(1) Virgin - material zone

(2) Decomposition zone

(3) Reaction or char zone

The interfaces that separate these zones are somewhat indistinct, but even so the zones can be defined by the principle phenomena found in each.

In the virgin material zone, the phenomena are relatively simple. The temperatures are low enough that changes in chemical properties of the material are negligible, and heat is transferred by simple conduction.

In the decomposition zone, energy is absorbed by the fragmentation and scission of molecules. As the temperature of the material increases, the decomposition reactions become more vigorous and cause a substantial polymer weight loss. Decomposition of some inorganic fillers also occurs, and occluded water is lost. Two energy – transfer modes are present in the decomposition zone:

(1) Transfer by conduction

(2) Transfer by pyrolysis and subsequent loss of hot combustion products

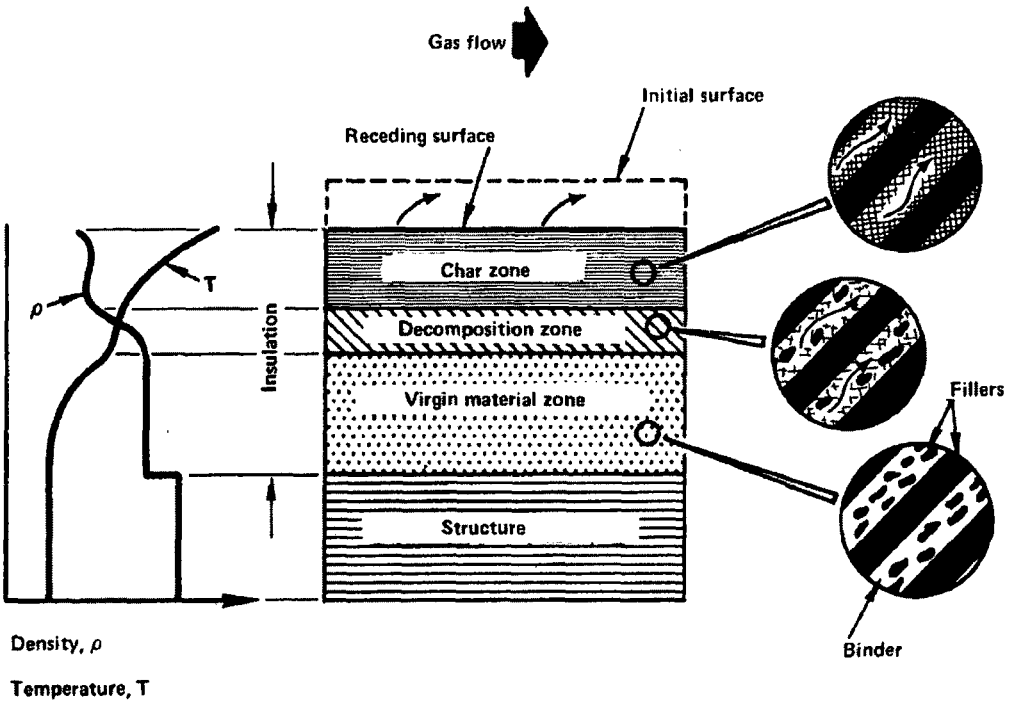

Fig (3.51) Model of ablating insulation [100]

As the temperature of the reaction increases, a large percentage of the total energy accommodated in the overall ablation process is absorbed by cracking and heating of pyrolysis gases. The magnitude of the energy absorption depends on the chemical content of the materials involved and on the temperature at which the reaction occurs. In general, the majority of decomposition reactions are endothermic.

In the char zone, phenomena are similar to those in the decomposition zone. The principle difference being the particular reactions involved. The decomposition reaction produces a residue that continues to decompose and finally yields a residue that is primarily elemental carbon. Decomposition of inorganic components and pyrolysis gas

cracking are also characteristic of this zone. Cracking of the low-temperature pyrolysis gas may result in the deposition of carbon within the char layer, the so called "coking" effect.

As exposure to the motor combustion environment continues, surface material is eroded. The term "surface regression" is used to describe the total effect of various modes of surface loss. These modes include:

(1) chemical effects:

- Surface chemical reactions of char-layer components with propellant gases and particles (usually liquid)
- Subsurface reactions (usually pyrolysis) in the char zone and the decomposition zone

(2) physical effects

- Surface erosion due to particle impingement and shear stress imposed by skin friction
- Thermal stress induced by heat transfer
- Subsurface weakening due to mechanical and thermal stresses in the char layer and the decomposition zone: i.e., spallation due to internal pressure created by pyrolysis gas

(3) Combinations of chemical and physical effects

Charring ablators are used in a greater variety of thermal environments because of their ability to withstand a much higher heat flux. In the charring ablator, the ablative material acts as a heat sink, absorbing all of the incident heat flux and causing the surface temperature to increase quickly. At reaction temperature, endothermic chemical

decomposition occurs: the organic matrix pyrolizes into carbonized material and gaseous products. The passage of heat-absorbing gases through the charred surface provides further insulative performance and thickens the boundary layer, reducing the convective heat transfer. The charring is a continuous process: as the charred surface is eroded by the severe surface environment, more char forms to take its place. Research shows that the char layer formed after decomposition reduces the heat flux passing through it. This blocking action can reduce the net heating of the ablative material by more than 50%. [104-106].

The heat flow rate through the thickness x is

$$q = -KA \frac{dT}{dx}$$

Since the area A is constant, the only way to reduce the heat flow rate through the thickness is to reduce the thermal conductivity of the material by 50 % since we need to find the temperature gradient through the thickness (dT/dx).

3.2.2.2.1 Ablation model for 1 layer of insulation

By applying this condition and by creating the geometry as shown in Fig (3.17) in the mat lab PDE tool and by entering the properties of insulation material (based on a hybrid reinforcement of CCF and KP) and steel as shown in Table (3.3) and taking into account the reduction in thickness of the insulation material due to ablation.

Solving the problem for 60 seconds of total time and with increment of 0.01 second for 4 sub steps of time:

1- Solving from 0 -1 second, the geometry of the model is as shown in Fig (3.17). After 1 second the insulation material loses 0.005 mm of thickness which corresponds to the experimental ablation rate of this material. A layer of 0.1 mm thickness has a temperature

above 1440 C (the decomposition temperature of KP). In the next run for solution we assume this layer (0.1 – 0.005 = 0.0995 mm) has thermal conductivity 0.1465 W/ m.C. This thermal conductivity is half of the experimental thermal conductivity of the insulation material (experimental thermal conductivity of 25 phr CCF + 25 phr KP based EPDM = 0.293 w/m.C). The assumption in reduction of thermal conductivity is due to the formation of char layer with thickness 0.0995 mm which reduces the heat flux passing throught it by more than 50 %. The temperature distribution as a function of thickness at 1 second time is shown in Fig (3.52). The total reduction in thickness after 1 second will be 0.005 mm as shown in Fig (3.19).

2- Solving from 1 -10 seconds, for the geometry shown in Fig (3.19). After 9 seconds the insulation material loses 0.045 mm of thickness. The total reduction in thickness after 10 seconds will be 0.05 mm as shown in Fig (3.20). A layer of 0.15 mm thickness has a temperature above 1440 C (the decomposition temperature of KP). In the next run for solution we assume this layer (0.1 – 0.05 = 0.095 mm) have thermal conductivity 0.1465 w/ m.C. This thermal conductivity is half of the experimental thermal conductivity of the insulation material (0.293 W/m.C). The assumption in reduction of thermal conductivity is due to the formation of total (new + from step 1) char layer with thickness 0. 095 mm which reduces the heat flux passing throught it by more than 50 %. The temperature distribution as a function of thickness at 10 seconds time is shown in Fig (3.52).

3- Solving from 10 -30 seconds, for the geometry shown in Fig (3.20). After 19 seconds the insulation material loses 0.095 mm of thickness. The total reduction in thickness after 30 seconds will be 0.15 mm as shown in Fig (3.21). A layer of 0.3 mm thickness has a temperature above 1440 C (the decomposition temperature of KP). In the next run for

solution we assume this layer (0.3 – 0.15 = 0.15 mm) have thermal conductivity 0.1465 w/ m.C. This thermal conductivity is half of the experimental thermal conductivity of the insulation material (0.293 W /m.C). The assumption in reduction of thermal conductivity is due to the formation of total (new + from step 1 + from step 2) char layer with thickness 0. 15 mm which reduce the heat flux passing throught it by more than 50 %. The temperature distribution as a function of thickness at 30 seconds time is shown in Fig (3.52).

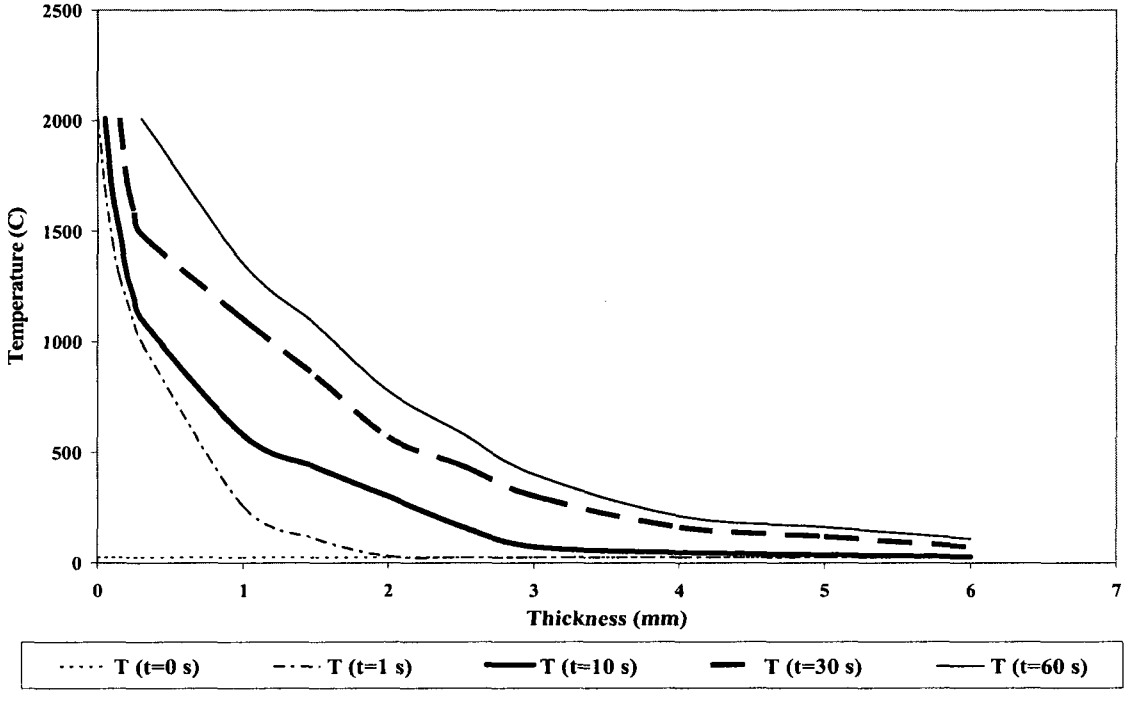

Fig (3.52) Temperature distribution as a function of thickness at different times for 1 layer (CCF and KP) based insulation

4- Solving from 30 -60 seconds, for the geometry shown in Fig (3.21). After 29 seconds the insulation material loses 0.145 mm of thickness. The total reduction in thickness after 60 seconds will be 0.3 mm as shown in Fig (3.22). A layer of (0.9 – 0.3 = 0.6 mm) thickness has a temperature above 1440 C (the decomposition temperature of KP). The

temperature distribution as a function of thickness at 60 seconds time is shown in Fig (3.52).

By using the same geometry [as shown in fig (3.17)] used before but with layer of insulation material based on KP alone in the mat lab PDE tool and by entering the properties of insulation material and steel as shown in Table (3.4) and taking into account the reduction in thickness of the insulation material due to ablation. By doing the same last 4 sub steps but with the reduction for thermal conductivity from 0.171 to 0.08505 W/m.K., the temperature distribution as a function of thickness at different times is shown in Fig (3.53).

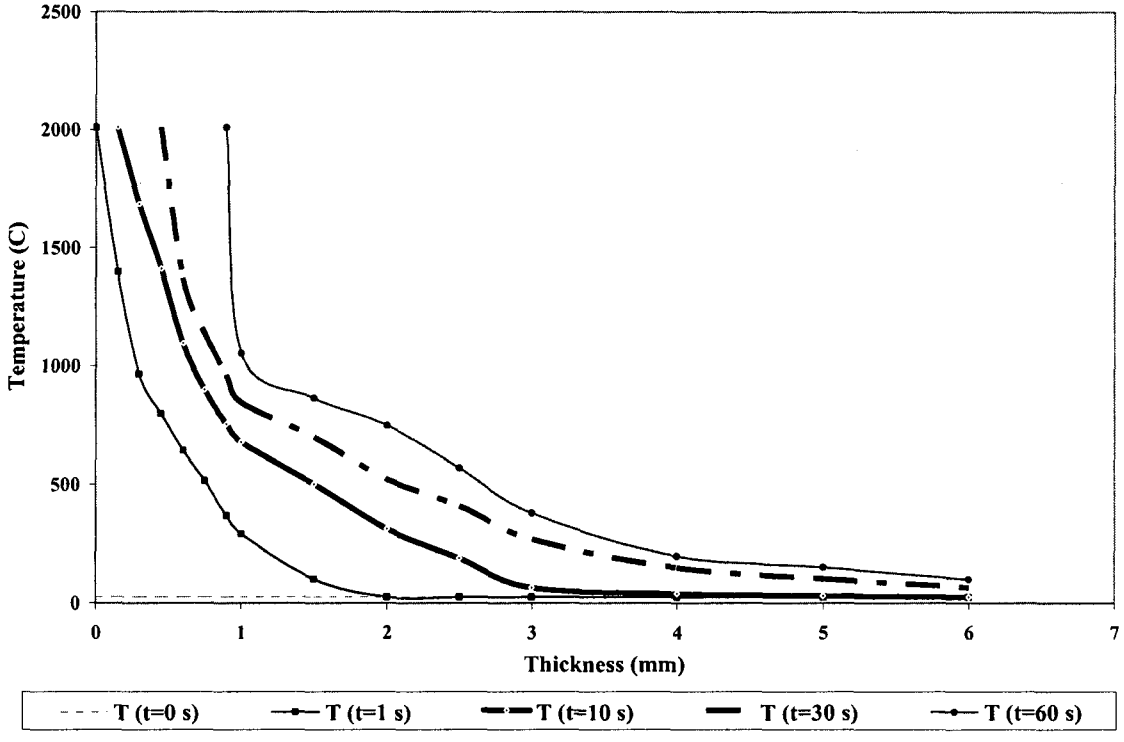

Fig (3.53) Temperature distribution as a function of thickness at different times for 1 layer (KP) based insulation

By using the same geometry [as shown in fig (3.17)], But with layer of insulation material based on CCF alone in the mat lab PDE tool and by entering the properties of insulation material and steel as shown in Table (3.5) and taking into account the reduction in thickness of the insulation material due to ablation. By doing the same last 4 sub steps but with the reduction for thermal conductivity from 0.453 to 0.2265 W/m.K, [and by considering the layers of char formed after a temperature above 1000 C (the decomposition temperature of epoxy sizing of chopped carbon fiber)], the temperature distribution as a function of thickness at different times is shown in Fig (3.54).

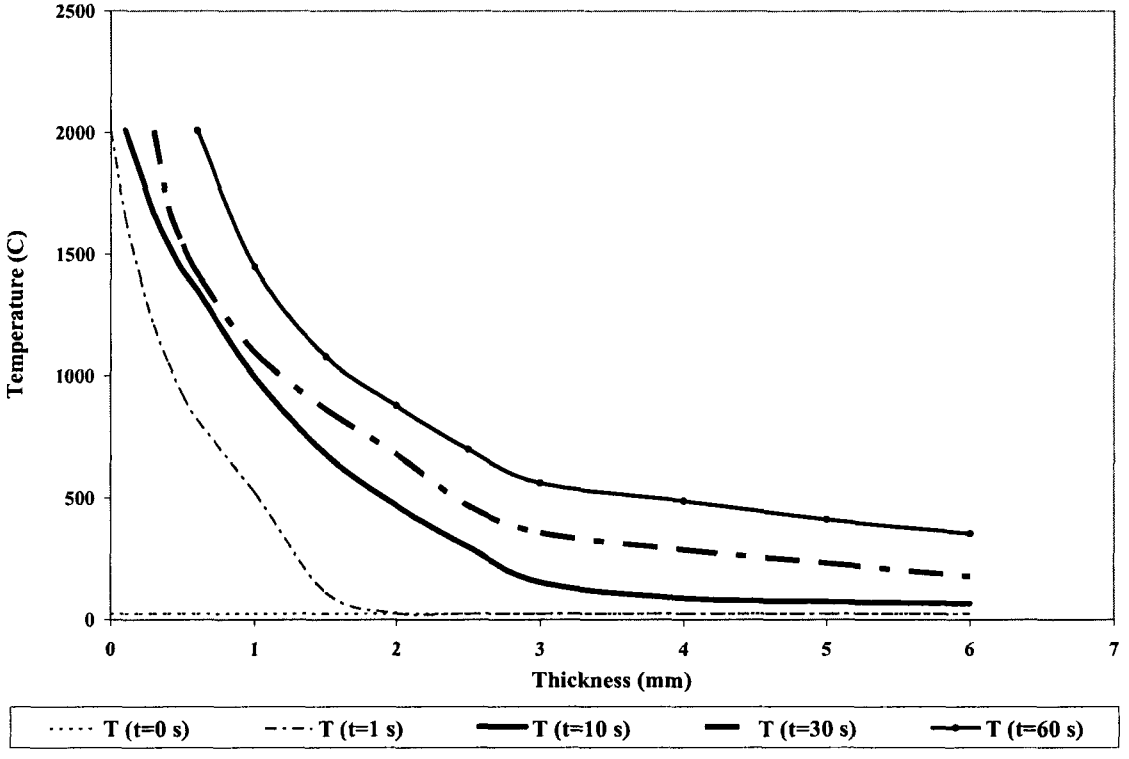

Fig (3.54) Temperature distribution as a function of thickness at different times for 1 layer (CCF) based insulation

3.2.2.2.2 Ablation model for 2 alternative layers of insulation

By creating a new geometry as shown in Fig (3.33) in the mat lab PDE tool and by entering the properties of insulation material and steel as shown in Table (3.6) and taking into account the reduction in thickness of the insulation material due to ablation.

By doing the same last 4 sub steps but with the reduction for thermal conductivity from 0.453 to 0.2265 W/m.K for CCF based layers and with the reduction for thermal conductivity from 0.171 to 0.0855 W/m.K for KP based layers according to the distance from the surface. And by considering the layers of char formed after a temperature above 1000 C (the decomposition temperature of epoxy sizing of chopped carbon fiber) for CCF based layers and a temperature above 1440 C (the decomposition temperature of KP) for KP based layers.

The temperature distribution as a function of thickness at different times is shown in Fig (3.55).

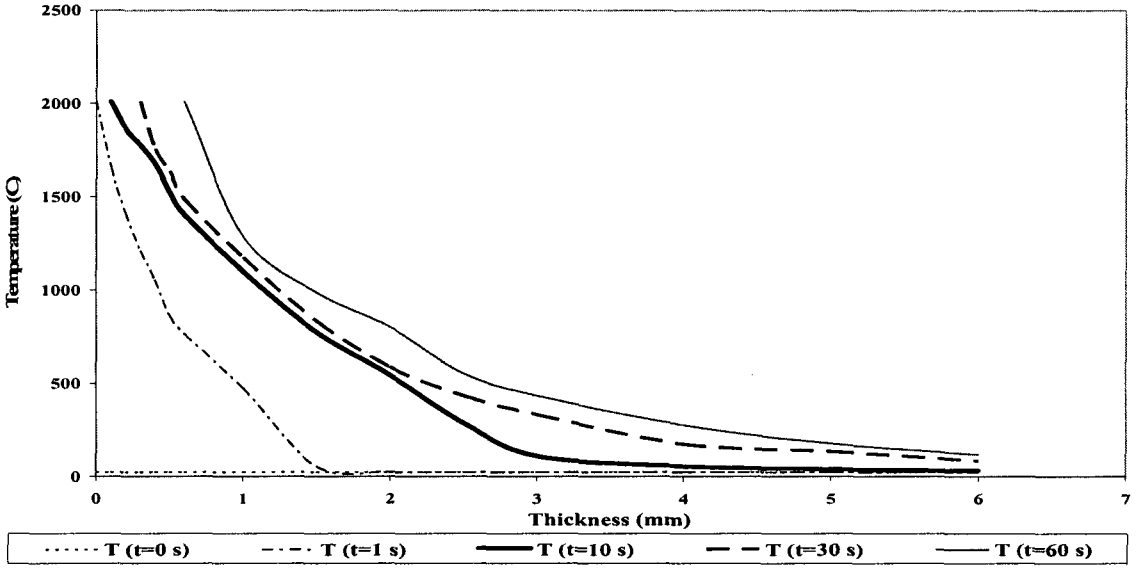

Fig (3.55) Temperature distribution as a function of thickness at different times for 2 layers (CCF or KP) based insulation

3.2.2.2.3 Ablation model for 4 alternative layers of insulation

By creating a new geometry as shown in Fig (3.39) in the mat lab PDE tool and by entering the properties of insulation material and steel as shown in Table (3.6) and taking into account the reduction in thickness of the insulation material due to ablation. The temperature distribution as a function of thickness at different times is shown in Fig (3.56).

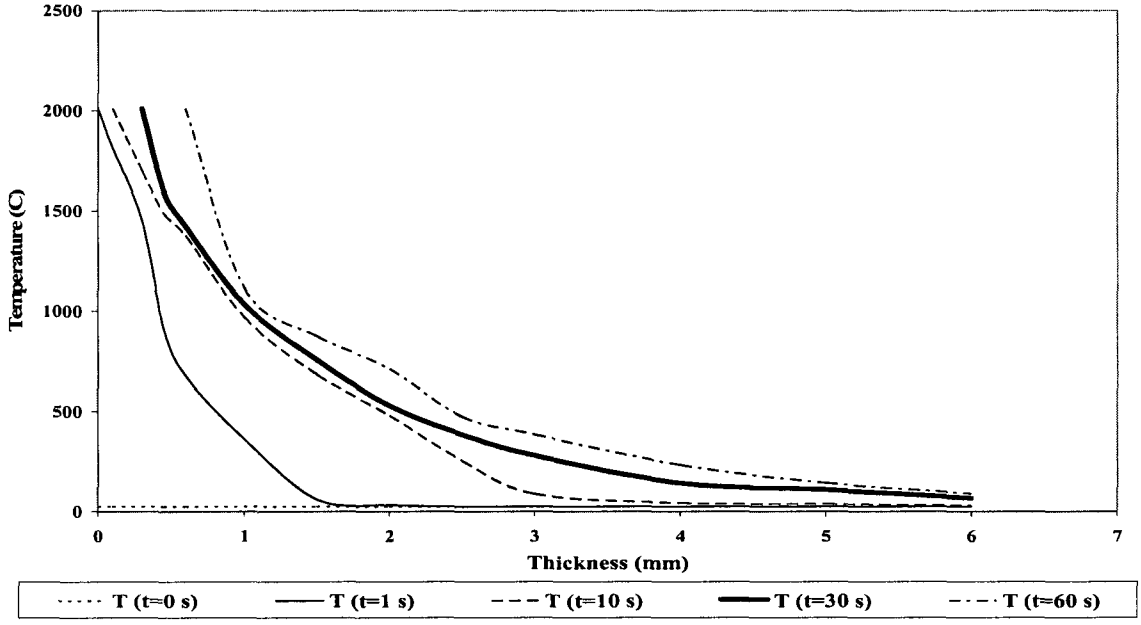

Fig (3.56) Temperature distribution as a function of thickness at different times for 4 layers (CCF or KP) based insulation

3.2.2.2.4 Ablation model for 6 alternative layers of insulation

By creating a new geometry as shown in Fig (3.45) in the mat lab PDE tool and by entering the properties of insulation material and steel as shown in Table (3.6) and taking into account the reduction in thickness of the insulation material due to ablation. The temperature distribution as a function of thickness at different times is shown in Fig (3.57).

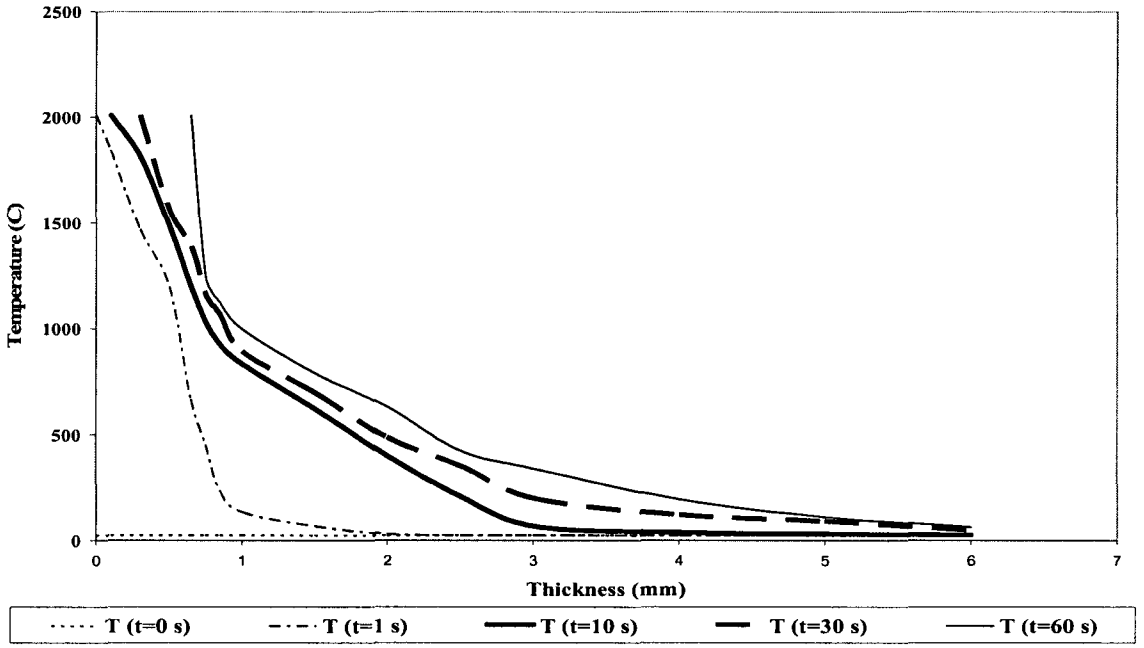

Fig (3.57) Temperature distribution as a function of thickness at different times for 6 layers (CCF or KP) based insulation

A summary of all the analysis shows the temperature of a point in the bottom surface of steel in Table (3.8)

N	Layers geometry	Temperature at surface of steel (°C)
1	1 layer of hybrid (CCF + KP) based insulation	109
2	1 layer of CCF based insulation	355
3	1 layer of KP based insulation	99
4	2 layers of single reinforcement (CCF or KP) based insulation	118
5	4 layers placed alternatively of single reinforcement (CCF or KP) based insulation	88
6	6 layers placed alternatively of single reinforcement (CCF or KP) based insulation	64

Table (3.8) Temperature comparison for different insulations geometries at the bottom surface of steel

3.2.2.3 Experimental and theoretically temperature results of ablation test

According to ASTM-E-285-80 the ablation tests were done by preparing samples of the insulation material with 3 mm thickness and length 20 cm and width 20 cm and the sample is weighed before the test. Then it is bonded to a steel piece with the same dimensions using the special adhesive Epon 828 and Epicure which is specified for gluing of rubber to steel and with adhesive thickness approximately 0.3 mm. Then a high accurate thermocouple is fixed in the back of steel sheet and the insulation material is subjected to MAPP torch (2010 °C) for 60 seconds. The temperature rise in the back of steel is recorded as function of time.

For 50 phr CCF based insulation the temperature rise in the back of steel is recorded as function of time versus that predicted from modeling as shown in Fig (3.58).

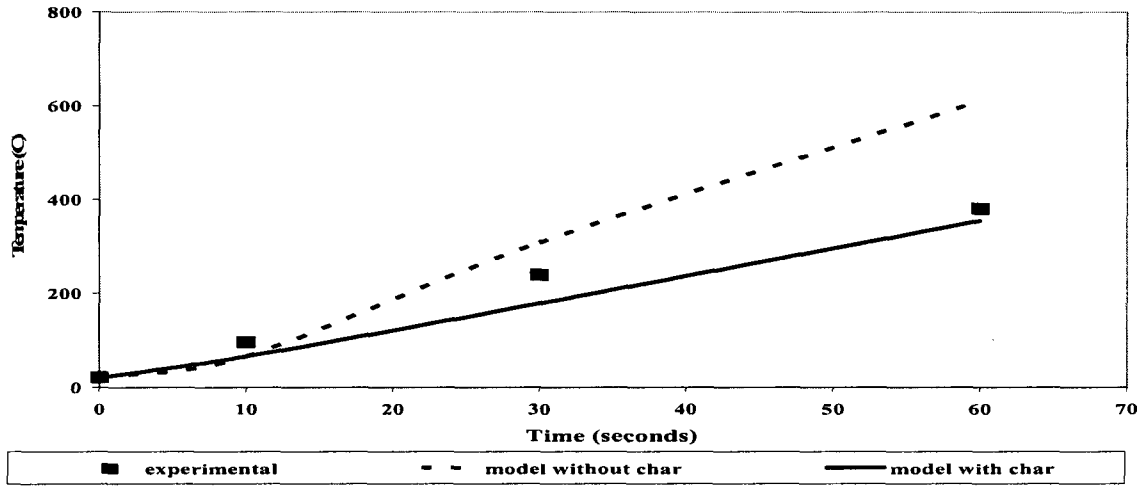

Fig (3.58) Experimental temperature rise in the back of steel as function of time versus these predicted by models for 50 CCF based insulation

The difference is very large between the predicted from model without considering the properties of char and experimentally measured, while it is reasonable between the

predicted from model with considering the properties of char and experimentally measured.

For 30 phr KP based insulation the temperature rise in the back of steel is recorded as function of time versus that predicted from modeling as shown in Fig (3.59).

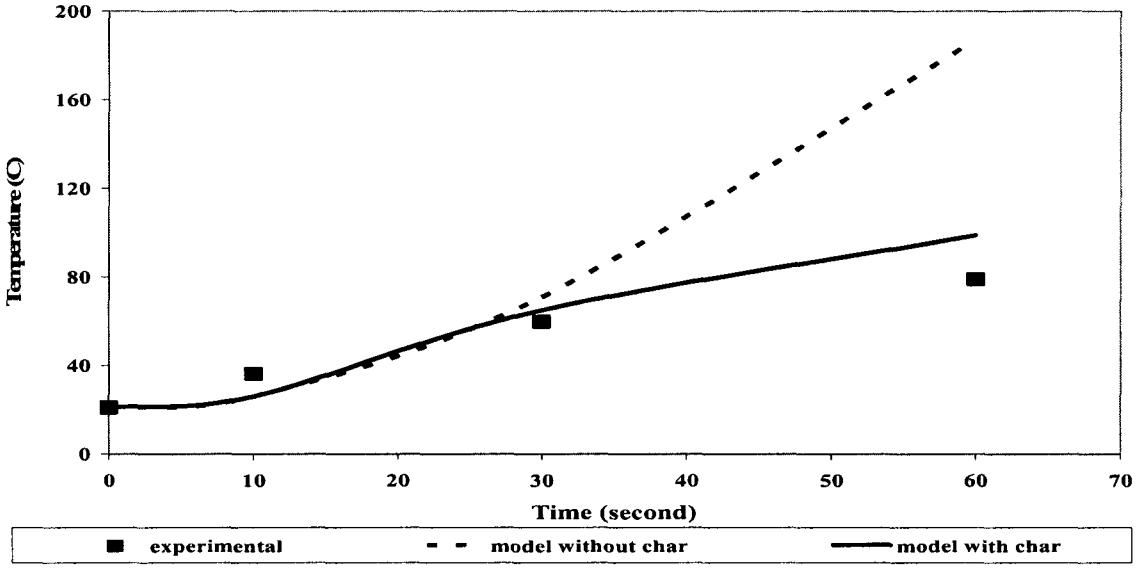

Fig (3.59) Experimental temperature rise in the back of steel as function of time versus these predicted by models for 30 KP based insulation

The difference is very large between the predicted from model without considering the properties of char and experimentally measured, while it is reasonable between the predicted from model with considering the properties of char and experimentally measured.

For 25 phr CCF + 25 phr KP based insulation the temperature rise in the back of steel is recorded as function of time versus that predicted from modeling as shown in Fig (3.60).

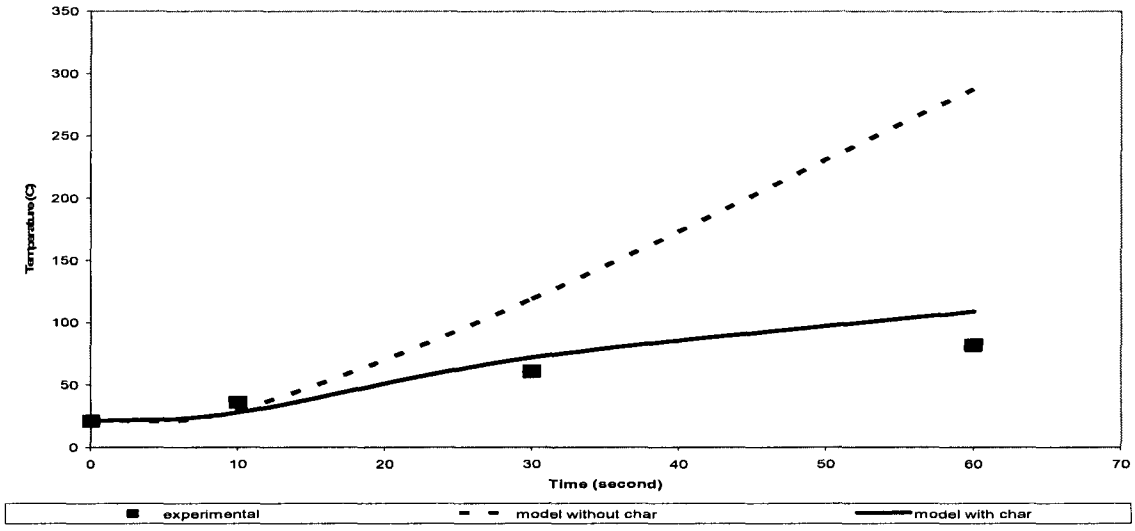

Fig (3.60) Experimental temperature rise in the back of steel as function of time versus these predicted by models for 25 phr CCF + 25 phr based insulation

The difference is very large between the predicted from model without considering the properties of char and experimentally measured, while it is reasonable between the predicted from model with considering the properties of char and experimentally measured.

Chapter 4

Development of the thermal insulation in prepreg form

Analysis of the thermal conductivity along the thickness direction of the sample reveals that the random phase distribution may not be the most efficient arrangement. In the composition of the three phases, the common phase is rubber, which serves as a matrix holding the other phases together. Between the chopped carbon fibers and Kevlar pulp, one phase is highly thermally conductive (chopped carbon fiber) and the other (Kevlar pulp) is not. By using the rule of mixtures for phases connected in parallel (layers of the components aligned parallel to the heat flow), in series (layers of the components aligned perpendicular to the heat flow), in random order (The Maxwell–Eucken model assumes a dispersion of small spheres within a continuous matrix of a different component) and in completely random order (The EMT model assumes a completely random distribution of all the components) the prediction of the thermal conductivity for the composite was made.

Using a volume fraction of 25 phr for chopped carbon fiber and 25 phr for Kevlar pulp inside 100 phr EPDM, using the conductivity values of 6.4 $W\,m^{-1}\,K^{-1}$ for chopped carbon fiber, 0.04 $W\,m^{-1}\,K^{-1}$ for Kevlar pulp and 0.36 $W\,m^{-1}\,K^{-1}$ for EPDM, the thermal conductivities for the composite in the different cases are as follows:

0.165 $W\,m^{-1}\,K^{-1}$ for series distribution

1.313 $W\,m^{-1}\,K^{-1}$ for parallel distribution

0.434 $W\,m^{-1}\,K^{-1}$ for random distribution (Maxwell Eucken)

0.479 $W\,m^{-1}\,K^{-1}$ for completely random distribution (EMT)

It can be seen that connection in series is the best arrangement for having low thermal conductivity, which is the objective of this development. If one can rearrange the phases from being randomly distributed to connection in series, one may obtain better insulation using the same amount of materials.

In addition, the work done for modeling of the ablation test [Ch 3] shows that using alternative layers of 50 phr CCF and 30 phr KP based insulation will show improvement in lowering the temperature in the back of steel over using only one layer of 50 phr CCF based insulation, 30 phr KP based insulation and 25 phr CCF + 25 phr KP based insulation. Also the numerical simulation for the heat transfer through the sample shows that the larger is the number of layers (meaning the thinner is the thickness of the sub layers) the better is the result (the smaller is the thermal conductivity) as shown in Fig (4.1).

So a question arises as how to manufacture the insulation material in the prepreg form and how to put the plies in a specific stacking sequence and cure it to perform a laminate of the insulation material.

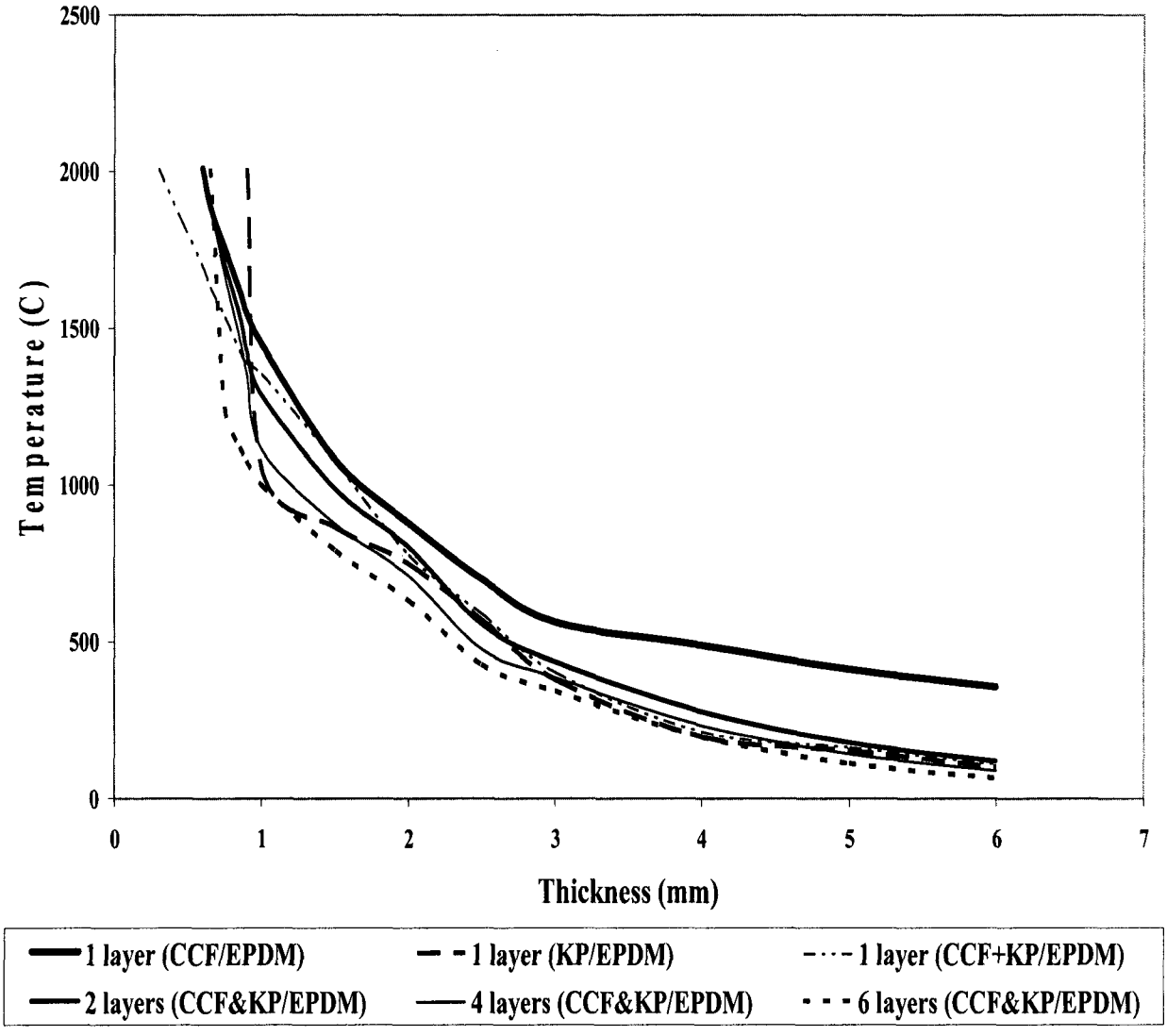

Fig (4.1) Temperature distribution as a function of thickness (after 60 seconds) for different number of layers based laminate

4.1 What is prepreg

Pre-impregnated composite material (prepreg) is used widely in the manufacture of composite parts. Prepreg is a combination of uncured resin and fiber reinforcement, which is in a form that is ready for molding and curing into the final composite part. By pre-impregnating the fiber reinforcement with resin, the manufacturer can carefully

control the amount and location of resin that is impregnated into the fiber network and ensure that the resin is distributed in the network as desired. It is well known that the relative amount of fibers and resin in a composite part and the distribution of resin within the fiber network have a large effect on the structural properties of the part.

Basically, a general prepreg consists of a fiber reinforcement impregnated to a pre-determined level with a resin. The resin system will usually be a matrix offering a broad range of properties. Stringent control of resin content and dispersion eliminates the risk of fiber fraction variation and resin-rich areas, which ultimately control laminate performance.

There are several advantages to using a prepreg instead of hand laying layers of reinforcement.

1) Good resin content means maximum strength properties and general performance.

2) Good resin content means part uniformity and repeatability. Without the pitfalls of human lamination techniques, there will be neither resin rich areas nor dry spots. Thickness will be uniform and every part that comes out of the mold has a theoretical likelihood of being identical.

3) Less mass and less waste.

4) Optimum cured network. After the heat curing cycle is completed, the part is ready for service.

5) Better surface finish. Mold preparation and mold release are easier

A process for preparing prepreg from polymer in the rubber form (elastomers) is very difficult and this is the first time research is done on this area. In addition, how to arrange the phases to have connection in series is a big challenge. When the three phases are

mixed together (in addition to the flame retardant material), they produce a random pattern. In order to have the arrangement in series as shown in Fig (4.2), one needs to place the Kevlar phases in alternating positions with the chopped carbon fiber phases. That means that one needs to produce thin layers of CCF/EPDM and thin layers of KP/EPDM and then place them on top of each other alternatively. EPDM is an elastomeric material. EPDM solids are produced by cross linking the rubber. Cross linking agents are added to form link between the rubber molecules. If there is insufficient amount of cross linking, the thin layers will be too liquid and they can not be handled. If too much cross linking has formed, the rubber will not be sticky. If the CCF/EPDM layers and the KP/EPDM layers are not sticky, they will not bond to each other and the assembly can not be made. Experimentation was carried out to determine the appropriate amount of cross linking agent so that the thin layers can be solid enough to be handlable and yet liquid enough to be sticky for bonding purpose afterwards. This type of thin layers is termed EPDM prepregs. Another set of experimentation was carried out to determine the appropriate curing cycle during the molding process to press the thin layers together.

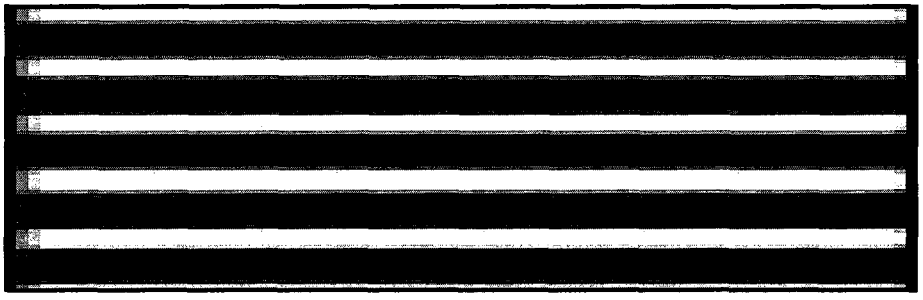

Fig (4.2) Series alignment in composites

It takes a long time to convert EPDM based master batch into the prepreg form. One important difficulty is the stickiness of raw EPDM before cure. Consequently, there is a

need to find ways and means of reducing this stickiness in EPDM at least at the surface to fabricate the prepreg to provide repellence from the mold and the release film.

The regular form of materials supplied in the prepreg is reinforcement in the textile fabric impregnated by a low viscous resin such as woven carbon or woven glass impregnated with epoxy resin. These materials can be stored, shipped and handled at room temperatures and is cured using a specific curing cycle.

The candidate pre-preg considerations should include storage life, open mold life and be sufficient to meet the properties of this application. This should allow for lay-up and subsequent rapid cure on large composite parts. Shelf life should be at the maximum possible within the capabilities of rubber system.

Pre-preg properties will be assessed and provided to ensure adequate performance; such as matrix content, fiber area weight, cured ply thickness, density, adhesion, etc.

The target here is to get the master batch result from the C. W. Brabender mixer and fabricate it to the prepreg form with sufficient degree of cure and then fabricate the final laminate with a specific stacking sequence and get the maximum degree of cure.

Appropriate resin content can be achieved by mixing well all the constituents inside the C. W. Brabender mixer and follow the mixing procedure.

4.2 Development of the insulation material in the prepreg form

The objective is to design, fabricate, and test a pre-preg system with the optimized matrix and reinforcement content. The system must have the final production environment, limitations, and quantities required for the application. Handling properties of the final pre-preg must be manufacturing friendly, and be able to be used with the standard set of

tools and procedures available in a typical clean room of a composite manufacturing facility.

The mixing procedure for mixing the master batch of the insulation by using the C.W. Bra bender is:

1- Warm the specified amount of EPDM (Trilene 67) inside a beaker on the furnace at 90 °C for 30 min. to allow easy flow into the mixing chamber of the C.W. Bra bender mixer

2- Operate the mixer for 50 rpm and 90 °C and then put the Trilene 67 amount in for 5 min.

3- Put the specified amount of the AP (ammonium polyphosphate) for 5 min.

4- Put the specified amount of CCF (chopped carbon fiber) or KP (Kevlar pulp) for 10 min.

5- Put the specified amount of PCA (peroxide cross linking agent) for 5 min.

6- Stop the Bra Bender and Extract the master batch for curing.

The only difference between mixing to get a master batch for prepreg manufacturing or curing directly a one layer laminate is the amount of peroxide cross linking agent (PCA) used. Different mixing cycles were done to perform optimization trials to get the optimum phr content of PCA during mixing which will result in minimum degree of cure for the prepreg and maximum degree of cure for the laminate of the insulation.

It appears from the different mixing trials that to get a master batch for directly curing a one layer laminate, the PCA is used with full amount for curing [100 phr EPDM + 60 phr AP + CCF and/or KP (reinforcement) + 6 phr PCA]. While for the case of getting a master batch for prepreg manufacturing, the PCA is used with a percentage not exceeding 50 % of the total amount for curing (100 phr EPDM + 60 phr AP + CCF or KP

(reinforcement) + 3 phr PCA). The rest of PCA (6 phr – 3 phr) will be used to be applied between the prepreg layers inside the mold to get the full cured layered laminate.

The mold for fabrication of thermal insulation in the prepreg form is designed according to the shape and the thickness of the required prepreg. The regular mold for production of one layer laminate of thermal insulation with dimension (300 x 150 x 3 mm) is used. Different spacers with different thicknesses (0.3, 0.4, 0.5 and 0.6 mm) with the same width and length of the mold cavity was done to get the minimum thickness of the prepreg.

The fabrication of the insulation can be done under a press where the homogenous mixture as a master batch is put inside the mold with specific weight calculated by density and size of insulant material.

Two factors were taken in consideration for the experimentation trials to get EPDM based prepregs. The first one is the thickness of the prepreg and the objective is to have it as low as possible. The second factor is the time required to perform the prepreg under the press and the objective is to have it as short as possible to save cost and at the same time to get the minimum degree of cure for repellence of the prepreg from the mold and the release film in addition to have the maximum degree of cure in fabrication of the laminate.

4.2.1 CCF/EPDM prepreg

4.2.1.1 Estimation of the optimum time for fabrication of the CCF/ EPDM prepreg

Master batches with composition (100 phr EPDM + 60 phr AP + 50 phr CCF + 3 phr PCA) were used. Different curing cycles were done to get the minimum degree of cure for the resulting prepreg by fixing the curing temperature (170°C), the curing pressure

(2.5 MPa) and prepreg thickness (1 mm) and lower the curing time (90 min for full cure then cooling to room temperature usually takes 30 minutes). Different times were used. By lowering the heating time from 60, 30, and 15 to 10 minutes then cooling to room temperature for 30 minutes, it was found that repellence of the CCF/ EPDM prepreg is easy without any effect on the geometry and continuity of the prepreg. When 2.5 minutes heating time was used, the repellence of the CCF/ EPDM prepreg was very difficult and there was separation of the prepreg into two parts, one sticks to the upper release film and the other sticks to the lower release film. This means that the force of repellence is lower than the adhesion force between the CCF/ EPDM prepreg surface and the release film.

When 5 minutes heating time was used then cooling for 30 minutes, the repellence of the CCF/ EPDM prepreg was not too difficult and there was stickiness of the few parts of the prepreg into the lower and upper release films, few stick to the upper release film and the rest sticks to the lower release film. This means that the force of repellence is still lower than the adhesion force between the CCF/ EPDM prepreg surface and the release film but not too much. In this case the prepreg was repelled successfully but without the complete geometry and continuity.

When 6 minutes heating time was used then cooling for 30 minutes, the repellence of the CCF/ EPDM prepreg was sufficient without any difficulty and there was not any stickiness of the any parts of the prepreg into the lower and upper release films, This means that the force of repellence is little bit more than the adhesion force between the CCF/ EPDM prepreg surface and the release film but not too much. In this case the prepreg was repelled successfully with the complete geometry and continuity.

So as a result the minimum degree of cure was obtained by using 170°C temperature and 2.5 MPa pressure for 6 minutes and then cooling to room temperature as shown in Fig (4.3). Using curing time less than 6 minutes, it is difficult to repel the CCF based prepreg from the Teflon based glass fabric because EPDM still sticks to the Teflon sheet (the surface cure of the EPDM layer is not enough to permit repellence from the Teflon film). While using curing time more than 6 minutes, the surface cure of the EPDM layer is too much to permit repellence from the Teflon film. So as a result higher surface thickness was cured which contradicts the basic requirement of the prepreg form to have the minimum degree of cure.

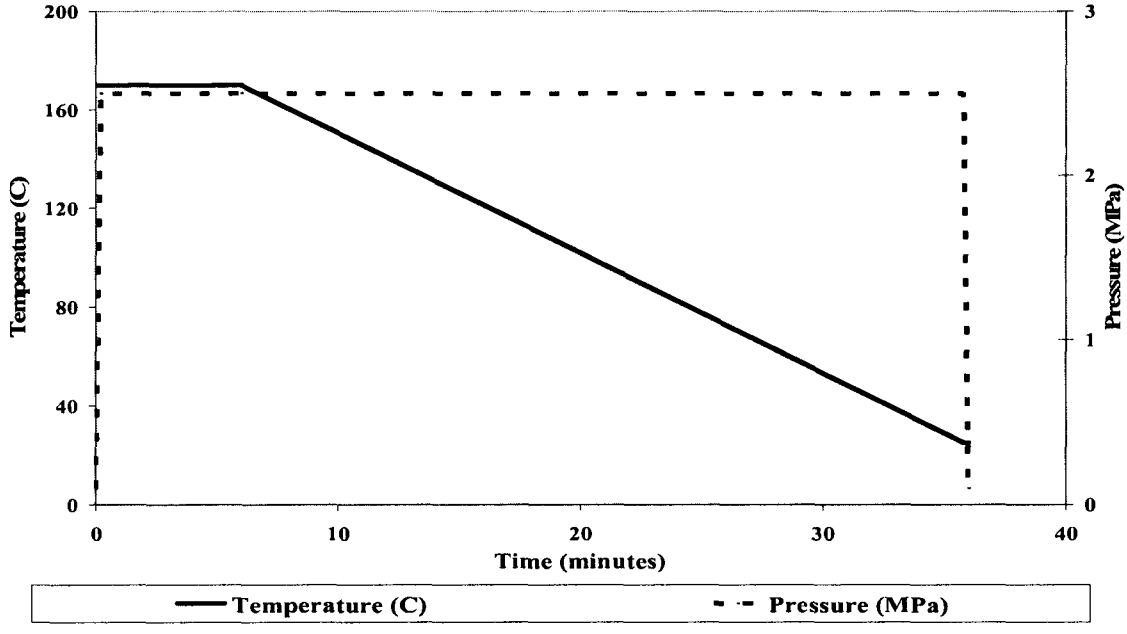

Fig (4.3) Fabrication conditions for CCF based prepreg

4.2.1.2 Estimation of the optimum thickness for fabrication of the CCF/ EPDM prepreg

Different curing cycles were done to get the minimum degree of cure for the resulting prepreg by fixing the curing temperature (170°C), the curing pressure (2.5 MPa), for 6

minutes heating then cooling to room temperature and lowering the prepreg thickness. Different thicknesses were used by adjusting the mold cavity by spacers with different thicknesses. By lowering the thickness from 1 to 0.8 and to 0.6 mm, it was found that repellence of the CCF/ EPDM prepreg is easy without any effect on the geometry and continuity of the prepreg. When 0.4 mm thickness was used, the repellence of the CCF/ EPDM prepreg was difficult and the prepreg was not continuous. When 0.5 mm thickness was used, the repellence of the CCF/ EPDM prepreg was sufficient without any difficulty. In this case the prepreg was repelled successfully with the complete geometry and continuity.

This means that the minimum thickness which can obtain for CCF / EPDM prepreg is 0.5 mm.

Fig (4.4) shows the CCF based EPDM master batch (output of C. W. Brabender mixer) inside the mold and the resultant prepreg after application of the 2.5 MPa pressure and 170 °C for 6 minutes.

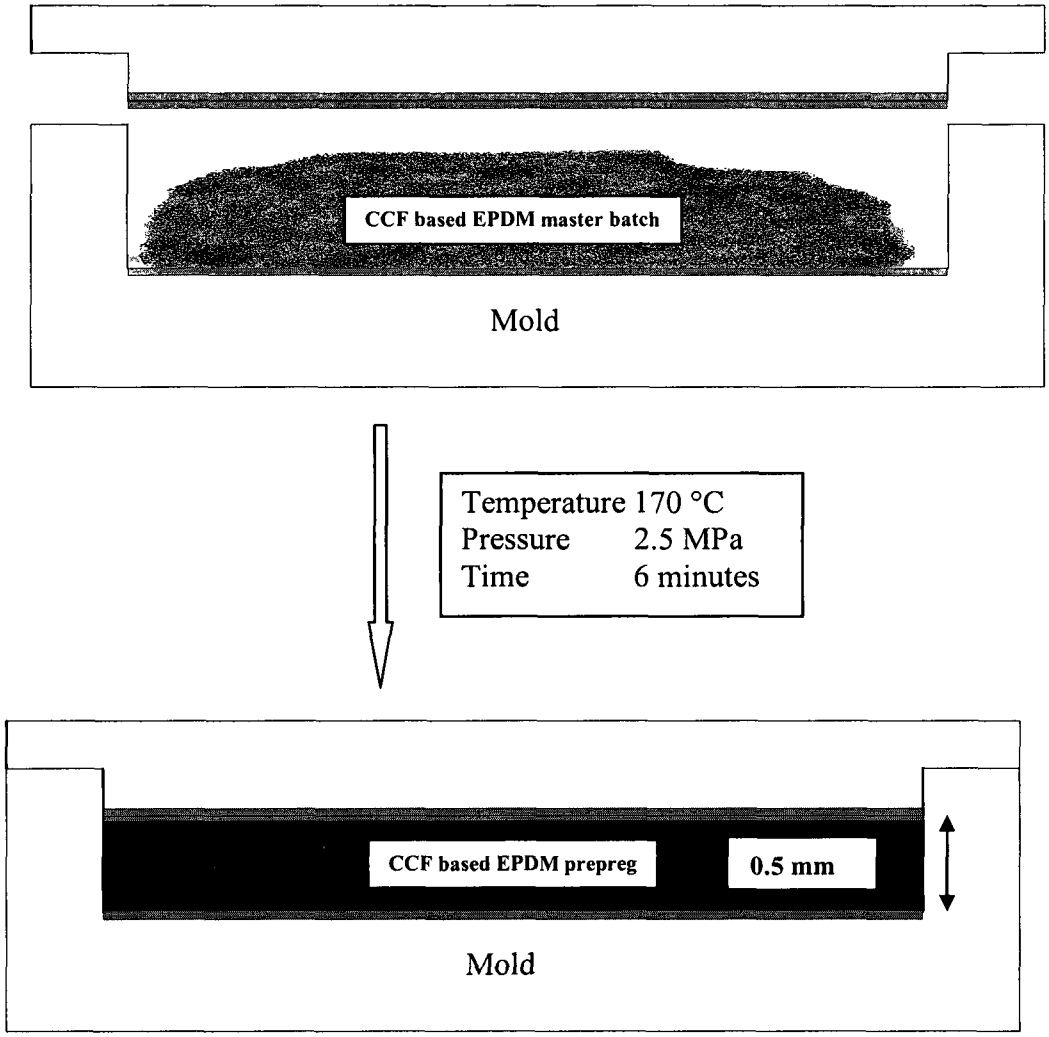

Fig (4.4) CCF based EPDM prepreg fabrication

Fig (4.5) shows the prepreg based on 100 phr EPDM + 60 phr AP + 50 phr CCF + 3 phr PCA with thickness 0.5 mm.

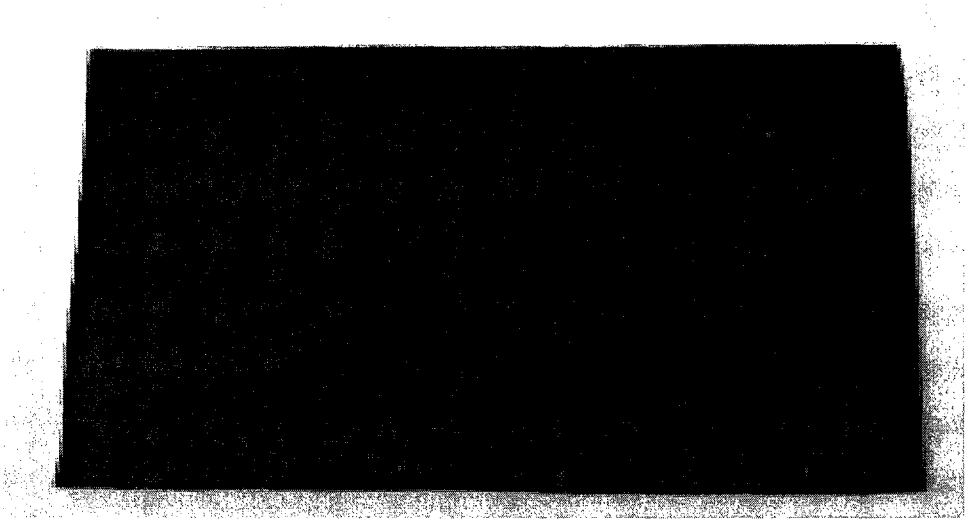

Fig (4.5) A prepreg based on CCF with thickness 0.5 mm

4.2.2 KP/EPDM prepreg

4.2.2.1 Estimating the optimum time for fabrication of the KP/EPDM prepreg

Insulation master batch with composition (100 phr EPDM + 60 phr AP + 30 phr KP + 3 phr PCA) was used. Different curing cycles were used to get the minimum degree of cure for the resulting prepreg by fixing the curing temperature (170°C), the curing pressure (2.5 MPa) and prepreg thickness (1 mm) and lower the curing time from (90 min for full cure). Different times were used. By lowering the time from 60, 30, 15, 10, 5 to 2.5 minutes, it was found that repellence of the KP/ EPDM prepreg is easy without any effect on the geometry and continuity of the prepreg. When 1 minute time was used, the repellence of the KP/ EPDM prepreg was very difficult and there was separation of the prepreg into two parts, one sticks to the upper release film and the other sticks to the lower release film. This means that the force of repellence is lower than the adhesion force between the KP/ EPDM prepreg surface and the release film.

When 1.5 minutes time was used, the repellence of the KP/ EPDM prepreg was not too difficult and there was stickiness of the few parts of the prepreg into the lower and upper release films, few stick to the upper release film and the rest sticks to the lower release film. This means that the force of repellence is still lower than the adhesion force between the KP/ EPDM prepreg surface and the release film but not too much. In this case the prepreg was repelled successfully but without the complete geometry and continuity.

When 2 minutes time was used, the repellence of the KP/ EPDM prepreg was sufficient without any difficulty and there was not any stickiness of any parts of the prepreg into the lower and upper release films. This means that the force of repellence is little bit more than the adhesion force between the KP/ EPDM prepreg surface and the release film but not higher much. In this case the prepreg was repelled successfully with the complete geometry and continuity.

The minimum degree of cure was obtained by using 170°C temperature and 2.5 MPa pressure for 2 minutes and then cooling to room temperature as shown in Fig (4.6).

Using curing time less than 2 minutes, it is difficult to repel the KP based prepreg from the Teflon based glass fabric because EPDM still sticks to the Teflon sheet (the surface cure of the EPDM layer is not enough to permit repellence from the Teflon film). While using curing time more than 2 minutes, the surface cure of the EPDM layer is too much to permit repellence from the Teflon film. So as a result higher surface thickness was cured which contradicts the basic requirement of the prepreg form to have the minimum degree of cure.

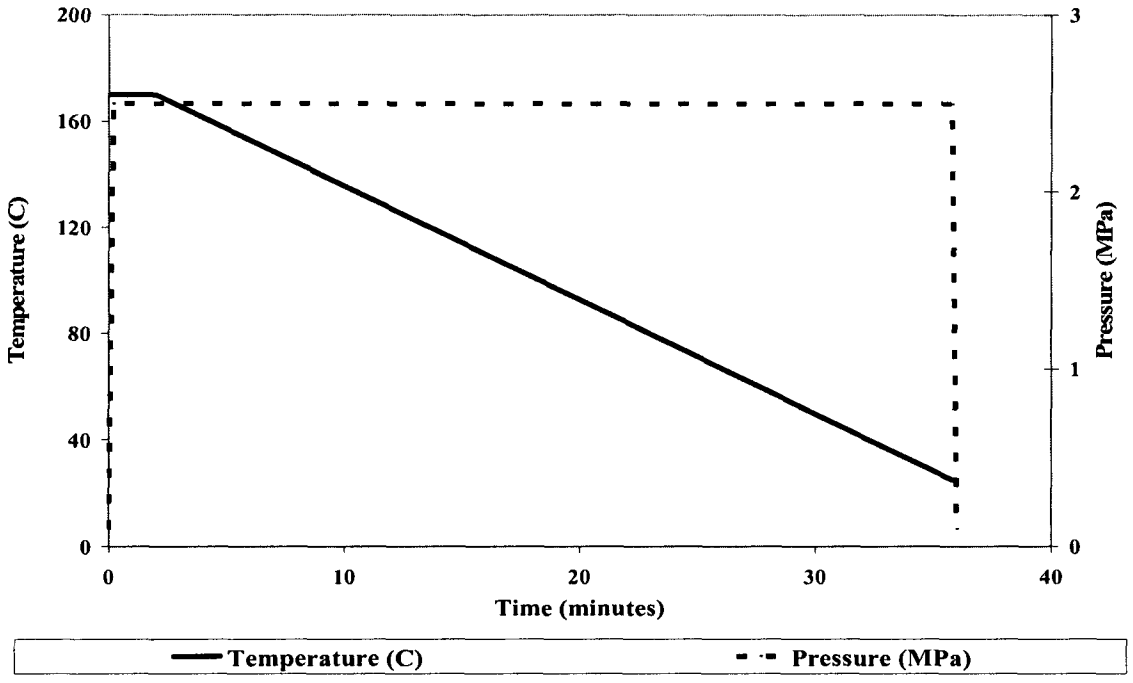

Fig (4.6) Fabrication conditions for KP based prepreg

4.2.2.2 Estimating the optimum thickness for fabrication of the KP/ EPDM prepreg

Different curing cycles were done to get the minimum degree of cure for the resulting prepreg by fixing the curing temperature (170°C), the curing pressure (2.5 MPa), for 2 minutes heating then cooling to room temperature and lowering the prepreg thickness. Different thicknesses were used by adjusting the mold cavity by spacers with different thicknesses. By lowering the thickness from 1, 0.8, 0.6 to 0.4 mm, it was found that repellence of the KP/ EPDM prepreg is easy without any effect on the geometry and continuity of the prepreg. When 0.2 mm and 0.3 thicknesses were used, the repellence of the KP/ EPDM prepreg was difficult and the prepreg was not continuous. When 0.4 mm thickness was used, the repellence of the KP/ EPDM prepreg was sufficient without any difficulty. In this case the prepreg was repelled successfully with the complete geometry

and continuity. This means that the minimum thickness which can obtain for KP / EPDM prepreg is 0.4 mm.

Fig (4.7) shows the KP based EPDM master batch (output of C. W. Brabender mixer) inside the mold and the resultant prepreg after application of the 2.5 MPa pressure and 170 °C for 2 minutes.

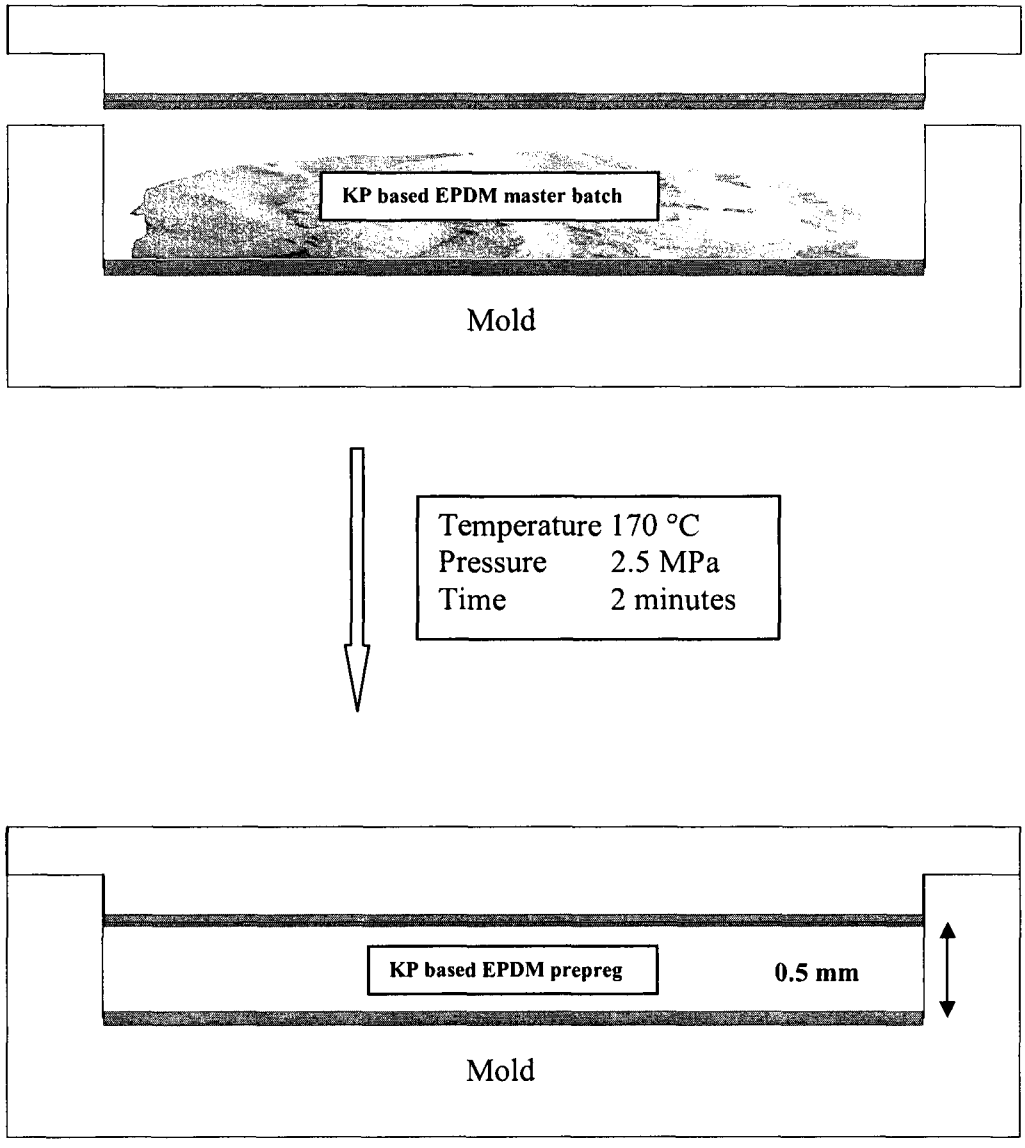

Fig (4.7) KP based EPDM prepreg fabrication

Fig (4.8) shows the prepreg based on 100 phr EPDM + 60 phr AP + 30 phr KP + 3 phr PCA with thickness 0.5 mm.

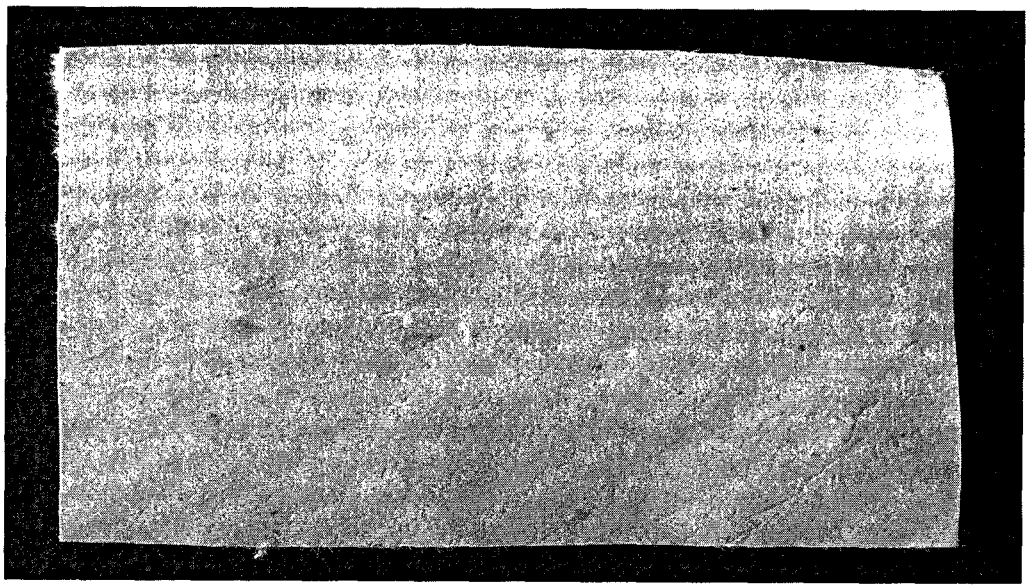

Fig (4.8) A prepreg based on KP with thickness 0.5 mm

After many fabrication cycles, it appears that the minimum thickness that can be obtained for the prepreg without affecting the properties and continuity of the material is 0.5 mm for CCF/EPDM prepreg and 0.4 mm for KP/EPDM prepreg.

To agree with the numerical modeling when equal thicknesses of the sub layers were used, equal thicknesses of CCF/EPDM prepreg and KP/EPDM prepreg of 0.5 mm were used in fabrication of the laminate.

The prepreg is partially cured on the surface with thickness around 20 μm on both sides (with a very low cross-link density) and the center of the prepreg [0.5 mm – (2 x 0.02 mm)] is completely uncured (the same form as the output master batch from mixer) which means that full cure can be achieved in fabrication of the laminate as shown in Fig (4.9).

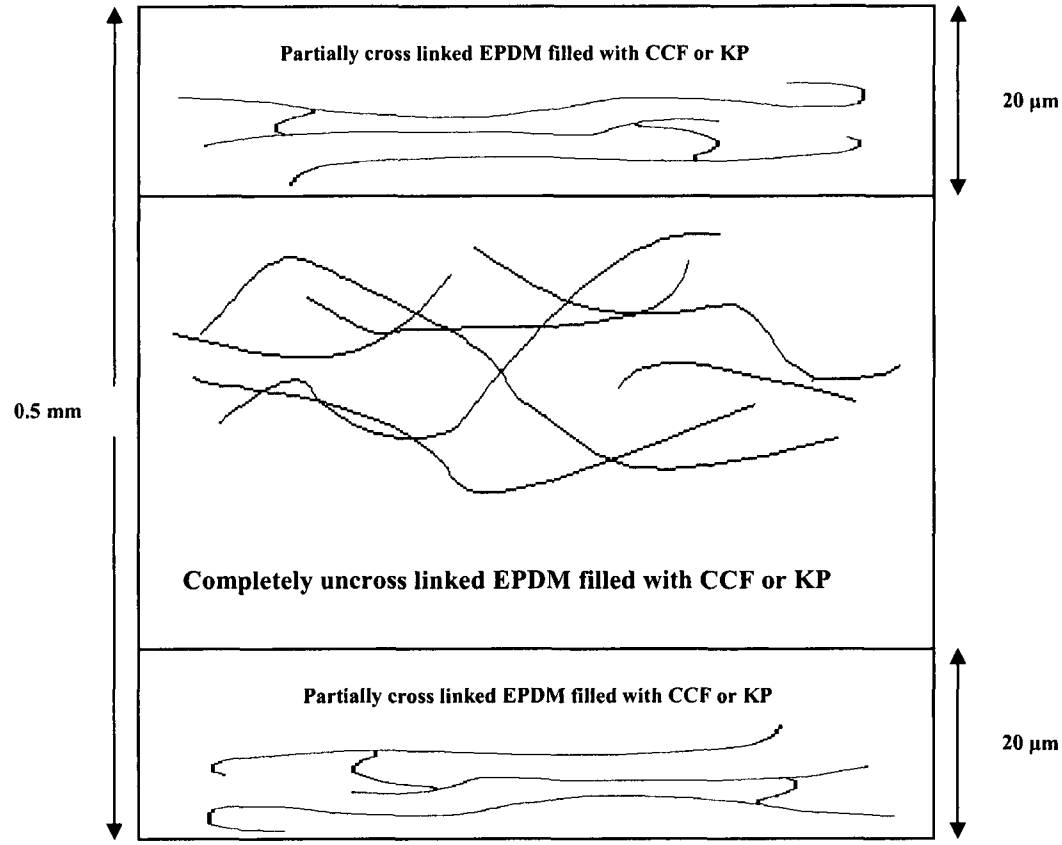

Fig (4.9) CCF or KP based EPDM prepreg curing state

The partiall curing on the surface with thickness around 20 μm on both sides allows full cure and bonding between layers when fabrication of the full laminate (based on 6 prepreg layers) by PCA layers incorporated in between the prepreg layers and using the full curing conditions (170 °C, 2.5 MPa, 90 minutes).

The completely uncrosslinked EPDM filled with CCF or KP on the center of the prepreg with thickness around 0.46 mm (0.5 mm – 2 x 0.02 mm) will be full cured when application of full curing conditions (170 °C, 2.5 MPa, 90 minutes) during fabrication of the full laminate.

4.3 Curing of the prepreg layers to make a laminate

The goal was to develop an elastomeric based composite system which could be easily fabricated to complex curves and surfaces, which has equivalent or better physical, thermal, mechanical and ablative properties than the existing thermal insulators, and which would retain structural integrity when fabricated on a typical structure and cycled between the temperature extremes expected in the application.

Manufacturing of a laminate begins with thin layers of insulation materials in the prepreg form to form multiple stacked layers that are bonded (laminated) together with chemical bond to form a compact thermal insulation laminate.

To cure a laminate with a thickness 3 mm, 6 layers of insulation in the prepreg form are stacked alternatively, one prepreg layer based on CCF then one prepreg layer based on KP.

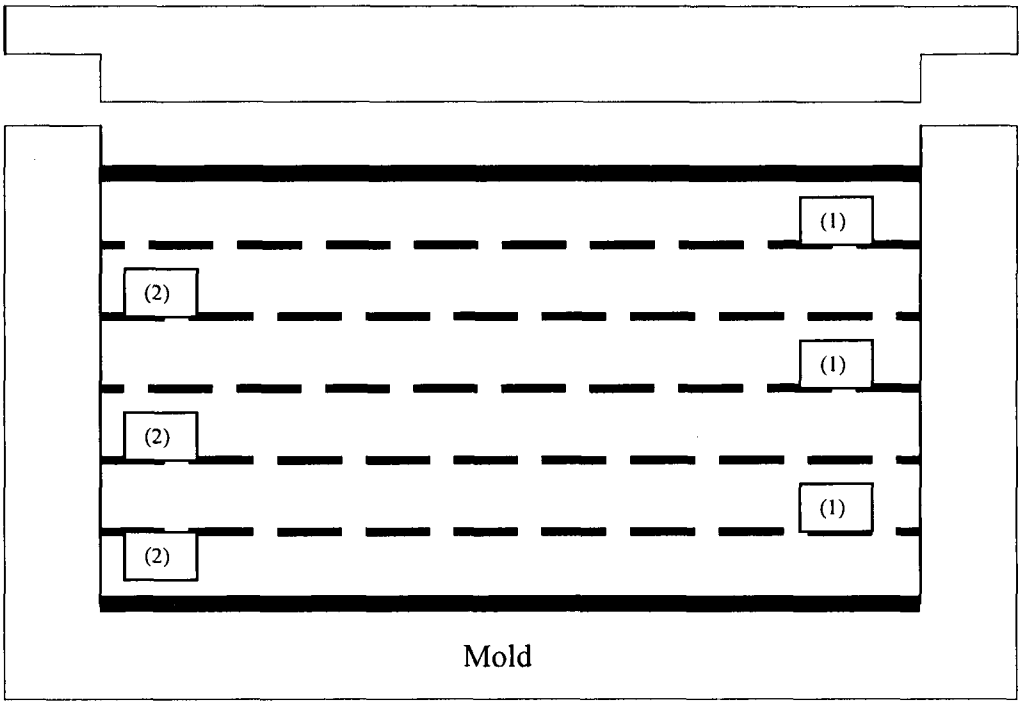

Fig (4.10) Layers of the laminate inside the mold before curing

PCA (white powder form) with the remaining amount (3 phr deducted from mixing) is placed in between the 6 layers in the mold (as 5 layers of PCA) as shown in Fig (4.10).

A legend to the drawing in Fig (4.10) is shown in Table (4.1).

All prepreg layers are placed between two thin layers of teflon coated glass fabric. The thickness of the film used is 0.075 mm (0.003 inch) and it is used to provide the high degree of repellence i.e. for easy removal of the laminate after curing.

The mold is then introduced to the press to cure the whole laminate using a curing cycle as shown in Fig (4.11).

Mark	representation
Thin solid lines	Mold male and female parts
Thick solid lines	Two layers of teflon based glass fabric
Thick dashed lines	Layers of PCA in between the prepreg layers
(1)	A prepreg layer with thickness 0.5 mm of EPDM + 60 phr AP + 50 phr CCF + 3 phr PCA
(2)	A prepreg layer with thickness 0.5 mm of EPDM + 60 phr AP + 30 phr KP + 3 phr PCA

Table (4.1) Graph legend for the curing of the laminate

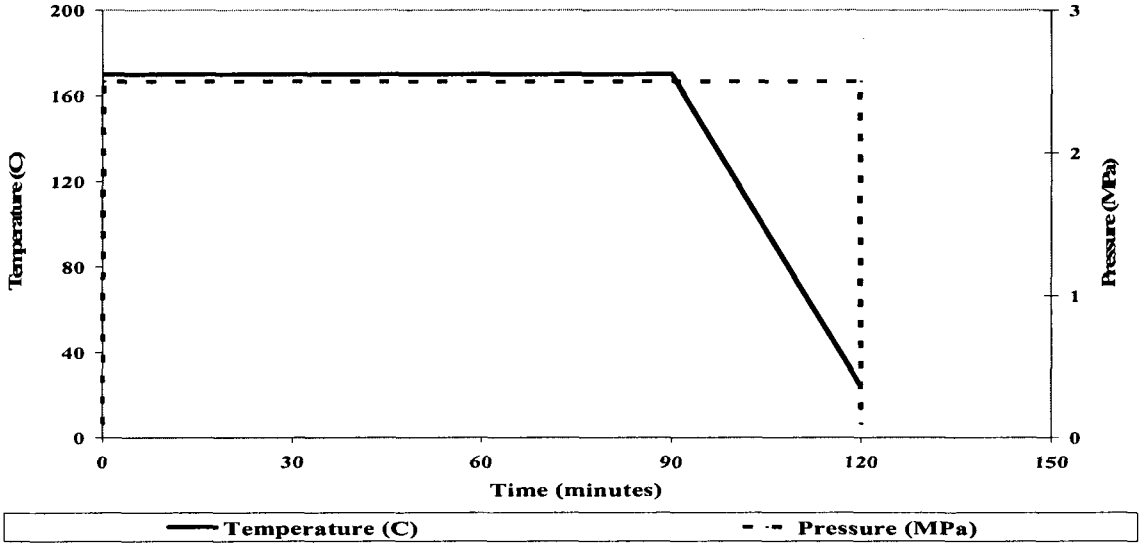

Fig (4.11) Curing conditions for the thermal insulation laminate

After application of the curing conditions (170 °C, 2.5 MPa, 90 minutes) to cure laminate, full cross linking happens in the insulation material as shown in Fig (4.12).

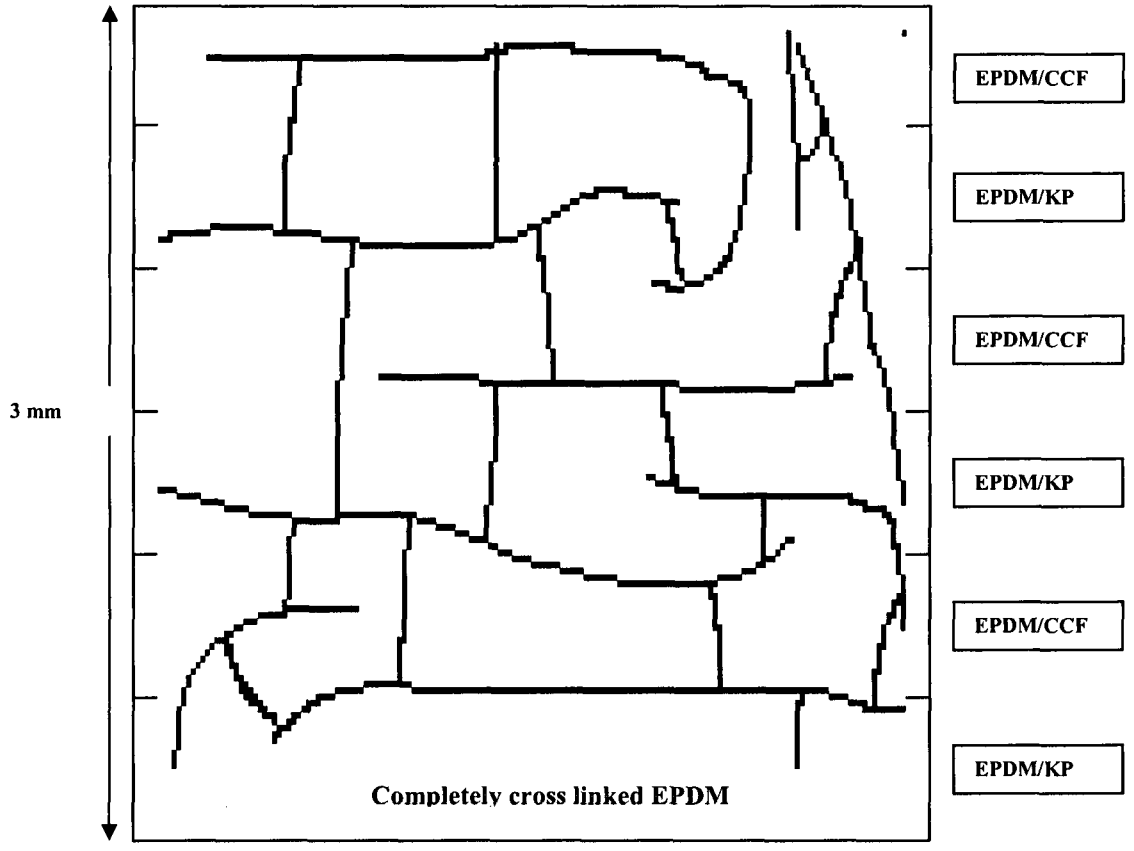

Fig (4.12) 6 layers CCF and/or KP based EPDM laminate curing state

4.4 Testing of the laminate

By cutting samples of the laminate and testing for physical, mechanical, thermal and ablative properties according to ASTM, laminate performance was obtained.

The TGA test indicates that an initial decomposition temperature for EPDM (matrix) occurs around 415 °C and the final decomposition is at 552 °C where EPDM decomposes to carbonaceous residue of free carbon. These provide a net effect of strong carbon based char which is highly erosion resistant. Also the tests indicate that an initial decomposition

temperature for ammonium polyphosphate (flame retardant agent) occurs around 579 °C and the final decomposition is at 726 °C.

The only stable ingredients above 1000 °C is CCF and KP which are stable up to 3200°C and 1450°C respectively, in addition to the carbon based char remains from decomposition of EPDM. This is clear where the remaining weight for the laminate sample just before 1000 °C is 27 % of the total insulation weight as shown in Fig (4.13). This is due to the insulation efficiency of KP and the high decomposition efficiency of CCF where CCF + KP work as a shield to EPDM, protect it against decomposition.

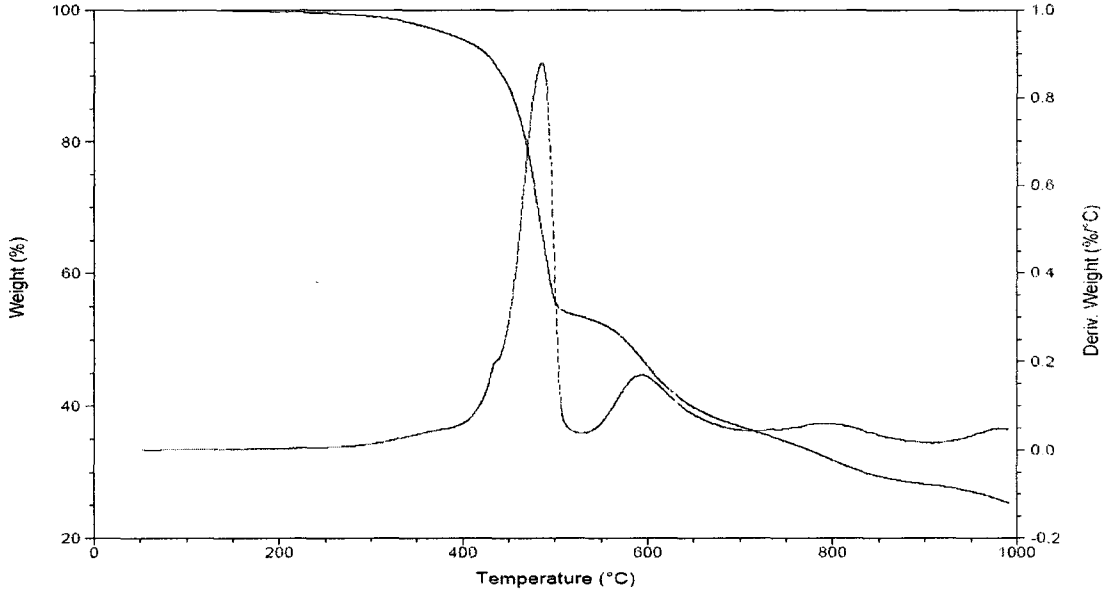

Fig (4.13) TGA, DTGA curves for a laminate fabricated from 6 layers

A list of physical, mechanical, thermal and ablative properties of the laminate consist of 6 alternative layers from 50 phr CCF based EPDM and 30 phr KP based EPDM is shown in Table (4.2).

property	unit	Testing value for laminate
Tensile strength	MPa	7.8 ± 0.5
Elongation	%	12.1± 1.2
Hardness	Shore A	88.9 ± 0.2
Density	gm/cm^3	1.239
Specific heat capacity	J/kg. °C	1691 ± 4
Thermal diffusivity	mm^2/sec	0.085 ± 0.002
Thermal conductivity	W/m. °C	0.178 ± 0.001
Ablation rate	mm/sec	0.006 ± 0.0002
Outer case temperature	°C	39.1± 0.5
TGA remaining weight	%	27 ± 0.5

Table (4.2) 6 layers CCF and/or KP based EPDM laminate properties

An ablation test is performed for the new laminate based on 6 alternative layers of 50 phr CCF and 30 phr KP the temperature rise in the back of steel is recorded as function of time.

For 6 alternative layers of 50 phr CCF and 30 phr KP based insulation the temperature rise in the back of steel is recorded as function of time versus that predicted from modeling as shown in Fig (4.14).

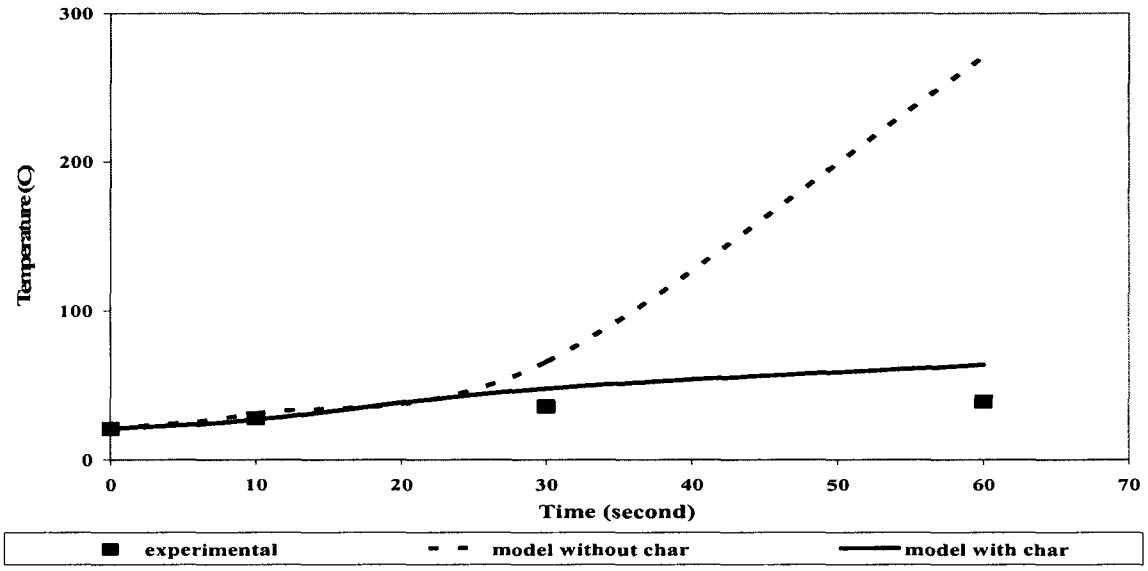

Fig (4.14) Experimental temperature rise in the back of steel plate as function of time versus that predicted by models for 6 alternative layers of 50 phr CCF and 30 phr KP based insulation

The difference is very large between the predicted from model without considering the properties of char and experimentally measured. Also there is good agreement between the predicted from model with considering the properties of char and experimentally measured.

For 6 alternative layers of 50 phr CCF and 30 phr KP based insulation the temperature rise in the back of steel for 180 second subjected to the torch is recorded as function of time is shown in Fig (4.15).

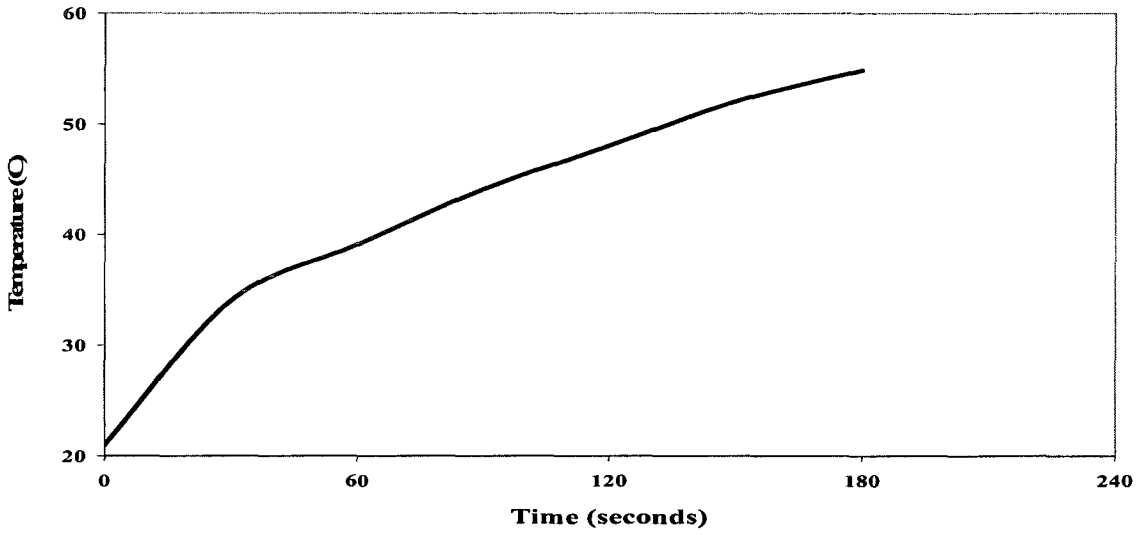

Fig (4.15) Experimental temperature rise at the back of steel plate as function of time for 6 alternative layers of 50 phr CCF and 30 phr KP based insulation (180 seconds)

It appears that the temperature rise at the back of steel after 180 seconds is only from 21°C to 54.6 °C.

4.4.1 Electrical conductivity

Currently used elastomeric-based insulation materials are electrically insulating, exhibiting high volume resistivities, and, hence, a poor ability to dissipate static charge. The ability to dissipate static charge is considered to be an important quality for the thermal insulator. An insulator possessing this quality is able to bleed off or dissipate charges that build up on the insulator surface. An insulator having a high electrical resistivity does not dissipate static charge timely, thus creating a potential for static charge to build up to a dangerous level. When the electric field increases to the point that breakdown of the air occurs or a path to ground for the static charge is inadvertently provided, the discharge can be dangerous. Physical harm to personnel and flash fires are

possible. Conventional silica-filled EPDM insulation is electrically insulating, having resistivities ranging from 1×10^{14} to 1×10^{16} Ohm·cm. An insulator is considered to be able to dissipate static charge if its volume resistivity is in the range of from 1×10^{5} to 1×10^{12} Ohm·cm. Asbestos-filled NBR, which is one of the few currently used insulation materials that is considered to be able to dissipate static charge, has a volume resistivity in the range of 1×10^{11} to 1×10^{12} Ohm·cm. However, the use of asbestos in rocket motors has lost favor due to reported health dangers associated with asbestos [107].

Measurement of the volumetric electrical resistivity of the laminate composed of 6 alternative layers of 50 phr CCF and 30 phr KP based insulation was done by using the HP Agilent 4339B High Resistance Meter. The volumetric electrical resistivity of the laminate is 3.6×10^{7} Ohm·cm. This value makes the laminate able to dissipate the static charge during propellant combustion.

The comparison between the temperature rise at the back of steel (after 60 seconds) obtained by numerical calculations considering the properties of char, without considering the properties of char and the experimentally measured is shown in Table (4.3).

It appears that the best insulation geometry which protects the case is 6 layers placed alternatively of single reinforcement (CCF or KP) based insulation where the maximum temperature of the case is 39.1°C. This temperature is very low for this type of insulation. A photo of the cross section of a laminate consist of 6 layers placed alternatively of single reinforcement (CCF or KP) is shown in Fig (4.16).

N	Layers geometry	Temperature (°C) (numerically without char properties)	Temperature (°C) (numerically with char properties)	Temperature (°C) (experimentally measured)
1	1 layer of hybrid (CCF + KP)	288	109	82
2	1 layer of CCF based insulation	611	355	317
3	1 layer of KP based insulation	187	99	79
4	6 layers placed alternatively of single reinforcement (CCF or KP) based insulation	271	64	39.1

Table (4.3) Theoretical and experimental temperatures comparison for different insulation geometries at the bottom surface of steel

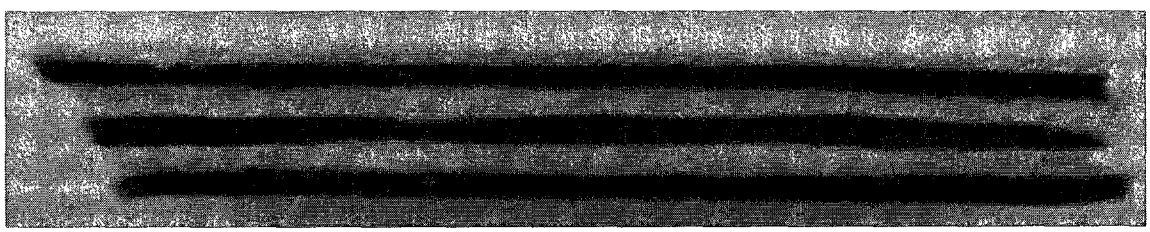

Fig (4.16) Cross section photo of a laminate consists of 6 alternative layers of (CCF or KP) based prepreg

Current application requires that the contribution of the solid rocket motor propellant combustion in the surface temperature of the solid rocket motor case should not exceed 150 °C. This is due to two reasons.

1- During the solid rocket mission, when the rocket leaves the inner zone with gravity (lower than 100 miles above the earth surface in altitude) to the higher zone without gravity (higher than 100 miles above the earth surface in altitude), it travels with very high speed where it is subjected to a very high external thermal load due to friction. Due to the net thermal load from inside (due to propellant combustion) and outside (due to

friction) the rocket motor may endanger the case if the contribution of the solid rocket motor propellant combustion in the surface temperature of the solid rocket motor case exceeds 150 °C.

2-The thermal insulation layers applied to the solid rocket motor case using high temperature adhesives (usually Epon 828 and Epicure) and the maximum operating temperatures for these types of adhesives is around 300 °C. So if the contribution of the solid rocket motor propellant combustion in the surface temperature of the solid rocket motor case exceeds 150 °C, the temperature of the adhesive may be more than 300 °C. At that time separation of the insulation from the case may happen and then explosion may occur.

As a result if the contribution of the solid rocket motor propellant combustion in the surface temperature of the solid rocket motor case (using 3 mm thick insulation) is 39.1 °C for 60 seconds combustion, 54.9 °C for 180 seconds combustion the mission will be safer. For longer combustion times (more than 5 minutes) the thickness of the insulation laminate can be increased more than 3 mm to accommodate this.

4.5 Comparison

Physical and mechanical properties comparison between 25 phr CCF + 25 phr KP based insulation and the laminate (composed of 6 alternative layers of 50 phr CCF based prepreg and 30 phr KP based prepreg) are shown in Fig (4.17).

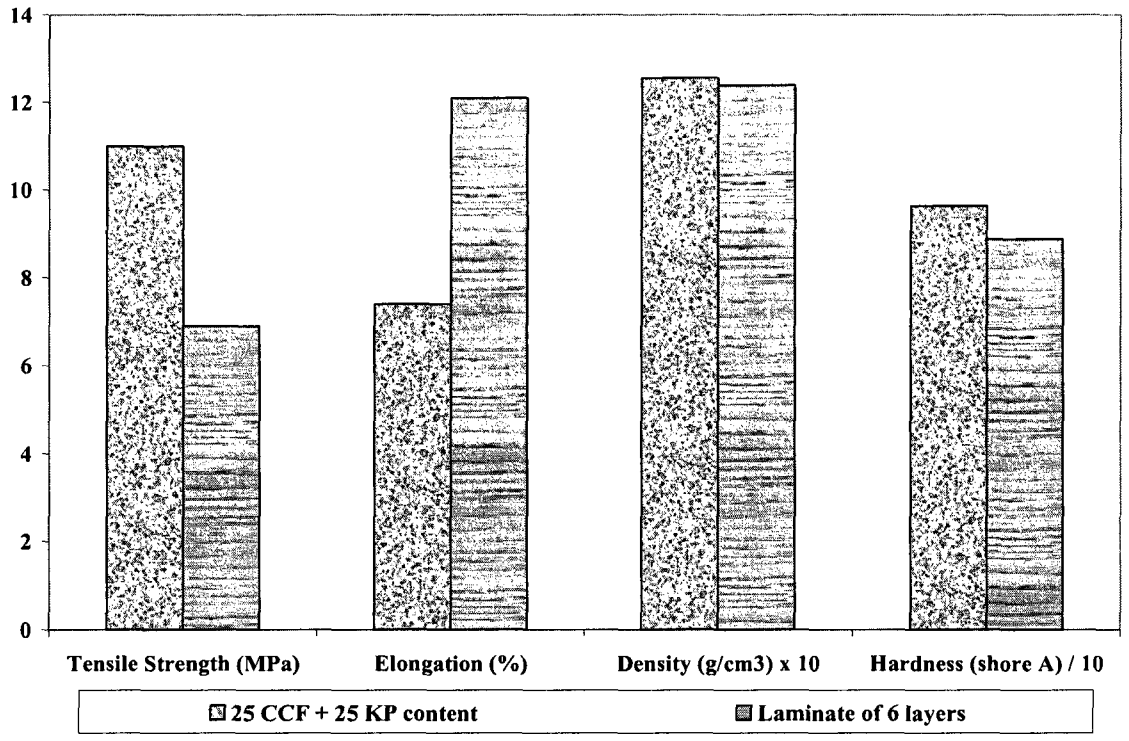

Fig (4.17) Physical and mechanical properties comparison between 25 phr CCF + 25 phr KP based insulation and the laminate (composed of 6 alternative layers of 50 phr CCF based prepreg and 30 phr KP based prepreg).

It appears that the better composition in tensile strength as solid rocket motor application is 25 phr CCF + 25 phr KP based EPDM. And the best composition in elongation, density and hardness as solid rocket motor application is the laminate (composed of 6 alternative layers of 50 phr CCF based prepreg and 30 phr KP based prepreg) are shown in Fig (4.17).

Thermal and ablative properties comparison between 25 phr CCF + 25 phr KP based insulation and the laminate (composed of 6 alternative layers of 50 phr CCF based prepreg and 30 phr KP based prepreg) are shown in Fig (4.18).

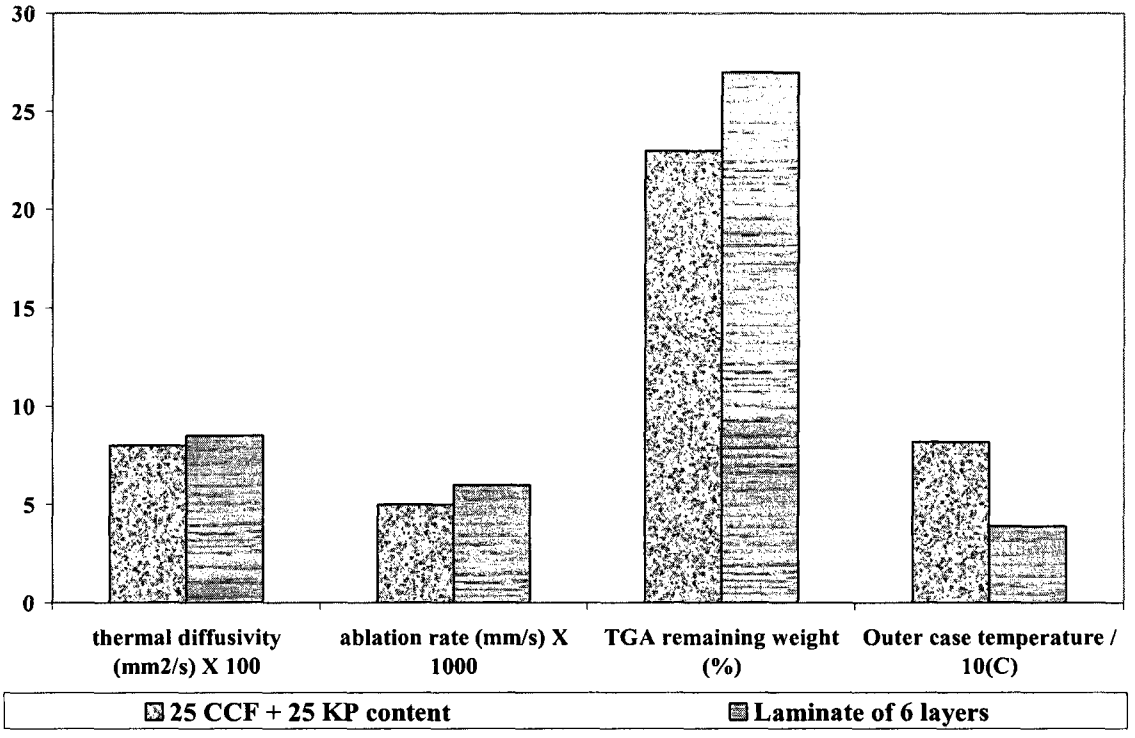

Fig (4.18) Thermal and ablative properties comparison between 25 phr CCF + 25 phr KP based insulation and the laminate (composed of 6 alternative layers of 50 phr CCF based prepreg and 30 phr KP based prepreg).

It appears that the better composition in thermal diffusivity and ablation rate as solid rocket motor application is 25 phr CCF + 25 phr KP based EPDM. And the better composition in TGA remaining weight at 1000 °C and outer case temperature as solid rocket motor application is the laminate (composed of 6 alternative layers of 50 phr CCF based prepreg and 30 phr KP based prepreg) as shown in Fig (4.18).

The ablation rate for a laminate (3 mm thick) consists of 6 layers placed alternatively of single reinforcement (CCF or KP) is 0.006 mm/second. The ablation rate of one layer insulation with 3 mm thickness composed of EPDM + 25 phr chopped carbon fibers + 25

phr Kevlar pulp + 60 phr ammonium polyphosphate is 0.005 mm/second. This was obtained by using a torch with a flame temperature of 2010 °C. The ablation rate of the laminate is little higher than that for the one layer hybrid based insulation. The reason for this can be explained by considering that the one layer hybrid based insulation consists of 6 sub layers of the same material as shown in Fig (1)and compare this geometry with that of the laminate as shown in Fig (4.19).

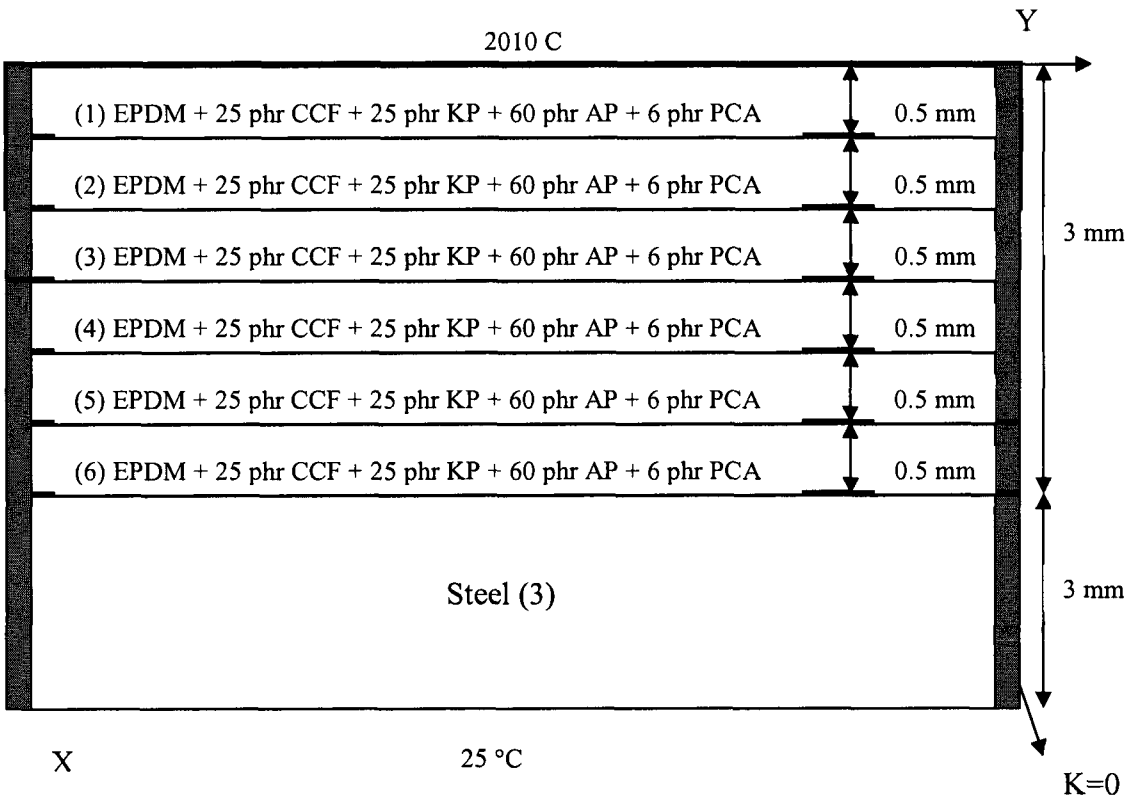

Fig (4.19) Ablation geometric model for 6 sub layers of hybrid (CCF + KP) based insulation)

The thermal conductivity of the first sub layer in the one layer hybrid based insulation with thickness 0.5 mm is 0.198 W/m. °C. This small thermal conductivity reduces the heat flux passing to the second layer; as a result, the temperature may be lower than the decomposition temperatures of all the phases inside the second layer. This leads to no

thickness reduction in the second layer. In the first layer, it consists of 4 phases; (EPDM) The matrix, the reinforcement [2 phases, one is chopped carbon fiber (CCF) and the second is Kevlar pulp (KP)], the flame retardant (ammonium polyphosphate). The different phases have different initial and final decomposition temperatures. From The TGA tests, EPDM (matrix) starts to decompose at around 415 °C and the final decomposition is at 551 °C where EPDM decomposes to carbonaceous residue of free carbon. Also the tests indicate that an initial decomposition temperature for ammonium polyphosphate (flame retardant agent) occurs at around 575 °C and the final decomposition is at 722 °C. The only stable ingredients above 1000 °C is CCF and KP which are stable up to (final decomposition temperature) 3445°C and 1450°C respectively, in addition to the carbon based char remains from decomposition of EPDM. This combination of conduction and decomposition temperatures gives the ablation rate of 0.005 mm/second.

The case of for a laminate (3 mm thick) consisting of 6 layers placed alternatively of single reinforcement (CCF or KP) is shown in Fig (4.20). The thermal conductivity of the first layer in the one layer hybrid based insulation with thickness 3 mm is 0.453 W/m. °C [Table (2.8)]. This high thermal conductivity conducts heat to the second layer; as a result, the temperature may be higher than the decomposition temperatures of many phases inside the second layer. This results in reduction of the thickness (ablation) in the second layer. In the first layer, it consists of 3 phases; (EPDM) the matrix, the reinforcement [1 phase, chopped carbon fiber (CCF)], and the flame retardant (ammonium polyphosphate). The different phases have different initial and final decomposition temperatures. From The TGA tests, EPDM (matrix) starts to decompose at

around 410 °C and the final decomposition is at 547 °C where EPDM decomposes to carbonaceous residue of free carbon. Also the tests indicate that an initial decomposition temperature for ammonium polyphosphate (flame retardant agent) occurs at around 575 °C and the final decomposition is at 722 °C. The only stable ingredient above 1000 °C is CCF which is stable up to (final decomposition temperature) 3445°C, in addition to the carbon based char. So this layer has a higher resistance to decomposition than that of the first layer of the hybrid based insulation due to the presence of higher amount of chopped carbon fibers. At the same time this layer has a thermal conductivity (0.453 W/m. °C) which is more than two times that for the first layer of the hybrid based insulation (0.198 W/m. °C). This combination of conduction and decomposition temperatures gives the ablation rate of 0.006 mm/second.

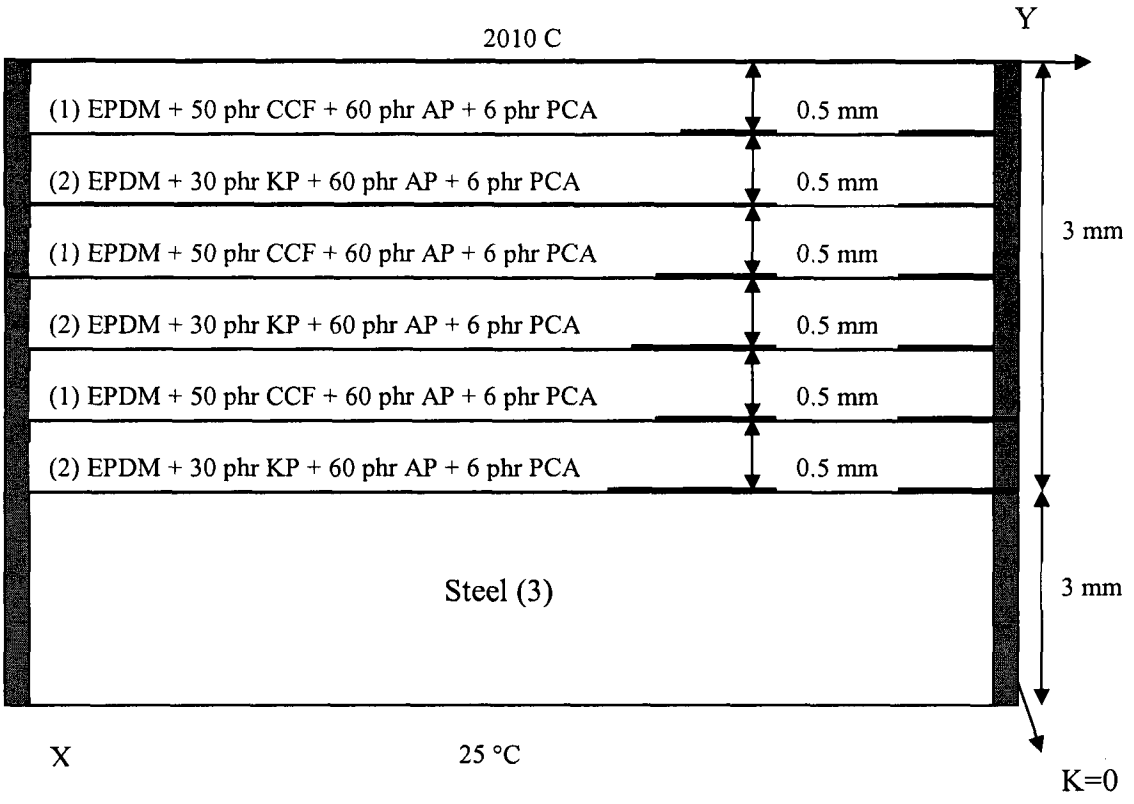

Fig (4.20) Ablation geometric model for a laminate consists of 6 layers placed alternatively of single reinforcement (CCF or KP) based insulation)

A laminate (composed of 6 alternative layers of 50 phr CCF based prepreg and 30 phr KP based prepreg) shows the better performance (physical, mechanical, thermal and ablative properties) as solid rocket motor application over all the other compositions discussed on the thesis work.

Comparison between the experimental and theoretically predicted (based in model with considering the properties of char) temperatures in the back of steel versus time for different samples is shown in Fig (4.21).

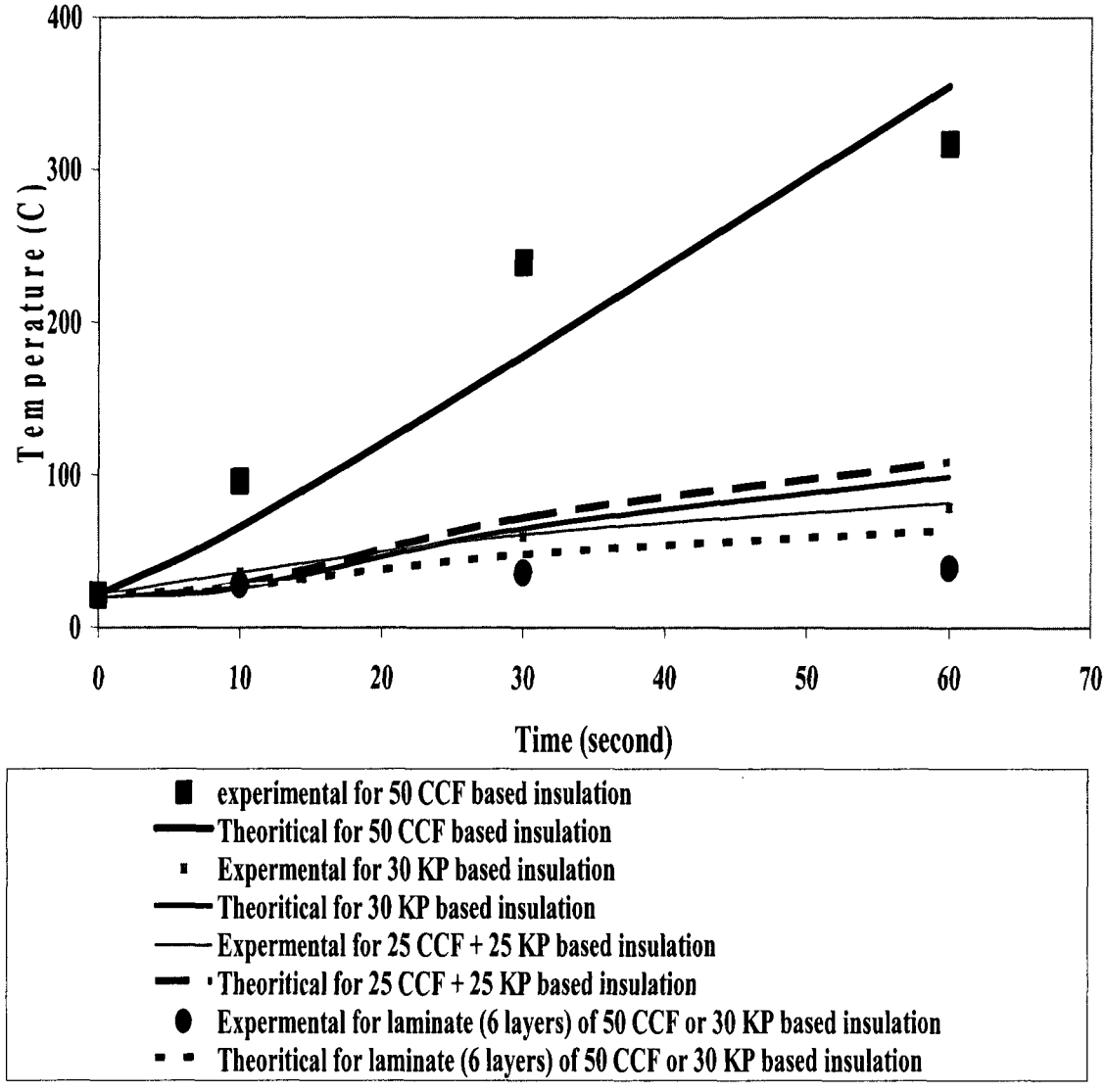

Fig (4.21) Experimental temperature rise in the back of steel as function of time versus these theoretically predicted for different samples

It appears that the better thermal insulation composition and configuration is a laminate that consists of 6 layers stacked alternatively of 50 phr CCF and 30 phr KP based prepregs. This composite laminate when used as solid rocket motor insulation will increase the temperature of the solid rocket motor case from 21 °C to 39.1 °C after 60 seconds and from 21 °C to 54.1 °C after 180 seconds.

4.6 Laminate density calculations

Density calculations were performed for the final insulation for 6 layers placed alternatively of single reinforcement (CCF or KP) based insulation and single layer of hybrid (CCF + KP). The densities of EPDM, CCF, KP and AP are 0.86, 1.81, 1.44 and 1.6 gm/ cm^3 respectively. Table (4.4) shows that using insulation consisting of 6 layers placed alternatively of single reinforcement (CCF or KP) reduces the total density by 1.33 % over using insulation consists of single layer of hybrid (CCF + KP). This reduction can be in the order of few hundreds of kilograms in big rockets.

Material	**Total weight [M] (gm)**	**Total volume [V] (cm^3)**	**Density [M/V] (gm/ cm^3)**	**Average Density (gm/ cm^3)**
100 phr EPDM + 25 phr CCF + 25 phr KP + 60 phr AP	210	$V_{EPDM} + V_{CCF} + V_{KP} + V_{AP}$ =185.0	1.14	1.14
100 phr EPDM + 50 phr CCF + 60 phr AP	210	$V_{EPDM} + V_{CCF} + V_{AP}$ = 181.4	1.16	1.125
100 phr EPDM + 30 phr KP + 60 phr AP	190	$V_{EPDM} + V_{KP} + V_{AP}$ = 174.6	1.09	
Density reduction (gm/ cm^3)				0.015
Density reduction (%)				1.33

Table (4.4) Densities calculations and comparison for different insulation geometries

4.7 Ply adhesion test

Determination of the bond strength or ply adhesion of the layers was done by unaxial tension test according to ASTM Designation: D 7005 – 03. 2.5 cm x 2.5 cm x 3 mm piece

of the laminate is bonded, by using EPON 828 and Epicure, to two aluminum substrates with dimensions 10 cm x 2.5 cm x 1 mm each. A front and side view of the sample is shown in Fig (4.22) a, b respectively.

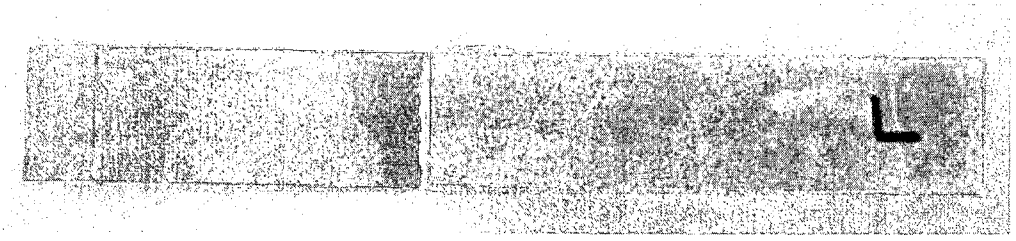

(a) Front view

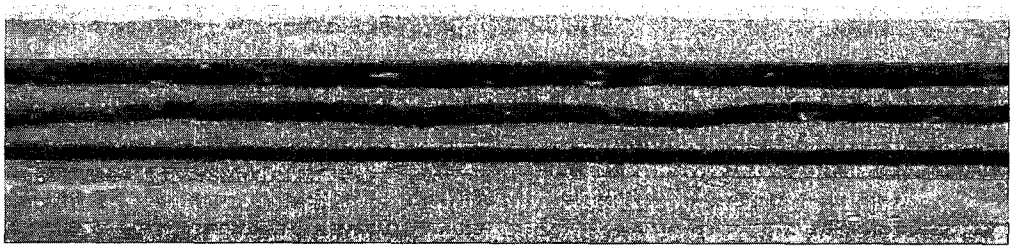

(b) Side view (cross section of a laminate piece inside 2 aluminum substrates)

Fig (4.22) Bonding test sample from the laminate

The axial displacement – force curve for the sample is shown in fig (4.23).

It appears from the curve that the laminate can withstand a maximum axial load of 537 N. after this load separation of the laminate happens from the aluminum substrate (adhesive failure) while the laminate sub plies is still bonded without separation of the layers. The bond strength or ply adhesion of the laminate is higher than the maximum recorded axial force. This maximum axial force is corresponding to a shear stress of 0.85 MPa.

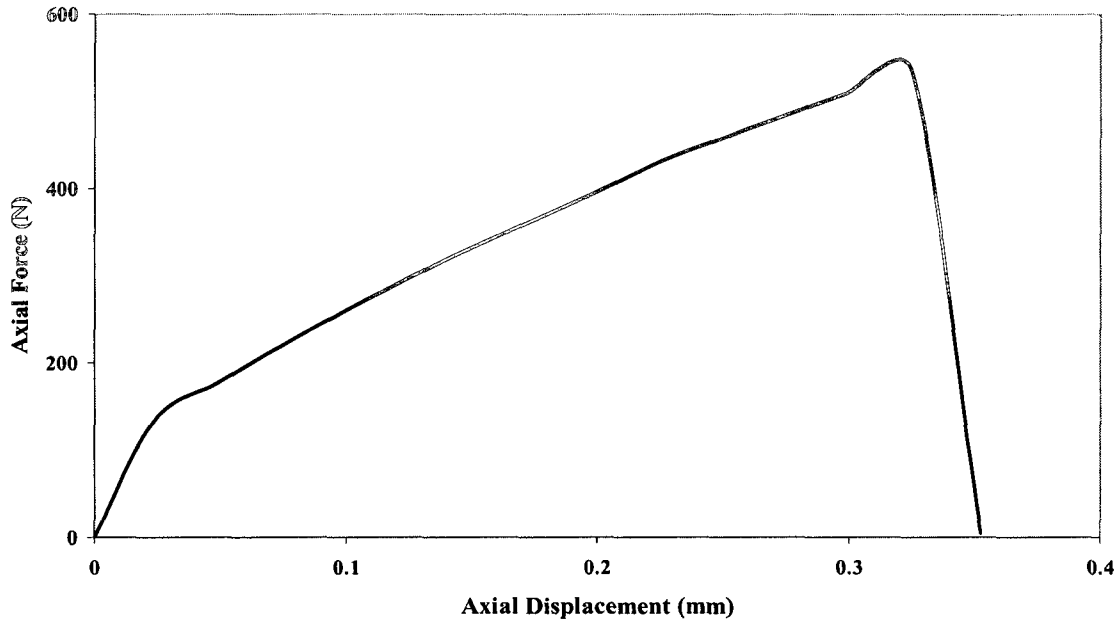

Fig (4.23) The axial displacement – force for the laminate composed of 6 alternative layers

A sample from 25 phr CCF + 25 phr KP based EPDM was prepared with the same procedure and dimensions (A front and side view of the sample is shown in Fig (4.24) a, b respectively).

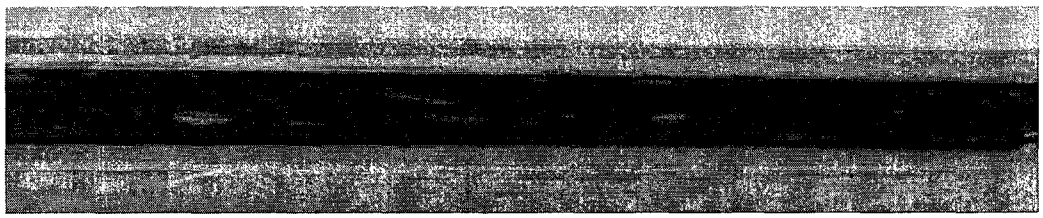

(a) Side view (cross section of a hybrid based EPDM piece inside 2 aluminum substrates)

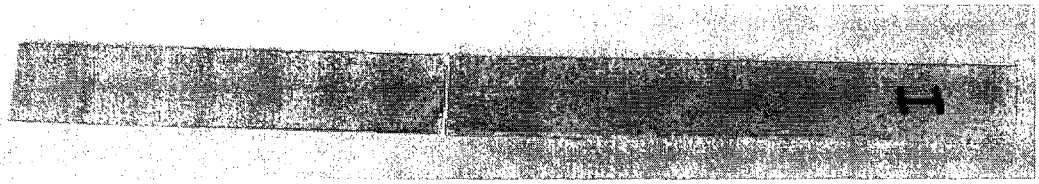

(a) Front view

Fig (4.24) Bonding test sample from CCF + KP based EPDM

The axial displacement – force curve for the sample is shown in Fig (4.25).

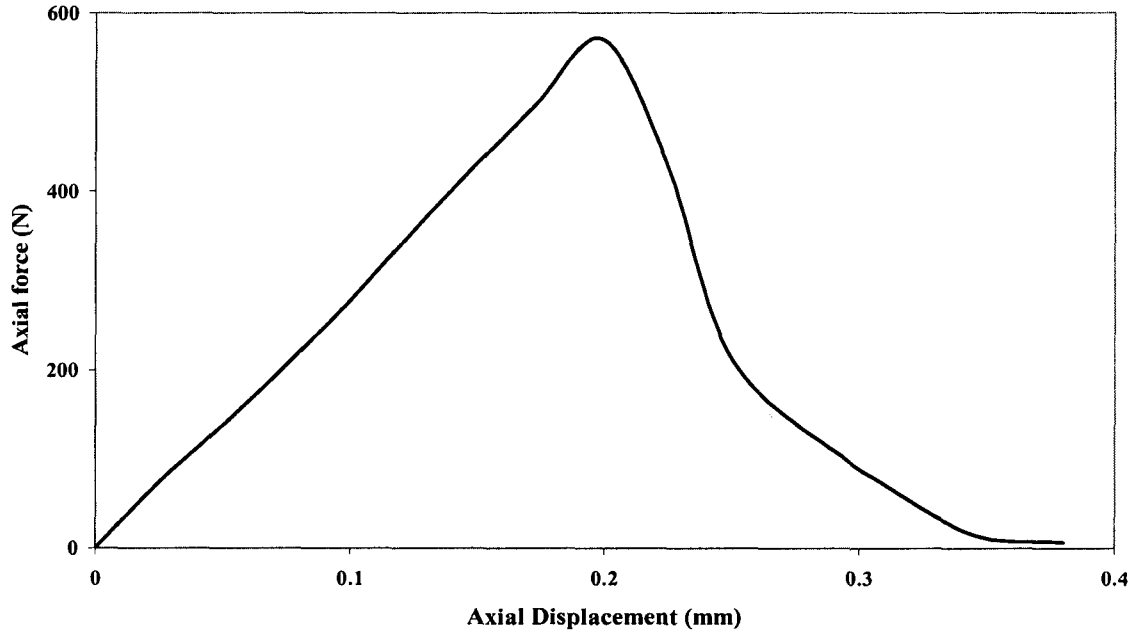

Fig (4.25) The axial displacement – force for CCF + KP based EPDM

It appears from the curve that a piece of CCF + KP based EPDM can withstand a maximum axial load of 570 N. After this load separation of the piece happens from the aluminum substrate (adhesive failure). The bond strength of the rubber based piece is higher than the maximum recorded axial force. This maximum axial force is corresponding to a shear stress of 0.88 MPa.

4.8 Contribution in lowering case temperatures

Current application requires that the contribution of the solid rocket motor propellant combustion in the surface temperature of the solid rocket motor case should not exceed 150 °C.

For an insulation layer of 3 mm thickness composed of EPDM + 25 phr chopped carbon fibers + 25 phr Kevlar pulp + 60 phr ammonium polyphosphate, this insulation is used to insulate a steel case. The problem in using the hybrid is that you can not guaranty that all

the fibers nearly aligned perpendicular to heat flow. Suppose that after mixing and curing of the insulation chopped carbon fibers aligned as shown in Fig (4.26) and Fig (4.27). Points A, B, C and D will be in dangerous situation because the chopped carbon fibers (thermal conductivity = 6.4 W/m.C) worked as conductive chains which conduct heat flux fast, this will raise the temperature of point A quickly result in failure of the adhesive layer which bonds the insulation to steel. This should lead to catastrophic explosion of the solid rocket motor.

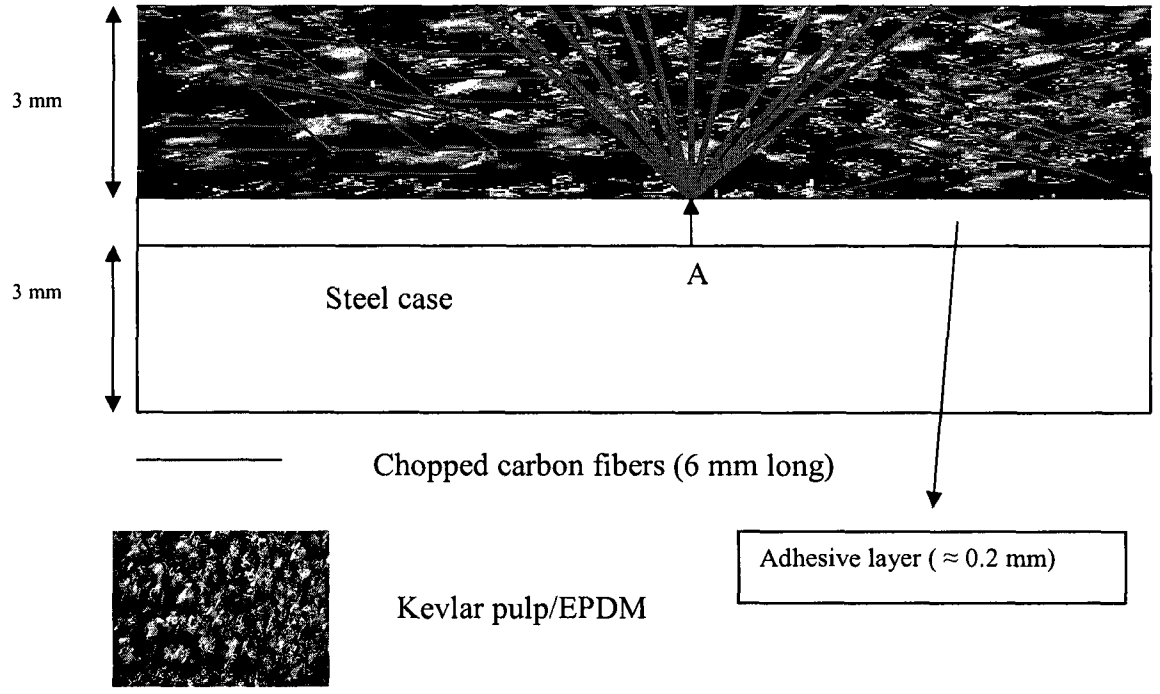

Fig (4.26) Schematic layout for the alignment of the different phases when using one layer insulation with 3 mm thickness composed of EPDM + 25 phr chopped carbon fibers +25 phr Kevlar pulp + 60 phr ammonium polyphosphate

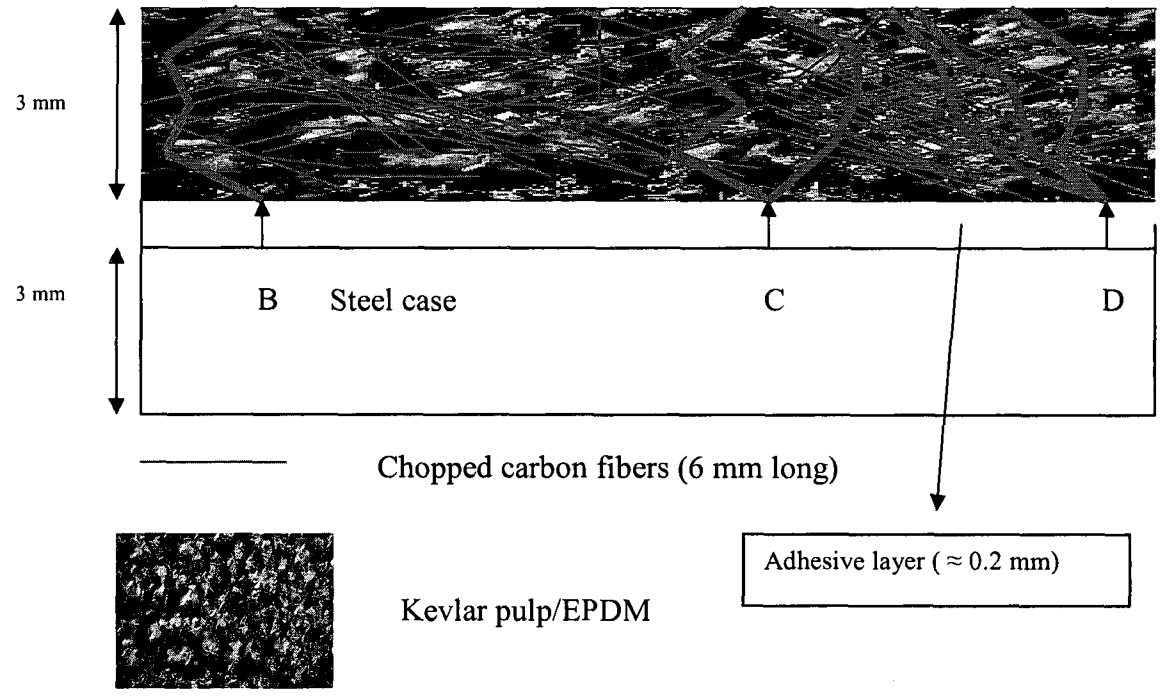

Fig (4.27) Schematic layout for the alignment of the different phases when using one layer insulation with 3 mm thickness composed of EPDM + 25 phr chopped carbon fibers +25 phr Kevlar pulp + 60 phr ammonium polyphosphate

While in the case of using a laminate consists of 6 layers placed alternatively of single reinforcement (CCF or KP) the situation will be different and safe as shown in Fig (4.28). This is because

1- The resistance to conduction is increased by the layers of KP/EPDM which have very low thermal conductivity

2- The larger is the number of layers; the physical structure converges to the series model which gives the lowest thermal conductivity

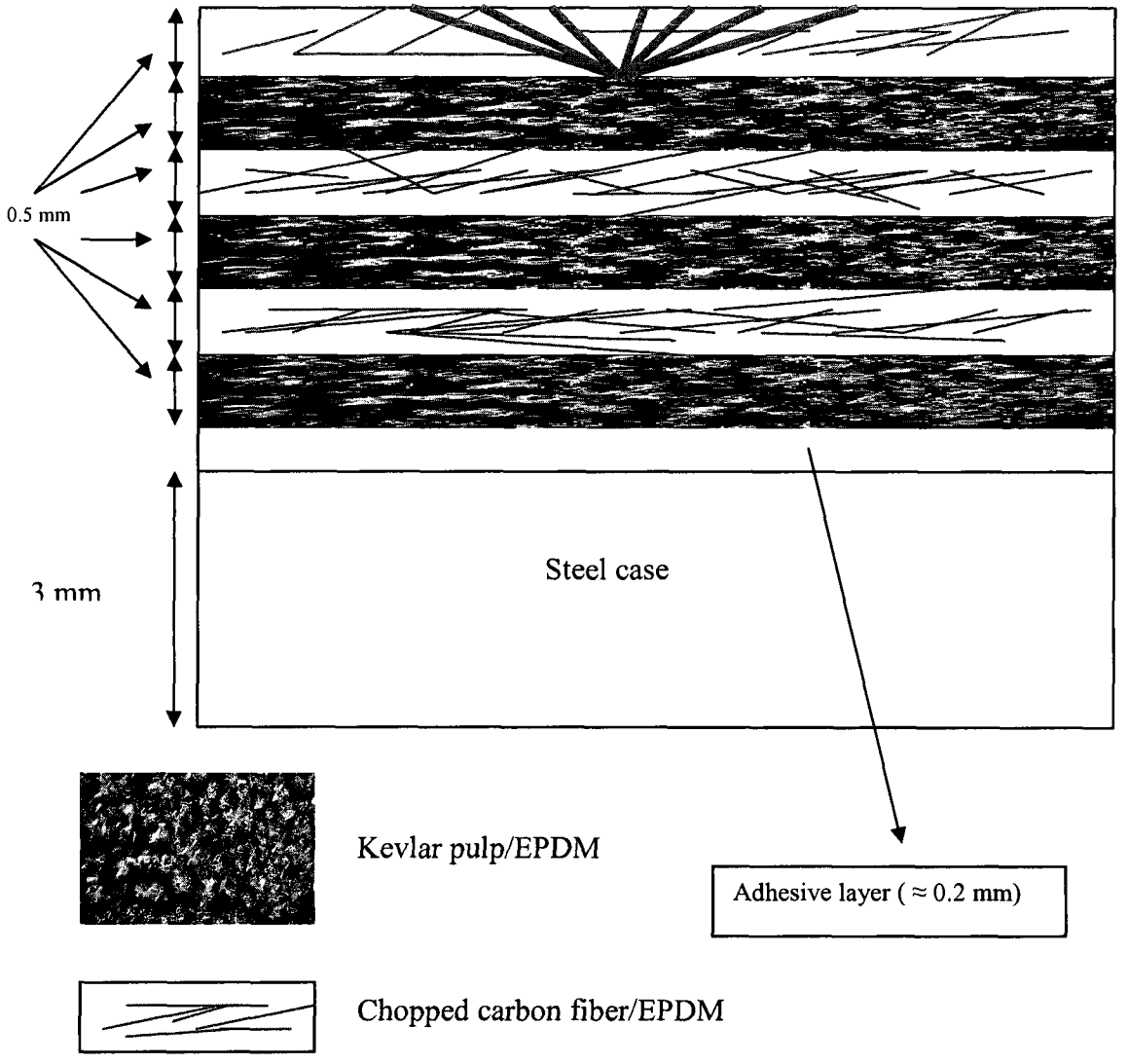

Fig (4.28) schematic layout for the alignment of the different phases when using a laminate consists of 6 layers placed alternatively of single reinforcement (CCF or KP) with 3 mm thickness as insulation

Chapter 5

Summary and Contributions

5.1 Summary

Work was performed to:

a) Define, evaluate, and demonstrate new concepts for a new manufacturing process for reinforced elastomeric thermal shields, while maintaining high ablation performance and resistance to the service conditions of application.

b) Develop a new technique for the manufacturing of new prepregs made of EPDM matrix reinforced with chopped carbon fibers or Kevlar pulp.

All material and formulation selections were made jointly by the selection of the most promising combination of matrix, and reinforcement. Physical, thermal, mechanical and ablation performance of the candidates was compared to currently used insulators. The material systems were started on a broad base and through various screening and selection phases resulted in the final system as shown in Fig (5.1).

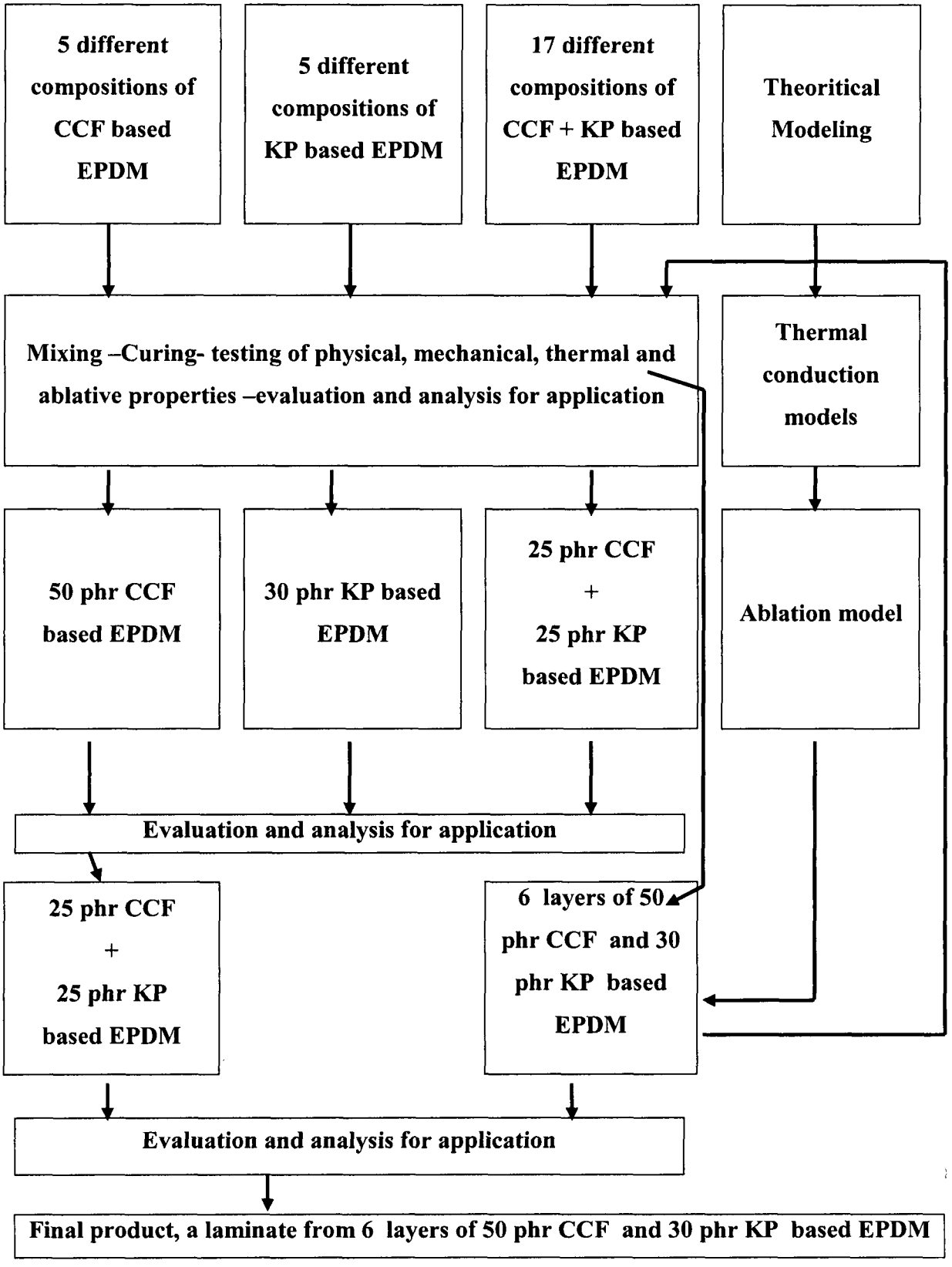

Fig (5.1) Scheme of the performed work

The approaches to achieve a new manufacturing process included investigation of the processing of the reinforced elastomeric master batch result from the mixer to get it in prepreg form. These materials and approaches were evaluated by consideration of manufacturing ease and by critical performance criteria of ability to withstand service temperature environment and satisfactory ablation performance.

After various screening and evaluation phases, one material system was selected, properties were generated, and a thermo-structural analysis made. The material system is a laminate consists of layers stacked alternatively of 50 phr CCF or 30 phr KP based EPDM in the prepreg form. The number of layers is specified according to the required thickness of the final insulation laminate taking into account that the thickness of the prepreg is 0.5 mm

Modifications of these materials were tested in an ablation environment simulating the propellant combustion conditions of a solid rocket motor for long time. The materials exhibited high heats of ablation combined with minimum shape change to indicate feasibility for this application in addition to high insulation efficiency (reduction of case temperature). These formulations and alignment met the performance criteria.

The development work introduced new concepts for composite synthesis based in elastomeric matrices. Elastomeric Prepregs are now exploited by new fabrication techniques and offer a cost-effective high performance route to composite construction. This generation of prepreg matrix systems will offer further improvements in workshop handling, reduced time processing and controlled stacking levels, improving laminate quality. This also opens further opportunities for the wider application of this versatile material in the rocket motor insulation industry. This can also be applied in exhaust pipes

as example in civilian applications. In addition the elastomeric based prepregs may be stored in large rolls in an uncured, or at most a partially cured, state until ready for use for laminate fabrication. As a result, a new fabrication technique was defined and demonstrated using discontinuous reinforcements to get a composite laminate based on elastomeric matrices.

The properties of a laminate with thickness 3 mm and composed of 6 layers stacked alternatively of 50 phr CCF or 30 phr KP based EPDM in the prepreg form are shown in Table (5.1).

Property	**Unit**	**Testing value for laminate**
Tensile strength	MPa	7.8 ± 0.5
Elongation	%	12.1± 1.2
Hardness	Shore A	88.9 ± 0.2
Density	gm/cm^3	1.239
Specific heat capacity	J/kg.k	1691 ± 4
Thermal diffusivity	mm^2/sec	0.085 ± 0.002
Thermal conductivity	W/m.k	0.178 ± 0.001
Ablation rate	mm/sec	0.006 ± 0.0002
Outer case temperature	°C	39.1± 0.5
TGA remaining weight	%	27 ± 0.5

Table (5.1) 6 layers CCF and/or KP based EPDM laminate properties

5.2 Contributions

The original aspects of this work are:

a- The development of a new arrangement for making more efficient insulant (by the connection in series of different phases)

b- The development of techniques to make the EPDM prepregs.

c- The development of techniques to make the layered insulant samples.

d- The simulation to provide the optimal configuration for lowest thermal conductivity.

e- The development of a new ablation model for reinforced elastomeric thermal shields

Immediate uses for the invention are:

a- Insulants for rocket motor cases

b- Liners for exhaust pipes in cars

c- Liners for conduits of high temperature and high velocity flowing gases.

Publications

(a) Patent

A declaration of invention entitled:

'Insulants based on elastomeric layered laminate for conduits of high temperature and high velocity gas streams and process for manufacturing thereof'

was accepted for filing.

The original aspects of the invention are:

a- The development of a new arrangement for making more efficient insulant (by the connection in series of different phases)

b- The development of techniques to make the EPDM prepregs.

c- The development of techniques to make the layered insulant samples.

d- The simulation to provide the optimal configuration for lowest thermal conductivity.

(b) Papers

- Journal papers (1)

1- Ashraf F. Ahmed, S.V. Hoa "Thermal insulation by heat resistant polymers for solid rocket motor insulation" Journal of composite materials, USA (under review).

- Conference papers (6)

1- Ashraf F. Ahmed, S.V. Hoa "Development and analysis of a hybrid reinforced composite material for solid rocket motor insulation" American Society for Composites 23rd annual technical conference, Sept. 9-11, 2008, Memphis, TN, USA.

2- Ashraf F. Ahmed, S.V. Hoa "Improvement of the properties of insulating polymers using chopped carbon fiber for solid rocket motor insulation" (CARBON 2008) conference, July. 12-18, 2008, Nagano, Japan.

3- Ashraf F. Ahmed, S.V. Hoa "Improvement of the properties of insulating polymers using aramid fiber for solid rocket motor insulation" 13th international conference on applied mechanics and mechanical engineering (AMME-13), May. 27-29, 2008, Cairo, Egypt.

4- Ashraf F. Ahmed, S.V. Hoa "Development of asbestos free composites for solid rocket motor insulation" 22nd Canadian Congress of Applied Mechanics, May 31st to June 4th, 2009, Halifax, Nova Scotia Canada.

5- Ashraf F. Ahmed, S.V. Hoa "Optimization and thermal conduction modeling for a hybrid reinforced composite material for solid rocket motor insulation" 17th International Conference on Composite Materials, ICCM-17, 27 - 31 Jul 2009, Edinburgh International Convention Centre (EICC), Edinburgh, UK.

6- Ashraf F. Ahmed, S.V. Hoa "Ablation Model for Reinforced Elastomeric Thermal Shields" American Society for Composites 24th Annual Technical Conference - held jointly with Canadian Association for Composites Structures and Materials, September 15th – 17th, 2009, Newark, Delaware.

Future work

1- Evaluate the performance of the developed thermal insulation laminate as application inside the exhaust pipe and predict the effect of use in the operation and shelf life time of the exhaust pipe.

2- Using CCF, KP and Silica (Aerosil R-982) as a new reinforcement for EPDM will be done. Fabrication of prepregs from CCF/ EPDM, KP/ EPDM and silica/ EPDM and evaluate the performance of a laminate composed of different sublayers of these prepregs (with different stacking sequence) with respect to the volume fractions of the selected materials in addition to investigation of physical, mechanical, thermal and ablative properties of these materials. Where Aerosil have density 0.05 gm/ cm^3 which may be result in more light insulation without affecting the other properties of the insulation material.

3- Carbon flakes, KP and Silica (Aerosil R-982) can be used as a new reinforcement for EPDM. Fabrication of prepregs from carbon flakes/ EPDM, KP/ EPDM and silica/ EPDM can be done. Evaluation of the performance of a laminate composed of different sublayers of these prepregs (with different stacking sequence) with respect to the volume fractions of the selected materials in addition to investigation of physical, mechanical, thermal and ablative properties of these materials can be done.

4- Using CCF + carbon flakes, KP and Silica (Aerosil R-982) as a new reinforcement for EPDM can be done. Fabrication of prepregs from CCF + carbon flakes/ EPDM, KP/ EPDM and silica/ EPDM can be done. Evaluation of the performance of a laminate composed of different sublayers of these prepregs (with different stacking sequence) with

respect to the volume fractions of the selected materials in addition to investigation of physical, mechanical, thermal and ablative properties of these materials can be done.

References

1- NASA space vehicle design criteria. "Solid rocket motor internal insulation" .NASA sp -8093, 1976.

2- Wang Zheng, Yongqiang Hu " Solid Rocket Motor" 1st ed., Astronautics industry Press, Beijing, 1993, pp. 229-236.

3- Guillot, David. G. Novel,"Method of insulating a rocket motor" US patent no 5352312, Oct 4, 1991.

4- Guillot, David. G. "Method of insulating case of solid propellant rocket motor" USA Patent Application No. 20020018847, 14 February 2002.

5- Kakade, S.D.; Navale, S.B. & Narsimhan, V.L. "Studies on interface properties of propellant liner for case-bonded composite propellants". Journal of Engineering Materials , 2003, 21, 73-85.

6- F. Cauty, C. Erades and J. C. Godon. "Experimental study of the degradation of an internal thermal insulator". Office national detudes et de recheches aerospatials, Chatillon , France, 2000.

7- Guillot, David. G. Novel, "Method of insulating a case of a solid propellant rocket motor" US patent no 6893597, May 17, 2005.

8- Guillot, David. G. Novel, 'EPDM rocket motor insulation' US patent no 6787586, Sept. 7, 2004.

9- Guillot, David. G. Novel, 'EPDM rocket motor insulation' US patent no 6566420 May 20, 2003.

10- Guillot, David. G. Novel, 'EPDM rocket motor insulation' US patent no 5644000, July 1, 1997.

11- Guillot, David. G. Novel, 'Low density thermoplastic elastomeric insulation for rocket motor' US patent no 5644110, July 20, 1997.

12- Guillot, David. G. Novel, 'thermoplastic elastomeric internal insulation for rocket motors for low temperature applications' US patent no 5399599, March 21, 1995.

13- Roberto Isopi, Eros Pittarelli, Antonio Sebasta 'Development of Low density insulators for space motors' SNIA Viscosa, Space and defense division, Via Sicilia 162, Rome, Italy, 1979.

14- Vernon W. Fitch and Norman F. Eddy. "Space shuttle solid propellent rocket motors, asbestos filled insulation replacement." Thiokol Corporation , Ogden, UT, 1997.

15- Mathew S. Bell, William F. S. Tam. "ASRM case insulation design and development. Composite structure laboratory". NASA –CR-191947, Aerojet general corporation, October 10, 1992.

16- Jancey Bell, "Rocket motor insulation using phosphonitrilic elastomeric compositions" US patent, Jun 18, 1991.

17- A. J. Kinloch and R. J. Young, *Behavior of polymers*, Elsevier Science Publishers, Ltd., London, 1983.

18- Yalin Guo, Guozheming Qiu, Aihua Liu. "Study of a liquid insulation for the solid rocket motor". Departement of Applied Chemistry, School of Science, Northwestern polytechnical university, Xian, shaanxi 710072, China, Xian aerospace composites research institute,china, 2006.

19- Weili Wu, Dajun Chen , Weili Wu, College of Chemistry and Engineering, Qiqihar University, Qiqihar 161006, China, "Thermal and Mechanical Properties of Dough Modeling Compound Reinforced Ethylene Propylene Diene Monomer/Silicon Rubber Composites", Polymer Composites—2006.

20- Saha Deuri, A.; Bhowmick, A.; Ghosh, R.; John, B.; Sriram, T. & De, S.K. "Thermal and ablative properties of rocket insulator compound based on EPDM". Polym. Deg. Stab., 1998, 21(1), 21-28.

21- Yu. A. Kumzerov, L. S. Parfeneva, I. A. Smirnov "Thermal and acoustic properties of chrysotile asbestos" Physics of the solid state journal, Vol. 47, 370-373, 2005.

22- Chase, Michael John, Smith, Derek Anthony and Dudley, Michael Alan "Rocket motor with ablative insulating casing liner" US Patent 3973397, August 10, 1976.

23- Ratte, Jacques, Duchesne, Gonzague and Carignan, Pierre "insulation system for rocket motors" United States Patent 4148675, Oct 4, 1979.

24- Junior, Kenneth E. and Byrd, James D."Aramid polymer and powder filler reinforced elastomeric composition for use as rocket motor insulation" US Patent 4492779, January 8, 1985.

25- Junior, Kenneth E., Byrd, James D. and Hightower, Jr., James O." Polybenzimidazole polymer and powder filler reinforced elastomeric composition for use as a rocket motor insulation" US Patent 4600732, July 15, 1986.

26- Byrd, James D., Davis, Robert T."Delayed quick cure rocket motor liner" US Patent 4601862, July 22, 1986.

27- Herring, Liles G."Elastomeric insulation compositions for rocket motors" US Patent 4663065, May 5, 1987.

28- Herring, Liles G. "Elastomeric insulating materials for rocket motors" US Patent 4878431, November 7, 1989.

29- Chang, Suae-Chen "Rocket motor insulation using phosphonitrilic elastomeric compositions" US Patent 5024860, June 18, 1991.

30- Guillot, David G "Method of insulating a rocket motor" US Patent 5352312, October 4, 1994.

31- Guillot, David G. "Low density thermoplastic elastomeric insulation for rocket motors" United States Patent 5498649, March 12, 1996.

32- Graham, Mark, Levi, Lane and Clarke, Brett "Durable motor insulation" US Patent 5821284, October 13, 1998.

33- Hutchens, Dale E., Cohen, Norman "Low smoke rocket motor liner compositions" US Patent 6051087, April 18, 2000.

34- Pennington, William L., Skolnik, Edward G. and Davidson, Thomas F. "Non-Asbestos insulation for rocket motor casing" US Patent 6265330, July 24, 2001.

35- Harvey, Albert R. and Ellertson, John W. "Rocket motor insulation containing hydrophobic particles" US Patent 6606852 issued on August 19, 2003.

36- Harvey, Albert R. and Ellertson, John W "Fiber-reinforced rocket motor insulation" US Patent 6691505, February 17, 2004.

37- Guillot, David G "Method of insulating a case of a solid propellant rocket" US Patent 20050028514, February 10, 2005.

38- Fan, Jun-Ling and Ho, Wen-Dar "Rocket motor insulation containing coated hydrophilic fillers" US Patent 20050054754, March 10, 2005.

39- Fan, Jun-Ling "Elastomeric insulating composition for a solid propellant rocket motor" United States Patent 6953823, Oct 11, 2005.

40- Fan, Jun-Ling, Tsai, Shr-Hau, Tu Fu-Hua and Tu Yao-Tsai "Low density rocket motor insulation" US Patent 20070112091, May 17, 2007.

41- Gajiwala, Himansu M. and Guillot, David G. "Polybenzoxazole-filled nitrile butadiene rubber compositions, articles incorporating the same, and a method of insulating a rocket motor with the same" US Patent 20070254988, November 1, 2007.

42- Guillot, David G and Harvey, Albert R. "EPDM rocket motor insulation" US Patent 7371784, May 13, 2008.

43- Gajiwala, Himansu M." Low-cost, low-density, ablative rubber insulation for rocket motors" United States Patent 7461503, September 9, 2008.

44- D. Sanschagrin and G. Couture. " Development of an asbestos free insulant for rocket motors". Defence research establishment Valcartier , 2459, Pie IX blvd. north, Courcelette, Quebec, Canada G0A 1R0,1996.

45- Woods, C. D. Myers, Jr, F. F., Davidson, T. F., and Ludlow, T. L., "Replacement of asbestos in smokeless insulators for rocket motors" Report number MMT3811, ARC propulsion Division, Gainesville, VA., april 1984.

46- S. S. Aggour, M. A. Elshendidy, S. M. Elmarsafy and A. F. Ahmed ' Improvement of the properties of insulating polymers'Journal of Eng., Vol 10, Egypt, 2006.

47- Muraleekrishnan, R.; Bandyopadhyay, G.G.; Catherine, Korah Bina; Ravindran, P.V.; Muthiah, Rm & Kannan, K.G. MACRO. 'Effect of diene type on thermal and mechanical characteristics of EPDM'. In Proceedings of the International Conference on Advances in Polymer Technologies, 14-17 December 2004, Thiruvananthapuram. pp. 340, India.

48- Herring, Liles G. "Elastomeric insulating materials for rocket motors". Hercules Inc. USA Patent No. 4, 501, 841, 26 February 1985. 12pp.

49- Karpeles, Richard & Grossi, Anthony V. "EPDM Rubber technology". In Handbook of elastomers, edited by Anil K. Bhowmik, and H.L. Stephens. Marcel Dekker Inc, USA, 2001. pp. 845-76.

50- Robert A. Rhein "Thermally stable elastomers" NWC TP 6372 Naval Weapons Center, China lake, California 93555, 1983.

51- Channel prime alliance, Dupont Company, Ethylene Propylene Diene polymers, Technical guide for polymers, Sept. 2004.

52- C.M. Bhuvaneswari, M.S. Sureshkumer, S.D. Kakade, and Monaj Gupta. "Ethylene – propylene rubber as a futuristic elastomer for insulation of solid rocket motor". Defence Science Journal, Vol 56, No.3 july 2006 pp.309-320.

53- C.M. Bhuvaneswari, S.D. Kakade, V.D. Deuskar, A.B. Dange and Manoj Gupta "Filled Ethylene-propylene Diene Terpolymer Elastomer as Thermal Insulator for Case-bonded Solid Rocket Motors" Defence Science Journal, Vol. 58, No. 1, January, 2008, pp. 94-102

54- Uniroyal Chemical Company, Inc., Trilene liquid polymers, Uniroyal Chemical Technical guide for liquid polymers, June 2002.

55- M. Akiba, A. S. Hashim,' Vulcanization and crosslinking in alstomers' Prog. Poly. Sci., Vol. 22, 475-521, 1997.

56- Achintya K. Sen, A. S. Bhattacharyya, P. P. De and Anil K. Bhowmick "Studies on crosslinking of EPDM- PE blends by thermoanalytical techniques" Journal of ThermalAnalysis, Vol. 37, 19-38, 1991.

57- Keller, Robert C. "Peroxide curing of ethylenepropylene elastomers". Rubber Chem. Technol., 1988, 61(2), 238-54.

58- Carbon fibers, ASM Handbook, Volume 21, Composites, 2001.

59- Paul J. Walsh," Carbon fibers" Zoltek Corporation, 2001

60- R. Bacon and C.T. Moses, High-Performance Polymers—Their Origin and Development, R.B. Seymour and G.S. Kirshenbaum, Ed., Elseveir, 1986, p 341.

61- G.G. Tibbetts, Carbon Fiber Filaments and Composites, J.L. Figueiredo et al. Ed., Kluwer Academic Publishers, 1990, p 73–94

62- Zolteck corporation, Advanced fibers systems, "Technical guide for carbon fiber", USA, 2006.

63- Aramid fibers, ASM handbook, 2003

64- Dupont advanced fibers systems, Technical guide for KEVLAR, USA, 2005.

65-Catherine A. Yezzi, Barry B. Moore. "Characterisation of Kevlar/ EPDM rubbers for use as rocket motor case insulators". Atlantic Research Corporation, 7511 Wellington road, Gainesville, Virginia 22065, 1986.

66- James J. Seidlek, "Elastomer/ aramid fiber dispersion" US patent, February 21, 1995.

67- SIGMA ALDRICH' Technical guide for peroxides' 2005.

68- Culverhouse, D. "Compounding rubber for fire resistance". Rubber World, 188(1), 18- 24, 1983.

69- C. W. Brabender Instruments, Mixers, Technical guide, 2004.

70- INSTRON, Shore A hardness, Technical guide, 2001.

71- NETZSCH Instruments, Nano Flash LFA 447 TM, System data sheet, 2005

72- Douglas B. Cook and Frederick M. Perkins. "Assessment of EPDM elastomer change using the thermal flash method –calibration studies". Thiokol Corporation, Brigham City, Utah, 1993.

73- D. Cook and F. Perkins. "Assessment of EPDM elastomer change using the thermal flash method", AIAA Missile Sciences Conference, 22-24 February, 1993, Monterey, CA.

74- TA instruments, Differential Scanning Calorimeter (DSC), Technical guide, 2002.

75- TA instruments, Thermo Gravimetric Analyzer (TGA), Technical guide, 2002.

76- BERNZOMATIC TORCH, TS 4000T trigger – start torch, Technical guide, 2006.

77- PIONEER DIETECS COORPORATION, ASTM specimen cutting dies for tensile testing, Technical data sheet, 2004.

78- ASTM D412 – 02, Standard Test Methods for Vulcanized Rubber and Thermoplastic Elastomers —Tension.

79- ASTM D2240 - 05 Standard Test Method for Rubber Property—Durometer Hardness.

80- ASTM E1461 - 07 Standard Test Method for Thermal Diffusivity by the Flash Method.

81- ASTM E 1269 – 01 Standard Test Method for Determining Specific Heat Capacity by Differential Scanning Calorimetry.

82- A. Y Uyarel and L Pektas'A thermal analysis investigation of new insulator compositions based on EPDM and phenolic resin' Journal of Thermal Analysis, Vol. 46 (1996) 163-176

83- ASTM E 1641 – 99, Standard Test Method for Decomposition Kinetics by Thermogravimetry.

84- E. A. Turi Ed. 'Thermal characterization of polymeric materials' Academic Press, New York, 1981.

85- Saha Deuri, A. & Bhowmick, Anil K. "Degradation of rocket insulator at high temperature". J. Therm. Anal., 1987, 32, 755-70.

86- A.M. Helmy. "Thermal analysis of solid rocket motor's heat insulation materials".Teledyne, Mccormick Selph, Hollister, California, USA, 1983.

87- R. E. Morgan, A. S. Prince, and S. A. Selvidge, Thiokol propulsion, Science and engineering Huntsville operations, Brigham city, Utah and J. Phelps, C. L. Martin,T. W. L awrence. National aeronautics and space administration, Marshall space flight center, Huntsville, Alabama. "Non – asbestos insulation testing using a plasma torch". July 2000.

88- Daniel S. Nelson, Andrew S. Prince. "An experimental method for evaluating the char tenacity of fiber- reinforced insulation materials", Joint Propulsion Conference and Exhibit, Indianapolis, USA; 27-29 June 1994.

89- ASTM E 285 – 02, "Standard Test Method for Oxyacetylene Ablation Testing of Thermal Insulation Materials".

90- Jianfeng Wang , James K. Carson , Mike F. North , Donald J. Cleland , "A new approach to modeling the effective thermal conductivity of heterogeneous materials". International Journal of Heat and Mass Transfer 49 (2006) 3075–3083.

91- Y. Benveniste, "On the effective thermal conductivity of multiphase composites", Journal of Applied Mathematics and Physics (ZAMP) Vol. 37, September 1986.

92- Karthik Ramani and Aparna Vaidyanathan ,"Finite element analysis of effective thermal conductivity of filled polymeric composites", Journal of Composite Materials 1995; 29; 1725.

93- MoranWang, JinkuWang, Ning Pan, Shiyi Chen and Jihuan He "Three-dimensional effect on the effective thermal conductivity of porous media", Journal of physics D, Vol. 40, 260–265, 2007.

94- Karthik Ramani and Aparna Vaidyanathan 'Finite Element Analysis of Effective Thermal Conductivity of Filled Polymeric Composites' Journal of Composite Materials; Vol. 29; 1725, 1995

95- Juliane Floury & James Carson & Q. Tuan Pham' Modeling Thermal Conductivity in Heterogeneous Media with the Finite Element Method' Journal of Thermal Analysis, Vol. 46, 177-189, 1996.

96- By Y. Benveniste 'On the effective thermal conductivity of multiphase composites' Journal of Applied Mathematics and Physics(ZAMP), Vol. 37, September 1986.

97- V. A. Osipova and Kh. A. Kyaar 'Calculation of the thermal conductivity of heterogeneous materials with disordered structure' Translated from Inzhenerno-Fizicheskii Zhurnal, UDC 536.21, Vol. 41, no 4, 607-616, 1981.

98- H. Hatta, M. Taya,' Effective thermal conductivity of a misoriented short fiber composites', Journal of applied physics, Vol 58 (7), 2478-2486, 1985.

99- R. C. Progelhof, J. L. Throne, R. R. Reutsch, "Methods for predicting the thermal conductivity of composite systems', a review", Polymer engineering science 16, 615-625, 1976.

100- I. J. Gruntfest "Ablation" in ECT 2nd ed., Vol. 1, pp. 11–21, General Electric Company.

101- 'Ablation process and environment' Kirk-Othmer Encyclopedia of Chemical Technology.

102- E. R. Stover "Ablative Materials" in ECT 3rd ed., Vol. 1, pp. 10–26, P. W. Juneau, Jr., and J. P. Brazel, General Electric Company.

103- M. B. Khan' An Investigation of the Ablation Behavior of Advanced Ultrahigh-Temperature EPDM/Epoxy Insulation Composites' polymer-plastics technology and engineering, Vol. 35, 187-206, 1996.

104- Hongqing, He & Yan, Hong 'Ablation model of EPDM' Tuijin Jishu, 20(4), 36-39, 1999.

105- A. A. Donskoy, "Elastomeric heat- shielding materials for internal surfaces of missile engines" International journal of polymeric materials, 1996, Vol. 31, pp. 215-236.

106- Donald L. Schmidt "Ablative polymers in aerospace technology" J. Macromol. SCI.- CHEM., A3(3), PP. 327-365, May, 1969.

107- Harvey, Albert R., Ellertson, John W. "Fiber-reinforced rocket motor insulation" US Patent 6691505, February 17, 2004.

Appendix

- **Tensile strength:** the stress at which a material breaks or permanently deforms

- **Strain:** The geometrical measure of deformation representing the relative displacement between particles in the material body, i.e. a measure of how much a given displacement differs locally from a rigid-body displacement.

- **Hardness:** the material's resistance to permanent indentation. It refers to various properties of matter in the solid phase that gives it high resistance to various kinds of shape change when force is applied.

- **Durometer:** One of the several measures of the hardness of a material

-**Thermal conductivity:** The property of a material that indicates its ability to conduct heat.

- **Specific heat capacity:** also known simply as **specific heat**, is the measure of the heat energy required to increase the temperature of a unit quantity of a substance by a certain temperature interval.

- **Thermal decomposition**: also called **thermolysis**, is defined as a chemical reaction when a chemical substance breaks up into at least two chemical substances when heated. The reaction is usually endothermic as heat is required to break chemical bonds in the compound undergoing decomposition.

- **The decomposition temperature:** The temperature at which the substance decomposes into smaller substances or into its constituent atoms.

- **Terpolymer:** a polymer made from three or more monomers

- **Ablation** is defined as the removal of material from the surface of an object by vaporization, chipping, or other erosive processes

- **The mechanism of ablation:** The material absorbs heat by increasing in temperature and changing in chemical or physical state, the changes usually being accompanied by loss of surface material.

- **Prepreg**: A combination of uncured resin matrix and fiber reinforcement, which is in a form that is ready for molding and curing into the final composite part.

- **A laminate:** A material constructed by uniting two or more layers of material together. The process of creating a laminate is **lamination**, which in common parlance refers to the placing of layers of materials in uncured state and curing them with heat and/or pressure, usually with a curing agent to form the final composite part.

- **The Glass transition temperature:** is the temperature at which an amorphous solid such as glass or a polymer, becomes brittle on cooling, or soft on heating

- **Viscosity:** A measure of the resistance of a fluid which is being deformed by either shear stress or extensional stress. Also it describes a fluid's internal resistance to flow and may be thought of as a measure of fluid friction.

- **Mooney viscosity**: The shearing torque resisting rotation of a cylindrical metal disk (or rotor) embedded in rubber within a cylindrical cavity.

- **Heat flux** or **thermal flux**, sometimes also referred to as **heat flux density** or **heat flow rate intensity** is a flow of energy per unit of area per unit of time

- **Electrical resistivity** (also known as **specific electrical resistance** or **volume resistivity**) is a measure of how strongly a material opposes the flow of electric current.

A low resistivity indicates a material that readily allows the movement of electrical charge. The SI unit of electrical resistivity is the ohm meter (Ω m).

Bond strength (ply adhesion): Amount of force required (per unit width) to separate plies of material or materials in peeling mode plus the force to bend the plies.